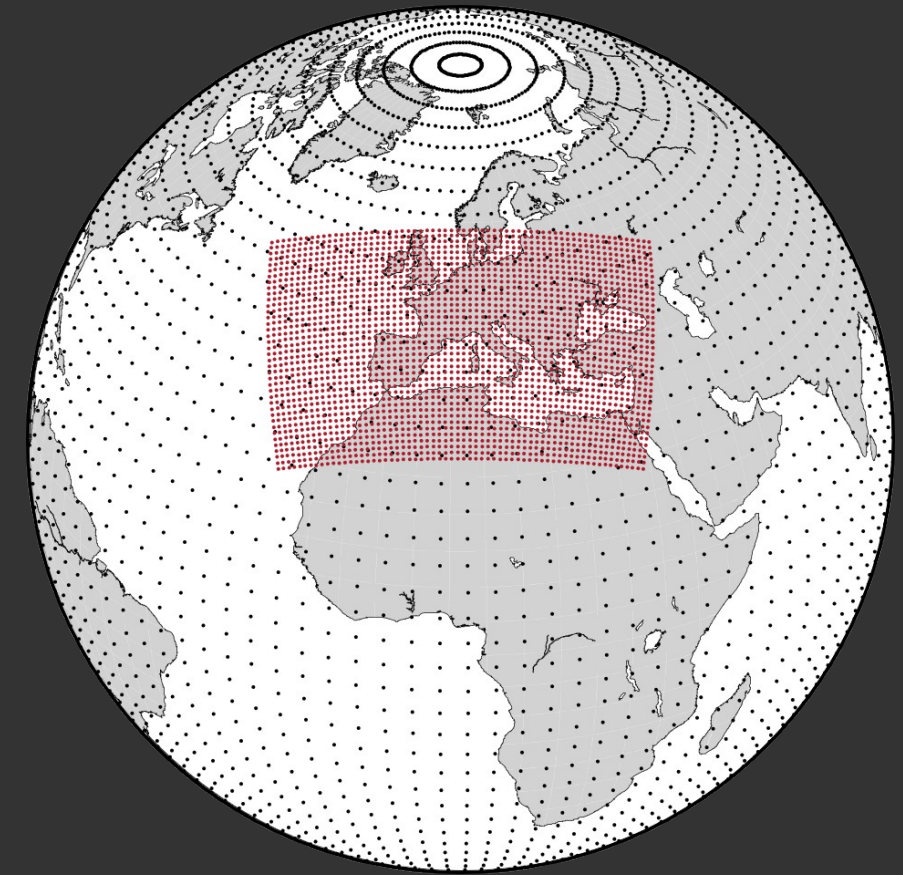
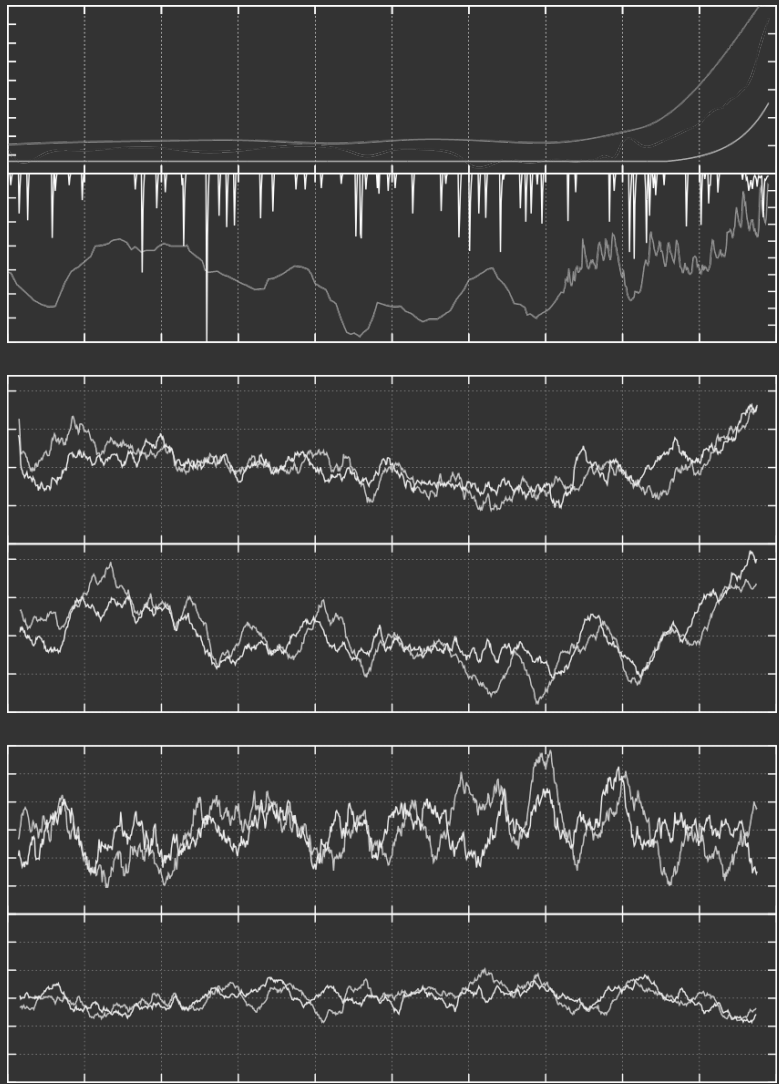


2011

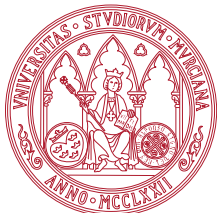
# Regional modelling of climate evolution in the last millennium and future projections

Regional modelling of climate evolution in the last millennium  
JUAN JOSÉ GÓMEZ NAVARRO



JUAN JOSÉ GÓMEZ NAVARRO





Universidad de Murcia

**Modelización regional de la evolución climática del último  
mileno y proyecciones de futuro**

**Regional modelling of climate evolution in the last  
millennium and future projections**

*Memoria presentada para optar al Grado de Doctor por:*

JUAN JOSÉ GÓMEZ NAVARRO

*Director: Juan Pedro Montávez Gómez*

2011



*Science is what we understand  
well enough to explain to a computer.  
Art is everything else we do.*  
**-Donald E. Knuth-**

*Ciencia es todo lo que entendemos  
suficientemente bien como para explicárselo  
a un ordenador. Arte es todo lo demás.*  
**-Donald E. Knuth-**



# Agradecimientos

Hay muchas personas que, de una u otra manera, han contribuido a que esta tesis llegue a algún puerto. En un lugar destacado, todo esto no habría sido posible sin la ayuda de Juan Pedro. No han sido pocas las discusiones de ciencia (y de lo que no es ciencia) en «la sala de fumar», sin las cuales no habría aquí nada que escribir. Me ha enseñado básicamente todo lo que sé de modelos, de clima y de contar chistes (de algunas cosas me ha enseñado más que de otras). Espero que tengamos muchas más discusiones enriquecedoras en el futuro. Otro lugar destacado lo tiene el que fue mi director (al menos oficialmente) durante casi la mitad de mi Tesis. Agradezco a Rafa su altruismo y buen rollo, que me ha permitido disfrutar de la beca FPU que ha hecho posible esto. Pero sobre todo, gracias porque si algo sé de cómo escribir Ciencia es gracias a él y sus manías. Nunca olvidaré ese regalo.

En segundo lugar, quiero agradecer a los que han sido mis «jefes temporales» en las diversas estancias que he hecho a lo largo de estos cuatro años. En orden de aparición, gracias Hugo por esas largas noches en Antigonish rodeados de mosquitos tigre canadienses, comiendo pebre y bebiendo vino hasta acabar existencias. Gracias Edu por ser un máquina, por los chutes de conocimiento que me has inoculado y porque en definitiva sin tu ayuda esta tesis sería más floja todavía. Gracias también a Jürg por dedicarme parte de su más que escaso tiempo, y a Elena por ser un inestimable apoyo en aquellas tierras germanas. Y aunque no han sido estancias propiamente dichas, muchas gracias a Fidel por ayudarme en todos los *papers* que he escrito. Gracias por esas estimulantes discusiones, por su paciencia y su predisposición a ayudar, por su enervante modestia, y en general por ser tan *maravilloso*.

Esta tesis es la formalización por escrito del trabajo efectuado durante cuatro años en el despacho de los becarios, y gracias a ellos ese trabajo ha sido más llevadero.

Gracias a Manolo por mostrarme la larga senda del Rock, a Santi (y su risa) por ser la alegría del despacho, a Sonia por enseñarme a correr el modelo y ser mi compañera de fatigas y a veces desdichas, a Raquel porque gracias a ella mi empanada mental es menos escandalosa, a Juan por ser el informático friki que siempre quise tener a mi lado, y a Félix por ser el compañero de despacho remoto. Gracias también a los otros miembros del celebérrimo grupo MAR: Juanan, Rocío, Zaida, y sobre todo a Pedro por ayudarme mil veces con el inglés y en la redacción de los *papers*. Así mismo, gracias a todos los compañeros, becarios y no becarios, del CIOyN: Manu, Pablo, María, Jaime, Eli, Elisa, Juanfran, Hugo, Jose, Javier, Javi, Adela, Andrés, Miguel... y sobre todo gracias a los que olvido mencionar.

Me gustaría agradecer también a las personas anónimas que mantienen grandes proyectos de desarrollo de software libre de calidad, sin el cual sin duda no habría podido hacer Ciencia ni escribir esta tesis. Así mismo, me gustaría agradecer a la gente que he ido conociendo durante estos años en la fauna de internet, y que también han dejado su huella en esta tesis (aunque sólo sea por retrasarla). Gracias a la gente de los foros de Migui, y en especial a Gonzalo Medina, L<sup>A</sup>T<sub>E</sub>X-man, por enseñarme a componer una tesis casi sin volverme loco.

Gracias al Ministerio de Educación por la beca FPU (Ref. AP-2006-04100) que ha financiado mi trabajo durante estos cuatro años. Agradezco al Ministerio de Medio Ambiente el haber aprobado los proyectos ESCENA (Ref. 20080050084265) y SALVASINOBAS (Ref. 200800050083542), así como al Ministerio de Ciencia y Tecnología por el proyecto SPECMORE (Ref. CGL2008-06558-C02-02/CLI). Estos proyectos han permitido pagar congresos, viajes y publicaciones.

Muchas gracias a mi familia: abuelos, tíos, primos, hermanica, cuñás, suegros, a la Hera y en especial a mis padres Pepe y Rosario, por apoyarme siempre y animarme a seguir adelante. También quiero mencionar a Zeferino, que ha soportado las chapas de mi tesis en el pueblo y me ha abierto su casa siempre que la he necesitado. Pero sobre todo gracias a Vanesa, que es la que realmente ha sufrido el que esta tesis exista. No sólo eso, sino que sin su sentido de la realidad probablemente nunca hubiera hecho el ánimo de ponerme finalmente a escribir. Muchas gracias Vane, esta tesis está dedicada a ti.

# Resumen

El estudio del clima y su evolución es una cuestión de interés general. Las sociedades modernas están expuestas a variaciones climáticas, que hoy sabemos que en tiempos pasados han jugado un importante papel en el auge y declive de diversas civilizaciones. Entender la evolución climática, su variabilidad, sus causas y mecanismos, así como determinar hasta qué punto puede estar condicionada por la acción de la mano del hombre es una cuestión compleja que supone un reto para la Ciencia contemporánea. Actualmente existe una fuerte evidencia de que la Tierra está sufriendo un proceso de Cambio Climático que carece de antecedentes en los últimos miles e incluso cientos de miles de años. Así mismo, todo parece indicar que las actividades humanas (cambios en los usos de suelo, deforestación, emisión de gases de efecto invernadero, etc.) está jugando un papel importante en este proceso. Sin embargo, pese a que los mecanismos físicos que relacionan el incremento en el nivel de los gases de efecto invernadero con el aumento en la temperatura son bien conocidos desde hace décadas, es difícil establecer una relación causal directa, puesto que el sistema climático es un complejo conjunto de subsistemas interrelacionado a diversas escalas espaciales y temporales, de manera que su comportamiento no es deducible a partir de sus partes por separado.

El estudio del clima es también interesante desde el punto de vista del avance científico, puesto que es un área que presenta muchas preguntas sin resolver. Su análisis está limitado por la evidente imposibilidad de llevar a cabo experimentos controlados. Así pues, la climatología es una ciencia con un fuerte componente descriptivo, que se basa en la cuidadosa observación y recopilación de datos. Esta tarea es a su vez difícil debido al tamaño del sistema de estudio y las complejas interconexiones que en él existen, que impiden el estudio de subsistemas cerrados. En este sentido, la climatología ha dado un enorme paso hacia delante tras la incorporación de redes de estaciones meteo-

rológicas globales, y más tarde satélites meteorológicos, que han permitido monitorizar el estado global del clima en cada instante. Otro enorme paso hacia delante en la climatología ha sido propiciado por el enorme aumento de la capacidad computacional, que ha posibilitado la introducción de modelos computacionales que simulan el sistema climático. Estos modelos permiten, dentro de las limitaciones de un modelo, que es una mera simplificación de la realidad, hacer experimentos controlados donde diversos parámetros pueden ser modificados para analizar su impacto en el sistema climático. En particular se pueden utilizar tanto para realizar proyecciones de Cambio Climático, basadas en ciertas hipótesis sobre la evolución de factores socio económicos, como para reconstruir la variabilidad climática en el pasado en función de la estimación de ciertos forzamientos externos.

Existen diversos tipos de modelos climáticos en la actualidad. Esta Tesis se concentra en dos de ellos: Modelos de Circulación General y Modelos Climáticos Regionales. Los primeros tienen en cuenta el sistema climático en su totalidad (atmósfera, océano, litosfera, criósfera, etc.), y simulan su evolución en todo el globo en su conjunto. La ventaja de este tipo de modelos es que simulan todos los intercambios de materia, energía y momento entre los diferentes componentes del sistema, y sólo dependen de una condición inicial, así como los forzamientos externos al sistema. El inconveniente es su enorme coste computacional, que limita su resolución espacial (del orden de cientos de kilómetros). Por el contrario, un modelo regional simula sólo un área limitada, con unas fronteras bien definidas. Así pues, los flujos de materia y energía a través de estas fronteras han de ser proporcionados externamente, por lo que un modelo de estas características necesita estar acoplado a un modelo global que facilite esta información. La ventaja de este tipo de modelos es su menor coste computacional, que permite su implementación a mayor resolución espacial (del orden de decenas de kilómetros).

Para la realización de esta Tesis se han realizado una serie de simulaciones climáticas para el futuro y el pasado con una versión climática desarrollada en nuestro grupo del modelo regional MM5 acoplado a diversos modelos globales (ECHO-G y ECHAM5)<sup>1</sup>. El dominio de estudio es la Península Ibérica, un área con una compleja diversidad climática que no puede ser reproducida con la baja resolución de los modelos globales, y que por tanto la hace óptima para llevar a cabo experimentos regionales que permitan evaluar el valor añadido de éstos. Así mismo se encuentra en un área especialmente sensible ante la problemática del Cambio Climático, como se detalla a lo largo de esta Tesis. La resolución espacial del modelo es 30 km, lo que permite

---

<sup>1</sup>Las simulaciones globales han sido utilizadas como datos de entrada para llevar a cabo las simulaciones regionales, pero su ejecución fue llevada a cabo previamente por diversas instituciones ajenas al desarrollo de esta Tesis. Para el desarrollo de esta Tesis sólo se han llevado a cabo simulaciones regionales.

reproducir circulaciones regionales introducidas por la interacción con los principales sistemas montañosos peninsulares. Por otro lado, hay una parte de la Tesis dedicada a una ambiciosa simulación efectuada sobre un domino que abarca toda Europa con una resolución de 45 km. El potencial de esta simulación radica en la mejora en las comparaciones entre simulaciones y las reconstrucciones de gran calidad disponibles para Europa. El objetivo principal de esta Tesis es desarrollar y analizar una base de datos de alta resolución climática sobre la Península Ibérica y Europa, tanto de proyecciones de cambio climático como de simulaciones del último milenio, que permita poner el actual calentamiento global en un contexto climático más amplio, así como relacionarlo con factores naturales.

Se ha llevado a cabo una simulación sobre la Península Ibérica del último milenio acoplada al modelo global ECHO-G. Esta simulación ha sido conducida mediante la reconstrucción de tres tipos de factores externos: variaciones en la intensidad de radiación solar, en la concentración de gases de efecto invernadero y efectos estimados en el balance radiativo de la actividad de grandes volcanes. Se ha evaluado la capacidad de esta simulación para reproducir un clima realista acorde con observaciones y simulaciones conducidas por reanálisis. Esto ha permitido caracterizar el valor añadido del modelo regional en este tipo de simulaciones, que se aprecia más cuando nos concentramos en la alta frecuencia y en variables cuya interacción con la orografía es importante, como la precipitación. También se ha evaluado la capacidad del sistema MM5-ECHO-G para reproducir de manera realista la relación entre la Oscilación del Atlántico Norte (NAO por sus siglas en inglés) y la precipitación sobre la península. Esto ha servido para estudiar esta relación a lo largo del último milenio, que a su vez permite conectar reconstrucciones independientes basadas en datos *proxy*<sup>2</sup> de precipitación y este índice climático durante el último milenio. Se ha llevado a cabo una comparación entre los resultados de la simulación y dos reconstrucciones ajustadas a una malla de temperatura y precipitación. No se ha identificado un buen acuerdo entre éstas y el resultado de la simulación, lo que puede ser interpretado de diversas formas: problemas en las reconstrucciones usadas para forzar las simulaciones, incapacidad del modelo para desarrollar un clima consistente y realista a partir de unos forzamientos realistas, así como fallos en las reconstrucciones de temperatura y precipitación. Sin embargo, la metodología, si bien permite identificar discrepancias, no permite discriminar las razones de éstas.

---

<sup>2</sup>Proxy es una palabra inglesa que no admite fácil traducción al castellano. Un proxy es una observación de algún fenómeno que de manera indirecta contiene información climática. Así por ejemplo el grosor de anillos de árboles, documentos sobre inundaciones y sequías o testigos de hielo en glaciares de Groenlandia son ejemplos de datos *proxy* utilizados para reconstruir el clima.

Por otro lado, se ha analizado el papel de la variabilidad interna en simulaciones regionales. La evolución del clima es una combinación de diversos factores naturales y humanos, que están superpuestos a un nivel indeterminado de variabilidad intrínseca del sistema climático que proviene de su naturaleza caótica. Esto dificulta la tarea de identificar qué fracción del calentamiento observado es debida a causas antrópicas. La comparación de dos simulaciones que comparten los forzamientos externos, pero parten de condiciones iniciales diferentes, permite evaluar el papel de la variabilidad interna con respecto a estos últimos. Para llevar a cabo este enfoque, se han realizado dos simulaciones de 1000 años sobre la Península Ibérica con una resolución de 30 km, lo cual supone un reto técnico en sí mismo debido a su enorme costo computacional. El análisis conjunto de estas simulaciones ha permitido determinar que la evolución de la temperatura está en gran parte determinada por la evolución de los forzamientos externos, mientras que la precipitación está dominada por la variabilidad natural. Esto explica una parte importante de la diversidad de resultados que se obtienen en proyecciones de cambios en la precipitación durante el siglo XXI. Un resultado inesperado de este estudio es que, pese a la influencia generalizada de la variabilidad natural en la precipitación, hay ciertas áreas en donde su efecto es menor, por lo que esta variable responde de manera consistente frente a los forzamientos. La identificación de estas áreas es fundamental porque es en ellas donde una comparación entre los resultados de la simulación y las reconstrucciones presenta un mayor potencial.

Una parte importante de la Tesis contiene los resultados de una simulación efectuada para toda Europa con una resolución espacial de 45 km durante el periodo 1500-1990. Se ha valorado la capacidad de simular un clima realista, para lo cual se ha comparado con observaciones reales, que comienzan a principios del siglo XX. Se ha valorando tanto la capacidad de obtener un valor medio realista como la distribución de probabilidad de temperatura y precipitación en diversas áreas características como la Península Ibérica, Los Alpes, Las Islas Británicas, etc. Así mismo se ha comparado esta simulación con diversas reconstrucciones disponibles para Europa durante el periodo simulado.

Por otro lado, se han llevado a cabo cuatro proyecciones de Cambio Climático. Para ello se han utilizado dos modelos globales (ECHO-G y ECHAM5) como condiciones de contorno, así como dos diferentes escenarios para cada uno de ellos (A2 y B2 para ECHO-G y A2 y B1 para ECHAM5). El análisis conjunto de estas cuatro proyecciones ha permitido analizar características comunes y específicas, lo que a su vez permite acotar las incertidumbres. Para ello se ha evitado la utilización de un enfoque de futuro menos presente. En lugar de ello se han utilizado técnicas estadísticas basas en el Análisis de Componentes Principales. Esto ha permitido encontrar que la estructura de los

patrones de calentamiento durante el siglo XXI es consistente, y que la diferencia entre diversos escenarios se limita a la intensidad del calentamiento. Se ha identificado que la estación más sensible al calentamiento es verano, lo cual tiene como consecuencia una continentalización del clima. Así mismo se ha distinguido entre la evolución de temperaturas máximas y mínimas, lo que ha permitido identificar un incremento del rango diario de temperaturas, que es así mismo característico de climas continentales.

Finalmente, se exploran algunas aplicaciones de las simulaciones llevadas a cabo para la realización de esta Tesis. Una de las aplicaciones de las simulaciones ha utilizado las series simuladas de temperatura y precipitación sobre un área que abarca la región de Andalucía para evaluar la capacidad de un novedoso método de reconstrucción, basado en el análisis de periodos extremos, para obtener una reconstrucción de la media y la varianza de las distribuciones de probabilidad de estas dos variables. Para ello se han utilizado las series como pseudorealidad a reconstruir, y se ha generado un pseudoproxy a partir de ellas. Se ha aplicado el método a este pseudoproxy para hacer una pseudoreconstrucción que posteriormente puede ser comparada con la serie original de la simulación. Esto ha permitido evaluar la capacidad de la metodología, así como estimar un intervalo de confianza para las reconstrucciones reales. Adicionalmente, se ha utilizado la consistencia física del modelo para evaluar las teleconexiones que se establecen entre un nuevo índice climático basado en la zonalidad del viento en el área del Canal de la Mancha con campos como temperatura y precipitación en el área de Europa. Este índice se ha reconstruido usando diarios de navegación de barcos de la Armada Británica, y mediante una comparación con observaciones reales se han establecido una serie de relaciones en el corto periodo instrumental. El modelo ha permitido valorar la consistencia de estas teleconexiones, así como evaluar su evolución temporal en períodos de tiempo climáticos, más allá de los registros instrumentales.

Esta Tesis constituye un paso adelante en cuanto a la utilización de modelos de alta resolución en un contexto paleoclimático. Se han simulado aproximadamente 3000 años con alta resolución, lo que ha permitido abordar cuestiones antes inaccesibles, como el valor añadido de este tipo de modelos en paleoclima o el papel de la variabilidad interna. Así mismo, se ha generado una enorme base de datos, desde proyecciones de Cambio Climático a simulaciones del último milenio. Estos datos están actualmente siendo utilizados por diversos investigadores, desde la comunidad de reconstrucciones climáticas hasta estudios de Impacto Ambiental. Como fruto de estas colaboraciones se están llevando a cabo actualmente varios estudios de diversa índole. Algunas de ellas ya han sido publicados o enviados a publicación, mientras que otros lo serán a lo largo de los próximos meses.



# Abstract

The study of climate and its evolution is a matter of general interest. Modern societies are exposed to climatic variations, which have played an important role during the past in the rise and fall of civilizations. Understanding the evolution of climate, its variability, its causes and mechanisms as well as determining at what extent it can be conditioned by the action of mankind is a complex task that represents a challenge to contemporary Science. There is now strong evidence that the Earth is undergoing a Climate Change process without precedent in the last thousand or even hundreds of thousands of years. Also, it seems that the anthropogenic activity (changes in land use, deforestation, emission of greenhouse gases, etc.) is playing an important role in this process. However, although the physical mechanisms linking the increase in the concentration of greenhouse gases with rising temperatures are well known for decades, it is difficult to establish a direct causal relationship, since the climate system is a complex set of interrelated subsystems at different spatial and temporal scales, whose behavior is not deducible from its separate parts.

The study of climate is also interesting from the standpoint of scientific progress, since there are still many open questions. Its analysis is however limited by the obvious impossibility of conducting controlled experiments. Thus, climatology is a science with a strong descriptive component, based on careful observation and data collection. This task is itself difficult because the size of the target system and the complex interconnections existing, which hampers the study of closed subsystems. In this sense, climatology has taken a huge step forward after the incorporation of global networks of weather stations, followed by weather satellites, which have allowed monitoring global climate state at every instant. Another huge step forward in climate has been fostered by the enormous increase in computing power, which has made possible the introduction of

computer models that simulate the climate system. These models allow, within the limitations of a model, which is a mere simplification of reality, performing controlled experiments where different parameters can be modified to analyze its impact on the climate system. In particular, they can be used both for developing climate change projections, based on certain assumptions about the evolution of socio-economic factors, as well as trying to reconstruct past climate variability based on estimations of certain external forcings.

There exist various types of climate models at present. This Thesis focuses on two of them: General Circulation Models and Regional Climate Models. The former take into account the whole climate system (atmosphere, ocean, lithosphere, cryosphere, etc.), and simulate their evolution across the planet as a whole. The advantage of such models is that they simulate all matter, energy and momentum exchanges between the different components of the system, and only need initial conditions as input, as well as a set of external forcings. Their drawback is however the huge computational cost, which limits their spatial resolution (in the order of hundreds of kilometers). By contrast, a regional model simulates only a limited area domain, with well defined borders. Thus, matter and energy flows through these borders have to be provided somehow externally, so a model with these features need to be coupled to a global model providing this information. The advantage of this type of model is its lower computational cost, allowing its implementation to greater spatial resolution (the order of tens of kilometers).

For the realization of this Thesis a number of climate simulations have been performed for the future and the past with a climate version, developed in our group, of the regional model MM5, coupled to two global models (ECHO-G and ECHAM5)<sup>3</sup>. The target domain is the Iberian Peninsula, an area with a complex climatic diversity that can not be reproduced with the low-resolution state-of-the-art global models, and therefore makes it optimal for conducting regional experiments to assess their added value. It has also been identified as a hotspot in climate change, as detailed throughout this Thesis. The spatial resolution of most simulations in this Thesis is 30 km, which is capable of solving the physics introduced by the interaction with major mountain systems in the Iberian Peninsula. On the other hand, there is a chapter in this Thesis devoted to a simulation conducted on a domain covering Europe with a resolution of 45 km. The main objective of this Thesis is to develop and analyze a data base of high-resolution climate simulations over the Iberian Peninsula and Europe. This database encompasses climate

---

<sup>3</sup>The global simulations have been used as input to perform regional simulations, but they were previously run by several institutions not related to this Thesis. For the development of this Thesis only regional simulations have been conducted.

change projections as well as palaeosimulations, which allow putting the current global warming in a longer climatic context, as well as relate it with natural factors.

A simulation of the Iberian Peninsula in the last millennium coupled to the global model ECHO-G has been carried out. This simulation has been conducted by the reconstruction of three types of external factors: variations in total solar irradiance, the concentration of greenhouse gases and estimated effects on the radiative balance of the activity of large volcanic events. The ability of this simulation to reproduce a realistic climate, consistent with observations and reanalysis-driven simulations, has been assessed. This has permitted to characterize the added value of this type of regional simulations, which is especially apparent looking at the high frequency domain, and in variables whose interaction with the topography is more important, such as precipitation. Additionally, the ability of the ECHO-G-MM5 system to reproduce realistically the relationship between the North Atlantic Oscillation (NAO) and precipitation over the Iberian Peninsula has been assessed. This has allowed studying this relationship over the last millennium, which in turn connects independent reconstructions based on proxy data of this climate index and the rate of precipitation during the last millennium. A comparison between the simulation results and two gridded reconstructions of temperature and precipitation has also been carried out. It has not been identified a good agreement between them, which can be interpreted in several ways: problems in the reconstructions of the external forcings used to drive the simulations, failures in the climate models to develop a consistent and realistic climate from the reconstructed forcings, or problems in the temperature and precipitation reconstructions. However, although the methodology identifies discrepancies, it can not discriminate their underlying reasons.

On the other hand, we have analyzed the role of internal variability in regional climate palaeosimulations. Climate variability is a combination of natural and anthropic factors, which are superimposed to an indeterminate level of intrinsic variability of the climate system coming from its chaotic nature. This makes difficult to identify what fraction of the observed warming is due to anthropogenic causes. However, the comparison of two simulations sharing external forcings, but being initialized differently, allows assessing the role of internal variability with respect to the latter. In order to utilize this approach, two simulations of 1000 years over the Iberian Peninsula with a resolution of 30 km have been performed, which is itself a technical challenge due to the huge computational cost involved. The joint analysis of these simulations has been used to establish that temperature evolution is largely governed by the evolution of external forcings, whereas precipitation is dominated to a great extent by natural variability. This explains an important part of the diversity of results obtained on pro-

jected changes in precipitation during the 21st century. An additional and unexpected result of this study is that, despite the widespread influence of natural variability in rainfall, there are certain areas where its effect is smaller, so this variable consistently responds to the forcings influence among simulations. The identification of these areas is an important result, because they are where a comparison between the results of the simulation and the reconstruction presents higher potential.

An important part of this Thesis contains the results of a simulation performed throughout Europe with a spatial resolution of 45 km during the period 1500-1990. It has evaluated the ability of the model setup to simulate a realistic climate; thus, it has been compared with instrumental observations, beginning in the early 21st century. Both the ability to obtain a realistic average value, as well as the probability distribution functions of temperature and precipitation characteristics in different areas, such as the Iberian Peninsula, Alps, British Isles, etc. has been assessed. This simulation has been also compared with a number of high-quality reconstructions of several variables in the European area for the simulated period.

Additionally, four regional climate change projections have been performed for the Iberian Peninsula. In order to drive them, two global models (ECHO-G and ECHAM5) have been used to generate the boundary conditions, and two different scenarios for each of them (A2 and B2 for ECHO-G and ECHAM5 A2 and B1) have been considered. The joint analysis of these four projections allows analyzing common and specific characteristics, which in turn can limit the uncertainties. The future-minus-present approach has been avoided. Instead, statistical techniques based on Principal Component Analysis have been employed. This has allowed finding consistent warming patterns during the 21<sup>st</sup> century, and determining that the difference between scenarios is just in amplitude, not in spatial structure. The most sensitive season to the projected warming has been identified to be summer, which yields a climate continentalization. The study also distinguishes between the evolution of maximum and minimum temperatures, which has permitted to identify an increased daily range of temperatures, which is also a characteristic of continental climates.

Finally, this Thesis explores some applications of the simulations carried out for the realization of this Thesis. The first uses the simulated series of temperature and precipitation over an area encompassing the region of Andalusia to assess the ability of a novel reconstruction method, based on the analysis of extreme periods, to obtain a reconstruction of the mean and standard deviation probability distributions of these two variables. For this, the original simulated series has been used as pseudoreal series to be reconstructed, and a pseudoproxy has been generated from them. Then, the methodology has been applied to the pseudoproxy to generate a pseudoreconstruction,

which can be compared with the original series. This allows evaluating the ability of the methodology, and to estimate confidence intervals for the reconstructions, once it is applied to actual proxy data, in this case documentary evidence. In another exercise, we use the physical consistency of the model to evaluate a set of teleconnections established between a new climate index based on the zonality of the wind in the area of the English Channel with other climate fields such as temperature and precipitation in the area of Europe. This index has been reconstructed using logbooks of ships of the British Army, and by comparison with observations, a number of large-scale relationships have been established for the short instrumental period. The model has allowed assessing the consistency of these teleconnections, as well as its time evolution in longer climate periods, far beyond the instrumental record.

This Thesis is a step forward in the use of high resolution models in a palaeoclimatic context. About 3000 years of high resolution simulations have been conducted, which has helped to address issues previously inaccessible, such as the added value of palaeoclimate simulations, and the role of internal variability. Also, it has generated a huge database from climate change projections to simulations of the last millennium. This data is currently being used by several researchers, from proxy reconstructions community members to Environmental Impact Studies. As a result of these collaborations, several studies of various kinds are currently being conducted. Some of them have already been published or submitted for publication, while others will be finished over the next months.



# Publications

Some of the main results of the analysis of the simulations presented in this Thesis have been published so far in the next list of articles:

- Gómez-Navarro, J.J., Montávez, J.P., Jiménez-Guerrero, P., Jerez, S., García-Valero, J.A., and González-Rouco, J.F.: Warming patterns in regional climate change projections over the Iberian Peninsula, *Meteorologische Zeitschrift*, 19, 275–285, 2010.
- Gómez-Navarro, J.J., Montávez, J.P., Jerez, S., Jiménez-Guerrero, P., Lorente-Plazas, R., González-Rouco, J.F., and Zorita, E.: A regional climate simulation over the Iberian Peninsula for a the last millennium, *Climate of the Past*, 7(2), 451–472, 2011.
- Gómez-Navarro, J.J., Montávez, J.P., Jerez, S., Jiménez-Guerrero, P., Lorente-Plazas, R., González-Rouco, J.F., and Zorita, E.: Internal and external variability in regional simulations of the Iberian Peninsula climate over the last millennium, *Climate of the Past Discussion*, 7, 2579-2607, 2011
- Gómez-Navarro, J.J., Montávez, J.P., Jerez, S., Jiménez-Guerrero, P., Lorente-Plazas, R., González-Rouco, J.F., Zorita, E., Luterbacher, J., and García-Bustamante, E.: A simulation of the European regional climate over the past 500 years, In preparation.

As a result of the collaborations with scientist in parallel research areas, the generated data base has made possible the following works to be prepared:

- Jiménez-Guerrero, P., Gómez-Navarro, J.J., Jerez, S., Lorente-Plazas, R., García-Valero, J.A., and Montávez, J.P.: Variation of Secondary Inorganic Aerosols (SIA) in Europe for the 21st century (1991-2100), *Atmospheric Environment*, 45, 1059–1063, 2011.
- Rodrigo, F.S., Gómez-Navarro, J.J., and Montávez, J.P.: Climate variability in Andalusia (southern Spain) during the period 1701–1850 AD from documentary sources: evaluation and comparison with climate model simulations, *Climate of the Past Discussion*, 7, 2297-2339, 2011.
- Dorado-Liñán, I., Buntgen, U., González-Rouco, J.F., Zorita, E., Montávez, J.P., Gómez-Navarro, J.J., Brunet, M., Heinrich, I., Helle, G., and Gutierrez, E.: Tree-ring proxy based temperature reconstructions and climate model simulations: Cross-comparison at the Pyrenees, *Climate of the Past Discussions*, 7, 3919-3957, 2011.
- Jiménez-Guerrero, P., Montávez, J.P., Gómez-Navarro, J.J., Jerez, S., and Lorente-Plazas, R.: Impacts of climate change on gas-phase pollutants and aerosols in the Iberian Peninsula for the late XXI century, *Atmospheric Environment*, Submitted.

During the PhD, I have also been involved the following published or submitted works:

- Jerez, S., Montávez, J.P., Gómez-Navarro, J.J., Jiménez-Guerrero, P., Jiménez, J., and González-Rouco, J.F.: Temperature sensitivity to the land-surface model in MM5 climate simulations over the Iberian Peninsula, *Meteorologische Zeitschrift*, 19(4), 363–374, 2010.
- Jerez, S., Montávez, J.P., Gómez-Navarro, J.J., Jimenez, P.A., Jimenez-Guerrero, P., Lorente-Plazas, R., and Gonzalez-Rouco, J.F.: The role of the land-surface model for climate change projections over the Iberian Peninsula, *Journal of Geophysical Research*, Accepted for publication.
- Jerez, S., Montávez, J.P., Jiménez-Guerrero, P., Gómez-Navarro, J.J., Lorente-Plazas, R., and Zorita, E.: Assessment of the role of the parameterization schemes from a multi-physics ensemble of present-day climate simulations over the Iberian Peninsula, *Climate Dynamics*, Submitted.
- Jerez, S., Montávez, J.P., Gómez-Navarro, J.J., Fernández, J., Lorente, R., García-Valero, J.A., and Jiménez-Guerrero, P.: A multi-physics ensemble of climate change

projections over the Iberian Peninsula: mean changes, uncertainties and leading processes, *Climate Dynamics*, Submitted.

- Jiménez-Guerrero,P., Jorba, O., Pay, M.T., Montávez, J.P., Jerez, S., Gómez-Navarro, J.J., and Baldasano, J.M.: Comparison of two different sea-salt aerosol schemes as implemented in air quality models applied to the Mediterranean Basin, *Atmospheric Chemistry and Physics*, 11, 4833–4850, 2011.
- García-Valero, J.A., Montávez, J.P., Jerez, S., Gómez-Navarro, J.J., Lorente-Plazas, R., Jiménez-Guerrero, P: A seasonal study of the Atmospheric Dynamics over the Iberian Peninsula based on Circulation Types, *Theoretical and Applied Climatology*, Submitted.



# Contents

<b>Agradecimientos</b>	<b>i</b>
<b>Resumen</b>	<b>iii</b>
<b>Abstract</b>	<b>ix</b>
<b>Publications</b>	<b>xv</b>
<b>1 Introduction</b>	<b>1</b>
1.1 The climate and its evolution . . . . .	2
1.1.1 Climate variability . . . . .	2
1.1.2 Palaeoclimatology and Climate Change Projections . . . . .	7
1.2 Climate models and climate reconstructions . . . . .	10
1.2.1 Global circulation models . . . . .	10
1.2.2 Regional climate models . . . . .	14
1.2.3 Reconstructions of past climate . . . . .	15
1.3 The target regions . . . . .	18
1.3.1 The Iberian Peninsula . . . . .	18
1.3.2 Europe . . . . .	21
1.4 Objectives and structure of this Thesis . . . . .	21
<b>2 Regional paleosimulation for the IP</b>	<b>25</b>
2.1 Introduction . . . . .	25
2.2 Description of simulations, data employed and methodology . . . . .	28
2.3 Value added by the RCM . . . . .	33

2.3.1	Mean values . . . . .	34
2.3.2	Temporal variability . . . . .	38
2.3.3	Main variability modes . . . . .	43
2.3.4	Regional climate and synoptic conditions: NAO . . . . .	46
2.4	Climate in the last 1000 years in the IP . . . . .	48
2.4.1	AOGCM versus RCM simulation . . . . .	48
2.4.2	Comparison with proxy-based reconstructions . . . . .	54
2.5	Summary and Conclusions . . . . .	59
<b>3</b>	<b>Internal variability in regional paleosimulations</b>	<b>63</b>
3.1	Introduction . . . . .	64
3.2	Description of the simulations . . . . .	66
3.3	Results . . . . .	68
3.3.1	Correlation as a measure of internal variability . . . . .	68
3.3.2	Forced vs. unforced evolution of temperature and precipitation .	71
3.3.3	Physical meaning of the correlations . . . . .	73
3.4	Summary and Conclusions . . . . .	83
<b>4</b>	<b>Warming patterns in climate change projections</b>	<b>87</b>
4.1	Introduction . . . . .	88
4.2	Methodology . . . . .	89
4.2.1	Experiment description . . . . .	89
4.2.2	EOF analysis . . . . .	91
4.3	Results . . . . .	92
4.3.1	Warming patterns . . . . .	93
4.3.2	Temporal evolution . . . . .	99
4.4	Discussion . . . . .	103
<b>5</b>	<b>European simulation over the past 500 years</b>	<b>107</b>
5.1	Introduction . . . . .	108
5.2	Methodology and data employed . . . . .	110
5.2.1	Climate models . . . . .	110
5.2.2	Observations and reconstructions . . . . .	113
5.3	Model skill in reproducing observed climate . . . . .	115
5.3.1	Climatologies . . . . .	115
5.3.2	Summary of the validation . . . . .	121
5.4	Modeled and reconstructed climate . . . . .	123

5.4.1	Gridded reconstructions . . . . .	123
5.4.2	Reconstruction of Central European Temperature series . . . . .	133
5.4.3	Reconstruction of Stockholm January-to-April mean temperatures	136
5.4.4	Modeled and observed temperatures records in Central England .	136
5.5	Summary and conclusions . . . . .	140
<b>6</b>	<b>Some applications of regional climate palaeosimulations</b>	<b>143</b>
6.1	Introduction . . . . .	143
6.2	Reconstructing climate in Andalusia from documentary evidence . .	145
6.2.1	Reconstruction methodology . . . . .	145
6.2.2	Building pseudoproxies . . . . .	146
6.2.3	Results . . . . .	147
6.3	Testing physical consistence of the Westerly Instrumental Index (WII)	151
6.3.1	Definition of the Index . . . . .	151
6.3.2	NAO vs. WII . . . . .	152
6.3.3	Large-scale relations found in the simulation . . . . .	154
6.3.4	Temporal consistence of the relations . . . . .	154
6.4	Warm anomaly in Northern Europe in 1730s . . . . .	156
6.4.1	Evidence in climate reconstructions . . . . .	158
6.4.2	Lack of evidence in the simulation and pseudoreality . . . .	158
6.4.3	Results . . . . .	159
6.5	Temperature reconstruction in the Pyrenees . . . . .	162
6.5.1	Reconstructions methodology . . . . .	162
6.5.2	Comparison with simulations . . . . .	163
<b>7</b>	<b>General conclusions</b>	<b>167</b>
<b>Bibliography</b>		<b>174</b>



# Chapter 1

## Introduction

There is famous quote, many times attributed to Mark Twain, which states that “*climate is what you expect, weather is what you get*”. I can not make sure whether he is the author or not<sup>1</sup>, but whoever is, I believe that once you realise what climate is about, you have to agree. Unlike the weather, which you can see, enjoy and even suffer in your everyday life, you can not experience directly the climate with your senses. Just as you can neither get half a right side when throwing a single coin, nor have one children and a half, you can not touch or feel the climate. This though, pretty obvious in principle, has deep impacts in how we study and define climate.

Climate is the set of statistical properties that define the weather in a given location. But in statistics there is always place for some sort of subjectivity, and this is not an exception. The mean state of a climate variable can be defined in a thirty-years period window, but it can be longer if different arbitrary definitions are employed. Similarly, extreme events can be defined as those which exceed the percentile 10 in a probability distribution function, but a smaller threshold may be chosen depending on the study. This statistical approach to the study of the climate (which is unavoidable by the own definition of the climate) blurs the answers we can get for important question regarding the past and future climate evolution. Thus, before trying to answer important questions such as “*is climate going to change within the XXI century due to anthropogenic influence?*” one has to be sure that he/she understands what this question means, which tools exists to deal with this problem, and even more important, which are the limits of our knowledge. In this respect, answering properly climate questions is impossible

---

<sup>1</sup>wikiquote states that its author is not Mark Twain, but Robert A. Heinlein, a science fiction author.

without taking into account the many acknowledged uncertainties present in Science in general, and in Climatology in particular. And of course, the problem is that people in general, and policy makers in particular, have no time (I would say no interest too) in taking the time needed to understand properly the points exposed above.

This Thesis deals with climate and climate variability, focusing on the Iberian Peninsula (IP) and Europe. The most employed tool is a Regional Climate Model (RCM), as further explained below. The next chapters face questions such as to what extent the current warming is unprecedented, which are the limitations of climate models and what could potentially happen if greenhouse gases (GHG)<sup>2</sup> keep raising at the same rate as in the last decades.

## 1.1 The climate and its evolution

As stated above, climate is the statistical description of the weather. Hence, although it can not be directly measured, it influences human activities. In particular, climate variations may have been associated to the raise and fall of civilizations, mainly due to effects on water supply and agricultural productivity (deMenocal, 2001; Weiss and Bradley, 2001; Patterson et al., 2010). Thus, the current global warming presents an important challenge to modern civilizations, which already experience many direct and indirect impacts of this change (Mann et al., 2009; Shanahan et al., 2009). However, due to the inherent complexity of the climatic system, the many remaining uncertainties, and the lack of long high quality observational series to study the evolution of past climate, is not a trivial task to assess to what extent the current climate change is unprecedented, and what is the role of the anthropogenic activities on it.

### 1.1.1 Climate variability

As already reported in the early studies of Lorenz (1963), the physical laws governing the atmospheric dynamics are intrinsically affected by chaotic behaviour. This implies, among other things, that the numerical simulation of the system is strongly dependent on the initial conditions, and small departures from the “correct” initial condition yields to large changes after few time steps. This is what makes the weather prediction impossible beyond a couple of weeks, regardless the quality of the model, the impressive improvements in computational power and the increasing quality of the input data used

---

<sup>2</sup>Greenhouse gases are those responsible for the greenhouse effect in the atmosphere, further explained below.

to initialize the numerical models of the atmosphere. This drawback is indeed sometimes used to argue against the climate change projections in the form of the question: “*if we can not predict the weather for the next 10 days, how are we going to be able to predict the climate in the next 100 years?*”.

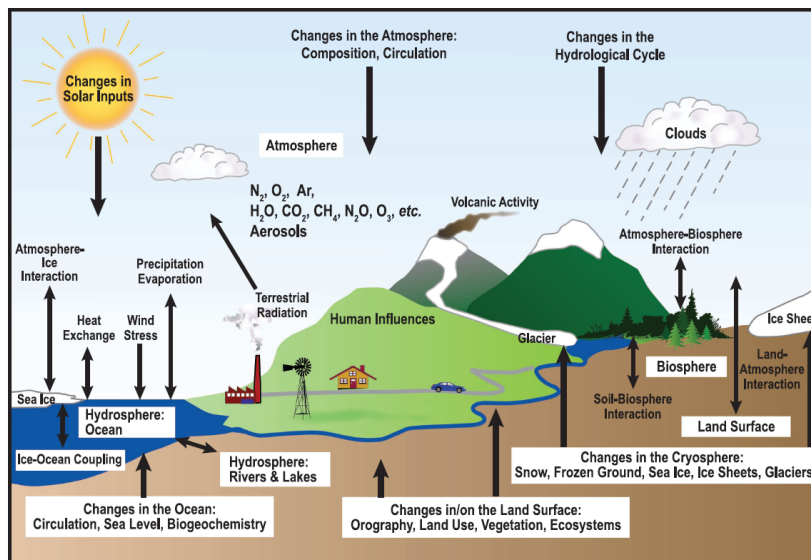
This is indeed a fair question whose answer is straightforward, but not always well understood for the society. Weather forecast and climate change projections<sup>3</sup> are different problems, dealing with different branches of Science and using different tools (admittedly with some parts in common) trying to answer different questions. From a mathematical point of view, weather forecast is an initial condition problem, whereas climate change projection is a boundary conditions problem (Giorgi and Bi, 2005). In weather forecast, a deep knowledge of the initial condition (this is, a perfect measure of the current state of the atmosphere) is fundamental, whereas modifications in the climate elements such as GHG concentrations, land use changes, etc. do not play an important role since these elements do not change appreciably in the time periods considered in weather forecast, and they can be considered constant. However, climate change projections deal with different time scales, where the initial conditions play a weak role as they are “forgotten” by the chaotic system in several days, entering in an equilibrium state what is what we call, in a statistical sense, climate. Then, climate change projections try to study how external modifications in the climate elements (which are the boundary conditions of the problem) such as the GHG concentrations, aerosol, land use cover, etc. modify this equilibrium state.

Figure 1.1 illustrates the many subsystems that compound the climate system. The solar radiation is the incoming energy that feeds the atmospheric movements. The power we receive from the Sun as short wave energy is fairly constant in time, although it slightly varies in an unpredictable<sup>4</sup> way along ages, and these variations have had deep fingerprints in the climate variations during the last millennium (Eddy, 1976; Crowley, 2000; Bradley et al., 2003). As soon as this energy reaches the atmosphere, which is of course another important part of the climatic system, the incoming radiation suffers a number of physical processes which are further illustrated in Figure 1.2. Part of the incoming energy is directly reflected by the clouds and the surface towards space. The remaining part is absorbed and heats the different components of the climatic system such as the oceans, the soil or the atmosphere. This heating increases the

---

<sup>3</sup>Sometimes the term “prediction” is used instead of “projection”. When talking about climate change and how it is studied with climate models, they refer to the same thing. In this Thesis I will refer to climate change projections.

<sup>4</sup>Sun variations remain mostly unpredictable due to the lack of a deep understanding on the physical processes underlaying the Sun dynamics.



**Figure 1.1:** Schematic view of the many components of the climate system and its main interactions. Source: (IPCC, 2007a).

temperature, which in turn increases the emission of long wave radiation. This feedback is maintained until the total outgoing radiation equals the incoming radiation. However, the atmosphere contains gases that absorb part of the outgoing long wave radiation, and this modifies the balance, forcing the atmosphere and the surface to further warm until a new equilibrium is reached and the outgoing radiation is able to balance all the incoming radiation. This mechanism, widely known as the greenhouse effect, was proposed as early as in 1827 by Joseph Fourier. Later on, John Tyndall discovered in 1861 that the primary contributors to this trapping are not the dominant constituents of the atmosphere, N<sub>2</sub> and O<sub>2</sub>, but trace gases, particularly water vapor and carbon dioxide, which constitute less than 1% of the atmospheric mass. Nowadays, none in scientific community doubts that the greenhouse effect is responsible for the Earth to be warmer than it should be in the absence of atmosphere, and that modifications in its composition may potentially have a warming (or cooling) effect at global scale (for a modern review of the greenhouse effect and how it is reinforced by positive feedbacks in the climate, the reader is referred to Held (2000)). The atmosphere is also very important because its lower part (namely the troposphere) is responsible for the weather, and it has the shortest response time, varying from minutes to weeks. The oceans are

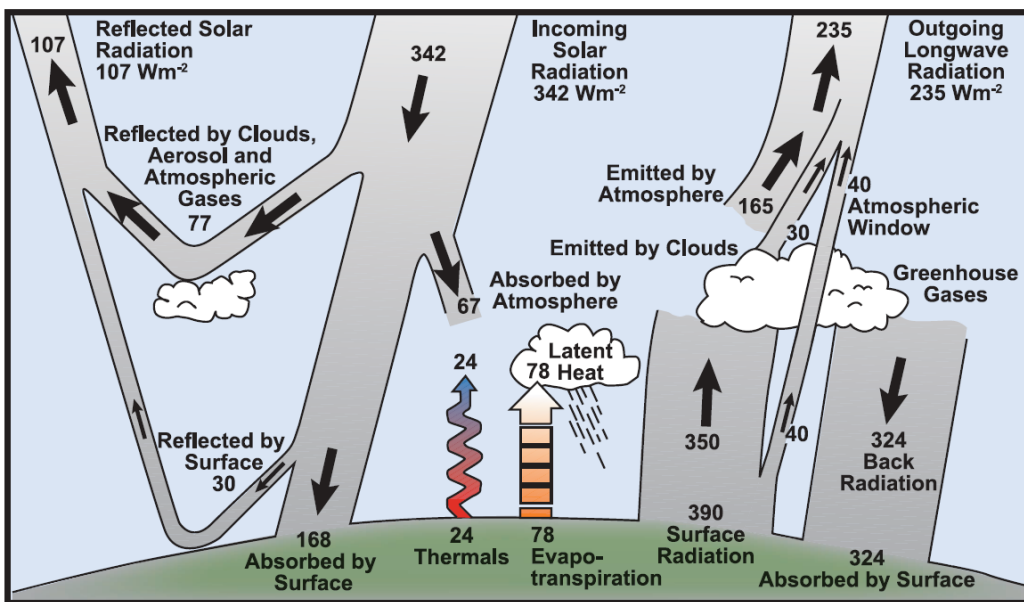


**Figure 1.2:** Radiation balance in the atmosphere. Most of the incoming energy is short wave radiation. Part of this radiation is reflected back to space, and part is absorbed. The absorption warms the climatic system, and in turn it emits energy in the form of long wave radiation. Source: (IPCC, 2007a).

other important component of the system, whose response time is slower than the atmosphere, although abrupt changes in ocean circulation it is thought to have played an important role in sudden past climate changes (Bigg et al., 2003). An important point to consider when discussing the warming observed in the last decades is the large thermal capacity of the water, which ameliorates climate variations and is responsible for the greatest amount of heat that the oceans are absorbing during the last decades (Barnett et al., 2001). The lithosphere and cryosphere are other important components which play an important role in the large climate changes in the history of the planet, but their response time is much lower, from years to millions of years, and depending on the study in many cases they are considered as constant.

But even more important than the components of the climate system, are their interactions. They exchange energy, matter, momentum, etc., and the study of the climate system has to take into account the feedbacks these exchanges imply. These feedbacks can be positive or negative. An important example of a negative feedback is the relation

between higher temperature and the increase rate of emitted long wave radiation discussed before, which plays a fundamental role in the thermal equilibrium of the Earth. On the other hand, positive feedbacks are thought to be responsible for a great part of the observed warming in the last decades (Hansen et al., 2011), and they include the reduction of albedo due to the melting of the ice cover in many areas of the planet (Curry et al., 1995), the increase of water vapour content in the atmosphere due to the larger evaporation rate in the presence of higher temperatures (Soden et al., 2002) or the liberation of large amounts of methane due to the reduction of the permafrost cover (Davidson and Janssens, 2006; Schneider von Deimling et al., 2011). The interaction, in form of feedbacks, between the different components of the climate system reaches a dynamic equilibrium which is what we denominate generically climate, and departures from this equilibrium determine the climatic variations. This equilibrium state is however dependent on some external and internal factors which may shift it, which are the so-called forcings. The modification of the concentration of GHGs in the atmosphere due to the human activities is an example of an anthropogenic forcing. Other anthropogenic forcing includes modification in land use (which implies the modification of the albedo) (Pongratz et al., 2009) or the liberation to the atmosphere of large amounts of aerosols, which influence the cloud formation and has also an important effect in the global albedo. There are however other forcings modifying the equilibrium state of the climate which are not related to human activities. Natural fluctuation in the solar power discussed above is an example. Another important natural forcing are big volcano events, whose main effect is to increase the aerosols in the atmosphere (Robock, 2004). It is widely accepted that the overall effect of volcano events is a global cooling the years following the eruption, and this forcing may have played an important role in cold period such as the Dalton Minimum (a cold period around the year 1800) (Wagner and Zorita, 2005). At longer temporal scales, modifications of the orbital parameters of the Earth around the Sun, continental drift, or changes the atmospheric composition due to natural biochemical processes are other examples of natural forcings which have modified the climate of the Earth during the last million years.

In addition to these forcings, the equilibrium state we defined before is not static. Instead, even if the forcings are kept constant in time, the climate naturally fluctuates at interdecadal or even larger time scales. This random fluctuations, which have their base in the chaotic nature of the climatic system, are denominated natural variability (Huubers and Curry, 2006). This natural variations affect the climate evolution at different temporal scales, increasing or hampering the climate modifications due to modification in the forcings. Large circulation modes such as the North Atlantic Oscillation (NAO) (Hurrell and van Loon, 1997) or the El Niño Southern Oscillation (ENSO) (Neelin et al.,

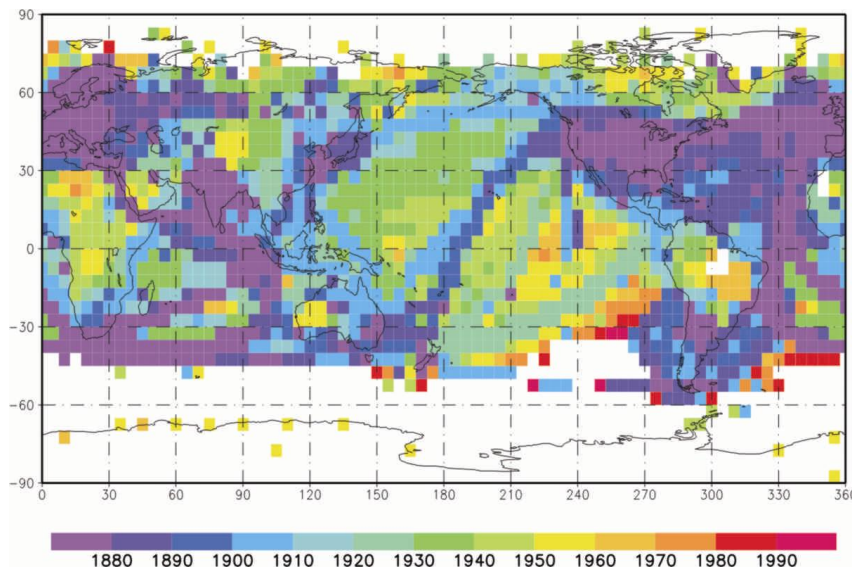


**Figure 1.3:** Scarcity of systematic observations of the state of the atmosphere. The colour represents the decade when systematic meteorological and climatological records began. Source: J.F González-Rouco, personal communication.

1998) are remarkable examples of the importance of internal variability at interannual time scales.

### 1.1.2 Palaeoclimatology and Climate Change Projections

As discussed above, the climate fluctuates due to the combination of forcings and the natural variability inherent to the climatic system. These variations during the last millennia have been the cause of migration and famine periods, and represent a challenge to modern civilizations (Büntgen et al., 2011). However, the human activities also represent a cause of climate forcing which is superimposed to the natural factors. In the last decades, a noticeable warming has been detected at a global scale (Luterbacher et al., 2004; Oreskes, 2004; Hegerl et al., 2011, among many others), which is accompanied by the increase of extreme events in some regions (Shanahan et al., 2009). Hence, the question that arises is whether the current warming is unprecedented, and to what extent it might be caused by anthropogenic causes.

Answering this question implies that we need to put the modern warming in a longer climatological context, where the human activities were of minor importance, and com-

pare the climate variability at centennial or millennial time scales. However, the systematic measure and documentation of the state of the atmosphere, began around the 19<sup>th</sup> century in few areas, as shown in Figure 1.3. In addition, although there is evidence of abrupt climate changes in the past (Alley et al., 2003), and the underlying mechanisms involved could play an important role in the future evolution of the climate, they are poorly understood. Thus, the analysis of the past climate is a valuable tool for understanding how climate evolves, what is the role of natural variability with respect to external forcings and how important the anthropogenic forcings are. It is also a good test bed for climate models, since their ability to reproduce the past evolution is a benchmark for their capabilities to project future climate changes (González-Rouco et al., 2009).

Climate change experiments are performed by means of climate models (further explained in the next section), and they are the most important tool to determine to what extent the climate change is anthropogenic, and what could be the future evolution of climate. There are however a number of problems to overcome before trying to project the evolution of the climate.<sup>5</sup> The first is the large number of uncertainties in the future evolution of external forcings. There are some of them which are just unpredictable with the current state of knowledge, such as the evolution of the solar power<sup>6</sup> or large volcanic events. There are other natural forcings which can be safely considered constant at the time scale the projection is designed for (typically 100 years), such as modification in the lithosphere (this is, the distribution of continents and oceans) or the orbital parameters of the Earth. The evolution of the Biosphere is another important factor which is affected by climate variations (indeed there are important feedbacks between both systems). However its evolution through the simulation is not considered in most simulations due to the many uncertainties in the complex mechanism that relate climate and life, and thus it is taken as constant. Finally, the anthropic forcings may determine critically the evolution of the climate. They include, but are not limited to, evolution in the concentration of GHGs, aerosols and modifications in land use (IPCC, 2007a). These factors are however affected by a huge uncertainty, since they depend on the future unpredictable socio-economical evolution of the current civilizations around

---

<sup>5</sup>An important problem is the uncertainties associated to the reliability of climate models, which is an important issue of climatology. However, assessing the uncertainties due to different model setup goes beyond the scope of the present study. The Thesis by Jerez (2011), developed in our group, deals with this topic.

<sup>6</sup>In the last centuries the Sun is showing a rather regular activity, following a 11-years cycle, but it was interrupted during the Maunder Minimum (Eddy, 1976) by unknown reasons. Since then, 24 of such cycles have been recorded, although the long-term future evolution of solar power remains unpredictable.

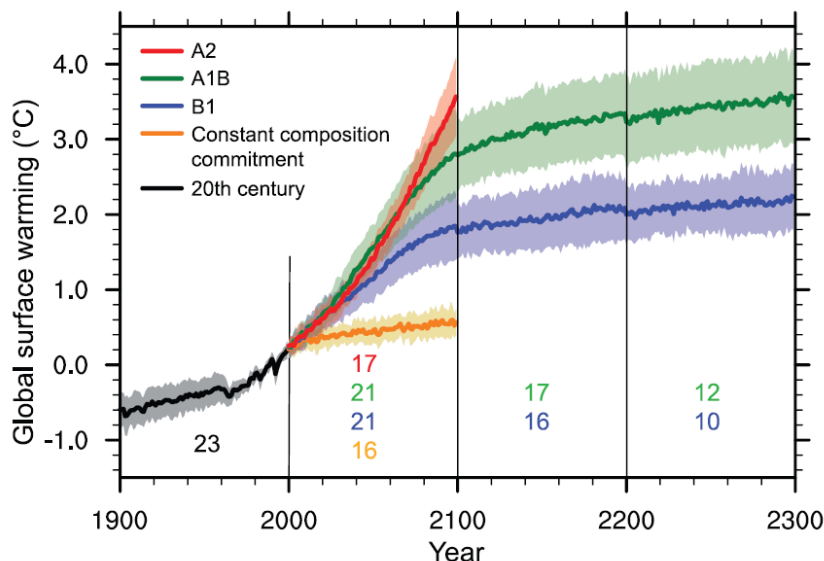


**Figure 1.4:** Ensemble mean series of several climate change projections of global surface temperature (relative to its mean value in 1980-1999) presented in the 4 th IPCC report. Black line denote observed temperature evolution during the last century, whereas grey shading is the uncertainty range. Red, green and blue colours denote the ensemble model mean temperature projected under the A2, A1B and B1 scenarios, respectively, which hypothesize different plausible evolution for the climate forcings during the next century. Orange line represents the evolution of simulated climate if the forcings would be kept constant to its value in the year 2000. The number in the figure is the ensemble size, which varies among scenarios, and the shading shows one standard deviation calculated among the model ensemble. Source: [IPCC \(2007a\)](#).

the globe. The only way to deal with such uncertainties is an statistical approach. A number of possible evolutions of the socio-economical factors, with their respective implications in the available technology, and thus in the future GHGs and aerosols emissions, are hypothesised. These hypothetic futures are denominated scenarios<sup>7</sup>. This input information is used to conduct simulations with several state-of-the-art Global Circulation Models<sup>8</sup> (GCM), and the results of this ensemble of simulations are considered in an statistical way (IPCC, 2007a). Figure 1.4 illustrates the result of this process by showing the ensemble mean series of global temperature as projected under several emission scenario.

## 1.2 Climate models and climate reconstructions

A deep knowledge on the long term past evolution of the climate is fundamental for understanding the climate processes and being able to project its future evolution. Palaeoclimatology provides the tools to gain insight about this question, which can be broadly classified in climate models and climate reconstructions. The formers try to numerically simulate a realistic climate by combining a large set of well established physical laws, and are a key point in climate science due to the impossibility to carry out controlled experiments in the real climate.<sup>9</sup> The latter tries to find out which was the evolution of the past climate, given the problem of the lack of direct measures in early periods, and are fundamental to put the current warming in a longer climatological context. This section introduces both methodologies.

### 1.2.1 Global circulation models

Numerical methods are used in many branches of Science. They normally deal with solving complex mathematical problems, such as finding the solution of a set of differential equations. A climate model is basically the result of merging many physical, chemical and sometimes even biological laws in a coupled system of partial differential equations which tries to reproduce the feedbacks between the elements of the climatic system (Trenberth, 2010). However, the resulting equations represent such a complex

---

<sup>7</sup>The uncertainties in the natural forcings are not considered in the scenarios. They ignore the unpredictable volcanic events and fix the solar power to the current value.

<sup>8</sup>Using many different models is a convenient way to assess the uncertainty in the models themselves.

<sup>9</sup>This is indeed a fundamental problem in climate science: you can not run a controlled experiment consisting in doubling the CO<sub>2</sub> content within the Earth's atmosphere and wait a hundred years taking careful measures just to test the anthropogenic warming hypothesis.

system that can not be solved analytically. A number of approximations has to be assumed in order to simplify the mathematical problem, and even in this case the use of computers to solve the resulting equations becomes mandatory.<sup>10</sup> However, the rising computational power has made possible the use of models of increasing complexity, which take into account explicitly a large number of the underlaying processes.

In a climate model, the general idea is discretizing the climatic system, getting a 3-dimensional grid covering the planet as illustrated in Figure 1.5, and to solve iteratively and numerically the temporal evolution of this system in discrete time steps given an initial condition, and taking into account the variations of external forcings. Depending on how strong the simplifications of the equations are, and on how many underlying processes are resolved explicitly by the model, there are several kind of models. There exist from simple Energy Balance Models (EBM) (North et al., 1981) to General Circulation Models, passing through Earth System Models of Intermediate Complexity (EMIC) (Knutti et al., 2002). This Thesis focuses on GCMs, which are those used for driving Regional Circulation Models (RCM), as further explained in the next section.

A GCM<sup>11</sup> consist in the coupling of several submodels, including at least a complete atmospheric model and an ocean model (Legutke and Voss, 1999; Jungclaus et al., 2006; Ammann et al., 2007; Jungclaus et al., 2010, among many others). Each of these models simulate the globe as a whole, and they are coupled in the sense that they run simultaneously and exchange energy, matter and momentum. The complexity of these models, as well as their spatial resolution has been growing in the last years IPCC (2007a). Current state-of-the-art include submodels to take into account the interaction between the atmosphere and the ice sheets, the chemistry in the atmosphere, carbon cycle, hydrological processes, etc. The atmospheric and oceanic components are subdivided also in a dynamical core and a set of parametrizations. The dynamical core solves numerically the fluid dynamic equations governing the large-scale circulation of the flow. However, this component is not able to simulate realistically subgrid-scale features which are fundamental in the atmospheric processes such as the cloud formation, local convective processes, interaction between the radiation and the air, formation of the Planetary Boundary Layer, etc. These processes have to be simulated including fur-

---

<sup>10</sup>The first successful numerical weather prediction was carried out in the famous computer ENIAC in 1950, and it was performed by a scientific team headed by John von Neumann. He was trying to find applications for this new computer, and the weather forecast met two essential conditions: it needs a heavy computation power, but it has also potential military applications (one has to take into account the historical context of the Cold War).

<sup>11</sup>Sometimes global models are referred as comprehensive Atmosphere-Ocean Global Circulation Model, AOGCM.

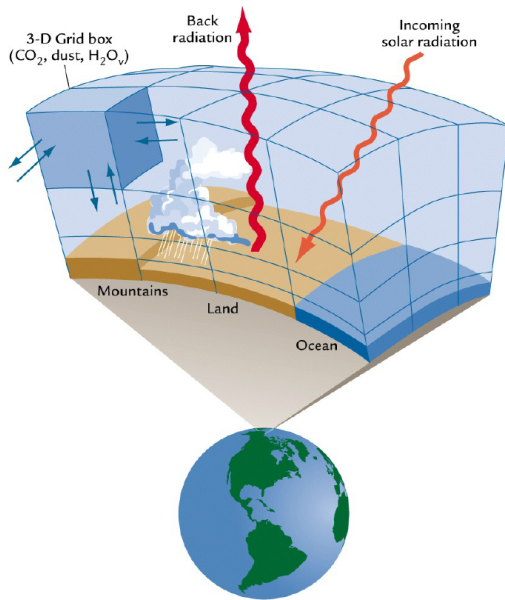


**Figure 1.5:** Ideal representation of the discretization process carried out in climate models. The space and time is mapped to a 3-dimensional mesh, and the equations governing different aspects of the climate are solved iteratively in each grid point during all the time steps needed to generate a simulation.

ther equations in form of semi-empirical or physical models, which are denominated generically parametrizations ([Stensrud, 2007](#)).

Due to the many submodels included in a GCM and the large number of grid points where these models have to be solved iteratively to cover the whole planet, they require a huge computational cost. However, since there is a compromise between the spatial resolution and the size of the time step for the numerical solution of the differential equations to converge ([Courant et al., 1967](#)), the solution to carry out these simulations can not be to increase the time step. Also, a realistic simulation of the many elements of the climatic system and their exchanges requires all these models to be run simultaneously. Thus, a common way to reduce the computational cost in these simulations is to use a relatively coarse spatial resolution. The consequence of this is that although their resolution has become finer with the increase of the computational power, most current models implement a spatial resolution around one hundred

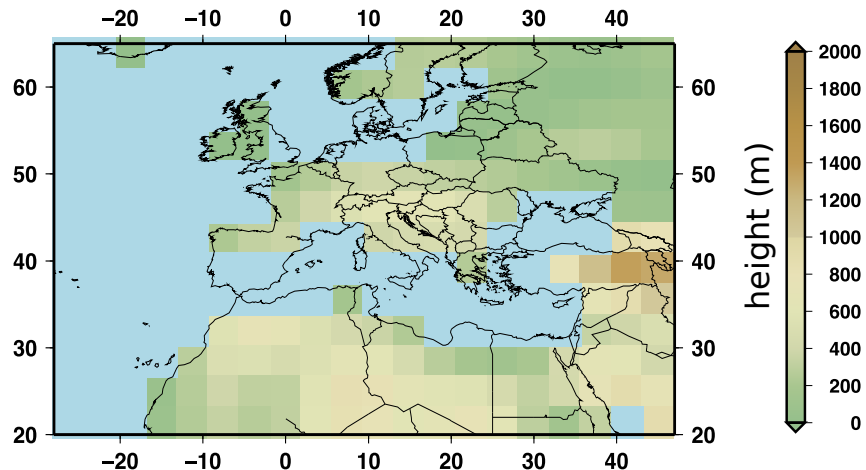


**Figure 1.6:** Typical spatial resolution of a GCM. In this case ECHO-G, which implements a spectral resolution T30 in the atmosphere. Figure represents the orography and ocean land mask in this model, which has been used to drive some of the regional simulations analyzed in this Thesis.

kilometers (see Figure 1.6, which shows the typical spatial resolution of a GCM over Europe). This resolution is enough to reproduce the large-scale features of the climate system, but precludes a correct representation of the local features of climate, which is determined by the interactions between the large-scale systems with the regional details. These details include a realistic orography, and the representation in the model of a better land use and vegetation cover, among others. Indeed many climatic variables depend on these local details.<sup>12</sup> In the palaeoclimate context this may be a problem because climate reconstructions are sometimes performed by means of several kind of indicators (further explained in the next section) which are affected by these local features, whereas palaeoclimate GCM experiments can not account for these details. This creates a gap between both approaches, making difficult the exercises of comparison, which are of great interest for the validation of models in a palaeoclimatic context as well as for testing the consistence of climate reconstructions. Thus, in order to bridge the gap between the large-scale simulated by GCMs and the local scale affecting climate records, downscaling techniques have to be applied to the GCM outputs.

<sup>12</sup>For example precipitation regimes vary in different sides of a mountain, although they are close to each other. However, the coarse resolution of many GCMs does not allow them to resolve the local circulation responsible for this asymmetric behaviour.

### 1.2.2 Regional climate models

There is a number of techniques to deal with the scale gap between the large-scale circulation, reasonably well reproduced by GCMs, and the regional climate produced by the details of the orographic features (Hewitson and Crane, 1996). These techniques are not used only in palaeoclimatology, but they are general-purpose tools used in climate change projections or weather forecast among other applications. There are broadly two main families of techniques: statistical and dynamical downscaling. The former uses statistical models to relate the large-scale circulation with the evolution of variables at local scale (Wilby et al., 1998; Zorita and von Storch, 1999; González-Rouco et al., 2000a; Xoplaki et al., 2004). These statistical models needs to be calibrated in a control period, after which then they can be used to predict the local variables using the large scale field as a predictor. Statistical techniques have the important advantage of being cheap computationally. However, their main drawback is that they assume that the relations established between predictand and predictor in the calibration period hold on for past or future periods of time. The other main tool to downscale the GCM fields is the dynamical downscaling. It consists of solving explicitly similar equations to those of a GCM (this is, they simulate the climate just as GCM do), but focusing in a limited area domain. The focus on a local area reduces the computational cost, thus allowing to increase the spatial resolution. This technique is widely known as Regional Climate Models (RCMs) (Giorgi et al., 1994, 2004a; Gómez-Navarro et al., 2010; Jerez et al., 2010; Gómez-Navarro et al., 2011a, among many others).

The main difference between regional and global models is that the former have boundaries. A GCM only needs an initial condition and the evolution of the forcings as input data, and it is able to develop a physically self-consistent pseudo climate responding to these forcings. However, a regional model does not only need the initial condition and the forcings, but the boundary conditions through the limits of its integration domain. Thus, RCM simulations have to be driven by a GCM simulations (in this sense, statistical and dynamical downscaling have the same limitation). Other than that, RCMs are very similar to GCMs. They have a dynamical core together with a set of parametrizations to simulate most of the important aspects of the atmosphere, as well as a number of submodels to characterise the land soil, the ocean<sup>13</sup> or the ice cover.

This Thesis analyses a number of simulations for the past and the future of the

---

<sup>13</sup>Most studies performed with RCMs so far, including this Thesis, do not simulate regionally the ocean. Instead, the information over the ocean such as temperature, sea ice, etc. is directly taken from the GCM simulation and spatially interpolated to the RCM grid. However, recent developments include the resolution of a regional ocean model vg. Xie et al. (2007).

climate of the IP and Europe performed with only one RCM, a climate version of the mesoscale MM5 (Grell et al., 1994a; Chen and Dudhia, 2001a,b; Fernández et al., 2007; Jerez et al., 2010), driven by several GCMs. The details of this model, its configuration and how it was driven, are further detailed along this Thesis.

### 1.2.3 Reconstructions of past climate

A deep knowledge of the past evolution of the climate system is fundamental to put the short instrumental period (see Figure 1.3) in a longer climatic context. However, since the systematic observation of the climate system only began recently (in climatic and geological time scales) a number of techniques have been developed to get insight of the possible climate evolution during the past. These techniques can be broadly classified into documentary evidence of human activities and natural proxies.

Documentary evidence consists of the study of historical documentation which may contain useful information about climatic events. It covers ecclesiastic ceremonies, urban annals, city and religious chronicles, brief reports of events, private correspondence, books of acts of church and city archives, medical studies, early newspapers, etc. (Brázil et al., 2005; Barriendos and Rodrigo, 2006; Rodrigo et al., 2011). Another important source of documents are navigation logs. For example Leijonhufvud et al. (2010) used the start of the sailing season in Stockholm (only possible once the Baltic sea is defrosted) to obtain a spring temperature reconstruction for the Baltic sea area. In general terms, the historical documentation tracks the evolution of variables which are closely linked to the human activities, remarkably temperature and precipitation. Although in some cases the documents contain objective measures with early scientific instruments, most documentation focuses on the occurrence of extreme events, such as large droughts or floodings. It is important to note that these events were extreme in the context of the living experience and the climatic mean state of the epoch in which the humans which left the writing documents live, so this information has a huge amount of subjectivity that the researcher has to try to isolate from the climate signal. Another limitation of this approach is that due to the very nature of these documents, historical climatology is limited to reconstruct the last centuries of the human history, and only in the areas where there are available written documents.

Natural proxies include a number of methodologies, some of which are briefly summarized here. An important source of climatic evidence is the growing rate on tree rings, known as dendroclimatology (Fritts, 1976; Briffa et al., 2004; Büntgen et al., 2011). The yearly growth of trees is influenced by several climatic factors. In some areas the limiting factor for this growth is the available water, whereas in others are mild

temperatures. Depending on the species and the location, the width, density and other parameters of the rings can be related with the evolution of several climatic variables. Samples of wood can be obtained without damaging the tree using manual devices as shown in Figure 1.7. These samples are analyzed trying to find a common climatic signal in the ring growth of many trees, and it has to be calibrated during an instrumental period (Dorado-Liñán et al., 2011). These samples record the growth of the tree during several years in the past, depending on its age. The older the tree, the farther back in time the record goes, and an advantage of this tool is that gives annual resolution. In addition to the sampling of living trees, the sampling of wood employed in early construction sites, churches, ships, etc. can be used to go further back in time. Joining the series from different living trees and dead wood, one can track the evolution of climate up to several thousands of years in the past with yearly resolution.



**Figure 1.7:** The drilling device used to extract wood samples is manual, and does not damage significantly the living tree. The samples are analyzed using X rays to measure the ring growth properties with great precision.

Ice cores are an extremely useful tool in palaeoclimatology (Legrand and Mayewski, 1997; Thompson et al., 2000). Small air bubbles are trapped within the snow in ice caps of Antarctica and Greenland. Every year a new layer of snow is naturally added, whereas older ones get buried up to hundred of meters with the pass of centuries (see Figure 1.8). As in the case of tree rings, the layers can be tracked back in the record with annual precision, and the deeper the layer, the older the sample. The chemical composition of the air bubbles contains valuable information about the past state of the atmosphere. GHG concentrations can be tracked with great precision. Big volcano events leave also a fingerprint in these records in form of ash and chemical compounds.

Some physical properties of water, such as the evaporation rate, depend on the isotopes composing the molecule. Thus, anomalies in the concentration of O<sup>18</sup> can be used to infer changes in temperature from the isotopic composition of water in the ice cores. Be<sup>10</sup> concentration can be used as a proxy for cosmic radiation, and thus solar activity, etc. The limitation of ice cores is its scarceness, especially during warm periods and near our target region, the IP.



**Figure 1.8:** Every year a new layer of snow is added in the ice caps in Antarctica, Greenland and glaciers around the globe. These layers can be tracked in ice core samples and used to date the samples back in time. The chemical composition of each layer is a valuable proxy of the climatic conditions in the past.

Other proxy indicators include the inversion of temperature profiles in boreholes (Beltrami, 2002), pollen records from continental and marine records as a proxy of vegetation cover, lacustrine sediments, isotopic composition of fossils of small marine animals, or the yearly growth rate of coral and shells, among others. All these indicators contain information on different aspects of the evolution of the climate, and it is the combination<sup>14</sup>, and specially the cross-validation of all of them simultaneously, what gives confidence about our capacity to reconstruct a plausible evolution of the climate.

Summarizing the information from the available climate reconstructions, the general picture is an extreme cold/arid period in the IP around 20 kyr ago known as the Last Glacial Maximum (LGM) with the sea level in a minimum of 130 m below the current level, 6 °C cooler and a maximum extension of the continental ice caps. However, approximately 11 kyr ago began the current interglacial, known as Holocene (Walker

<sup>14</sup>Often, many different types of proxy indicators are merged to get a single consistent reconstructions. This is the so-called multiproxy approach (Luterbacher et al., 2004).

et al., 2009), with a rapid warming and an increase in humidity. The maximum temperatures were reached in its initial phase, and since then they have been slowly decreasing until the beginning of the industrial period. Focusing in the evidence found for the last millennium in the Northern Hemisphere<sup>15</sup>, a large part of our knowledge (and also the estimations of the uncertainties) can be summarized as in Figure 1.9. The general picture is a relatively warm period extended until the first centuries of the millennium, the so-called Medieval Warm Anomaly (550-1300) (Bradley et al., 2003), followed by a cold period during roughly 1300-1850 denominated the Little Ice Age. This cold period includes some especially cold decades, such as the Late Maunder Minimum around 1700 (Eddy, 1976), a period characterised by extremely low solar power, or the Dalton Minimum around 1815, marked by an anomalous increase in the volcanic activity<sup>16</sup> (Wagner and Zorita, 2005). GHG concentrations hardly changed during the last millennium until the beginning of the industrial period. This increase has been accompanied by the parallel increase of the global temperatures, and indeed great part of the observed warming is attributable to this cause (Hegerl et al., 2011).

### 1.3 The target regions

This Thesis analyses the results of a number of climate simulations performed with a RCM over two regional domains: the Iberian Peninsula and Europe.

#### 1.3.1 The Iberian Peninsula

Most of the simulations presented in this Thesis are performed over the IP. Besides the personal reasons to chose this area in particular, it is an interesting area of study due to its high climate heterogeneity, in which the dynamical downscaling shows a great potential.

The IP is located in the transition area between the tropical and extra-tropical latitudes (see Figure 1.10). It presents sharp spatial contrasts of mean temperature and precipitation due to its complex topography and to its location at the southern fringe of the North Atlantic storm tracks (Font-Tullot, 2000). Additionally, due to the spatial gradient of the oceanic influence and the complex orography, the climate of the IP shows strong spatial gradients from the coast to the interior. Its climate varies from the

---

<sup>15</sup>Due to historical reasons, the number of available proxy records so far is considerably larger in this hemisphere.

<sup>16</sup>In 1815 the eruption of the Tambora volcano in Indonesia took place, one of the largest volcanic events in the record.

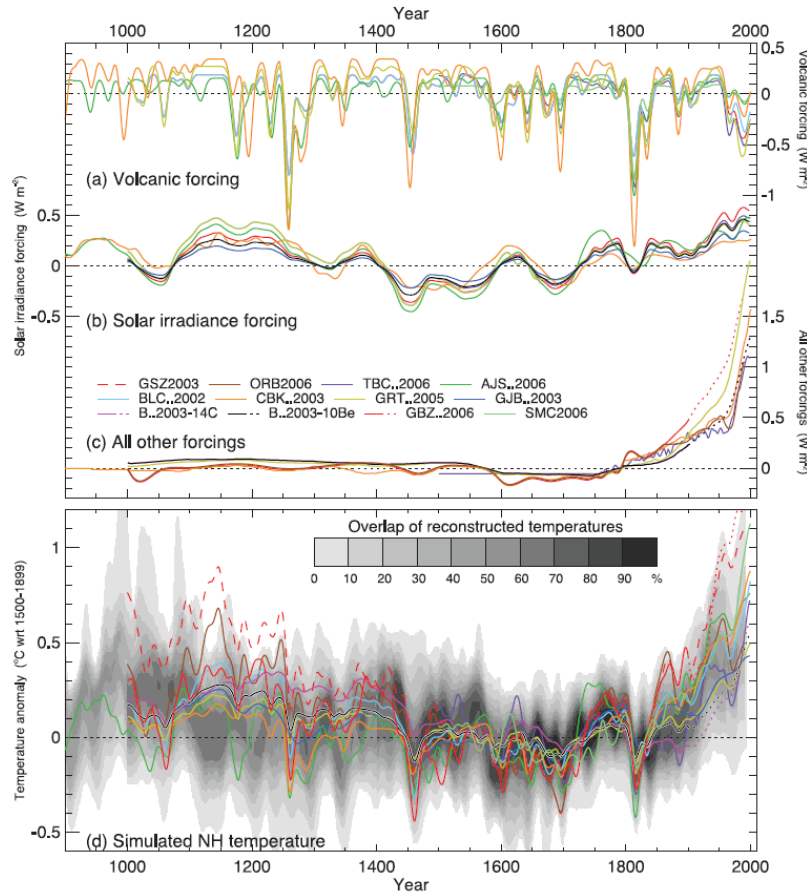


**Figure 1.9:** Reconstructions of several forcings and North Hemisphere temperature included in the 4th Assessment Report of the IPCC. Black shading denotes the uncertainty range estimated for the reconstructions. Source: (IPCC, 2007a).

Mediterranean semi-arid climate in the interior and the East, characterised by warm and dry summers with convective predominant precipitation and cold and humid winters with large-scale induced precipitation, to milder and wetter summers toward the north and west, mainly connected to large-scale synoptic systems including the North Atlantic Oscillation (Serrano et al., 1999; Font-Tullot, 2000; González-Rouco et al., 2000b). This complex climatic features hampers the climatic simulation of this region. Figure 1.6 illustrates how the coarse spatial resolution of a typical GCM is not able to catch the

orographic details, and how a RCM (see Figure 1.10) is a valuable tool for improving the climate simulations over this kind of areas.

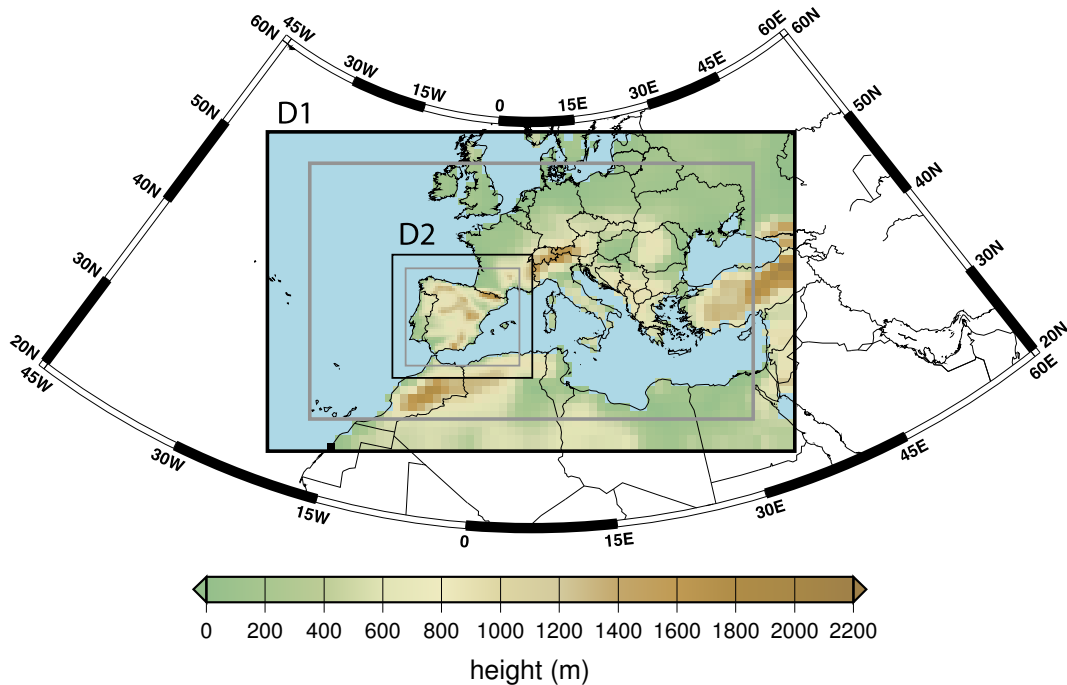


**Figure 1.10:** The 2 two-way nested domains of 90 and 30 km respectively, used to perform the regional simulations focusing on the IP.

Besides the challenge that implies this complexity, there are other motivations to downscale palaeoclimate and climate change simulations over this area. The IP, as part of the Mediterranean basin, has been identified as one of the most sensitive areas to the consequences of the climate change (Giorgi, 2006). In addition an hydrological deficit in a large part of the IP exists, as well as a known fragility of Mediterranean ecosystems and the societal dependence on water, which makes the IP particularly sensitive to rapid climate changes. However, impact studies of climate change demand high resolution projections capable to simulate realistically the sharp climatic contrasts of the IP discussed above. On the other hand, this area also has a great potential for exercises comparing reconstructions with palaeosimulations. There is abundant documentary evidence as well proxy indications over the IP (the CLIVAR report (Cacho et al., 2010) offers an intensive review on the information available and the state of the knowledge).

However, to date there are no long palaeoclimate simulations performed with regional models, which precludes the cross-validation of the reconstructions with models, and indeed this lack of simulations is pointed out in the referred report. The simulations analyzed in this Thesis contribute to fill this gap.

### 1.3.2 Europe

Chapter 5 analyzes a simulation encompassing Europe with two domains, the inner covering Europe with a spatial resolution of 45 km (see Figure 1.11). This area also poses great interest due to the even larger amount of reconstructions which have been developed in the last years (Luterbacher et al., 2004; Leijonhufvud et al., 2010; Büntgen et al., 2011, among others). However, although it has been extensively analyzed in the context of large project dealing with climate change projections such as PRUDENCE (Déqué et al., 2005) or ENSEMBLES (van der Linden P and J.F.B. Mitchell (eds.), 2009), less attention has been paid to palaeosimulations.

## 1.4 Objectives and structure of this Thesis

In the former sections, the need for a deep knowledge of the past evolution of the climate has been exposed. It has been discussed how climate models can be used to simulate the climate, and how they help understanding their different components and their interactions. Models can also be used to project the possible evolution of the climate under several hypothesis of evolution of the socio-economical factors. RCMs in particular have been introduced as a valuable tool to deal with the problem of the coarse spatial resolution of the state-of-the-art GCMs. However the skill of climate models needs first to be evaluated against observations, and the role of internal variability versus external forcings assessed. Thus, the objectives of this Thesis are various.

The first objective relies on creating a large database of high-resolution regional climate simulations for the IP and Europe. Simulations cover the palaeoclimatic period 1000-1990 under two different initial conditions, and they are later on continued until 2100 under several climate change scenarios. Hence, this database contains transient runs of several hundreds of years without gaps, which has no precedent in RCM literature. This huge database can be potentially used for several kind of researchers, from impact studies to climate reconstructions. Indeed, it is already being employed, as indicated through this Thesis.

However, before third-part researchers use this data for their needs, it must be validated. The comparison between the model simulations and observations, in order to

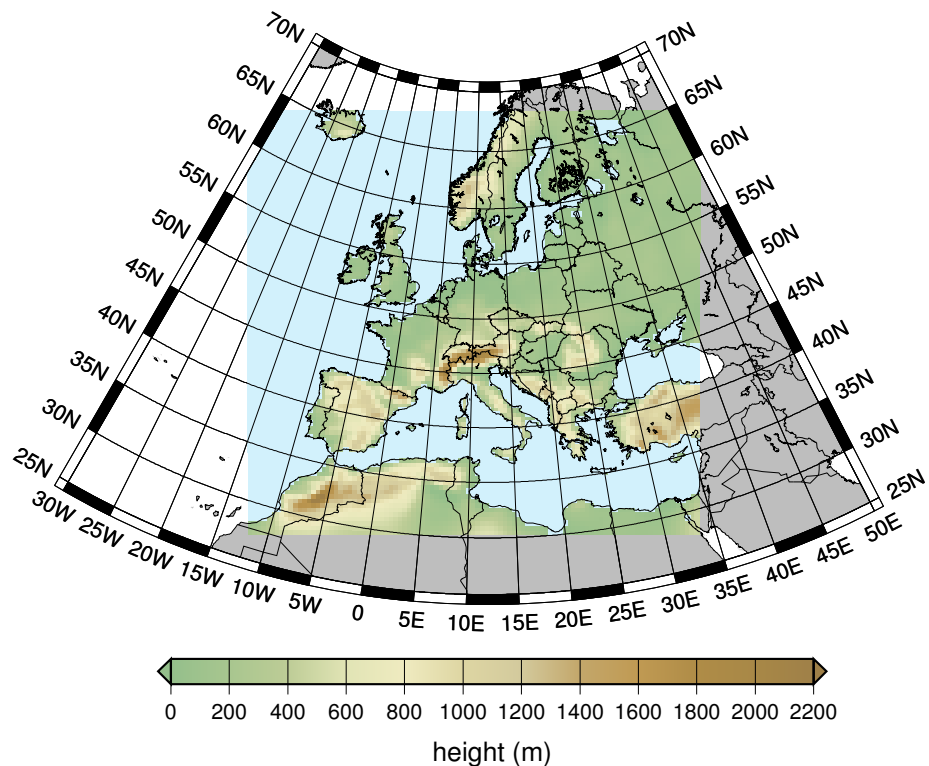


**Figure 1.11:** Regional domain used to perform the regional simulations focusing over Europe. The simulation was performed using 2 two-way nested domains of 135 and 45 km, respectively. However the analysis focuses on the inner higher resolution domain (shown here).

assess the model skill, is thus an important objective of this Thesis. This validation procedure must not only focus on the capability of the model to mimic mean values of temperature and precipitation, but it has to consider variability of temporal series, correct representation of main variability modes of several variables, and a realistic simulation

of the links between large-scale fields and orographic-induced features of regional climates, among others. On the other hand, given the great computational cost involved in generating this database, it is also important to state to what extent the high-resolution details introduced by the regional model improve significantly the results obtained with global state-of-the-art models. It is also important to identify whether there are some variables whose performance is not significantly improved by the RCM, since this would imply that GCM models might be also very useful in impact studies or comparison with reconstructions, without having to expend large computational resources in dynamical downscaling.

Another objective of this Thesis is to use the generated simulations to study the climatic evolution of the IP and Europe during the last centuries. In this sense, there is a strong evidence of cold periods in the last millennium, in particular within the period known as Little Ice Age (LIA). They are interesting because they represent evidence of strong climate changes in the recent past, and by studying them, researchers can gain insight in the nature of the current climate change. In particular, it is thought that these anomalous periods were partly driven by variations in the external forcings. However, the long-term climate variability is not easy to assess by studying the relatively short instrumental records. Analysing climate simulations allows to study the long-term evolution of climate and to test some plausible physical mechanisms behind these key periods.

Climate simulations of the past millennium allow the comparison exercise between the generated database with reconstructions of the climate. These comparison exercises are a great tool to identify errors or inconsistencies in climate reconstructions, but also represent a great testbed to benchmark the skill of climate models. Validation of climate models in long time periods is a key point of nowadays climatology, since climate models are used to perform climate change projections of several decades in advance, while they are only validated for shorter time periods during the instrumental period. On the other hand, climate simulations offer the concept of pseudoreality. Although they are simplifications of nature, climate models are built using well established physical laws, which ensures their self-consistency. Thus, the simulated climate is a simplified version of the actual one, but it is physically self-consistent. This allows to represent realistically some aspect of climate interactions, which can be used to test, in the simplified but controllable world of the simulation, some aspect of the methodologies used in climate reconstructions. Hence, another important objective of this Thesis is to use available reconstructions of climate in the target areas to compare them with climate simulations, as well as using the model to test key aspects of such reconstructions.

Climate variability is the combination of several external and internal factors super-

imposed to an undetermined level of natural variability. This variability is unpredictable by its own nature, and acts reinforcing or ameliorating the effect of the external forcings. Any climate simulation is affected by this noise level, which hampers the detection of an actual signal of climate change. The influence of natural variability is in general greater at regional scales, since spatial averaging filters out its effects. Hence, assessing the role of natural variability in regional climate simulations and its relative weight in the evolution of climate is another of the objectives of this Thesis.

Finally, an important objective of this Thesis is to analyse the warming patterns projected in regional climate simulations carried out under several emission scenario and driven by two different GCMs. In particular, our objective is to look for consistence of climate change patterns through the identification of major uncertainties in the ensemble generated. Our interest is to study the main characteristics of projected warming, such as its annual evolution, or the trends associated to maximum and minimum temperatures separately, which allow to assess in detail the changes expected in the climate of the IP.

The structure of this Thesis is as follows. Chapter 1 introduces the Thesis and justifies the methodologies employed. Chapter 2 describes and analyzes a paleosimulation for the IP comparing their results with several climate reconstructions. Chapter 3 deals with the problem of the internal variability, and characterizes its role in regional paleosimulations. Chapter 4 discusses several regional climate change projections for the IP, studying their uncertainties and common features. Chapter 5 testes a regional paleosimulation for Europe, assessing the skill of the model and comparing their results with a number of climate reconstructions. Chapter 6 illustrates some applications of the simulations carried out for the realization of this Thesis in the form of collaborations works with different researchers. Finally, Chapter 7 outlines the main conclusions obtained in this Thesis. All chapters include a short introduction and a methodology part which further describes their content.

# Chapter 2

## A regional climate simulation over the Iberian Peninsula for the last millennium

A high-resolution (30 km) regional paleoclimate simulation of the last millennium over the Iberian Peninsula (IP) is presented. The simulation was performed with a climate version of the mesoscale model MM5 driven by the global model ECHO-G. Both models were driven by the same reconstructions of several external forcing factors. The high spatial resolution of the regional model allows to realistically simulate many aspects of the climate in the IP, as compared to an observational data set in the reference period 1961-1990. Although the spatial-averaged values developed by the regional model are tightly driven by the boundary conditions, it is capable to develop a different realisation of the past climate at regional scales, specially in the high-frequency domain and for precipitation. This has to be considered when comparing the results of climate simulations versus proxy reconstructions. A preliminary comparison of the simulation results with reconstructions of temperature and precipitation over the IP shows good agreement in the warming trends in the last century of the simulation, although there are large disagreements in key periods such as the precipitation anomalies in the Maunder Minimum.

### 2.1 Introduction

In the last years considerable efforts have been devoted to the understanding of the internal variability and its role in the evolution of the climate in the last millennia (Bradley and Jones, 1993; Jones et al., 2001; Zorita et al., 2005; Mann et al., 2008;

Swingedouw et al., 2010, among others). This has allowed to frame the short instrumental period in a broader climatic context, and to understand some of the physical mechanisms responsible for the observed variability.

These efforts belong to two categories: climate reconstructions based on proxy indicators and climate model simulations. The former uses information from various indirect sources, including documentary records, tree rings, ice cores, etc. These sources provide information at various temporal resolutions about the past evolution of temperature and precipitation, among other variables (Bradley and Jones, 1993; Jones et al., 2001; Luterbacher et al., 2004; Mann et al., 2008). On the other hand, the use of comprehensive atmosphere ocean global circulation models (AOGCM) has become possible due to the impressive increase in computational power. This has allowed to perform simulations with state-of-the art global climate models over periods of several centuries (Zorita et al., 2005; Tett et al., 2007; Ammann et al., 2007; Swingedouw et al., 2010). Although the validation of these comprehensive models used for future climate projections can be performed by checking whether they are able to reproduce the main features of the actual climate, the reliability of climate models to realistically simulate climate changes is much more difficult to assess. The comparison of simulations of past climates with climate models with proxy-based climate reconstructions may thus increase the confidence put on future projections or identify drawbacks that should be corrected, thus improving the climate projections as well (González-Rouco et al., 2009).

However this comparison is burdened by two important factors. On the one hand climate reconstructions are based on data that is usually local or regional, whereas the present AOGCMs have a too coarse spatial resolution that precludes a realistic representation of the local features, which may strongly influence proxy records. This may cause important mismatches between simulations and reconstructions. For this reason, some of the comparison between model simulations and climate reconstructions over the past millennium performed so far have been limited to global or hemispheric scales (Jones et al., 2009). Several authors have also used a number of methodologies trying to overcome this problem. Stevens et al. (2008) grouped borehole temperature profiles into regional ensembles, to match the spatial resolution of the global AOGCM ECHO-G, of about  $3.75^{\circ}$ . These authors have, however, underlined the need for finer spatial resolution simulations. On the other hand the climate system fluctuates internally over a large frequency range (Huybers and Curry, 2006). Climate models are also affected by this natural variability, and hence one should not expect a complete agreement at interannual timescales when comparing the temporal evolution of model simulations and reconstructions, even if both are perfect (Yoshimori et al., 2005).

Regarding the spatial scale gap between model and reconstructions, downscaling

techniques are a common tool in meteorological and climate studies to address this problem. Driven by a AOGCM simulation, these techniques allow to take into account the effect of regional features, thus developing a more realistic climate for a limited area. In particular, dynamical downscaling methods, involving the use of Regional Climate Models (RCM), solve similar equations as a AOGCM does, but using higher resolution for a limited area domain. The higher spatial resolution, which implements a more realistic orography, allow them to simulate some features of regional climates, like synoptic scale disturbances, more accurately than current AOGCMs, and for this reason RCMs are extensively employed in climate change projections within the context of large projects such as PRUDENCE or ENSEMBLES (Déqué et al., 2007; van der Linden P. and J.F.B. Mitchell (eds.), 2009, and references herein). Nevertheless, to date there are few studies where these models have been used for paleoclimate applications (Graham et al., 2009; Zorita et al., 2010), or only cover short periods of time farther back in the past (Hostetler et al., 2000; Renssen et al., 2001; Kjellström et al., 2010; Strandberg et al., 2011).

In this study, we present the first results of a simulation performed with the regional model MM5 driven by the global model ECHO-G over the last millennium (1001-1990) for a domain encompassing the Iberian Peninsula (IP). This area presents sharp spatial contrasts of mean temperature and precipitation due to its complex topography and to its location at the southern fringe of the North Atlantic storm tracks (Font-Tullot, 2000). Hence it provides a good test bed to examine the skill of regional models in a paleoclimate context. For example, the precipitation in south-western part and the northern fringes of the IP is strongly influenced by the North Atlantic Oscillation, whereas precipitation along the Mediterranean coasts is much more weakly connected to the North Atlantic weather systems.

Although new climate reconstructions over diverse periods within the last millennium in the IP are being developed at this moment, to date there are only few available to compare against the simulations. In this study we focus on the gridded reconstructions of monthly, or seasonal, temperature and precipitation for the Western European region (Luterbacher et al., 2004; Pauling et al., 2006).

The paper is organised as follows: In Sect. 2 we describe the experiment set up of the AOGCM and the RCM, as well as the proxy reconstructions used for comparison with the simulations. We also describe some of the analysis tools employed in the paper. In Sect. 3 we evaluate the added value provided by MM5 to the climatology produced by ECHO-G for a reference period. For this purpose we use a simulation driven by meteorological reanalysis. In Sect. 4 we summarise the main features of the whole simulation, focusing on the differences between both models, and also compare the

simulation with several proxy-based reconstructions for the area of study. Discussions and conclusions are given in Sect. 5.

## 2.2 Description of simulations, data employed and methodology

For this study we have performed two simulations using different sets of driving conditions for a climate version of the regional model MM5. The first experiment (hereafter referred to as ERA40+MM5) is driven by ERA40 reanalysis (Uppala et al., 2005) for the period 1961-1990. Jerez et al. (2010) have already shown that this simulation is capable of reproducing realistically the main features of the climate in the IP, in particular considering temperature. The second experiment (hereafter referred to as ECHO-G+MM5) has been driven by the global model ECHO-G, and covers the last millennium almost entirely (1001-1990). We use the climate simulated in the first experiment, together with an observational data base, to benchmark the skill of the regional model to reproduce the present climate when it is driven by ECHO-G.

The ECHO-G global model driving the long RCM paleosimulation consists of the spectral atmospheric model ECHAM4 coupled to the ocean model HOPE-G (Legutke and Voss, 1999). The model ECHAM4 was used with a horizontal resolution T30 ( $\sim 3.75^\circ \times 3.75^\circ$ ) and 19 vertical levels. The horizontal resolution of the ocean model is approximately  $2.8^\circ \times 2.8^\circ$ , with a grid refinement in the tropical regions and 20 vertical levels. A flux adjustment constant in time and with zero spatial average was applied to avoid climate drift. This adjustment is an integral part of the coupled atmosphere ocean model ECHO-G, and is an ad-hoc solution to avoid the unavoidable long-term climate drift that occurs when coupling two models with imperfect representation of surface fluxes. The model ECHO-G is included in the model suite of the Fourth Assessment Report of the Intergovernmental Panel on Climate Change. Although it has a relatively low-resolution atmosphere compared to the resolution of other IPCC models like ECHAM5-OM ( $1.87^\circ \times 1.87^\circ$ ) or HadCM3 ( $2.75^\circ \times 3.75^\circ$ ), assessments of the quality of the IPCC models measured by their skill to simulate the present observed climatology rank ECHO-G among the best IPCC models. Specifically, for the extratropical Northern Hemisphere atmospheric circulation, the study by Gleckler et al. (2008) places ECHO-G as the third best model. In terms of simulated precipitation ECHO-G ranks as the seventh model, despite its coarser resolution.

The GCM simulation was driven by estimations of three independent sources of external forcings: greenhouse gases (GHGs) concentrations in the atmosphere, total solar irradiance (TSI) and an estimation of the global mean radiative forcing of stratospheric volcanic aerosols. The latter two effects are included through the introduction

of variations in an effective solar constant. Finally, it is important to note that although variations in land-use may have a strong impact in climate evolution, as clearly illustrated by Kleidon et al. (2000), this factor has not been included in the simulations. Land-use categories have been fixed to the present values, since to the author's knowledge there are not available reconstructions of this parameter for the last millennium over the Iberian Peninsula. Here we discuss briefly some general aspects of these forcings; for a full description of this simulation and their external forcings the reader is referred to González-Rouco et al. (2003); Zorita et al. (2005) and references therein.

The evolution of the considered forcings is depicted in Figure 2.1. The orange line represents the reconstruction employed for the variations of the TSI. Black lines show the estimated reduction in solar irradiance at the top of the atmosphere caused by volcanic eruptions. The sum of both lines is the effective solar constant that is implemented in the model to take into account both sources of external forcing. There is a series of maxima and minima in the TSI among which three minima around the years 1440, 1700 and 1810 stand out. These minima, which are remarked by grey bars in the figure, drive three respective minima in the near surface-air temperature (SAT) over the IP (see Figure 2.11). These minima match known cold periods in the past, as further explained below. Finally, green, blue and grey lines represent the evolution of nitrous oxide, carbon dioxide and methane, respectively. GHGs concentrations show a relatively constant value until 1850, roughly when the industrial period begins. Since then, all GHGs concentrations increase globally until the end of the simulated period in 1990. Both models, AOGCM and RCM, have been driven by identical external forcings to avoid physical inconsistencies.

The TSI reconstruction used in these simulations is described in (Crowley, 2000), and is based on ice core measurements of  $^{10}\text{Be}$ , residual  $^{14}\text{C}$  from tree ring records and an estimate of  $^{14}\text{C}$  from  $^{10}\text{Be}$  fluctuations. The series includes information from solar spots observations from roughly 1700 onwards, which explains the high-frequency variability of the series in the last centuries. However, a more recent reconstruction of this variable, e.g. (Krivova et al., JGR submitted) depicts a much smaller amplitude of the variance. In particular, these authors estimate a difference in total solar irradiance between the Late Maunder Minimum (a cold period around 1700) and late 20th century of  $1.25 \text{ W/m}^2$  (about 0.09%), meanwhile the past solar irradiance used in this simulation changes by 0.3%. These authors indicate a much stronger change in the ultraviolet spectral band, with an increase of about 50% since the Late Maunder Minimum. More recent simulations with the model ECHAM5-OM, which were driven by the reconstruction of TSI (i.e. without spectrally resolved changes) (Jungclaus et al., 2010) barely display a period of global lower temperatures similar to the Little Ice Age (LIA), distinct

from the background internal variability. This apparent contradiction might be due to different reasons: the LIA might not have been a global phenomenon, the sensitivity of the real climate to changes in solar irradiance is higher than the model sensitivity, global temperatures are more strongly affected by variations in the ultraviolet band, or the Krivova et al. model to reconstruct total solar irradiance is not correct. At this stage, it is difficult to highlight one of these explanations as correct. At any rate, assuming that present climate models are broadly correct, a low-amplitude reconstruction of past solar irradiance and the existence of an externally-forced global-scale LIA does not seem to be compatible at this moment. However it must be taken into account that this conclusion is limited due to the small number of simulations available to date.

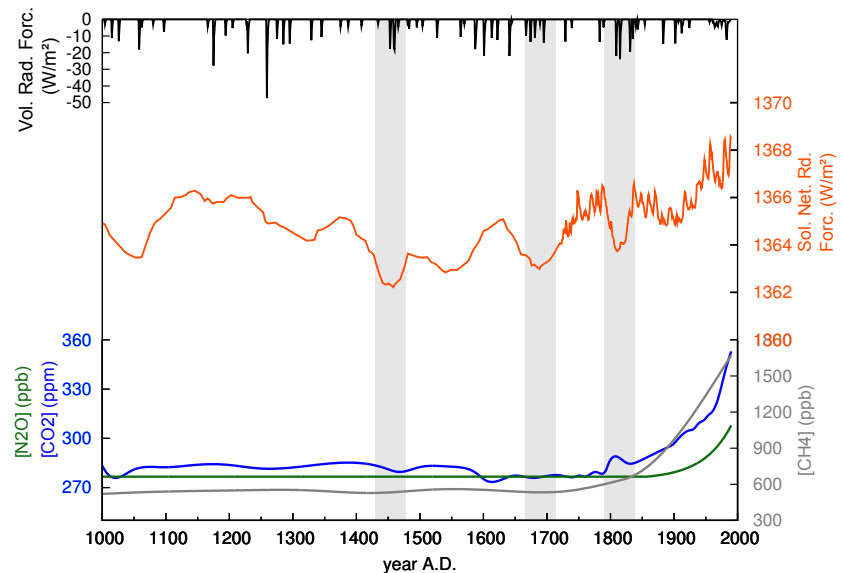


**Figure 2.1:** Reconstruction of the forcings for the last millennium employed in the simulations (Crowley, 2000). Orange line is the reconstruction of the total solar irradiance. Black line shows the estimated reduction in the effective short wave radiative balance in the top of the atmosphere due to big volcano events. Blue, green and grey lines show the evolution in the concentration of CO<sub>2</sub>, NO<sub>2</sub> and CH<sub>4</sub>, respectively. Grey bars indicate three important periods further discussed in the sections below.

The regional climate model used for the present study is a climate version of the Fifth-generation Pennsylvania-State University-National Center for Atmospheric Research Mesoscale Model (Dudhia, 1993; Grell et al., 1994a; Montávez et al., 2006; Gómez-

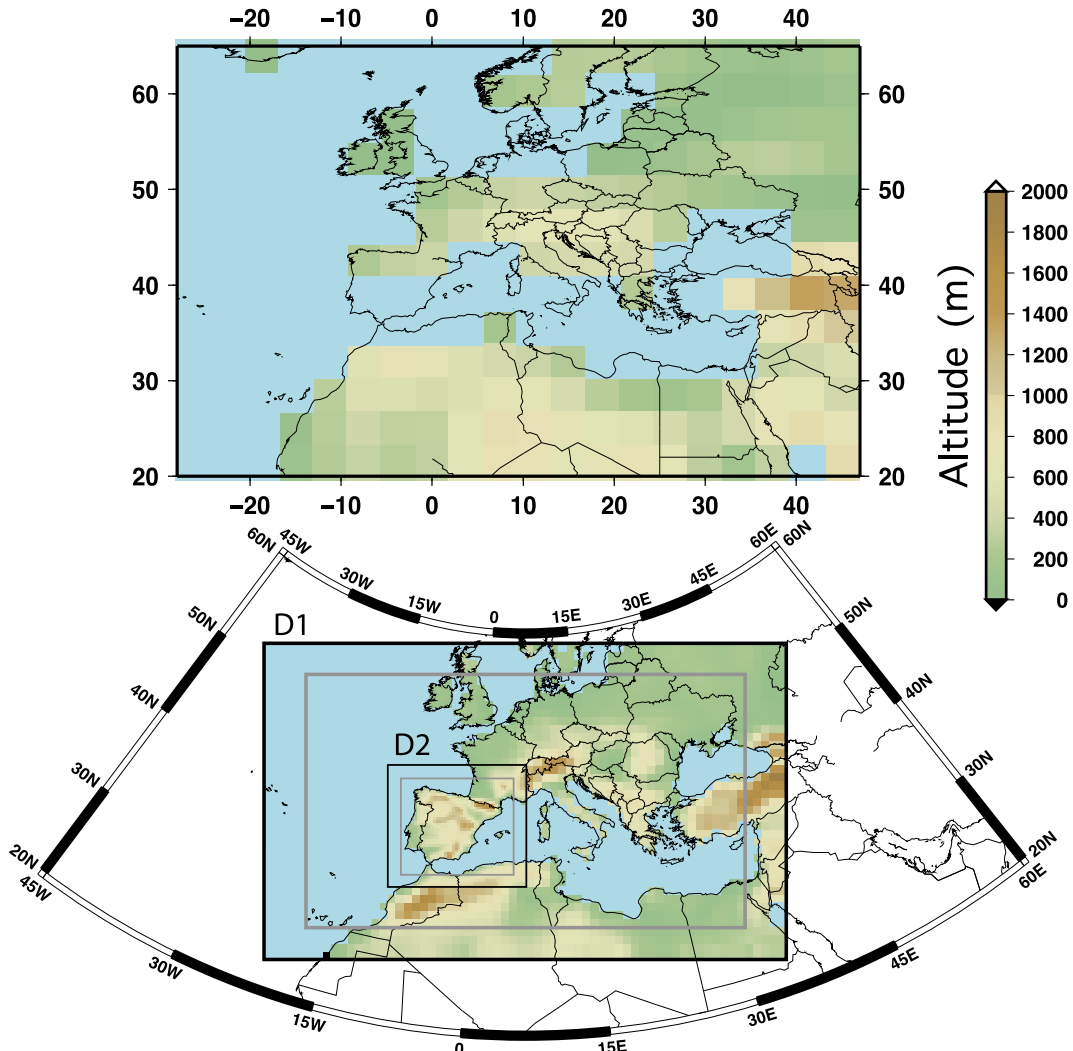


**Figure 2.2:** Land-sea mask and orography of the AOGCM simulation (up) and spatial configuration of the two 2-way nested domains of 90 and 30 km respectively used in the RCM simulation (down). The colour of the squares in both figures represent the topography implemented in the models. Blue squares represent ocean grid boxes. Only the area inside the grey square in the domain 2 is analysed hereafter.

Navarro et al., 2010). Figure 2.2 depicts the spatial resolution implemented in the AOGCM (up) together with the two double-nested domains with a resolution of 90 km and 30 km respectively employed in the RCM simulation (down). The outer domain (D1) covers Europe and the Mediterranean Sea since this area strongly influences the climate of the eastern part of the Iberian Peninsula (Font-Tullot, 2000). The inner domain (D2) covers the IP with higher resolution. The atmosphere is represented by 24 sigma levels in the vertical, with the top level at 100 hPa. The boundary conditions of the model ECHO-G are introduced into the outer domain of the RCM through a blending area of five grid points at the fringes of the outer domain, shown in grey squares in Figure 2.2. This area is excluded from the analysis hereafter.

The physics configuration in the RCM has been chosen in order to minimise the computational cost since none of the tested configurations provides the best performance for all kinds of synoptic events and regions (Fernández et al., 2007). The physical options implemented here are: Grell cumulus parametrisation (Grell, 1993), Simple Ice for microphysics (Dudhia, 1989), Rapid Radiative Transfer Model radiation scheme (Mlawer et al., 1997) and the Medium Range Forecast parametrization for boundary layer (Hong and Pan, 1996). The Noah Land-Surface model (Chen and Dudhia, 2001a,b) has been used, as it simulates more accurately the climate in dry areas, specially in summer over most of the IP (Jerez et al., 2010). Boundary conditions for D1 are updated every 6 hours in the ERA40+MM5 experiment, and every 12 hours in the ECHO-G+MM5 simulation.

In order to illustrate the added value provided by the model MM5, we compare the time series (mean value and variance) of the seasonal means from individual years of SAT and precipitation in a reference period (1961-1990) in the four data sets (ECHO-G, ERA40, ECHO-G+MM5 and ERA40+MM5) with the European Climate Assessment & Observations database (E-OBS) (Haylock et al., 2008). The E-OBS data set is a reconstruction of the evolution of SAT and precipitation for the recent past (1950-2006) which is the result of an interpolation of observational data to a high resolution regular grid ( $0.25^\circ \times 0.25^\circ$ ) that homogeneously covers Europe over land grid points. Specifically, we have used the third version of this data set. Although some problems regarding precipitation have been reported (Hofstra et al., 2009), we use this data base because it is commonly used for model validation purposes in large projects such as ENSEMBLES (van der Linden P. and J.F.B. Mitchell (eds.), 2009), and the daily temporal resolution of this data base allows the study of extreme events, which will be reported in future studies.

This comparison has been performed by means of Taylor diagrams (Taylor, 2001). These depict, in a polar coordinates graph, the correlation and variability ratio of two

series. Instead of showing correlation and variability of two temporal series, as the usual approach, the Taylor diagrams represent the spatial correlation and standard deviation ratio of two gridded spatial fields. To make all data sets comparable, the data of the four simulations have been spatially interpolated to the E-OBS grid, resulting in a total of 1209 grid cells over the IP after removing the ocean grid cells

In order to further evaluate similarities between the ECHO-G+MM5 and ERA40+MM5 simulations, we have performed an Empirical Orthogonal Function (EOF) analysis of the seasonal series of SAT and precipitation. This methodology reduces the high dimensionality of these fields, decomposing them into spatial patterns (EOFs) and associated principal components (PCs) ([von Storch and Zwiers, 1999](#)). By comparing the EOFs of both simulations we can get some insight about the differences and similarities of their spatial correlation structure.

Finally, some preliminary comparisons against proxy-based climatic reconstructions have been performed. We have employed the SAT reconstruction by [Luterbacher et al. \(2004\)](#) and the precipitation reconstruction by [Pauling et al. \(2006\)](#). Both data sets consist of monthly and seasonal series in a  $0.5^\circ \times 0.5^\circ$  regular grid over Europe. They are based on a large variety of long instrumental series, on indices based on historical documentary evidence and on natural proxies. These reconstructions have been performed with a Climate Field Reconstruction method. The reconstruction method is based on Principal Components (PC) regression, by which a multivariate statistical regression model is set up between the leading Principal Components of a gridded observational data set and the available proxy records. This statistical model is then used to reconstruct the temperature or precipitation Principal Components backwards in time and, by combining the reconstructed PCs with the spatial eigenvectors, the whole spatial field. We compare the seasonal mean series of SAT and precipitation in the model and in the reconstruction, but in both cases using only land points in their respective grids over the IP.

## 2.3 Value added by the RCM

This section aims to show the added value generated by the RCM with respect to the stand-alone AOGCM simulation. We compare the climatologies generated by MM5 when this regional model is driven by ECHO-G and ERA40 in a 30-years reference period (1961-1990), respectively. [Jerez et al. \(2010\)](#) illustrated how the downscaling of ERA40 performed with MM5 is capable to reproduce the main features of the SAT of the IP, but no equivalent study for MM5 has been performed for precipitation so far. For this reason we have also compared the results of the simulations with the E-OBS data

base, which contains information about SAT and precipitation.

### 2.3.1 Mean values

Figure 2.3 shows the mean value of the seasonal SAT for the reference period for all data sets. Each column depicts the result for each of the four models and the observational data set in this order: ECHO-G, ERA40, ECHO-G+MM5, ERA40+MM5 and E-OBS. Each row represents the mean climatology broken down by season. The large difference between ECHO-G and ERA40 (first and second columns, respectively) stands out. This difference is attributable to their different spatial resolution (coarser in ECHO-G), the differences in the formulation of ECHO-G and the IFS model employed to develop ERA40 and to the fact that the reanalysis data incorporates the information from observations of the actual climate (Uppala et al., 2005). Due to this assimilation process, ERA40 is a more reliable realisation of the recent past. Comparing both data sets, ECHO-G tends to develop too cold summers and too warm winters, leading to an underestimation of the amplitude of the annual cycle. Furthermore, the spatial resolution of ECHO-G does not allow to capture the orographic details of the IP (see Figure 2.2). In particular, the model is not capable of representing realistically some characteristics of the south of the IP, since it is defined as ocean grid-cells.

On the other hand, columns 3 and 4 in Figure 2.3 show the result of nesting MM5 into the former data sets. The similarities between these simulations are noticeable, and are also similar to the observations depicted in column 5. The resolution of MM5 is able to take into account the main geographical characteristics of the IP, as can be noticed by the cold areas in both columns, which correspond quite well with the higher altitude regions (see Figure 2.2). Important differences still remain, such as an underestimation up to 2 °C of the SAT in the southwestern parts of the IP in summer, and a similar magnitude of overestimation of winter SAT in the central region. This underestimation of the amplitude of the annual cycle seems to be predetermined by the driving AOGCM. Hence, although MM5 ameliorates this deficiency, it is not able to correct it completely.

A similar picture is found for precipitation (Figure 2.4). ECHO-G and ERA40 develop different rainfall patterns (see columns 1 and 2). In general, ECHO-G underestimates the amount of precipitation, more notably in the wettest parts of the IP in the North, where the underestimation is up to 150 mm/month in winter. This underestimation is stronger in winter and spring. The differences may be due to the coarser resolution of ECHO-G and its orography, which fails to discriminate between land and sea points at regional scale, but also to differences in the local and global circulation, as further discussed below. As in the case of SAT, MM5 tends to narrow these differ-

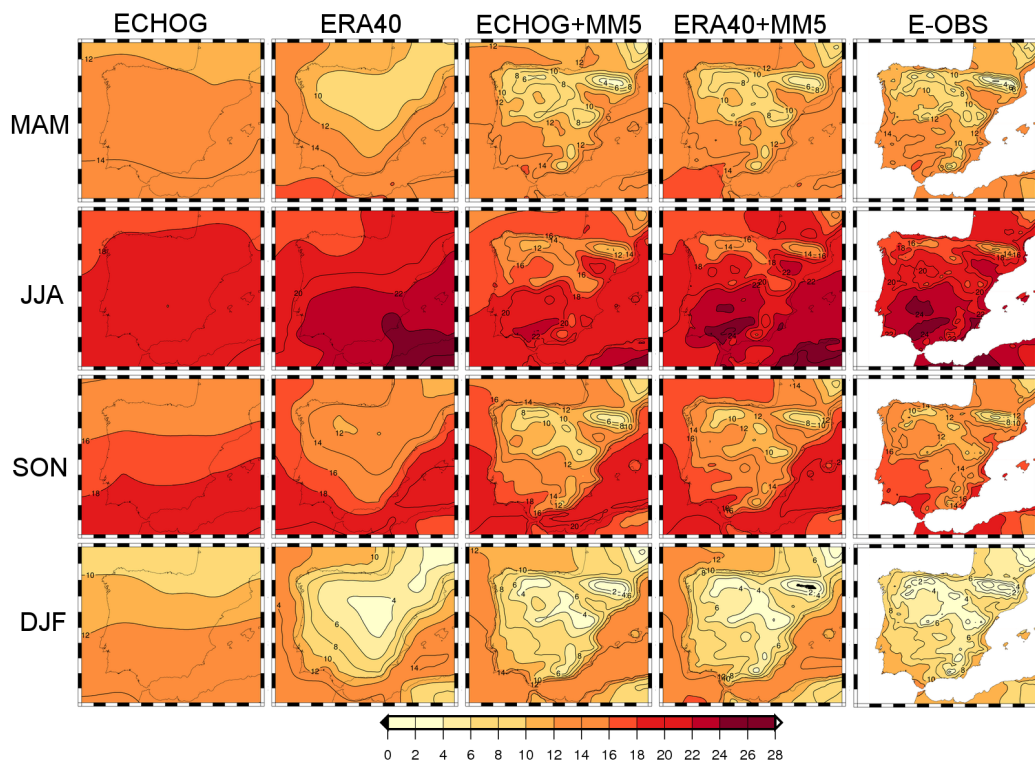


**Figure 2.3:** Mean value of SAT (in °C) in the period 1961-1990 for ECHO-G, ERA40, and MM5 nested to both (by columns) in all the seasons (by rows). Last column depicts the values for the E-OBS data base. All fields have been interpolated to a 7 minutes regular grid to ease the visual comparison.

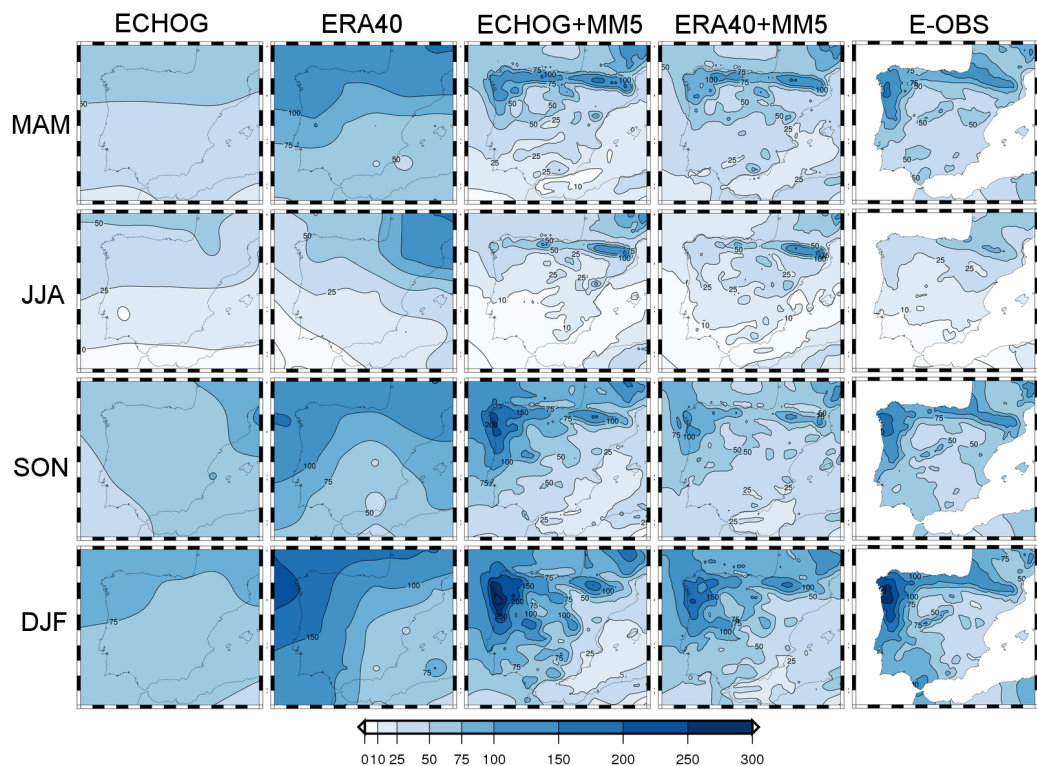


**Figure 2.4:** Mean value of monthly precipitation (in mm/month) in the period 1961-1990 for ECHO-G, ERA40, and MM5 nested to both (by columns) in all the seasons (by rows). Last column depicts the values for the E-OBS data base. All fields have been interpolated onto a 7-minute regular grid to ease the visual comparison.

ences, as can be appreciated in columns 3 and 4. In the case of precipitation there are nevertheless larger differences between the regional simulations. The main one is the overestimation of the precipitation in the ECHO-G+MM5 simulation in the Northwest of the IP in winter and autumn. Precipitation is underestimated in the south in warmer seasons.

As stated above, an important difference between ERA40 and the ECHO-G simulation is that the latter does not include assimilation of observations. Due to the internal variability of the AOGCM, some of the main circulation modes in the model may not be simultaneous with those observed in the actual climate. In the ERA40 reanalysis this temporal evolution matches the observed one, since it does include observational data assimilation. Thus, some of the differences in the ECHO-G+MM5 and ERA40+MM5 simulations in the 30-years period we have used as reference could be attributable directly to this cause, which is independent of the skill of the regional model. In particular, precipitation in the IP is known to be strongly influenced by NAO (Trigo et al., 2004), so differences in the state of this circulation mode in the reference period may explain part of the bias in the amounts of precipitation. Nevertheless there are other important factors more directly related to the skill of the model, further commented on below.

The improvement achieved by MM5 can be visualised in the Taylor diagrams (Figure 2.5). In these diagrams we compare, by season, the performance of the four model integrations when reproducing the mean SAT and precipitation in the reference period compared to the E-OBS data base. In particular each triangle in the figure depicts in polar coordinates the spatial correlation (angle) and standard deviation ratio (radius) between SAT mean values of each experiment and E-OBS. Similarly, each diamond represents the same calculation for precipitation. Climatologies of the four experiments have first been interpolated to the E-OBS grid to perform the calculations. ECHO-G underestimates SAT spatial variability in all seasons, as expected due to its coarse resolution. ERA40 performs better in this respect, although it is still not able to represent the many variations in the climate over the IP. When the RCM is driven by both data sets, it simulates a very similar variability, which is also close to the observed. Although this may be partly due to the similar spatial resolution of the RCM simulations and the E-OBS data base, it is evident that the use of MM5 brings the global data sets closer to the observations. Regarding the correlation, MM5 simulates a SAT pattern in both experiments which correlates with 0.95 with the observed one for each season, further highlighting the added value of the regional model. For precipitation we find a more complex behaviour. As before, ECHO-G systematically underestimates the spatial variability due to its coarse resolution. The correlation with the observations is high in summer because it is able to reproduce the observed North-South gradient, but in other

seasons it is very low. MM5 is able to improve both aspects, and the correlation between precipitation with observations is over 0.8 for all seasons. Correlation between precipitation in ERA40 and E-OBS is high in general, and thus MM5 is not able to improve this aspect very much. ERA40+MM5 shows, in general, lower spatial variability than ERA40, in some cases narrowing the differences between model and observations and in some others increasing them.

Summarising Figures 2.3 to 2.5, MM5 is able to improve several aspects of the present climate simulated by ECHO-G. On one hand, it increases the amplitude of the SAT annual cycle, which is underestimated by the AOGCM. The seasonal mean values of precipitation and SAT are strongly modulated due to the higher spatial resolution. The RCM narrows the differences between the climatological values of SAT and precipitation in ECHO-G and ERA40, which become very similar to the observations, as indicated by the Taylor diagrams. This points to an improvement in the characterisation of the climate over the IP, at least in the reference period, when the outputs of ECHO-G are used to drive MM5.

As indicated above, the main drawbacks in the climatologies of the ECHO-G+MM5 simulation with respect to ERA40+MM5 are the underestimation of the amplitude of the annual cycle of temperature and the overestimation of the winter precipitation in the Northwest. Besides the possible effect of the internal variability of the AOGCM on the simulated climatology in reference period commented on above, both biases could be explained by an overestimation of the zonal circulation in the atmospheric model ECHAM4, a feature common in many global climate models. In winter, the extra warm and wet oceanic wind is conductive of warmer temperatures to the IP, whereas in summer it tends to cold it. This explanation is supported by Ulbrich et al. (2009), who have shown the overestimation of the zonal circulation in the model ECHAM4, specially in the North Atlantic region.

### 2.3.2 Temporal variability

We have also examined the effect of MM5 on the simulated interannual variability of SAT and precipitation. The standard deviations of the seasonal mean temporal series of SAT are shown in Figure 2.6. As in Figures 2.3 and 2.4, columns 1 and 2 show the results for ECHO-G and ERA40. The main difference between these patterns is the strong underestimation of the interannual variability in winter and autumn in ECHO-G. Nevertheless, the underestimation is not constant across the four seasons, and in fact the variability in some areas of the North of the IP in summer and spring is overestimated with respect to ERA40. The corresponding simulations when MM5 is coupled to both

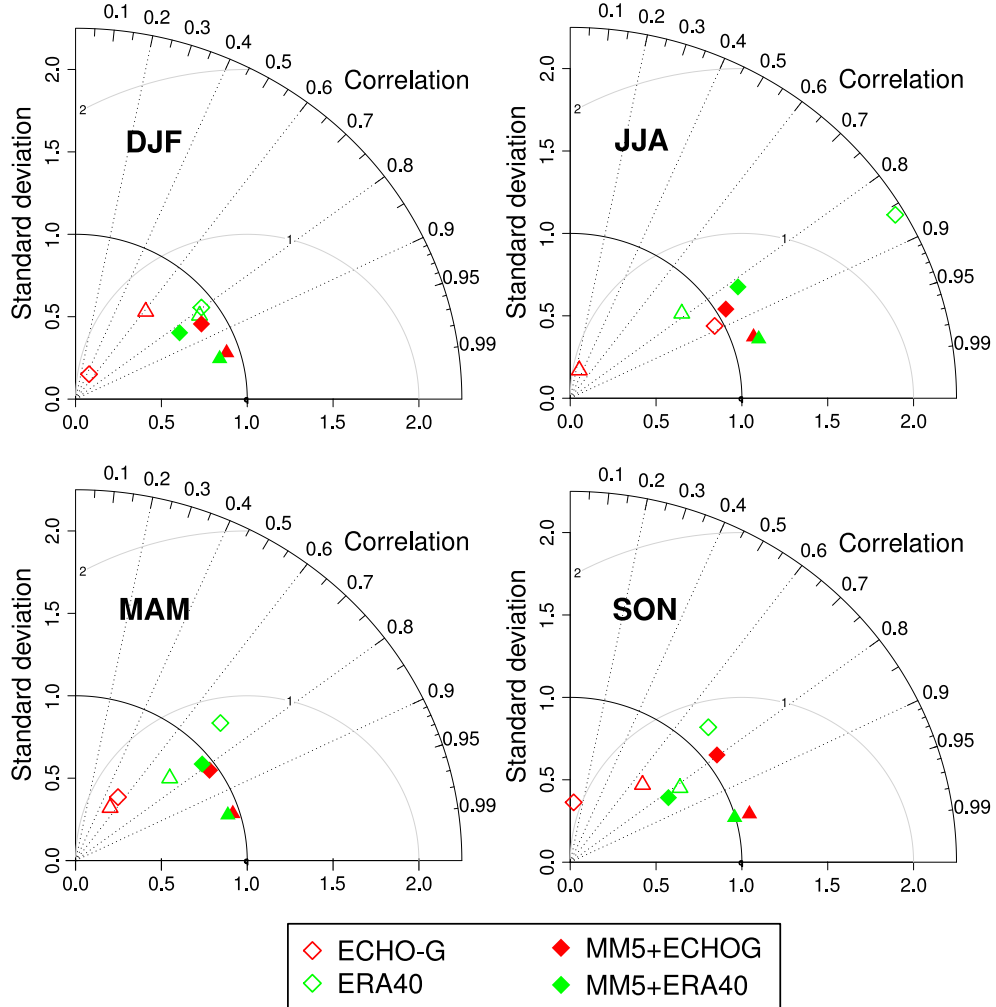


**Figure 2.5:** Taylor diagrams of the spatial structure of the mean SAT and precipitation in the reference period. Triangles represent the correlation and variance ratio between the SAT seasonal mean values obtained by the models against the values of the E-OBS database. Diamonds depict the same information regarding precipitation. Empty symbols represent the driving data, meanwhile filled ones represent the MM5 results. The colour distinguishes between ECHO-G (red) and ERA40 (green). All experiments have been interpolated to the E-OBS grid to perform the calculations.

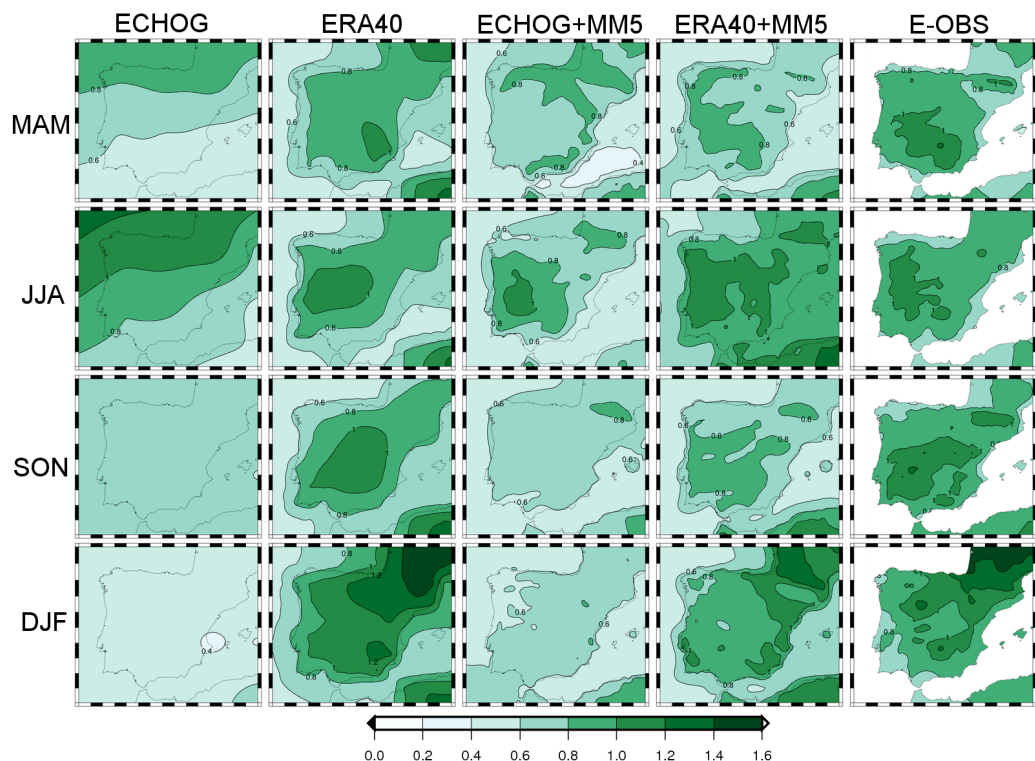


**Figure 2.6:** Standard deviation (in  $^{\circ}\text{C}$ ) of seasonal mean series of SAT in the period 1961–1990 for ECHO-G, ERA40, and MM5 nested to both (by columns) in all the seasons (by rows). Last column depicts the values for the E-OBS data base. All fields have been interpolated to a 7 minutes regular grid to ease the visual comparison.

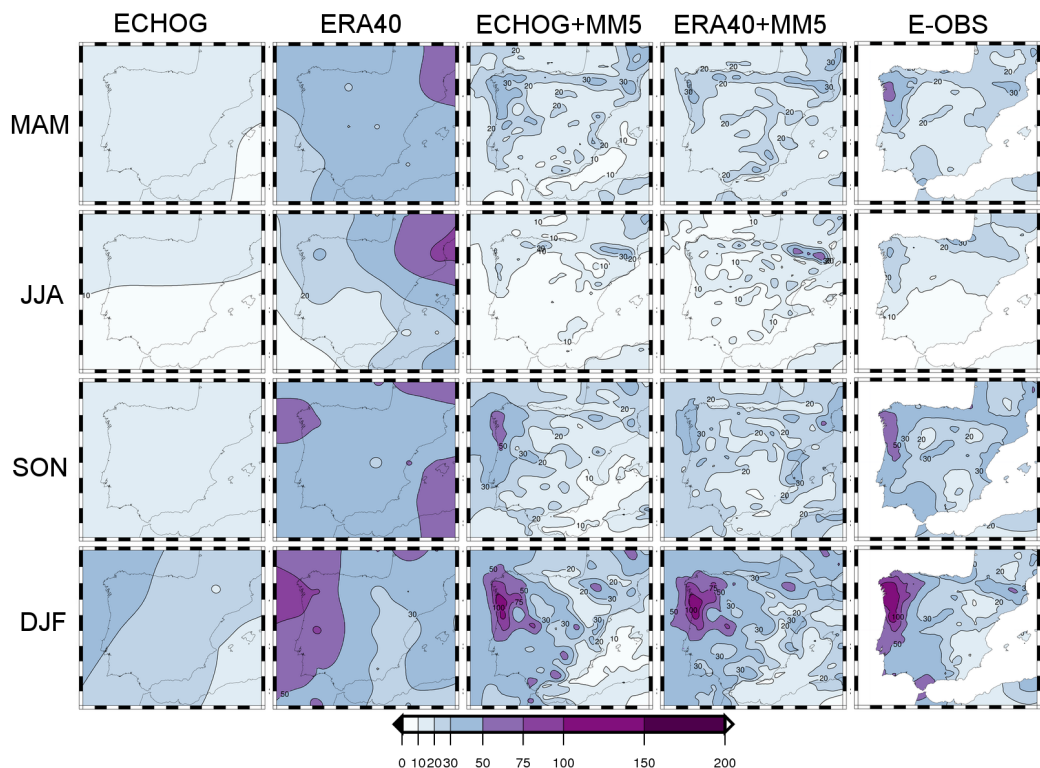


**Figure 2.7:** Standard deviation (in mm/month) of seasonal mean series of precipitation in the period 1961-1990 for ECHO-G, ERA40, and MM5 nested to both (by columns) in all the seasons (by rows). Last column depicts the values for the E-OBS data base. All fields have been interpolated onto a 7-minute regular grid to ease the visual comparison.

data sets are shown in columns 3 and 4 of the same figure, and column 5 depicts the same data for the E-OBS data base. ECHO-G+MM5 systematically underestimates the SAT variability with respect to ERA40+MM5, and there are large differences in their spatial structure, the mismatch being more noticeable in spring. Nevertheless the RCM is able to correct some of the main deficiencies of ECHO-G. For instance, it increases the interannual variability in autumn and winter, and decreases it in the North in summer, making the structure of the SAT variability more similar to the observations. Thus, the effect of MM5 is to correct ECHO-G by increasing and decreasing interannual variability, depending on the season and area, but in all cases narrowing differences between ECHO-G and ERA40, and reducing differences with respect to E-OBS.

Figure 2.7 depicts the same information regarding the interannual variability of the seasonal mean precipitation. As it could be expected, the wettest areas show a larger variability in every experiment. It is apparent that ECHO-G strongly underestimates the precipitation interannual variability in all seasons, more noticeably in summer (see columns 1 and 2). MM5 corrects some of these differences, increasing the variability in many areas. In particular, the pattern of precipitation variability is very similar in ECHO-G+MM5 and ERA40+MM5 (see columns 3 and 4), although there exists some underestimation of the precipitation variability in the Northwest of the IP in the ECHOG+MM5 experiment, mainly in the wettest areas. This contrasts with the fact that this simulation develops stronger precipitation amounts than ERA40+MM5 (Figure 2.4). These larger precipitations, together with their less variability, may be attributable to deficiencies in ECHO-G in reproducing the weather types that affect the climate over the IP, as well as a differences due to internal variability.

Summarising, ECHO-G tends to underestimate the regional interannual variability of the temporal series of SAT and precipitation over the IP in the reference period with respect to ERA40. MM5 is able to partly correct this drawback, with a general increase of interannual variability. Furthermore it also corrects the overestimation of SAT variability in the North of the IP in summer. The improvements introduced by the downscaling process may have an important impact in inter comparison exercises between proxy reconstruction and simulations, since the former are strongly influenced by local climate features, which are better reproduced by the RCM. For instance, there are areas with great potential for proxy studies, such as the Pyrenees, and other mountain ranges in the Southeast of the peninsula, in which MM5 clearly outperforms ECHO-G. Hence, comparison studies between ECHO-G+MM5 and reconstructions offer better reliability than between those and the AOGCM alone.

### 2.3.3 Main variability modes

Finally, we have investigated the coherence of the covariance structure of temperature and precipitation in the regional experiments driven by ECHO-G and ERA40 by means of an Empirical Orthogonal Function (EOF) analysis. This technique has been applied to the seasonal series of SAT and precipitation in the period 1961-1990 only over land grid points. It is important to note that the spatial patterns in the figures below are dimensionless, as they have been normalised to unit spatial variance. Hence, comparing the patterns does not indicate the amplitude of variability in each experiment, but only the relative spatial distribution of the correlation among the grid-cells. The comparison of the actual variability of both simulations has been presented in Figures 2.6 and 2.7.

Figure 2.8 depicts the first three EOF patterns of SAT. The ordering of the maps is as follows: columns 1 and 2 show the first EOF for ECHO-G+MM5 and ERA40+MM5, respectively. The second EOF for ECHO-G+MM5 and ERA40+MM5 are shown in columns 3 and 4. Finally, the third EOF is shown in columns 5 and 6. Each row includes a season, going from spring (first row) to winter (last row). The percentage of variance explained by each EOF is shown in Table 2.1. In both experiments and all seasons the percentage of variance explained by the first EOF is higher than 75%. The associated patterns present the same sign over the IP, and their shape is similar in both simulations. In summer, the form of the patterns seems to be related to the distance to the ocean, whereas in autumn they are rather correlated to altitude. It is interesting to note that a similar annual cycle in the variability patterns has been found in an ensemble of climate change projections (Gómez-Navarro et al., 2010). There are nevertheless important differences between simulations. In winter ECHO-G+MM5 develops a North-South pattern which does not match the West-East pattern found in ERA40+MM5 very well. The second and third EOFs explain much less percentage of variance in all cases, with similar amounts in both simulations. This supports the similarities between both simulations. The overall form of these patterns is in this case very similar. The largest differences are found in the third EOF patterns for winter, although the percentage of variance explained by these patterns is only around 3%.

Figure 2.9 depicts the first three EOF patterns for precipitation. Table 2.2 shows the percentage of variance explained by each pattern. The percentage of variance explained by the first EOF of precipitation is lower than for SAT. A prominent exception occurs in winter, for which the EOF explains a high percentage of variance, coherently in both experiments. Regarding the spatial structure of the leading EOF, it is pretty similar in both simulations, being more marked in the wettest areas in the North-West in coldest seasons and the higher altitude areas in the North-East of the IP in summer. There are

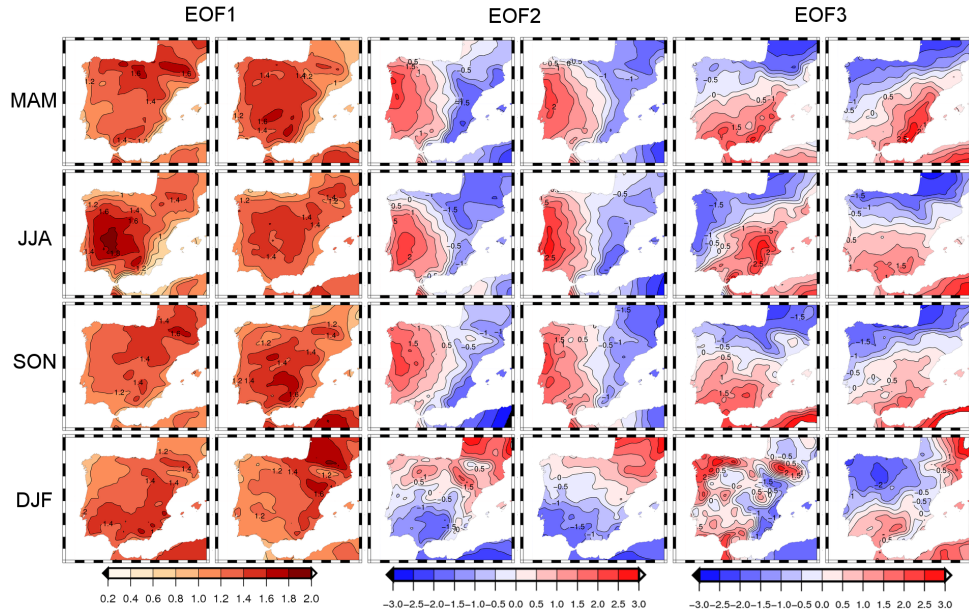


**Figure 2.8:** Normalised EOF patterns obtained from the seasonal mean series of SAT for the period 1961-1990 in the simulations ECHO-G+MM5 and ERA40+MM5.

	EOF1		EOF2		EOF3	
	ECG	E40	ECG	E40	ECG	E40
MAM	82.06	76.18	7.97	11.63	4.79	5.98
JJA	79.68	79.73	10.12	9.86	4.65	5.29
SON	82.95	80.14	7.67	10.88	3.28	3.29
DJF	79.21	88.56	7.32	6.91	3.28	3.29

**Table 2.1:** Percentage of variance explained by each EOF of the seasonal mean series of SAT. ECG denotes the ECHO-G+MM5 experiment whereas E40 denotes the ERA40+MM5 experiment.

nevertheless important differences in spring, and in autumn. ECHO-G+MM5 tends to overestimate the intensity of the EOF pattern in the North-West, developing a pattern similar to that for winter. This difference could be explained again by the overestimation of the zonal circulation in ECHO-G. This stronger flow of humid air forces the RCM to simulate precipitation events in autumn that are not present when the RCM is driven

by ERA40. This may point to an unrealistic frequency of certain weather types in the ECHO-G simulation, which leads to a misrepresentation of the precipitation variability in ECHO-G+MM5 in the warmer seasons, and can also affect the SAT field. The second and third EOF are more relevant in this case, as they explain an important share of the variance. Their patterns are shown in columns 3 to 6. There exists overall a good agreement between the two simulations.

The largest differences occur in summer, as ERA40+MM5 tends to develop a more pronounced pattern in the high-altitude areas. Again, this difference can be attributed to the overestimation of the zonal flow in ECHO-G in this season, since the climate in the MM5+ERA40 is more weakly forced by the advective flow. Note that in autumn the ordering of the second and third EOF seem to be swapped in both experiments. This is not surprising since the percentage of variance explained by these two EOFs for ERA40+MM5 is pretty similar, 13.42 and 13.30 respectively (see Table 2.2).

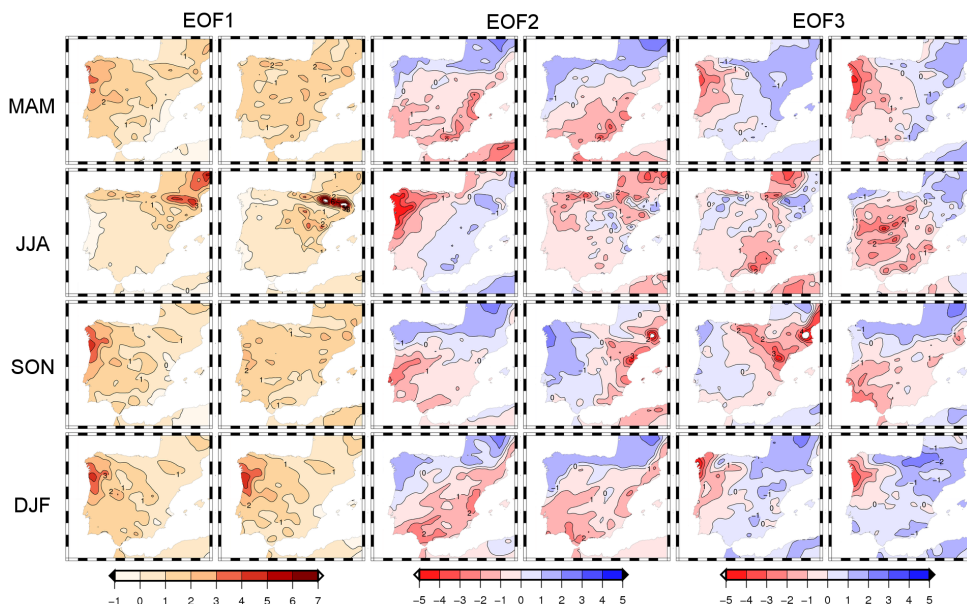


**Figure 2.9:** Normalised EOF patterns obtained from the seasonal mean series of precipitation for the period 1961-1990 in the simulations ECHO-G+MM5 (left) and ERA40+MM5 (right).

Overall, there is a relative good agreement between the EOF patterns in both simulations. In particular the EOF patterns varies coherently through the seasons and along

	EOF1		EOF2		EOF3	
	ECG	E40	ECG	E40	ECG	E40
MAM	45.70	40.27	18.16	19.84	10.67	9.99
JJA	34.61	36.87	16.91	15.92	7.68	11.27
SON	49.82	39.50	13.04	13.42	6.05	13.30
DJF	74.07	69.65	8.29	11.04	5.25	5.21

**Table 2.2:** Percentage of variance explained by each EOF of the seasonal mean series of precipitation. ECG denotes the ECHO-G+MM5 experiment whereas E40 denotes the ERA40+MM5 experiment.

the EOF hierarchy. The SAT patterns follow an annual cycle similar to the one found previously in an ensemble of climate change projections (Gómez-Navarro et al., 2010). Regarding precipitation, similar agreement between simulations is found in winter, although several differences linked to the overestimation of the zonal flow, appear in summer. Hence, not only mean values and variability of the climatologies developed by MM5 when coupled to ECHO-G are similar to ERA40, but also the main variability modes (with some deficiencies). This supports the idea that the dynamical downscaling of ECHO-G simulation is able to capture the main features of the present climate of the IP. Thus, provided that the boundary conditions of the AOGCM are relatively good, it can be expected that the RCM will also be able to reproduce the actual features of past climates. It is important to highlight that the dynamical downscaling process is able to display spatial gradients at regional scale that the AOGCM can not. For instance, precipitation in the Northwest of the IP is dominated by the zonal flow from the Atlantic ocean, whereas its effect in the South-Eastern areas is weaker. These details, which are due to regional features and are implicitly included in the proxy reconstructions, can barely be simulated by a coarse resolution AOGCM.

### 2.3.4 Regional climate and synoptic conditions: NAO

The North Atlantic Oscillation (NAO) is a well known variability pattern in the winter sea level pressure (SLP) field affecting the climate of the North Atlantic-European sector. In particular it strongly affects the precipitation events in winter in most parts of the IP (Trigo et al., 2004). To ascertain that the relationship between the NAO and the precipitation over the IP is robust in the observed climate, we have calculated the correlation map between a NAO index and the winter precipitation for the IP in the period 1950-1990. The NAO index is defined here as the standardised series of the principal

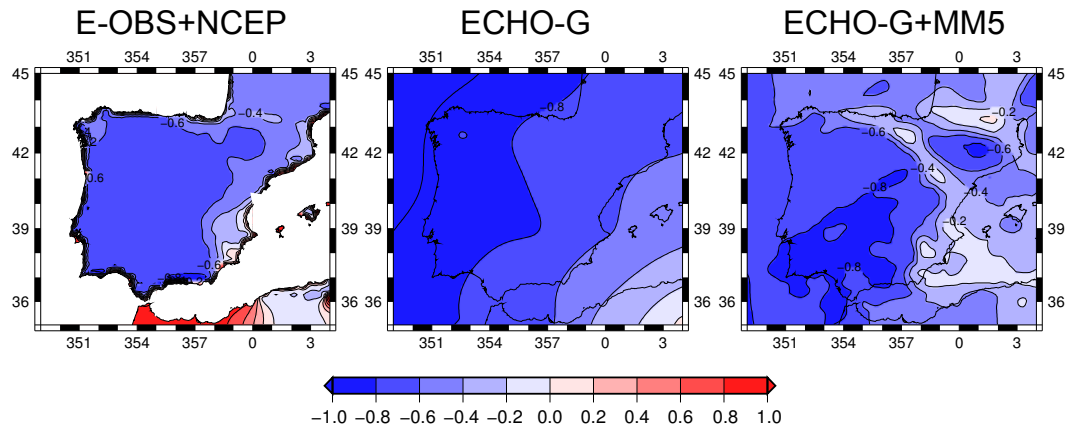


**Figure 2.10:** Correlation maps between NAO and winter precipitation over the IP as reproduce by ECHO-G (left), ECHO-G+MM5 (centre) and a combination of reanalysis for SLP and observations for precipitation (right). The NAO index is defined in the main text.

component associated to the leading EOF of the mean SLP in winter in the geographical box  $70^{\circ}\text{W}$  to  $50^{\circ}\text{E}$  and from  $20^{\circ}\text{N}$  to  $75^{\circ}\text{N}$ . To perform these calculations we have used the E-OBS data base of precipitation over the IP (Haylock et al., 2008) and the NCEP reanalysis (Kalnay et al., 1996) for SLP. The result is depicted in the left map of Figure 2.10. The correlation between this index and the winter precipitation is quite strong, reaching values of -0.6 over most of the domain. It is nevertheless less strong in the eastern parts, where the influence of the Atlantic flow in the precipitation regime is weaker.

We have investigated the link between the NAO variations and the precipitation within the models. The central map of Figure 2.10 depicts the result of same calculations as above but using the ECHO-G model for the same period. The model is capable of simulating this relationship, although it overestimates its importance (the correlation is below -0.8 in the Northwestern half of the IP). The precipitation in the Southeast seems to be also too strongly driven by this circulation mode, a feature which is not very realistic. The map on the right of the same figure shows the result when MM5 is used to simulate the climate over the IP. In this case, we have calculated the NAO index using the data simulated by the AOGCM, since the former area lies outside the domain of our regional simulation and the regional model introduces no significant modifications with respect to the driving model in this variable. Apart from the clear gain in spatial resolution, in this case the precipitation regime is quite different, and is not so strongly driven

by the Atlantic flow (correlation  $-0.6$  over most areas, although it reaches  $-0.8$  in some areas in the Southwest), approximating the simulation to the observations. In good agreement with them, the RCM is able to simulate areas in the Southeast where the precipitation is very weakly driven by NAO, and overall the spatial correlation between left and right maps over land points is  $0.7$ . Nevertheless, compared to observations, the RCM results are more affected by important orographic features like the Pyrenees or the Iberic System, around the center of the Iberian Peninsula. Since there is evidence of the reasonable skill of RCMs in complex orography areas such as the Alps (Frei et al., 2003), a plausible explanation for these differences could be that the observational data base is less reliable over mountains, since precipitation measures in these areas are specially scarce, and they are interpolated from data of nearby meteorological stations.

Thus, Figure 2.10 clearly illustrates another aspect of the added value by the RCM simulation: its capability to simulate realistically the physical connections between the large-scale systems simulated by the driving model and the response of the local climate to them. Nevertheless, and according to the comments made before, the temporal evolution of these circulation modes in the AOGCM is not directly driven by the external forcings, but it is strongly affected by internal variability. This has deep impacts in the evolution of precipitation over the IP (Luterbacher et al., 2010). For this reason, we should not expect in general a good agreement between NAO variations in the model and in the reconstructions. We will further discuss this aspect when comparing the model results with some reconstructions of the climate in the next sections.

## 2.4 Climate in the last 1000 years in the IP

In the former section we evaluated the added value of the RCM simulation and illustrated how the dynamical downscaling is able to narrow the differences between ECHO-G and ERA40 for a reference period. In this section we highlight the main features of the simulation performed with MM5 coupled to ECHO-G for the 1001-1990 period. We also perform some comparison with proxy-based reconstructions.

### 2.4.1 AOGCM versus RCM simulation

Figure 2.11 gives an overall idea of the path followed of the simulation. Upper panels represent the 31-years running mean of the SAT anomalies for winter and summer with respect to the period 1900-1990. Red lines correspond to ECHO-G and blue lines to ECHO-G+MM5. The series are averaged over an area which covers the entire IP,

including ocean grid-cells. The middle panel represent the same information but regarding the precipitation anomaly for the Northwest of the IP, whereas the lower panel refers to the evolution of the precipitation in the Southeast. We split the precipitation series into two areas because the precipitation regime and amount is quite different in these two areas, as shown in Figure 2.4. However SAT evolution is not so heterogeneous, and so we consider just the simple spatial average. We include ocean grid-cells to be consistent in the figure, since ECHO-G does not include any land grid-cell in the southeastern area. In this figure, the high correlation between the variations in both simulations for all seasons is apparent. This is not surprising since the AOGCM drives the RCM simulation. There are nevertheless some differences which will be discussed below. In general, discrepancies in the simulations should not be sought in the domain-averaged series but in their high resolution spatial structure, as illustrated later.

In the SAT series (upper panels of Figure 2.11), we may identify a warm initial condition, followed by a cold period which roughly covers 1400-1850, and ends with a warm trend which continues until the end of the simulations. These warm/cold periods match well with respective historical periods that are relatively well documented in other parts of the world and commonly denominated as the Medieval Warm Period and the LIA. The final warming trend from roughly 1850 to the end of the simulation is simultaneous with the rise of the concentration of GHGs as prescribed in the model run (Figure 5.1). The RCM tends to follow ECHO-G more weakly in summer, as we can clearly identify around 1120, 1410 or 1740 in this season.

Looking at higher frequency variability, several marked minima in the SAT anomalies can be identified around the periods 1430-1450, 1600-1620, 1675-1710 and 1800-1830, in general more noticeably in summer. Some of these cold periods match fairly well known historical periods, like the Spörer minimum (1420-1440), the Maunder minimum (1675-1710) and the Dalton minimum (1800-1830), which are marked with a grey band in the figure. Furthermore, they seem to be directly driven by variations in the external forcing (Figure 5.1). For this reason, we use hereafter these denominations to denote the anomalies in temperature and precipitation simulated by the model which coincide in time with these anomalies in the forcing conditions. Note that the model simulates also a cold period around 1620 that is not driven by any of the external forcings. This aspect will be further commented on in the final discussion in the context of internal variability of climate models. Interestingly, there are some minima that can be identified in all seasons, such as the Spörer minimum, whereas others, like the Maunder minimum, can hardly be identified in winter. This implies that the amplitude of the annual cycle is strongly reduced in the Maunder minimum, but not in other cold periods, and this suggests that the physical mechanism under different cold

periods could be very different.

Precipitation series show in general larger differences between the global and regional simulations. As in the case of SAT, this is specially noticeable in summer. The reason for this is that whereas winter precipitation in the IP is largely dominated by large scale systems (see the next section), and hence by the boundary conditions that drive the RCM, summer precipitation in the IP is more convective. As illustrated by Fernández et al. (2007), the effect of the higher spatial resolution and the different physical parametrisation of both models plays an important role in this precipitation regime, and thus explains the larger differences in summer. There are also important differences between the North West and the South East of the IP, one of the most important being the large difference in the variability of the series (which is linked to the mean precipitation). It is not so easy to identify in these series the low frequency signal of the LIA, but there exists an overall negative relationship with the SAT series, like a strong winter precipitation maximum around the Maunder Minimum and the opposite trends of both variables in summer over the last century. The temporal correlation of the 31-years running mean series of SAT and precipitation, both averaged over the whole IP, is -0.16 in winter and -0.83 in summer. Using a bootstrap method, the confidence interval for the correlation at the 95% level was found to be  $\pm 0.39$  and  $\pm 0.50$  for both seasons, respectively. Hence, although the winter anti correlation between precipitation and SAT can be due to chance, the summer case seems to be statistically significant. In fact, the relationship between drier and warmer conditions in the dry season has been reported in several climate change projections for the 21th century in the Mediterranean area (Giorgi and Bi, 2005), so our findings are coherent with these results, and reinforce some conclusions of these studies in the context of past climates. In winter, the negative correlation between these variables is weaker, partly due to the positive tendency they share in the last century.

As discussed above, some differences in the climatologies developed by the RCM and the AOGCM simulations are found at regional scales. For illustration, Figure 2.12 depicts the summer and winter SAT anomalies in the Maunder minimum with respect to the 1900-1990 period as simulated by ECHO-G (left) and ECHO-G+MM5 (centre) and reconstructed by Luterbacher et al. (2004) (right). In this section we focus on the differences between the AOGCM and the RCM. Although it is shown in the figure, comparison with proxy-based reconstructions is performed in the next section. The spatial average of the anomalies in both simulations is similar, as can be appreciated in Figure 2.11. Furthermore, anomalies are overall larger in summer than in winter in both simulations. However, the spatial distribution of the coldest areas is different. In the ECHO-G simulation they are located outside of the IP, decreasing to the Southeast to-

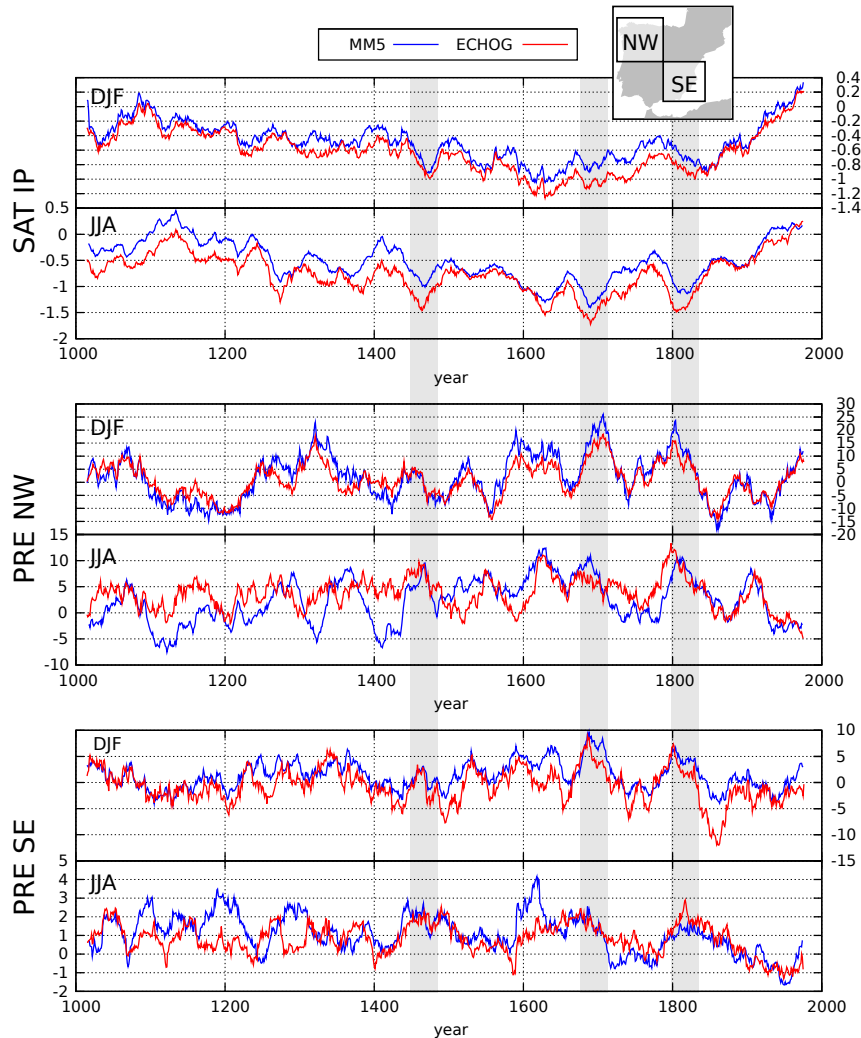


**Figure 2.11:** Anomaly series of SAT over the IP (upper panel, in  $^{\circ}\text{C}$ ) Northwest precipitation (middle panel, in mm/month) and Southeast precipitation (lower panel, in mm/month) in winter (DJF) and summer (JJA), respectively. The NW and SE subdomains are represented in the grey map in the top-right corner of the figure. Red line represents the series for ECHO-G and blue line for ECHO-G+MM5. Ocean grid-cells are also included in the calculations. Anomalies are calculated with respect to the period 1900-1990, and a 31-years running mean have been applied to all series. Grey bars indicate three cold periods discussed in the main text.

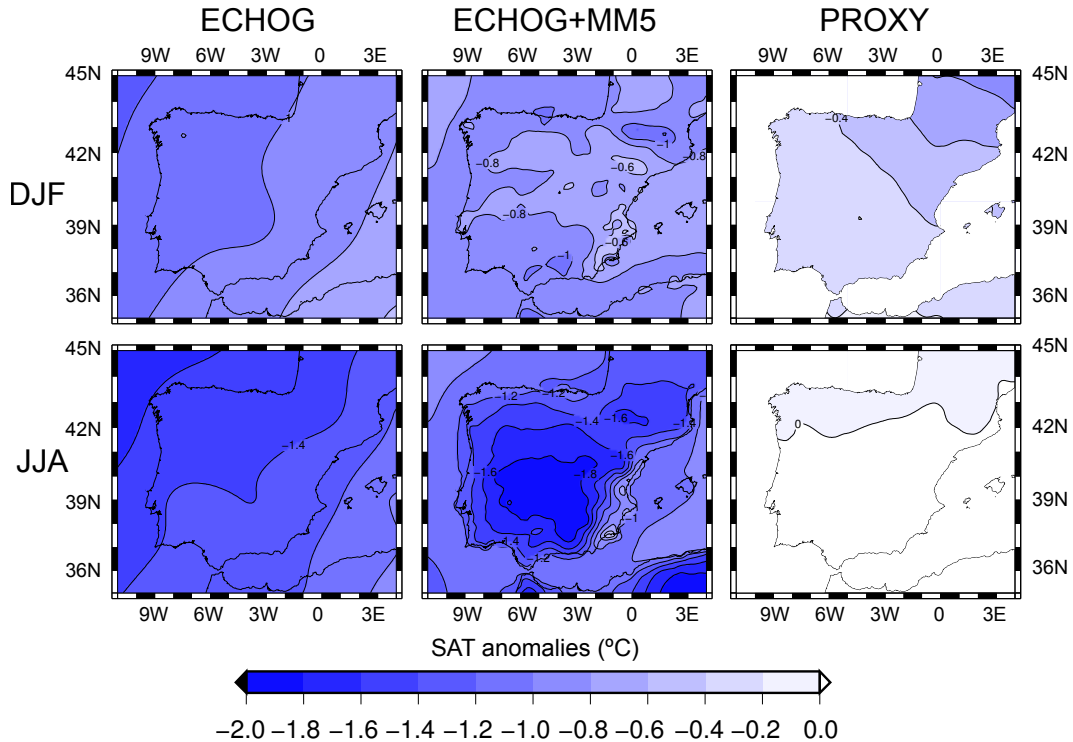


**Figure 2.12:** SAT temperature anomalies for winter (up row) and summer (bottom row) in the 1671-1700 period respect to 1900-1990. The figure shows the results for ECHO-G (left), ECHO-G+MM5 (centre) and the SAT reconstruction (right).

wards the Mediterranean Sea. The spatial structure of the anomalies is similar in both seasons. In the RCM simulation the coldest areas are rather located in the centre of the peninsula in summer, and in the higher areas in winter. It is interesting to note that similar spatial patterns, with the same seasonal cycle, were found for the warming patterns for the 21st century in regional climate change projections for the same area (Gómez-Navarro et al., 2010). Differences between the two simulations could be related to the coarse topography, as the south half part of the IP is defined as ocean, as can be seen in Figure 2.2. Similar differences are apparent for the rest of seasons and for the other cold periods (not shown).

Similarly, Figure 2.13 shows the same information as Figure 2.12 but for precipitation anomalies: winter and summer anomalies in the Maunder minimum for ECHO-G,

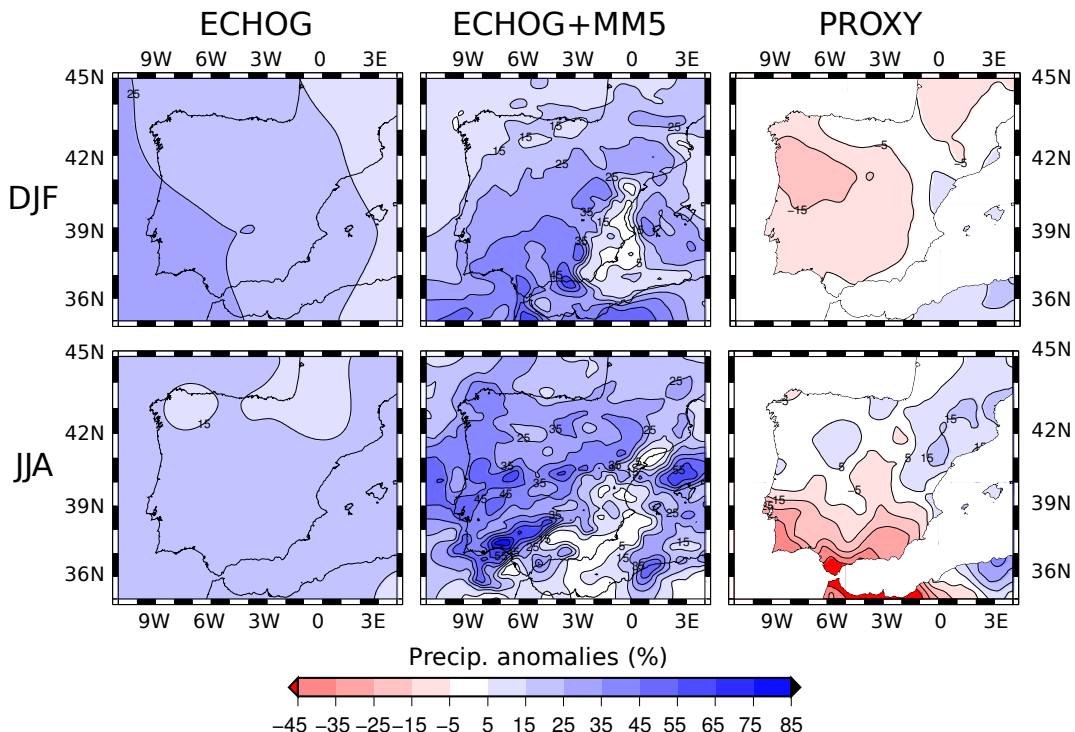


**Figure 2.13:** Precipitation anomalies for winter (up row) and summer (bottom row) in the 1671-1700 period respect to 1900-1990. The figure shows the results for ECHO-G (left), ECHO-G+MM5 (centre) and the precipitation reconstruction (right).

ECHO-G+MM5 and reconstructed by [Pauling et al. \(2006\)](#). ECHO-G simulates a homogeneous increase in precipitation about 20% for most of the IP in summer, and slightly higher in the West of the IP in winter. However, although the RCM also simulates an average increase of precipitation in both seasons (see Figure 2.11), its shape is very different. In fact, the high resolution model simulates a strong increase in precipitation in some areas of the Southwest of the IP. However, there are some areas in the Southeast where there is no increase of precipitation. This behaviour is inverted in autumn for the same period, where a strong increase of precipitation is observed in the Southeast in the MM5 simulation which is not present in ECHO-G (not shown).

In general, the low-frequency evolution of the RCM is dominated by the AOGCM, as is clearly illustrated in Figure 2.11. Nevertheless, the added value of the RCM appears in the high-frequency domain. Top (bottom) row in Figure 3.4 shows the correlation

between the annual series of SAT (precipitation) in every each grid point and the corresponding mean value for the IP domain in ECHO-G (left) and MM5 (right). The series have been previously filtered through a high-pass filter which only allows frequencies higher than  $0.3 \text{ yr}^{-1}$ . This filtering prevents the slow variations in the climate to increase the correlation among grid points in different locations of the domain. In SAT, ECHO-G is hardly able to make any differences between several areas within the IP. On the contrary, MM5 reduces the correlation between the mean behaviour of the IP and some areas in the Southeast, reaching values below 0.8. The corresponding maps in the low-frequency domain (not shown) are identically equal to 1, further indicating the strong influence of the driving model in the low frequency evolution of the RCM. In precipitation MM5 introduces larger differences. Although the correlation for precipitation series in ECHO-G is lower than for SAT, it displays a strongly homogeneous behaviour. Nevertheless, in the MM5 simulation there are areas near the Mediterranean Sea with evolution uncorrelated with the mean behaviour. The correlation pattern seems to be related to the main mountain systems (see Figure 2.2), which suggest that the improvement is, to a great extent, introduced by the more realistic orography.

The differences in the shape of anomalies of SAT and precipitation in both simulations are partly due to the higher spatial resolution of the RCM, which allows it to develop more realistic local dynamics. In addition, in large areas such as our outer domain, the regional model is able to generate its own synoptic scale circulation, which is slightly different from that of the AOGCM. The modification of this circulation may importantly affect the regional climate. These regional differences further illustrate how the RCM, although driven by the AOGCM, is able to develop quite different climatologies at local scales (Déqué et al., 2005). Nevertheless it is important to note that the improvements introduced by the RCM depend strongly on the variable of interest. In SAT, the AOGCM strongly drives the regional model, although it is still able to introduce some differences in the high-frequency. In precipitation, the RCM introduces large departures from the driving model, in part due to the strong impact of high-resolution orography in the precipitation events. The improvements introduced by the RCM may impact the inter comparisons between proxy-based reconstructions and model simulations, as the AOGCMs are not able to simulate local flow patterns which strongly modulate observed climate in a given area.

#### 2.4.2 Comparison with proxy-based reconstructions

Figure 2.15 shows the evolution of the anomalies in SAT (upper panel), Northwest precipitation (middle panel) and Southeast precipitation (lower panel) for the ECHO-

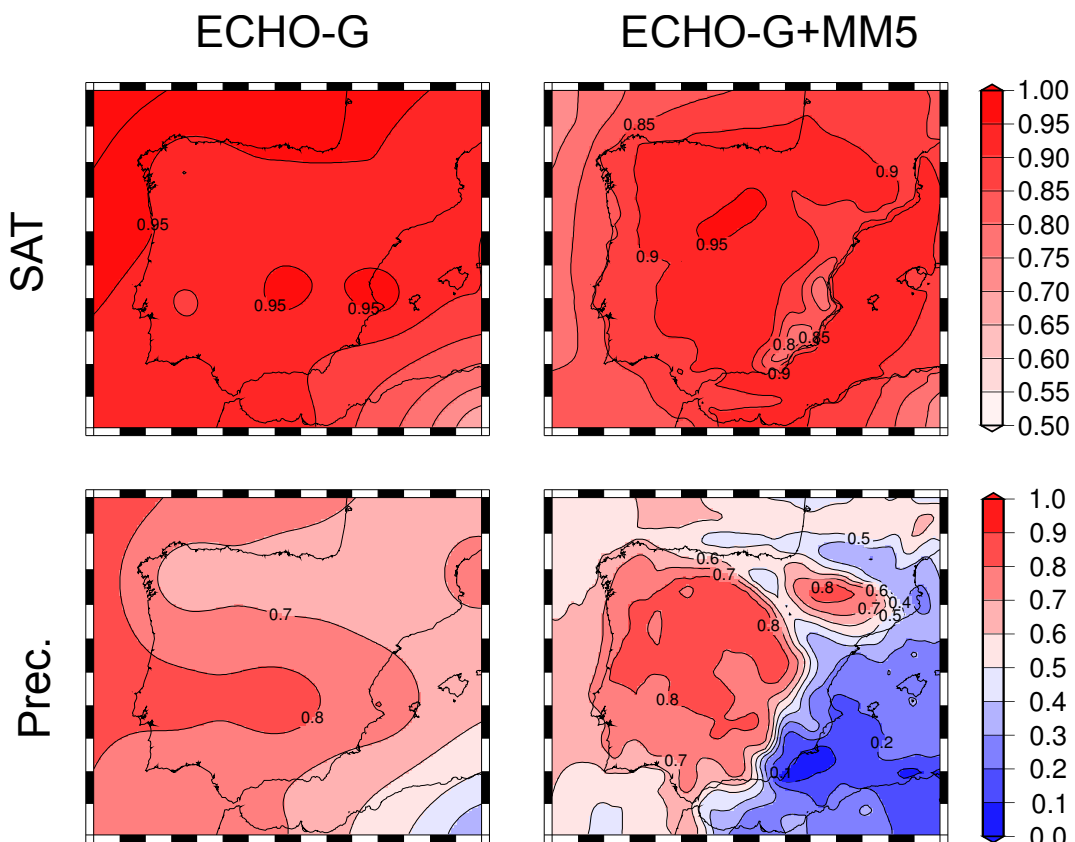


**Figure 2.14:** Top row: correlation between annual series of SAT in each grid point and the domain-averaged series corresponding to the ECHO-G (left column) and ECHO-G+MM5 (right column) simulations. Bottom row: the same calculation for precipitation. The correlation is calculated for the period 1001-1990, and the series have been low-frequency filtered to remove frequencies below  $0.3 \text{ yr}^{-1}$ .

G+MM5 simulation (blue line) and the corresponding reconstructions of SAT (Luterbacher et al., 2004) and precipitation (Pauling et al., 2006). As in Figure 2.11, the anomalies are calculated with respect to the period 1900-1990, but in this case ocean grid-cells of the model have not been considered to be consistent with the reconstructions. SAT winter series variability is similar, but it is higher in the simulation: standard deviation 0.27 and 0.20 in the model and the reconstruction, respectively. There is also a clear positive trend at the end of the period in both series, although in the model it begins around 50 years earlier. In general, the trends are larger in the model, which could be related to the fact that the model forcings do not include anthropogenic aerosols. In summer, reconstructions show less variability than the model (0.17 and 0.46, respectively), although the final trends are similar. The main difference is that, in both seasons, the model is between 0.5 and 1 °C colder than the reconstructions. The temporal agreement between model and reconstructions in the cold periods simulated by the model is not very good. In the columns 2 and 3 of Figure 2.12 we compare the winter and summer SAT anomalies for the Maunder minimum. Although the sign of the anomaly is the same, the reconstruction does not present the strong cold period in summer SAT as simulated by both models. There is a better agreement in winter in the intensity of this anomaly, although its spatial structure is also different.

Precipitation anomaly tends to be larger in the model than in the reconstructions in both season in the Northwest (see series in the middle panel in Figure 2.15). Variability of the 31-years running mean series of winter precipitation for the model and the reconstruction in the period 1500-1990 is similar for both the Northwestern (standard deviation 8.1 and 6.3 mm/month in the model and in the reconstruction, respectively) and Southeastern areas (standard deviation 3.0 and 2.2 mm/month in the model and in the reconstruction, respectively). There is also a good agreement in the upward final trend in the wet areas, where the precipitation variations are larger. Summer precipitation variability is nevertheless larger in the model in the wet area and lower in the dry area. The temporal agreement between the model and the reconstruction is also low. To illustrate these differences, in columns 2 and 3 of Figure 2.13 we compare the winter and summer precipitation anomalies for the Maunder minimum (1671-1700). The spatial structure of precipitation anomalies do not agree, and the mean values are also different (spatial-averaged anomalies of -4% and 22% in winter precipitation in the reconstructions and the model, respectively). In particular, the reconstruction shows a strong dry anomaly in the South in summer (decrease of precipitation up to 90%) that is opposite to the result obtained with the model.

However, with the information we have to date it is not easy to assess whether this mismatch is due to deficiencies of the reconstructions, of the model or of both. In ad-

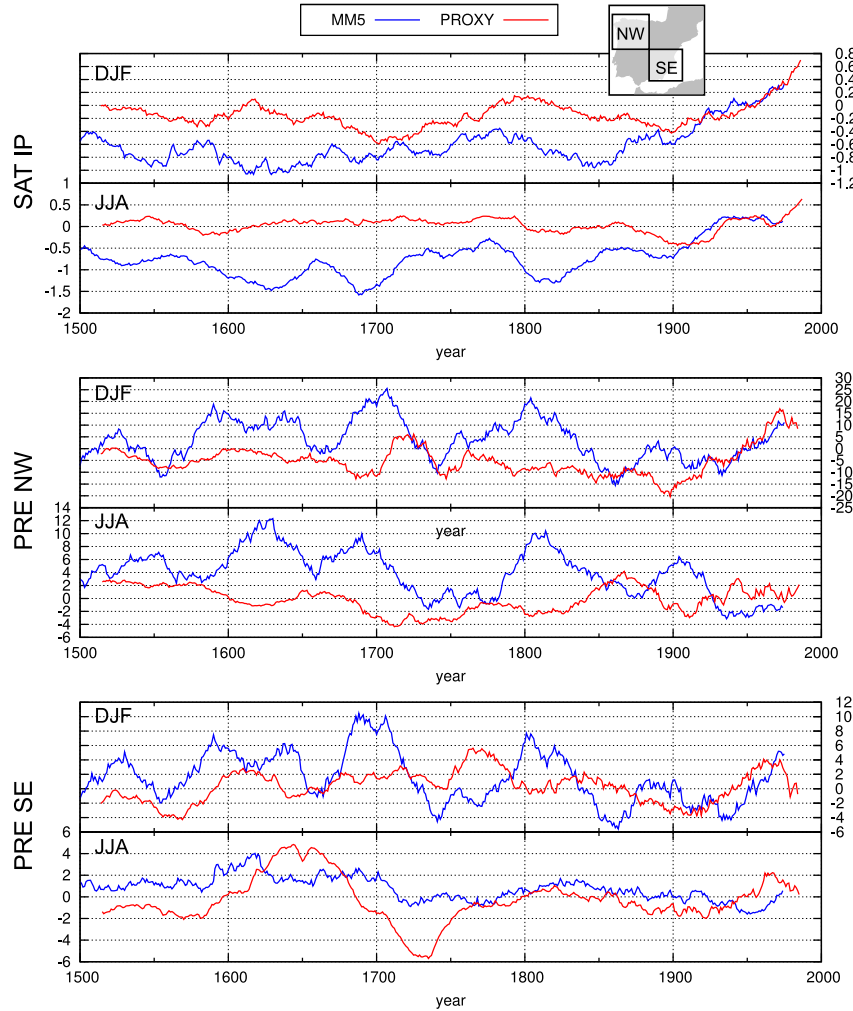


**Figure 2.15:** Anomaly series of SAT over the IP (upper panel, in  $^{\circ}\text{C}$ ) Northwest precipitation (middle panel, in mm/month) and Southeast precipitation (lower panel, in mm/month) in winter (DJF) and summer (JJA), respectively. The NW and SE subdomains are represented in the grey map in the top-right corner of the figure. Red line represents the series for the reconstructions and blue line for ECHO-G+MM5. Ocean grid-cells are excluded in the calculations. Anomalies are calculated with respect to the 1900-1990 period, and a 31-years running mean have been applied to all series.

dition, it is also possible and even probable that part of the variations in precipitation is caused internally and is not related to the external forcing. In that case, model and reconstructions should not necessarily agree. We have explored this possibility through the relations between NAO and precipitation. In section 3.4 we showed that MM5 is able to develop a realistic link between NAO and precipitation events over the IP. Figure 2.16a shows the precipitation anomaly series for the IP domain together with the NAO index simulated by ECHO-G+MM5 for the whole simulated period. We can appreciate how the Maunder minimum is characterised by the positive precipitation anomaly indicated above, and it can now be linked to the strong minimum in the NAO index. A similar behaviour can be found around the Dalton minimum. In fact, there is a clear anti-correlation between both series during all the simulation (the correlation coefficient between the NAO index and precipitation for the whole millennium is  $-0.84$ ).

Hence, according to Figure 2.16a, the positive precipitation anomaly during the Maunder minimum seems to be driven by a weaker NAO phase within the model. This allows us to test the precipitation reconstructions over the IP against independent reconstructions of the NAO index. The argument is as follows: we do not expect in general a good temporal agreement between the NAO index in the model and the reconstructions, since this circulation mode is strongly dominated by internal variability. Nevertheless the model is complex enough to simulate realistically the physical mechanisms which link the evolution of NAO and precipitation in the IP. Thus, if the NAO evolution in a given period in the model is by chance in phase with the evolution of the actual climate, the precipitation pattern developed by the model in that period would be a reliable version of the precipitation in the actual climate, and then it could be compared against reconstructions.

Figure 2.16b shows a NAO reconstruction performed by Luterbacher et al. (2002) (green line), together with the Pauling et al. (2006) precipitation series (blue line). These series show a realistic anti-correlation behaviour which is not surprising since they share some proxies and at some extent the NAO reconstructions includes precipitation proxies. In these reconstructions there is not such low NAO phase driving the strong positive precipitation anomalies, as it was observed in the simulation. Nevertheless there are large uncertainties in the evolution of NAO during the last millennium. To illustrate this, the recent NAO reconstruction by Trouet et al. (2009) is shown in the red line in the same figure. The Trouet et al. (2009) reconstruction is based on two proxy indicators, one of them also used by Luterbacher et al. (2002). However, there are large mismatches between them. In fact, the Trouet et al. (2009) record record is in slightly better agreement with the model evolution. In particular it exhibits a strong NAO index in the Medieval Warm Period which is weakened in the LIA. During the Maunder

Minimum it reaches a relative minimum, although it is not one of the strongest in the record, as is the case of the simulation. Nevertheless the agreement is low in general and rather inhomogeneous along the millennium.

Concluding, Figure 2.16 clearly illustrates how although NAO has a strong impact in precipitation events in the IP there are still large uncertainties in its evolution during the last millennium. Neither the model nor the different reconstructions agree in general. Although the model is able to develop a realistic link between NAO and precipitation, the evolution of this circulation mode is to a great extent dominated by variability, which makes the comparison with proxies difficult. In addition, since the proxy-based precipitation records discussed here show some skill (the Reduction of Error for the IP presented by [Pauling et al. \(2006\)](#) is positive, i.e. past winter precipitation estimates are better than climatology), to explain the differences between these reconstructions and the model will require further analysis.

## 2.5 Summary and Conclusions

The high spatial resolution simulation described in the previous sections represents an added value to previous paleosimulation performed with ECHO-G ([Zorita et al., 2005](#), and references herein). By means of a comparison with a dynamical downscaling performed with reanalysis data, MM5 was shown to be able to improve significantly the skill of ECHO-G in reproducing the observed climate in the IP in the 1961-1990 period. In particular, differences between climate developed in ERA40 and ECHO-G are larger than those for the corresponding regionalized data sets. Thus, the RCM narrows the differences between these two simulations. Furthermore, MM5 is able also to narrow differences between the climate developed by ECHO-G and the E-OBS data base. This supports the idea than the regionalization of a AOGCM paleosimulation may improve the quality of this model at regional scales. These improvements pertain to the modification of the seasonal variability, which is modified by MM5 bringing it closer to observations in the reference period. Nevertheless there are some differences in the simulations with respect to the observations in the reference period which are attributable to the inherent internal variability of the model, thus hampering the assessment of the skill of the model.

External forcings seem to have an important role in the simulation. There is a series of minima and maxima in the effective TSI that can be linked with corresponding cold/warm periods, and that match several known historical periods. In particular, the models are able to simulate the LIA and the Medieval Optimum as a direct response to radiation forcing. On the other hand, in the last 150 years of the 20th century there

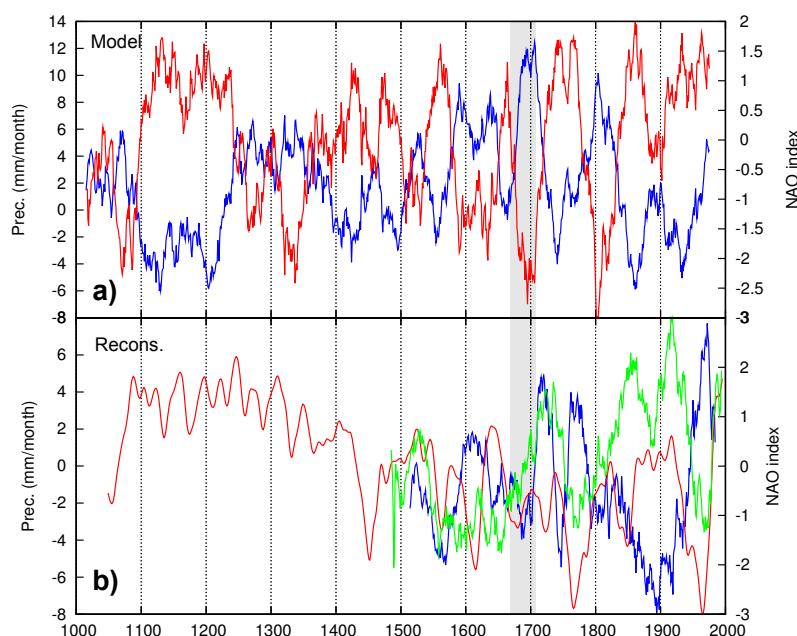


**Figure 2.16:** a) NAO index (red line) and precipitation (blue line) as simulated by ECHO-G+MM5 during the last millennium. b) NAO index as reconstructed by Luterbacher et al. (2002) (green line), by Trouet et al. (2009) (red line), and Pauling et al. (2006) precipitation series (blue line). All anomalies are calculated respect to the period 1900-1990 and averaged for the IP. Green line has been smoothed through a low-pass filter, meanwhile the rest of the series have been smoothed through a running mean of 31 years. Grey bar indicates the Maunder Minimum period discussed in the text.

is an increase of the temperature, which seems to be linked to the continuous rise of GHGs concentrations characteristic of the industrial period. There are nevertheless some cold minima that can not be explained by the external forcings, for instance in the period 1600-1620. This minimum seems to be caused by the internal characteristic variability of the AOGCM. If this is the case, this introduces an important uncertainty factor, since the amplitude of the internal variability could in principle even explain all the simulated minimum at this regional scales. This amplitude could be better estimated downscaling the control run with ECHO-G, using an ensemble of simulations using different AOGCMs, or even using the same AOGCM with different initial conditions. This avenue will be explored in future studies.

Although domain-averaged values of SAT and precipitation in the RCM simulation are very similar to those of the AOGCM in the same area, some important differences appear at regional scales. These can be more clearly found in the high-frequency evolution of the regional climate, or in the shape and intensity of SAT and precipitation anomaly patterns in a given period. For example, MM5 simulates a precipitation anomaly pattern in the Maunder minimum which is qualitatively different to that simulated by ECHO-G. In general, the differences introduced by the RCM are less noticeable for SAT than for precipitation, which is more strongly modified by the coarse resolution of the AOGCM. These differences introduced by the RCM may have an important impact in the inter comparison exercises between proxy-based reconstructions and model simulations.

We have compared the results of the model simulation with the SAT and precipitation reconstruction of Luterbacher et al. (2004) and Pauling et al. (2006) over the Iberian Peninsula, respectively. The model results tend to be colder than the reconstruction, more noticeably in the LIA. Winter SAT variability is similar, although the model overestimates it. However, in summer the reconstruction depicts clearly less variability. There is a relatively good agreement in the final trend in the 20th century. Precipitation series show similar variability in the model and in the reconstructions, although the correlation between both is low. In particular, the positive anomaly in precipitation simulated by the model does not seem to reproduce the reconstruction in the past centuries.

Overall, the high-resolution information added by MM5 to the ECHO-G simulation does not tend to narrow differences between the models and the reconstructions, specially for precipitation. Instead, MM5 is able to add high-resolution details to the AOGCM simulation, but following in general terms the path of the AOGCM which drives the simulation, especially in winter when the regional climate within the considered domain is more strongly governed by synoptic conditions. It is important to note that the RCM should narrow differences with reconstructions only in the case that the

RCM significantly reduces errors of ECHO-G in the last millennium and also in the case that the reconstructions employed here realistically represent the actual evolution of the past climate. Hence, we find that one of these conditions (or maybe both) is not met. In any case, the added value of the RCM is that it is able to simulate a physically consistent climate which takes into account the characteristics due to high resolution orographic features over the Iberian Peninsula. The simulated high-resolution, physically consistent, climate can be used to test some aspect of the reconstructions, such as variability of the series (which is a measure of the sensitivity of the climate to external forcings and its internal variability at regional scale), as well as test physical relationships between variables such as the link between large circulation modes and local events. This kind of questions can hardly be addressed within an AOGCM.

An important part of the disagreement between the simulated and reconstructed precipitation can be attributed internal variability in the model through the evolution of NAO in the model, although a complete explanation will require further analysis. This disagreement is important because it can be carried further to place confidence in the simulations of future climate in the Iberian Peninsula and the Mediterranean region in general. Climate projections indicate a strong decrease of precipitation in this region ([Giorgi and Bi, 2005](#)) with a high level of agreement across the suite of IPCC models ([IPCC, 2007b](#)). The ECHO-G model, also included in the IPCC suite, also simulates strong decreases of winter precipitation in the future under increasing concentrations of greenhouse gases. If the sign of the simulated precipitation changes disagrees with that of the reconstructions, the confidence placed on the future projections at regional scales would be compromised. However it is important to note that this argument depends on the kind of response of the climate to external forcing. In climate change projections, the magnitude of the external forcing lies outside anything that has been seen in the last millennium, and the response to the climate to this forcing can not be expected to be linear in general.

As future work, further intercomparisons between the the RCM simulation and newer proxy-based reconstructions that are being developed at this moment in the IP will be performed in order to validate more aspects of the simulation. On the other hand, more regional simulations will be carried out using different AOGCM simulations. The aim of these ensemble of simulations is to evaluate the importance of the internal variability of the AOGCM driving the simulation, and trying to separate its effect from the impact of the external forcings.

Chapter **3**

## Internal and external variability in regional simulations of the climate of the Iberian Peninsula over the last millennium

In this study we analyse the role of internal variability in regional climate simulations through a comparison of two regional paleoclimate simulations for the last millennium. They share the same external forcings and model configuration, differing only in the initial condition used to run the driving global model simulation. A comparison of these simulations allows us to study the role of internal variability in climate models at regional scales, and how it affects the long-term evolution of climate variables such as temperature and precipitation. The results indicate that, although temperature is homogeneously sensitive to the effect of external forcings, the evolution of precipitation is more strongly governed by random unpredictable internal dynamics. There are however some areas where the role of internal variability is lower than expected, allowing precipitation to respond to the external forcings. In this respect, we explore the underlying physical mechanisms responsible for it. This study identifies areas, depending on the season, in which a direct comparison between model simulations of precipitation and climate reconstructions would be meaningful, but also other areas where good agreement between them should not be expected even if both are perfect.

### 3.1 Introduction

The climate system fluctuates naturally over a large frequency range, from days to millions of years (Huybers and Curry, 2006). This variability is the combination of an undetermined level internal variability superimposed to the net effect of a number of external forcings. Some of these forcings have a natural origin, such as changes in the solar irradiance or the radiative effect of big volcano events, whereas others have an anthropogenic cause, like land use changes or the emission of greenhouse gases and aerosols to the atmosphere during the Industrial Era (Crowley, 2000; Stott, 2003).

In the context of anthropogenic climate change, it is important to have available reliable estimations of the amplitude of natural variability on multidecadal timescales and at regional spatial scales, since this variability may hinder the attribution of trends observed to the anthropogenic forcing. In this respect, recent detection and attribution studies (Hegerl et al., 2011) have shown the fingerprint of external forcings in the temperature evolution of climate at continental scale during the last millennium. This kind of detection and attribution exercises require long historical records of climate variability. However, observations are too short to reliably assess multidecadal or even centennial climate variations, and therefore the analysis of past climate is a valuable tool in the estimation of the amplitude of climate variability and its mechanisms.

The efforts to assess the role of natural variability in climate evolution belong to two categories: climate reconstructions based on proxy indicators and climate model simulations. Comparing both approaches is important to identify systematic errors in simulations, as well as drawbacks in the methodologies used in reconstructions (González-Rouco et al., 2009). In particular, the validation of climate models in a past climate context may increase the confidence placed in climate change projections. Nevertheless several limitations arise when comparing results from models and reconstructions.

One drawback is the scale gap between both approaches. Although the use of comprehensive atmosphere-ocean global circulation models (AOGCMs) has become possible due to the impressive increase in computational power (Zorita et al., 2005; Tett et al., 2007; Ammann et al., 2007; Swingedouw et al., 2010; Jungclaus et al., 2010, among others), their spatial resolution is still too coarse to take into account the regional climate features caused by fine orographic details. Climate reconstructions are thought very sensitive to these details, which are implicit in the information extracted from the proxies. This scale gap may be bridged using Regional Circulation Models (RCMs), which simulate the climate system for a limited domain (Kittel et al., 1998; Jerez et al., 2010, among others). This downscaling approach is commonly used in climate change projections (Jacob et al., 2007; Déqué et al., 2007; Gómez-Navarro et al.,

2010, among many others), but fewer studies exists nowadays focusing on the applications of RCMs in a paleoclimate context, partly due to the large computational cost involved (Diffenbaugh and Sloan, 2004; Zorita et al., 2010; Strandberg et al., 2011). In particular, most regional simulations available to date are too short to address the role of internal variability, or although long, they do not consider different runs (Gómez-Navarro et al., 2011a).

Another important limitation in the model-proxy comparison is the inherent internal variability of climate models. Just as the actual climate, the models are affected by a strong chaotic internal variability over a broad band of time scales. This implies that a complete agreement at interannual timescales should not be expected when comparing the temporal evolution of model simulations and reconstructions, even if both are perfect (Yoshimori et al., 2005). Several studies have previously analyzed the role of internal variability in climate simulations. Goosse et al. (2005) used an intermediate complexity model to perform 25 simulations of the last millennium. These simulations shared the same external forcings, only differing in their initial condition. This ensemble allowed them to detect the fingerprint of climate forcings in the long-term evolution of temperature at hemispheric and continental scale. However, they found that the role of internal variability becomes greater at regional and interannual timescales. Similarly, Servonnat et al. (2010) used an AOGCM to analyse the role of external forcings against internal variability, focusing on the evolution of surface temperature. They also pointed out the greater role of internal variability at regional scales, which may blur the effect of external forcings at sub-continental scale. However, due to the large computational cost involved, most studies so far do not consider the use of downscaling techniques to analyse explicitly the role of internal variability at regional scales, despite that climate proxies contain important information at these scales. The fingerprint of the forcings in precipitation is other aspect which is seldomly considered in the bibliography.

Thus, in this study we present a comparison of two simulations performed with a climate version of the mesoscale model MM5 driven by the AOGCM ECHO-G over the last millennium (1001-1990) for a domain encompassing the Iberian Peninsula (IP). The model configuration and the external forcings are the same in both simulations. The only difference lies on the initial condition used to run the two simulations in the global model, and thus these experiments allow us to investigate the role of external forcing in the evolution of several climate variables, not only temperature, compared to the magnitude of the internal variability of the model at regional scale. In particular, we focus on the evolution of near-surface air temperature (SAT) and precipitation (PRE) in winter (mean of December-January-February) and summer (mean of June-July-August).

### 3.2 Description of the simulations

The global model ECHO-G driving the RCM consists of the spectral atmospheric model ECHAM4 coupled to the ocean model HOPE-G (Legutke and Voss, 1999). The model ECHAM4 was used with a horizontal resolution T30 ( $\sim 3.75^\circ \times 3.75^\circ$ ) and 19 vertical levels. The horizontal resolution of the ocean model is approximately  $2.8^\circ \times 2.8^\circ$ , with a grid refinement in the tropical regions and 20 vertical levels. Two simulations were performed with this model configuration, both driven by the same reconstructions of several external forcings, which are depicted in the first two panels of Figure 3.1. Cyan, pink and grey lines represent the evolution of atmospheric carbon dioxide, nitrous oxide and methane, respectively. The orange line represents the reconstruction employed for the variability of the total solar irradiance (TSI). Black lines show the estimated equivalent reduction in solar irradiance at the top of the atmosphere caused by volcanic eruptions. The sum of both lines is the effective solar irradiance, which is implemented in the model to take into account both sources of short-wave external forcing. The two simulations (hereafter referred as ERIK1 and ERIK2) cover the last millennium almost entirely only differing in their initial condition (ERIK2 starts from a colder climate state). A full description of these simulations can be found in González-Rouco et al. (2003); Zorita et al. (2005) and references therein.

The RCM used to downscale the two AOGCM simulations is a climate version of the Fifth-generation Pennsylvania-State University-National Center for Atmospheric Research Mesoscale Model (Dudhia, 1993; Grell et al., 1994b; Montávez et al., 2006; Gómez-Navarro et al., 2010). A double-nesting scheme was implemented, with a lower-resolution (90 km) outer domain, covering Western Europe, and a higher-resolution (30 km) inner domain covering the IP. Both domains are two-way coupled between them, whereas the RCM is one-way coupled to the driving GCM. These domains, as well as the chosen physical parametrisation, are the same as those previously described by Gómez-Navarro et al. (2011a). The regional simulations have been driven with exactly the same external forcing reconstructions as in the global model simulations to avoid physical inconsistencies. The two downscaled simulations, which cover the period 1001–1990, will be referred hereafter as MM5-ERIK1 and MM5-ERIK2, respectively.

Here we analyse the role of internal variability at regional scales through a model-model comparison. Thus, the evaluation of the model skill in reproducing observations or climate reconstructions is beyond the scope of the present study. For a full description of the capabilities of this model configuration to reproduce a realistic climate over the IP, the reader is referred to (Gómez-Navarro et al., 2011a).

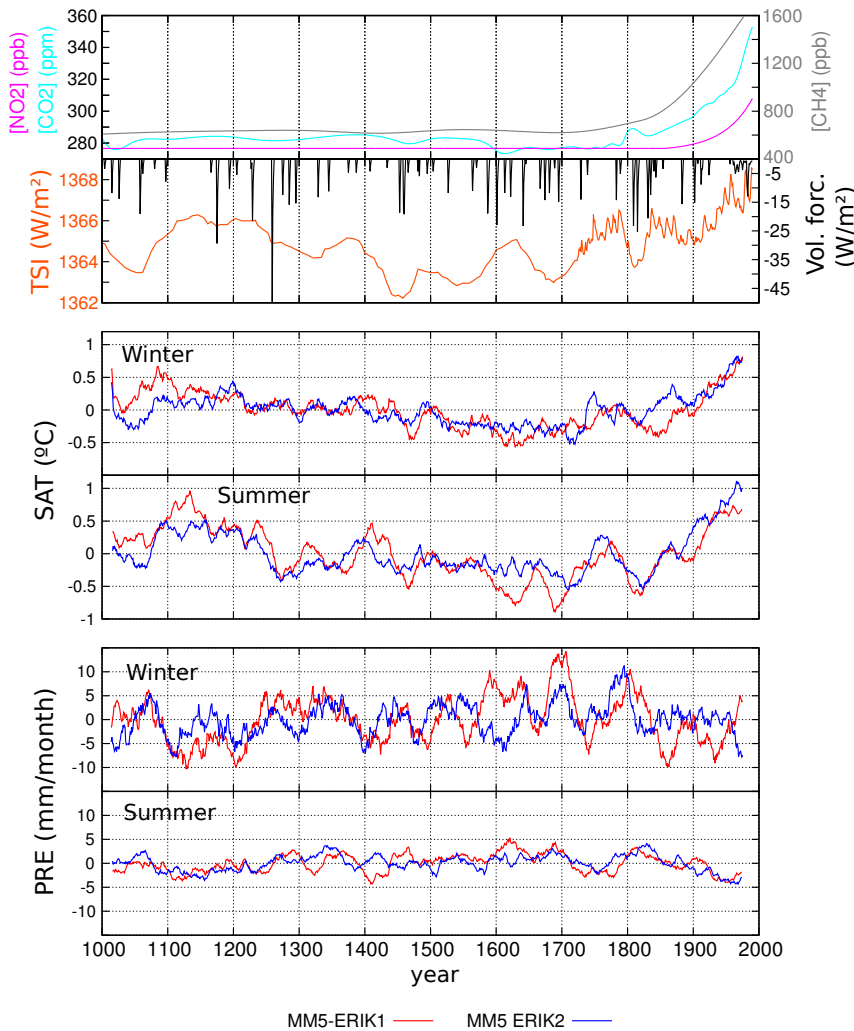


**Figure 3.1:** Evolution of the external forcings (first two panels), spatial average of SAT (two middle panels) and PRE (bottom panels) anomalies for winter (December–February) and summer (June–August). The MM5-ERIK1 and MM5-ERIK2 experiments are coloured red and blue, respectively. The eight series have been smoothed with a running mean of 31 years, and the same vertical scale has been applied to both seasons to emphasise their different variability.

### 3.3 Results

#### 3.3.1 Correlation as a measure of internal variability

Figure 3.1 depicts the evolution of the anomalies in SAT and PRE in winter and summer averaged over the IP in the two RCM simulations. The eight series have been smoothed with a 31 years running mean in order to filter out the high frequency signal and highlight the low-frequency variability. In the SAT series we can easily identify three main periods: a warm initial condition up to roughly 1400, followed by a long cold period which finishes around 1850 reverting to a stronger trend towards a warmer climate. These periods match the already known characteristic periods in the last millennium such as the Medieval Climate Anomaly, the Little Ice Age and the warmth of the Industrial Era. In particular, there are some noticeable cold periods such as the Spörer Minimum (around 1450), the Maunder Minimum (around 1700) and the Dalton Minimum (around 1810) which can be identified in the SAT series and are associated with a simultaneous reduction in the TSI and volcanic activity. The final trend can be linked to an increase in the TSI, but also with the large increase in GHG concentrations. In general terms, the impact of the external forcing in these cold periods seems to be more relevant in summer in both simulations, which show similar characteristics in terms of variability and temporal evolution.

The fingerprint of the forcings in the evolution of precipitation is however less apparent. Other than a slight decrease in precipitation, more noticeable in summer, since 1800 to the end of the simulation, it is not easy to identify the impact of external forcings on precipitation. Further, although the variability depicted by both simulations is similar in both seasons, their temporal agreement is lower than in the case of SAT, suggesting a stronger independence of precipitation of the external forcings. The variability of winter precipitation is stronger, as it corresponds to wetter conditions in this season in the IP, a feature correctly reproduced by both simulations.

Careful comparison of these two millennial simulation allows the study of the internal variability by quantifying the signal-to-noise ratio. This can be assessed through the calculation of the correlation of the temporal series associated to several variables in the two experiments. A simple conceptual model of the evolution of a climate variable that is partially driven by the external forcing may illustrate this point. The variable can be considered as a combination of the external forcing plus a contribution of noise due to the inherent chaotic nature of the simulation:

$$T = \alpha W + f \quad (3.1)$$

where  $T$  is the variable of interest,  $\alpha$  is a proportionality constant,  $f$  is the direct effect

of the external forcing in the variable and  $W$  is a normalised random variable representing internal variability, which is uncorrelated with the forcing. If we now perform several identical simulations, only differing in the initial conditions, we have several variables  $T_i$ . The point here is that random noise prevents correlation between these variables from being perfect. Instead, the correlation between these variables can be depicted as:

$$\text{cor}(T_i, T_j) = \frac{\text{Var}(f)}{\text{Var}(f) + \alpha^2} \quad (3.2)$$

where the variance of the variable is assumed to be the same in all the experiments (i.e.  $\text{Var}(T_i) = \text{Var}(T_j)$ ,  $\forall i, j$ ) and  $W$  and  $f$  are uncorrelated. Hence, according to the last equation, if forcing plays a strong role in the evolution of  $T$ ,  $\alpha$  can be considered negligible and the correlation is close to one. On the other hand, if the evolution of the variable depends strongly on the internal variability ( $\alpha$  is large), the right term in Eq. 3.2 becomes small and the evolution of the variable is not correlated between the different experiments. Thus, the correlation gives a quantitative measure of the relative role of internal variability in the evolution the different variables of the simulation, a parameter that will be used in the next section.

It is important to note nonetheless that the influence of the external forcing detected in this way may be dependent on the time scale, season and area. This is due to the different amplitude of internal variability, from daily to interdecadal, and to the amplitude of the external forcing at different time scales. In this study we have performed an analysis using different running means with increasing time intervals, in an attempt to identify the temporal scales at which the signal-to-noise ratio is stronger. Low-pass Fourier filters have also been employed to retain the low-frequency variability, which is more clearly governed by external forcings.

Another important aspect to consider is what correlation limit can be safely considered as statistically significant. Indeed, the running mean (or the Fourier filters) we apply to smooth the series introduces an artificial autocorrelation which could affect the calculations of correlation and overestimate its significance. Thus, the estimation of the confidence interval has to take into account this fact. We use a statistical test which calculates the correlation threshold numerically (Ebisuzaki, 1997), taking into account explicitly the artificial autocorrelation structure introduced in the smoothing process we apply to the series.

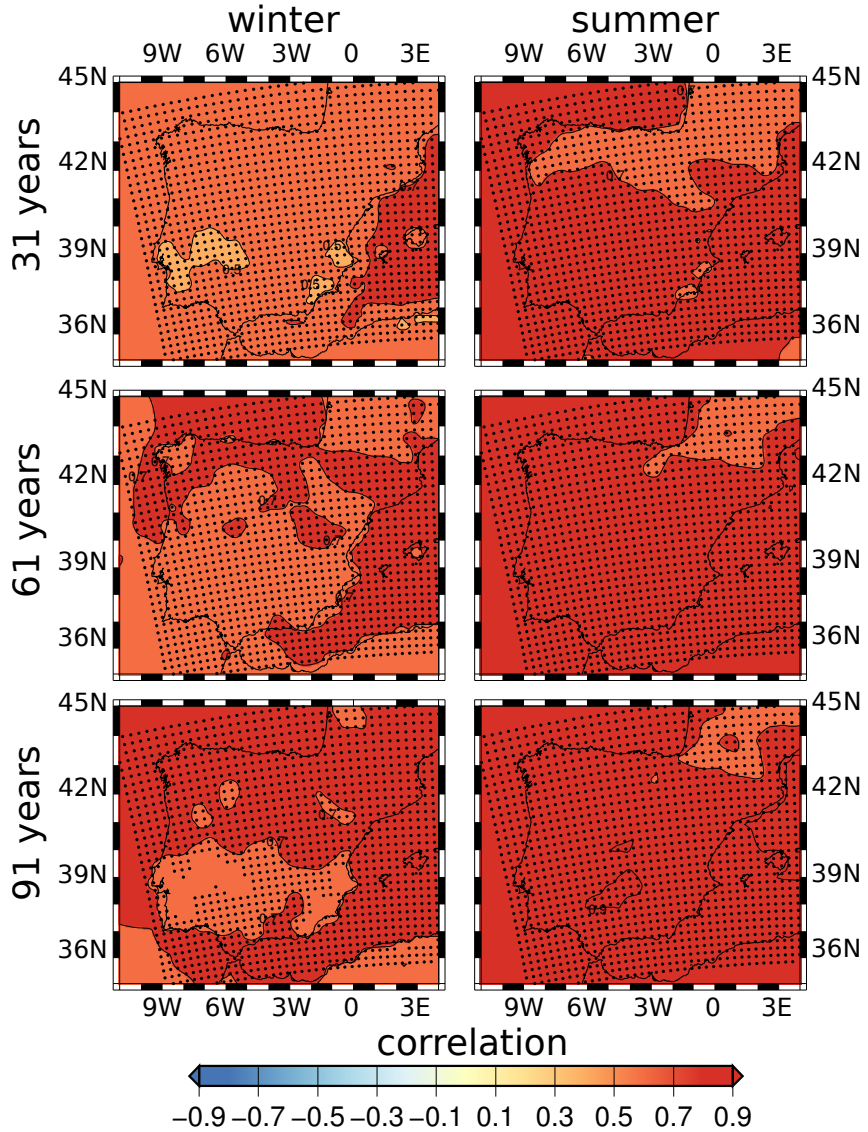


**Figure 3.2:** Correlation map of SAT series in winter (December–February, left column) and summer (June–August, right column) between the MM5-ERIK1 and MM5-ERIK2 experiments. The three rows represent the correlations calculated with the series smoothed by a running mean filter of 31 (top), 61 (middle) and 91 (bottom) years, respectively. Black circles denote grid points where the correlation is significant at the 95% confidence level according to a bootstrap method (Ebisuzaki, 1997).

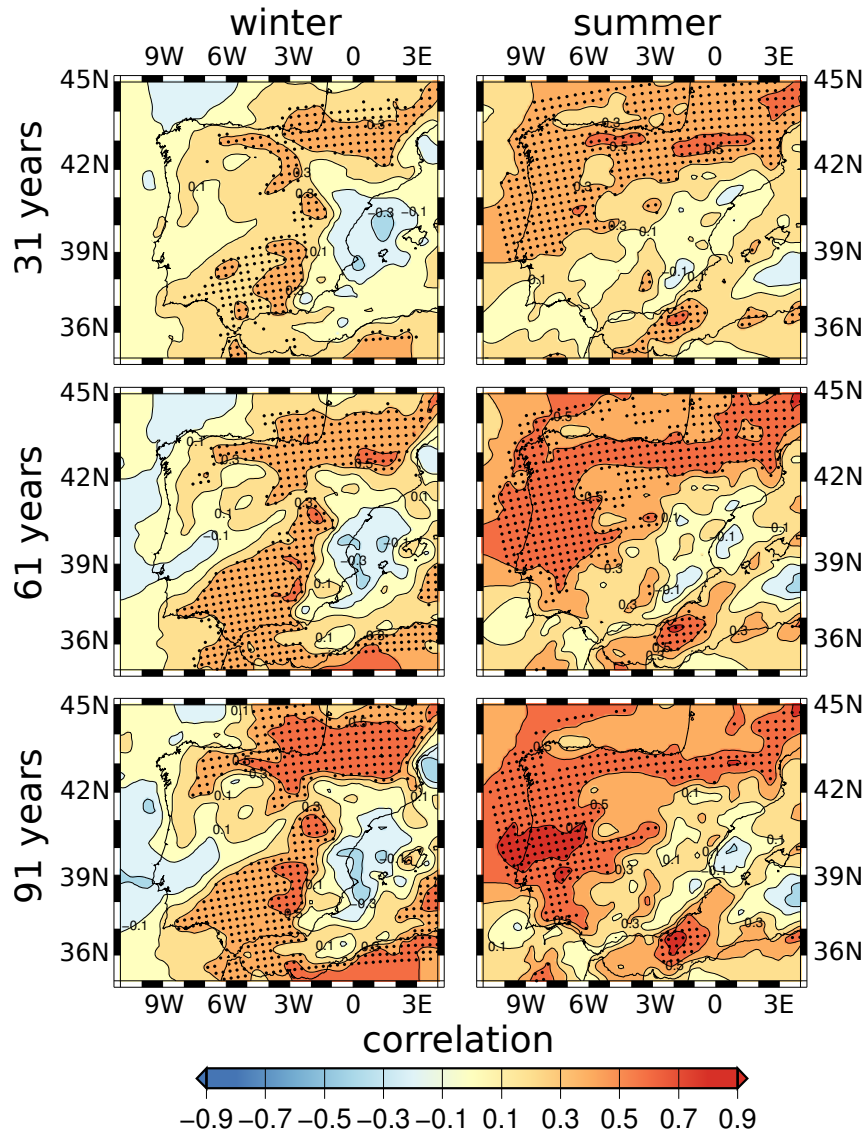
### 3.3.2 Forced vs. unforced evolution of temperature and precipitation

Figure 3.2 depicts the spatial distribution of the correlation between the SAT series simulated in the MM5-ERIK1 and MM5-ERIK2 experiments, both smoothed using three different running means. The evolution of this variable in the two experiments is highly correlated in both seasons (black circle denotes grid points where the correlation is significant at the 95% confidence level according to a bootstrap method (Ebisuzaki, 1997)), and it is quite steady over the domain. Correlation in summer is slightly stronger, and in both seasons tends to be somewhat greater when a stronger smoothing is applied. It is interesting to note that the spatial structure of the correlation is different in winter and summer, with stronger correlations in the southern part of the IP in summer, and stronger correlations in the north in winter. There are hardly any changes when different running means are applied. The main conclusion we can derive from this figure is that the evolution of SAT seems to be dependent on the evolution of the external forcings, and this result is valid everywhere in the IP. This result is quite reasonable, since near-surface temperature should be physically strongly modulated by the external forcing. The magnitude of the correlation is essentially independent of the degree of smoothing, which may be interpreted as the fact that the strongest influence of the external forcing is already attained at the smallest time scale probed here.

Similarly, Figure 3.3 depicts the same information for precipitation. In this case the correlation is in general lower, and, in some cases, even negative. There are, however, some well defined areas where this variable still exhibits a high and statistically significant correlation between experiments (denoted with a black circles, as in Figure 3.2). As in Figure 3.2, the correlation structure is different in winter and summer, and given a season, it hardly changes when a stronger smoothing is applied. In winter, the areas which most clearly respond to the forcings are the northeast of the IP and the main mountain systems such as the Pyrenees, and the Iberian and Betic systems. Conversely, the sensitive areas in summer are located in the west and north of the IP, and show no clear influence of the orographic features of the domain. We discuss a possible physical explanation for these patterns in the next subsection.

Given the length of the simulations, we have tried another test to evaluate the significance of the correlations. We divided the 990-year long series in two subseries of 495 years. We calculated the same correlations as in Figures 3.2 and 3.3 in the two periods, to check whether they are period-dependent. We found that the correlation patterns hardly change in different periods (not shown), which further suggests that the correlations found have a physical meaning, rather than just being a statistical artifact.

When we further analysed the significance of the correlations calculated in the for-



**Figure 3.3:** Correlation map of precipitation series in winter (December–February, left column) and summer (June–August, right column) between the MM5-ERIK1 and MM5-ERIK2 experiments. The three rows represent the correlations performed with the series smoothed through a running mean of 31 (top), 61 (middle) and 91 (bottom) years, respectively. Black circles denote grid points where the correlation is significant at the 95% confidence level according to a bootstrap method (Ebisuzaki, 1997).

mer section and their relationship with the smoothing applied to the series in Figure 3.4, the mean correlation for SAT was above a 95% confidence interval in both seasons and for all the tested running means, although in winter it tends to be slightly lower. The resemblance between series increases with longer smoothing, but it saturates around 50 years. The limit for the confidence interval increases monotonically with longer smoothing, and is greater for summer, when correlations are also higher. Apart from the non-smoothed series of winter temperature, nearly all grid points exhibit a correlation above the 95% confidence level, supporting our previous interpretation on the importance of the external forcings in the evolution of SAT in the IP during the last millennium.

From a regional modelling perspective, the results for precipitation are especially interesting. Figure 3.4 illustrates how the correlations for this variable are, on average, below the confidence level. Nevertheless, as mentioned above, there are areas where the correlation is still high. The dashed bar represents the percentage of grid points in the domain where the correlation is significant at the 95% confidence level, and Figure 3.3 allows their identification in different seasons. It is in these areas where the forcings plays an important role in the evolution of precipitation. They can only be identified through the use of a high resolution model, since the average spatial process dilutes the statistical confidence, as Figure 3.4 clearly illustrates. Another important aspect of these calculations is that they demonstrate that, although the correlation between experiments tends to be higher when longer smoothing is applied, the threshold for statistical significance is also larger, so that the number of grid points which show a significant correlation does not increase monotonically.

### 3.3.3 Physical meaning of the correlations

Although statistical significance is a necessary condition, it is not sufficient to assert that there is a causal relationship between the long-term evolution of forcings and SAT and PRE. The physical link between forcing and temperature is straightforward: the stronger the external radiative forcing, the higher the temperature. It depends neither on regional features nor on the season. The correlation map at global scale (not shown) between the external forcings and SAT is homogeneously positive over most of the globe, independent of the season, and it is similar in magnitude to that shown in Figure 3.2 for the IP.

However, the link between forcing and precipitation is less obvious. In principle, higher temperatures tend to increase the evaporation, and hence the moisture content of the atmosphere. However, higher temperatures would tend to reduce the relative

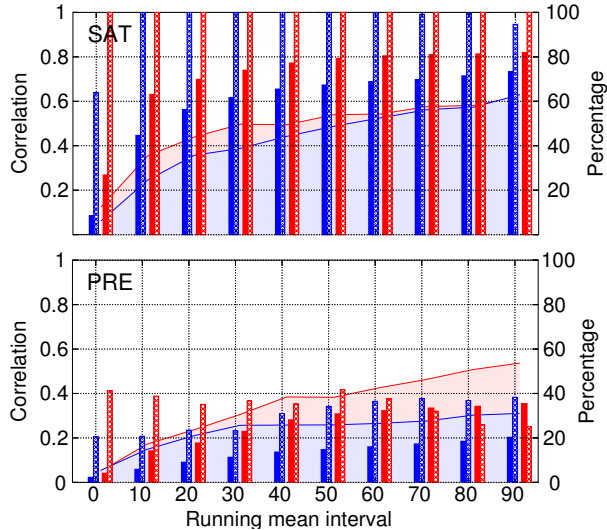


**Figure 3.4:** Significance of the correlations between the MM5-ERIK1 and MM5-ERIK2 series of SAT (top panel) and PRE (bottom panel) when using different running means to filter out the high frequency signal. Blue (red) color represents the results for December–February (June–August). The shaded area for each variable is the threshold for the correlation at the 95% confidence level, obtained through a bootstrap method (Ebisuzaki, 1997). Solid bars represent the mean correlation for the domain, whereas dashed bars represents the percentage of grid points in the domain which show a significant correlation.

humidity for a given level of moisture, which tends to diminish the cloud cover and precipitation. The net result may depend on the regional features, the large-scale circulation or the season. In fact, we found that the large-scale correlation between forcings and precipitation shows no clear homogeneous signal over the global (not shown), as in the case of SAT. Thus, the net effect of higher/lower forcings is dependent on other indirect factors such as modifications in the local circulation or the interaction with the orography. In addition, this relationship strongly depends on the season, as illustrated by Figure 3.3. For this reason, we have investigated the physical mechanism linking the evolution of precipitation and forcing separately for winter and summer, and focusing only in the IP, since in other areas it could be different. In the remaining part of this section we focus on the low-frequency variations, since they show a larger signal-to-noise ratio. To do so, we use a simple low-pass Fourier filter which eliminates the variability timescales shorter than 50 years. We analyse the low-frequency variations of SAT and PRE, separately, through an Empirical Orthogonal Function (EOF) analysis

(Hannachi et al., 2007), a methodology that reduces the high dimensionality of complex phenomena, such as climate, and has been used in other studies regarding long regional climate simulations (Gómez-Navarro et al., 2010). Finally, since we are interested in the variations relative to the mean state, and the precipitation over the IP is strongly heterogeneous (Serrano et al., 1999), we have used standardised precipitation series to avoid an over-representation of the wettest areas in the northwest of the IP. Hence, all EOF maps shown here are dimensionless.

The first EOF of the normalised low-frequency variations of SAT and PRE in summer in the experiment MM5-ERIK2 are shown in Figures 3.5a and 3.5b and explain 89% and 44% of the variance, respectively. The corresponding figures for MM5-ERIK1 are very similar and are not shown here. The associated Principal Components (PCs) for the two variables and experiments are shown in 3.5d, together with the external forcings. The close relationship between the evolution of SAT and PRE is apparent in the two simulations. The correlation between the PCs of SAT and PRE is 0.82 and 0.79 for the MM5-ERIK1 and MM5-ERIK2, respectively. Figure 3.5c shows the correlation map between the low-frequency evolution of the two variables for MM5-ERIK2 (the corresponding map for MM5-ERIK1 is similar and has also been omitted), and independently illustrates the close link between the two variables. The resemblance between the maps in Figures 3.5b and 3.5c can be better understood by looking at the PCs. The low-frequency variations of SAT are dominated by a spatially homogeneous EOF whereas the variations of precipitation display several spatial characteristics. The strong correlation between the PCs, as well as the high percentage of variance that the first EOF for each variable explains, drive the clear correlation between these variables and their spatial structure.

On the other hand, the correlations between the PCs of the two experiments are 0.81 and 0.34 for SAT and PRE, respectively. This is in good agreement with our previous finding of a stronger influence of the external forcings in the evolution of SAT than in the case of PRE. In addition, the similarity between the map in Figure 3.5c (or Figure 3.5b) and correlation maps in Figure 3.3 for summer is clear. Again, the explanation for the structure and intensity of these correlation patterns is better sought in the EOF analysis. The homogeneous first EOF together with the large amount of variability it explains and the large correlation between the associated PCs, force a high and homogeneous correlation between the SAT in the two experiments. On the contrary, the lower correlation between PCs associated with the evolution of precipitation in the two experiments precludes strong coupling between them. Despite this, the shape of the main variability mode is similar in the two simulations, and the correlation between both PCs is not negligible (0.35, statistically significant), which explains why the areas

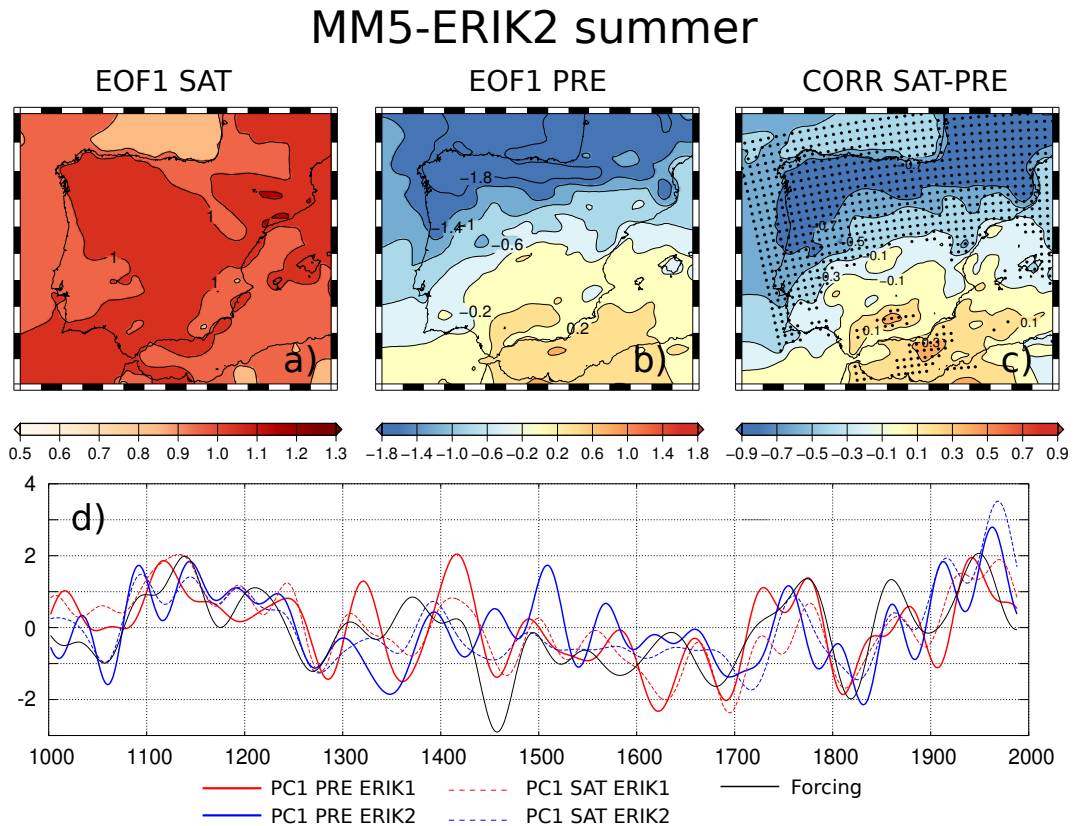


**Figure 3.5:** Evolution of the summer (June-August) SAT and PRE during the last millennium in the two simulations. The three top maps show the first EOF of the standardised SAT (Fig. a) and PRE (Fig. b), as well as the correlation between these two variables (Fig. c). All maps are dimensionless, and correspond to the MM5-ERIK2 experiment, since the corresponding maps for MM5-ERIK1 are very similar (not shown). Fig. d shows the normalised PCs associated with the two variables in the two experiments, as well as the external radiative forcing. All calculations were performed with the smoothed low-frequency series. Black circles denote grid points where the correlation is significant at the 95% confidence level according to a bootstrap method (Ebisuzaki, 1997).

most affected by this pattern stand out in the correlation maps of Figure 3.3.

Having identified that the response to the forcing in summer precipitation over the IP is due to the main variability mode, which has the same spatial structure and is clearly correlated in the two simulations, we sought the physical mechanism behind this link. First, we separately considered large-scale and convective precipitation. The correlation maps equivalent to those shown in Figure 3.3 for convective precipitation alone, depict very low values and no spatial structure, whereas the maps corresponding to large-scale precipitation look very similar to those in Figure 3.3 (not shown). This suggests that the response to forcing is in the large-scale field, in particular in the response of regional circulation to external forcings. To confirm this, Figure 3.6a shows the correlation between the low-frequency filtered series of external forcings and SLP for summer in the ERIK1 experiment (the map corresponding to ERIK2, not shown, exhibits the same pattern and supports the same physical explanation). We show the calculations in the AOGCM fields since this area lies outside the domain simulated by the RCM, and, in any case, the differences between the RCM and the AOGCM in the SLP field are small. This figure shows how the local circulation is affected by the driving forcings. In particular the strengthening of the Azores high reduces the large-scale precipitation over the northwest, whereas the low over Morocco has the opposite effect and is responsible for the simultaneous increase of precipitation in the southeast of the IP and over the Mediterranean Sea, which is precisely the shape of the first EOF shown in Figure 3.5b.

We analyzed the correlation pattern depicted in Figure 3.6a. It is closely related to the leading variability mode of simulated summer SLP, extracted through EOF analysis. In fact, the spatial correlation between the first EOF and the correlation pattern in Figure 3.6a is 0.68, whereas the percentage of variance explained by these patterns are 35% and 24%, respectively. This variability mode is not only present in the simulation, but also contributes significantly to variability in observations. Indeed, we found that the percentage of variance explained by this pattern in an observational dataset for SLP in summer for the 20th century (Trenberth and Paolino, 1980) is up to 18%. To show at what extent this pattern is sensible to forcings, we have projected this pattern onto the SLP field, considering not only the 990-years simulation, but also including a continuation of the ERIK1 simulation under the SRES scenario A2 of the 4th IPCC. This calculation defines a time series of the intensity of this mode through the simulation. This series is shown in Figure 3.6b, together with the 31-year running mean (the index corresponding to the projection of the correlation pattern onto observations in the 20th century is also shown in green for comparison). It becomes clearly stronger under the climate change projection, when the external forcings is specially intense,

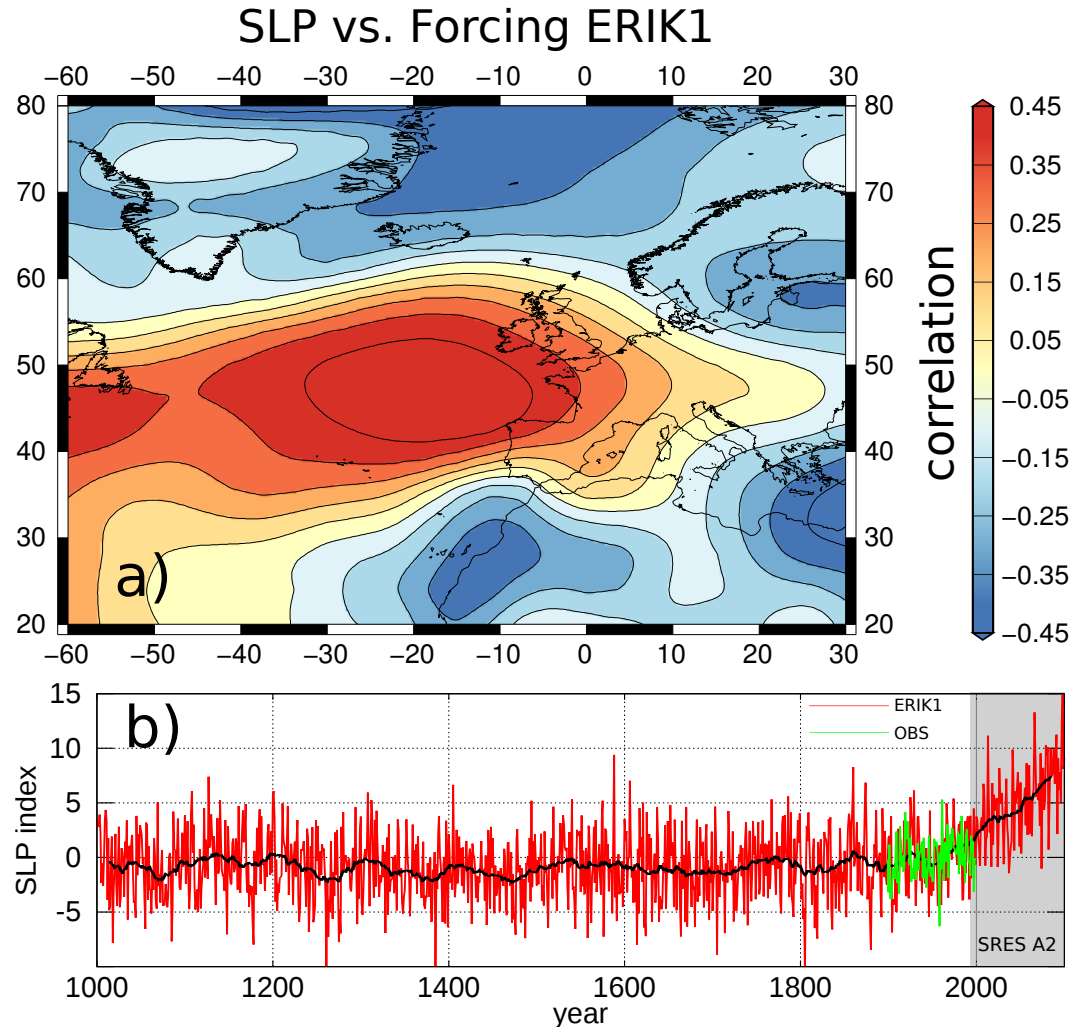


**Figure 3.6:** Top: Correlation between summer (June-August) SLP and external radiative forcings in the experiment ERIK1. We show the results in the AOGCM field, since this area lies outside the simulated domain by the RCM. The calculations were performed with the smoothed low-frequency series. Bottom: evolution of the climate index defined as the projection of the correlation map in Fig a onto the summer SLP field (red line), together with its 31-year running mean (black thick line). The projection of this pattern onto the observational dataset by Trenberth and Paolino (1980) is also shown (green line). Grey shadow indicates the time period where the prescribed forcings change from the paleosimulation to the future climate scenario SRES A2, with natural forcings kept constant.

and illustrates how this large-scale variability mode is stimulated by climate forcings. It is noticeable that the same mode is excited in the paleosimulation and in the climate change projection, although the forcings during the last millennium are mostly solar variability and volcanic activity, whereas in the A2 scenario these natural factors are kept constant, and only changes in greenhouse gases are prescribed.

The results for winter are different. As discussed above, Figure 3.3 shows how the correlation structure for winter is different from that of summer, which suggests that the underlying physical mechanism may also be different. Figures 3.7a, b and c are equivalent to Figures 3.5a, b and c for winter (as before, the following argument is based on the MM5-ERIK2 experiment, although it also holds for the MM5-ERIK1 experiment). The evolution of SAT in winter is dominated by a homogeneous EOF, with associated PCs that are strongly correlated in the two experiments (correlation 0.68). However an important difference between summer and winter is that in the latter, the leading EOF for precipitation (Fig. 3.7b) is very different from the correlation pattern between temperature and precipitation (Fig. 3.7c). The explanation for this difference has to be sought in the impact of large-scale circulation in the precipitation regime in winter over the IP. The North Atlantic Oscillation (NAO) is a variability mode of SLP in the North Atlantic area which strongly affects the winter precipitation amount in the IP, especially in the western parts (Trigo et al., 2004). The MM5-ECHO-G model is able to successfully reproduce this feature (Gómez-Navarro et al., 2011a). Figure 3.7d illustrates this by showing the correlation between the NAO index, defined as the PC associated to the first EOF of winter SLP in the North Atlantic area, and the precipitation series in each grid point. It is apparent how the areas most affected by NAO (Fig. 3.7d) are those standing out in the first EOF of precipitation (Fig. 3.7b). This means that in winter the main variability mode of precipitation is dominated by NAO variations. However, the correlation of the low-frequency variations of NAO in the two simulations is only 0.17 (below 0.27, the significance level at the 95% confidence level), indicating that this important circulation mode does not respond to the external forcing, but is dominated by internal variability in the AOGCM. This explains the generally lower impact of the driving forcing in the evolution of precipitation in winter. In winter, the fingerprint of the relationship between SAT and PRE illustrated in Figure 3.7c has to be sought in the second EOF. This is shown in Figure 3.7e and explains 18% of the low-frequency precipitation variance. We compare this second most important variability mode for winter precipitation with the correlation pattern between SAT and PRE. This mode of precipitation variability, once the influence of the non-forced NAO has been removed, responds to the forcings, as can be identified by comparing Figure 3.7e and the correlation maps for winter in Figure 3.3. In fact, the correlation between the PC

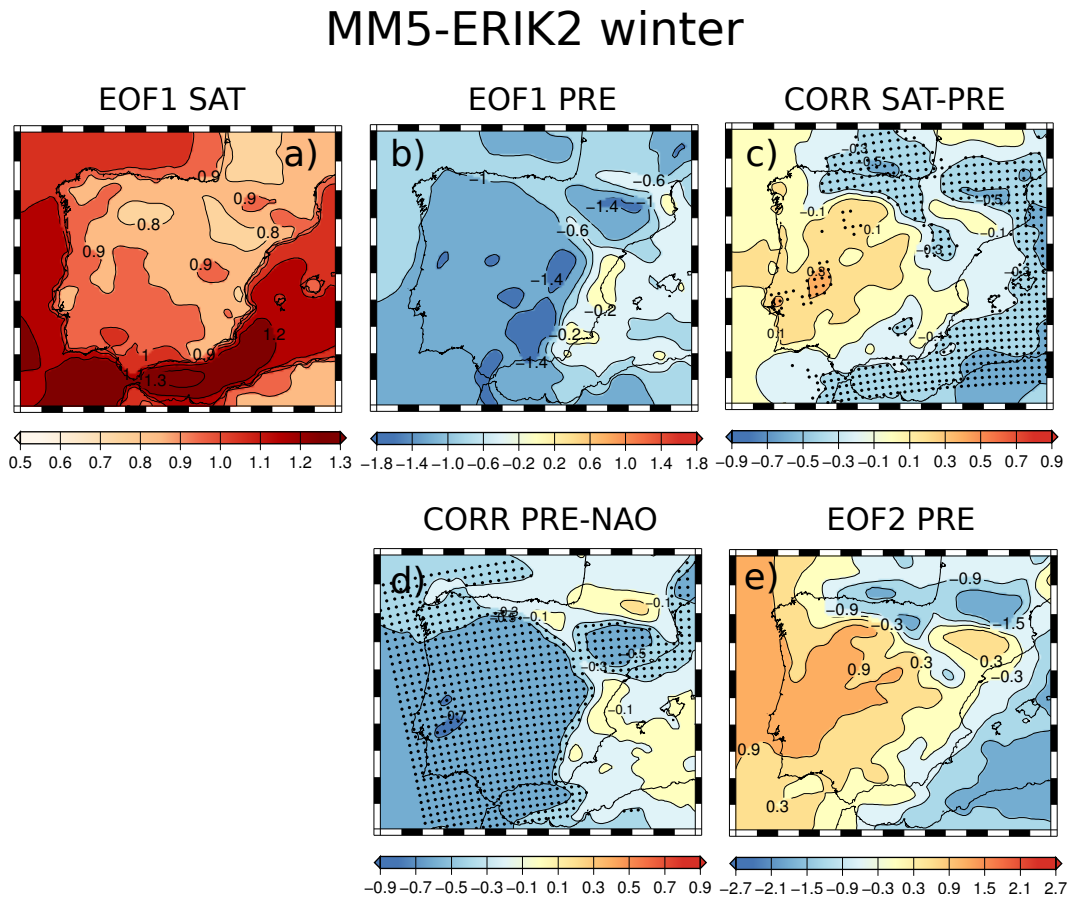


**Figure 3.7:** The three top maps show the first EOF of standardised series of winter SAT (Fig. a) and PRE (Fig. b), as well as the correlation between these two variables (Fig. c). Fig. d shows the correlation between the precipitation series and the NAO index, defined as the PC associated with the leading EOF of SLP in the North Atlantic area. Fig. e is the second EOF of winter precipitation. All maps are dimensionless and correspond to the MM5-ERIK2 experiment, since the corresponding maps for MM5-ERIK1 are analogous (not shown). The calculations were performed with the smoothed low-frequency series. Black circles denote grid points where the correlation is significant at the 95% confidence level according to a bootstrap method ([Ebisuzaki, 1997](#)).

associated to this precipitation mode and the PC associated with the SAT is 0.62 (0.66 in MM5-ERIK1).

The physical link between temperature and precipitation in winter described above, which is responsible for the resemblance between the evolution of the precipitation series during this season in the two simulations shown in Fig. 3.3, is not due to the response of the large-scale circulation to the external forcings, as the case of summer. Instead, it is due to interactions between the large-scale circulation and the orography of the RCM. Fig. 3.8a shows the correlation between the low-frequency evolution of precipitation series in the two simulations, together with the orography considered by the model (in green contours). The correlation is more intense near the main mountain systems such as the north side of the Pyrenees or the western part of the Iberian and Betic systems. This figure, together with the characteristic anti-correlation map between temperature and precipitation shown in Fig. 3.7c, suggests that there may exist a modulation in the condensation level, driven by temperature variations, which could affect specially the precipitation over mountain regions. To check this, the condensation level is estimated using the approximation of the difference between temperature  $T$  and dew point temperature  $T_d$

$$\text{CL} \propto (T - T_d). \quad (3.3)$$

Both variables measured in the surface (Lawrence (2005) presents a modern review on the relations between moisture, temperature and how they are related). Fig. 3.8b shows the correlation between temperature variations and the temperature differences in Eq. 3.3. There is a generally strong and positive relation between the height of the condensation level and the temperature (which is not an obvious result since the moisture content over the IP depends to a large extent on the evaporation rate in the Atlantic Ocean, which is lower in colder periods). The relation is stronger near the main mountain systems, although the correlation map also depicts sensitivity to the Atlantic flow on the windward side of the mountains. That is, in cold periods the condensation level sinks, especially on the windward side of the mountains, and this flavours the increase of precipitation in these areas. Hence, the physical link between precipitation and forcing in winter is through variations in the condensation level, directly modulated by variations in temperature. Surprisingly, despite the intensity of the noise due to internal variability in the winter precipitation, this mechanism is strong enough to leave an observable mark in the amount of precipitation in some areas over the IP, characterised by the orography. It is important to note that this mechanism can only be accurately reproduced within the context of a high resolution simulation capable of resolving the fine spatial scales involved.

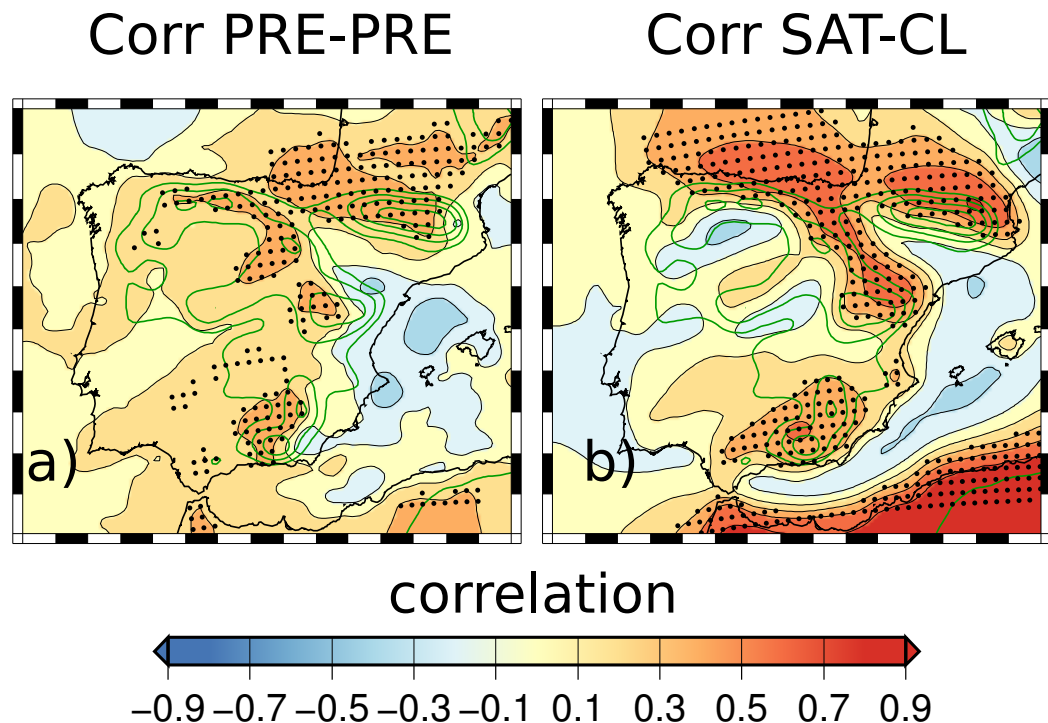


**Figure 3.8:** Physical response of winter precipitation over the IP. Fig. a) shows the correlation between precipitation series in the MM5-ERIK1 and MM5-ERIK2 experiments, and it is the analog to Figure 3.3 but using a low-pass filter instead of running means. Fig. b) depicts the correlation between the temperature and height of the condensation level in the MM5-ERIK2 experiment. All calculations were performed using the low-frequency series. Green contours indicate the terrain height above 500 metres spaced by 300 metres. Black circles denote grid points where the correlation is significant at the 95% confidence level according to a bootstrap method (Ebisuzaki, 1997).

### 3.4 Summary and Conclusions

In this study we have compared the evolution of SAT and PRE in two millennial paleoclimate simulations performed with a RCM with a spatial resolution of 30 km for the IP. The comparison allows us to evaluate the importance and magnitude of the internal variability in the evolution of these variables, relative to the influence of the reconstruction of external forcings used to drive the simulations. The underlaying argument is that if internal variability dominates the evolution of a given variable, the temporal correlation of the series associated to it in both experiments would be negligible.

The results indicate that the long-term evolution of SAT is strongly affected by the external forcings driving the simulation. This variable responds homogeneously to the external factors over the IP at most temporal scales. The evolution of precipitation is, however, more strongly governed by chaotic variability at regional scale. In particular, there are few areas in the IP, the main mountain system in winter and the North and West areas in summer, where the precipitation is significantly driven by external forcings. However, in many parts of the domain the influence of the external forcing can not be detected in the evolution of precipitation. It is important to note that the significance of the correlation emerges at regional scales, and is blurred when a spatial average is performed. This stresses the importance of high resolution simulations in exercises comparing the model results with proxy reconstructions of precipitation.

The influence of the external forcing on precipitation is especially weak in winter. This is due to the nature of the winter precipitation over the IP, which is dominated by variations in the NAO. The NAO seems to be quite insensitive to the external forcing in the simulations at the investigated timescales. Once the NAO signal is removed from the precipitation series, the leading variability pattern corresponds quite well with the areas which are more clearly able to respond to forcings. Summer precipitation is overall more strongly affected by variations in the forcing. Its main variability mode matches well the areas where summer precipitation responds to external forcing. In fact, we have been able to demonstrate that this precipitation mode is dominated by modulation of the large-scale SLP by the external forcing in summer. This is in contrast with the stronger contribution of the internal variability of SLP in winter. During this season, there are still some areas where precipitation responds the forcing, but, in this case, it is not through modification in the large-scale flow, but through the interaction between condensation level and orography.

Our findings regarding the impact of internal variability in the simulations may have a strong impact on how comparison between simulations and reconstructions are performed. In particular, we have been able to identify areas where we should not

expect good agreement between the model and the reconstructions, even if both are perfect. On the other hand, there are areas, mostly in the main mountain systems, where mismatches between both approaches can not be argued to be due to internal variability. These results stress the importance of RCMs in paleoclimate studies, since we have demonstrated that the physical mechanism responsible for the response of precipitation to external forcings in winter can only be realistically reproduced by using high resolution simulations.

It is important to note that some of these findings may be model-dependent. Different global models develop slightly different circulation patterns. At regional scale, interactions with orography strongly depend on the set of parametrizations employed (this is especially true for precipitation (Fernández et al., 2007)). Thus, the mechanisms proposed here may suffer modifications if different model configurations are employed. However, it is hard to address *a priori* these important issues with only two simulations. A larger ensemble of runs with different driving global models and set of parametrizations would be required to reinforce our findings, but it is nowadays computationally prohibitive. Thus, it is beyond the scope of this study to address these uncertainties.

A further important comment has to be made regarding the reconstructions of solar forcing used in these simulations. The evolution of the TSI used in these simulations is taken from Crowley (2000). However, a more recent reconstruction of this variable (Krivova and Solanki, 2008) depicts a much smaller amplitude of the variations. In particular, these authors estimate a difference in total solar irradiance between the Late Maunder Minimum and late 20th century of  $1.25 \text{ W/m}^2$  (about 0.09%), whereas the past solar irradiance used in these simulation changes by 0.3%. Yet an event more recent reconstructions of TSI over the Holocene (Shapiro et al., 2011) again points to an even wider amplitude of TSI variations than those used in these simulations, 0.4% change between the Late Maunder Minimum and late 20th century. It is beyond the scope of this study to analyse which of these reconstructions more realistically represents the past. The influence on our analysis of using reconstructions with lower amplitude in the simulation would be to reduce the term  $\text{Var}(f)$  in Eq. 3.2, and thus reduce the correlation of the same variable between simulations. Higher-amplitude reconstructions of past TSI would have the opposite effect.

A similar argument could apply to volcanic forcing, for which the uncertainties are still also large. In addition, the implementation of volcanic forcing in these simulations, simply as a reduction in the effective solar irradiance, possibly precludes a more realistic simulation of the volcanic winter warming at mid and high-latitudes due to the NAO response to differential effect of volcanic aerosols in the Tropics and high latitudes (Stenchikov et al., 2006; Fischer et al., 2007). According to this mechanism, winters

after volcanic eruptions should experience a stronger NAO and thus the IP would tend to receive less precipitation. This mechanism tends to increase the influence of the volcanic forcing and it would phase-lock the simulated precipitation in both simulations in periods with intense volcanic activity more strongly than is simulated by our model set-up.

Finally, some of these conclusions can be extended with caution to the climate change projections. In a forced scenario, the SAT can be expected to be influenced by external forcings, and hence their projections present a reasonable degree of confidence. Evolution of precipitation is nevertheless less reliable since its behaviour at regional scale is governed by greater uncertainty due to the influence of internal variability. This drawback is an addition to the well known uncertainties characteristic of precipitation projections under climate change scenarios (Christensen et al., 2007). Nevertheless, it has to be taken into account that our findings depend on the intensity of the external forcings. In climate change projections the intensity of external forcings is stronger, and thus the overall role of internal variability can be expected to be lower. In future works, a similar study should be carried out with different runs for the same climate change projection.



Chapter **4**

## Warming patterns in regional climate change projections over the Iberian Peninsula

A set of four regional climate change projections over the Iberian Peninsula has been performed. Simulations were driven by two General Circulation Models (consisting of two versions of the same atmospheric model coupled to two different ocean models) under two different SRES scenario. The XXI century has been simulated following a full-transient approach with a climate version of the mesoscale model MM5. An Empirical Orthogonal Function analysis (EOF) is applied to the monthly mean series of daily maximum and minimum 2-metre temperature to extract the warming signal. The first EOF is able to capture the spatial structure of the warming. The obtained warming patterns are fairly dependent on the month, but hardly change with the tested scenarios and GCM versions. Their shapes are related to geographical parameters, such as distance to the sea and orography. The main differences among simulations mostly concern the temporal evolution of the warming. The temperature trend is stronger for maximum temperatures and depends on the scenario and the driving GCM. This asymmetry, as well as the different warming rates in summer and winter, leads to a continentalization of the climate over the IP.

## 4.1 Introduction

Climate change is one of the problems of most concern, as pointed out by the last report of the IPCC (IPCC, 2007b). More specifically, the Iberian Peninsula (IP), as part of the Mediterranean Region, has been identified as one of the Hot-Spots of climate change (Giorgi, 2006; Diffenbaugh et al., 2007).

Projections of future climate can be performed by General Circulation Models (GCMs), whose external forcings are based on the IPCC Special Report on Emission Scenarios (SRES) (Houghton et al., 2001). These models reproduce large-scale circulation, but their performance in reproducing regional climate details is poor due to their coarse resolution (Rind et al., 1990; von Storch, 1995). For this reason, downscaling techniques are necessary in order to capture the fine scale structure of climate change, especially in areas with complex topography and great climatic diversity such as the IP (Font-Tullot, 2000).

Several downscaling techniques exist, such as statistical downscaling (Wilby et al., 1998; Trigo and Palutikof, 2001; Xoplaki et al., 2004), in which statistical/empirical models link the large-scale fields with local or regional variables, and dynamic downscaling, performed by means of Regional Climate Models (RCMs) nested to GCMs. The latter allows climate change projections at higher spatial resolution for a limited-area domain (Giorgi et al., 2004a,b; Raisanen et al., 2004; Solman et al., 2008; Nunez et al., 2009, and many others). The higher resolution and more complete physical representation reduce some driving GCM biases in the present climate and thus enhance the credibility of future climate change projections (Liang et al., 2008).

Climate change projections are nevertheless affected by three sources of uncertainty: emission scenario uncertainty, internal variability and model uncertainty. The first is caused mostly by external-to-climate factors such as the evolution of economy and technology. The second is inherent to the climate system, and its importance decreases at multidecadal time scales (Hawkins and Sutton, 2009). The last source, model uncertainty, is due to the misrepresentation in the models of some important physical processes. In regional climate change projections, model uncertainty arises from uncertainties in the GCM driving the simulation and from the RCM itself (Giorgi, 2005). These uncertainties can be evaluated through the spread in ensembles of equivalent simulations (Déqué et al., 2007; Jacob et al., 2007).

In the case of the European Continent, several studies have focused on assessing the accuracy on different RCMs in reproducing the climatology observed for a control period (usually 1960-1990) (Déqué et al., 2005; Jacob et al., 2007), as well as on evaluating the spread among climate change projections (Déqué et al., 2007). Many

of these works lie within the context of the PRUDENCE and ENSEMBLES projects (5Th and 6Th EU Framework Programme, respectively).

The most frequent approach adopted for the evaluation of projected warming is the future-minus-present method, which is based on the assumption that biases in simulated present-day and future climates will tend to cancel each other, and thus their difference captures the climate change signal. Although supported by intercomparisons between climate models (Kittel et al., 1998), this approach is very sensitive to the chosen periods due to the inherent internal variability of the climate models, especially at regional scales (Raisanen, 2001). Although computationally expensive, full transient simulations minimise the internal variability uncertainty due to the longer time series obtained.

The aim of this work is to check whether the projected warming over the IP is dependent, and to what extent, on the SRES scenario and the GCM version driving the regional simulation. For this purpose a set of four full transient regional climate change projections for the XXI century has been carried out using a climate version of the meteorological model MM5 (Fernández et al., 2007; Montávez et al., 2006, 2008) driven by two versions of the atmospheric model ECHAM coupled to two different ocean models, and two SRES scenarios. The physical configuration and domain setup is the same in all the experiments, as a study of the uncertainty linked to the RCM itself is not the aim of this work. In order to capture the warming signal, an Empirical Orthogonal Functions analysis is applied, following an approach similar to Zorita et al. (2005). This methodology, not previously employed in RCM studies, tries to overcome the problem linked to the internal variability of RCMs. The study focuses on the evolution of monthly mean series of daily maximum and minimum 2-metre temperatures separately.

## 4.2 Methodology

### 4.2.1 Experiment description

The regional climate model used for the present study is a climate version of the Fifth-generation Pennsylvania-State University – National Center for Atmospheric Research Mesoscale Model (Dudhia, 1993; Grell et al., 1994a; Montávez et al., 2006). Some other versions have been widely used in other regional climate change projections (Boo et al., 2006; Nunez et al., 2009)

Figure 4.1 depicts the two two-way nested domains with a resolution of 90 km and 30 km, respectively, employed in all the simulations. The mother domain covers Europe and the Mediterranean Sea, which has been shown to strongly influence the climate of

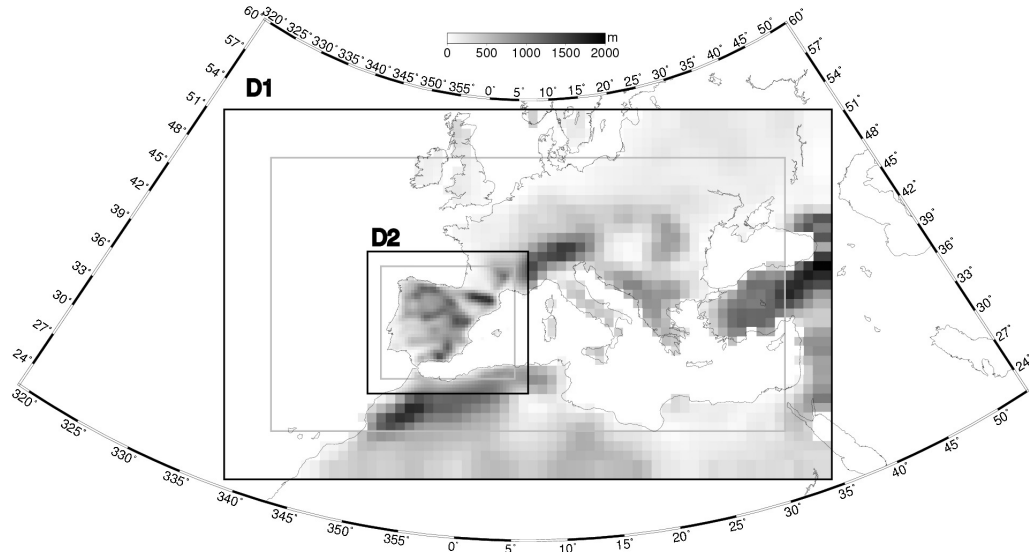


**Figure 4.1:** Nested domains D1 and D2 with 90 km and 30 km grid sizes, respectively, used in the simulations. The grey scale represents the orography seen by the model and grey rectangles indicate the blending area used for both domains.

the eastern part of the Iberian Peninsula (Font-Tullot, 2000). The second domain covers the IP with higher resolution. 24 sigma levels are considered in the vertical, with the top at 100 hPa. A blending area of five grid points, shown in grey squares in Figure 4.1, is excluded from the analysis hereafter.

The same physical configuration is used in all simulations. It has been chosen in order to minimise the computational cost, since none of the tested configurations provides the best performance for all kinds of synoptic events and regions (Fernández et al., 2007). The physical options implemented are: Grell cumulus parametrisation (Grell, 1993), Simple Ice for microphysics (Dudhia, 1989), RRTM radiation scheme (Mlawer et al., 1997) and MRF for planetary boundary layer (Hong and Pan, 1996). The Noah Land-Surface model (Chen and Dudhia, 2001a,b) has been used, as it simulates more accurately the climate in dry areas, especially in summer over the southern part of the IP (Montávez et al., 2008).

Four experiments have been carried out using two versions of the atmospheric model ECHAM coupled to two different ocean models (hereafter denominated ECHO-G and ECHAM5, respectively) as boundary conditions under two different SRES scenar-

Experiment	GCM	Scenario	Period
EGA2	ECHO-G	A2	1991-2099
EGB2	ECHO-G	B2	1991-2099
E5A2	ECHAM5	A2	2002-2099
E5B1	ECHAM5	B1	2002-2099

**Table 4.1:** Experiment alias, GCM used, SRES scenario and time period covered by the four experiments.

ios. Table 4.1 summarises the four experiments, with the GCM employed, the scenario and the period covered. It should be noted that the only difference between the chosen scenarios is the Green House Gas (GHG) concentrations.

The ECHO-G model driving the EGA2 and EGB2 experiments consists of the spectral atmospheric model ECHAM4 coupled to the ocean model HOPE-G (Legutke and Voss, 1999). The model ECHAM4 is used with a horizontal resolution T30 ( $\sim 3.75^\circ \times 3.75^\circ$ ). The horizontal resolution of the ocean model is approximately  $2.8^\circ \times 2.8^\circ$ , with a grid refinement in the tropical regions. A flux adjustment constant in time was applied to avoid climate drift. A more detailed description of the model can be found in (Zorita et al., 2005) and references herein. Boundary conditions are updated in the boundaries of the regional model every 12 hours.

The ECHAM5 model drives the E5A2 and E5B1 experiments. This consists of the atmospheric model ECHAM5 coupled to the Max Plank Institute Ocean Model (MPI/OM) (Jungclaus et al., 2006). The atmospheric model is used with a resolution T63 ( $\sim 1.875^\circ \times 1.875^\circ$ ), while the ocean resolution is about  $1.5^\circ \times 1.5^\circ$ . Boundary conditions were updated every 6 hours.

### 4.2.2 EOF analysis

In order to investigate the warming signal along the XXI century an Empirical Orthogonal Function (EOF) analysis was used (Lorenz, 1956; von Storch and Zwiers, 1999; Hannachi et al., 2007). This methodology reduces the high dimensionality of complex phenomena by decomposing a space-time field into spatial patterns and associated time indices :

$$T(t, \mathbf{s}) = \sum_{i=1}^N PC_i(t) EOF_i(\mathbf{s}),$$

where  $N$  is the number of modes contained in the field,  $\text{EOF}_i(\mathbf{s})$  are a set of functions defined for space and  $\text{PC}_i(t)$  their temporal coefficients, usually called Principal Components. The difference between the original field and the first member of the summation is the residual,

$$\begin{aligned}\text{Res}(t, \mathbf{s}) &= T(t, \mathbf{s}) - \text{PC}_1(t)\text{EOF}_1(\mathbf{s}) \\ &= \sum_{i=2}^N \text{PC}_i(t)\text{EOF}_i(\mathbf{s}).\end{aligned}$$

Therefore the analysis of the residual series has to be performed in order to evaluate whether the EOF analysis is able to filter out the warming signal trend.

To illustrate the methodology, the monthly series of daily maximum 2-m temperature for July in the EGA2 experiment (Table 4.1) is studied herein in detail. Similar results are produced for the rest of the months in every experiment. Figure 4.2 depicts the time evolution of the domain-averaged anomalies of maximum 2-m temperature for July, the corresponding  $\text{PC}_1$  and the residual. The correlation between the average 2-m temperature and the first PC is nearly one. The residual presents no trend and its variance is much smaller. The residual, which is dominated by  $\text{EOF}_2$  (not shown), has a bipolar structure, so the domain-averaged series is not sufficient to test the robustness of the methodology. For this reason, Figure 4.3 shows the complementary picture in the spatial domain for the same data set. The corresponding  $\text{EOF}_1$  is shown in the bottom-left panel of Figure 4.4. The original data set exhibits trends up to 1 K/decade in some central-west areas of the IP, decreasing in amplitude to the coast, while the residual trends are roughly one order of magnitude smaller. These two facts, plus the large amount of variance explained by  $\text{EOF}_1$  (89% of the total, Table 4.2), imply that this pattern contains the spatial structure of the warming pattern, as obtained by other authors for GCMs (Zorita et al., 2005).

### 4.3 Results

The EOF methodology presented in the previous section was applied independently to the monthly mean series of daily maximum and minimum 2-m temperatures for the four experiments. Table 4.2 depicts the amount of total variance explained by just the first EOF in each scenario, variable, and month, which is greater than 70% in all cases. Moreover the  $\text{EOF}_1$  is able to filter out the warming trend, and, for this reason, only the first EOF will be studied, below-referred to as the warming pattern.

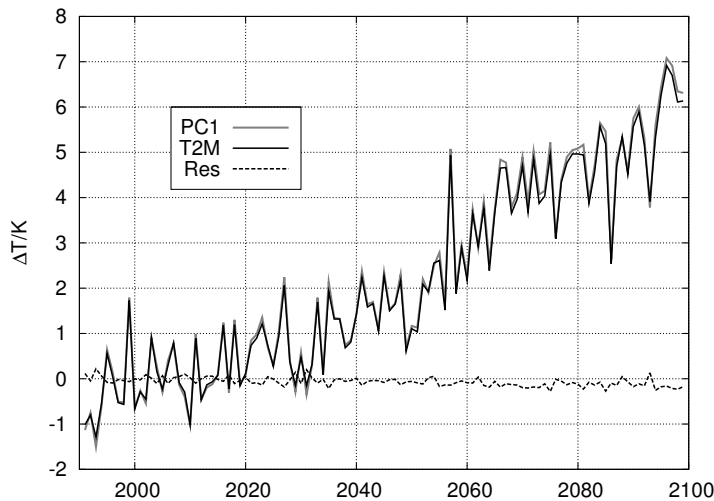
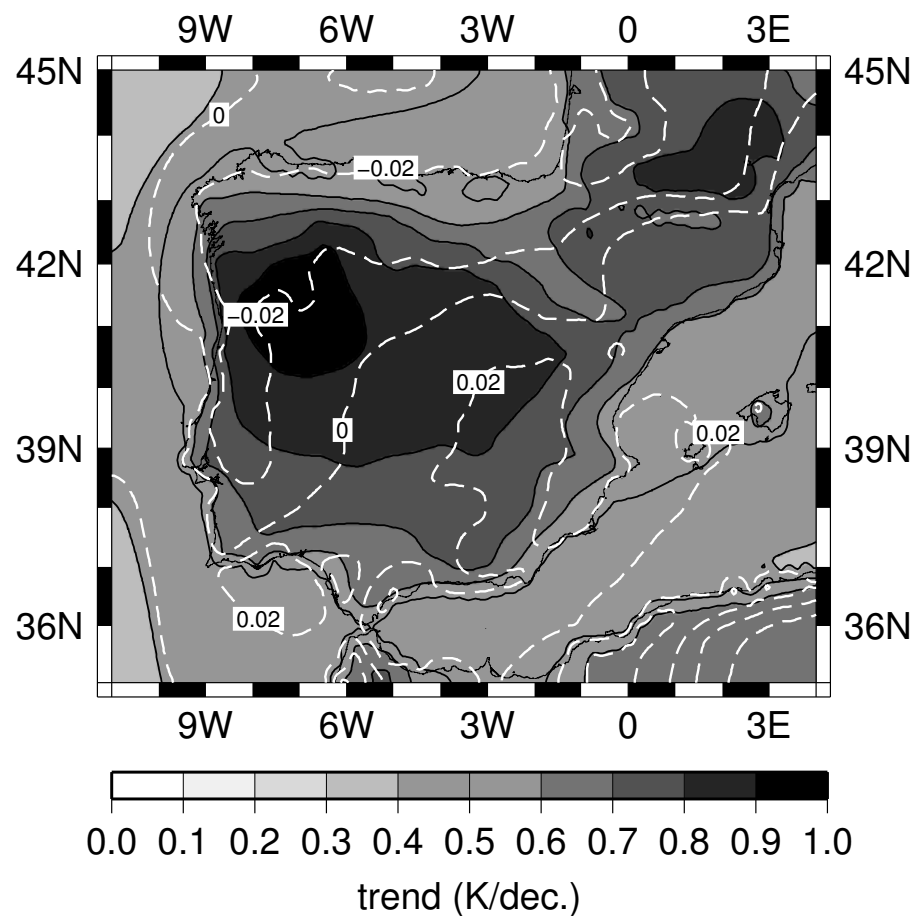


**Figure 4.2:** Anomalies in the spatial averaged maximum temperature versus  $PC_1$  and the residual. The series correspond to July monthly means for the EGA2 experiment.

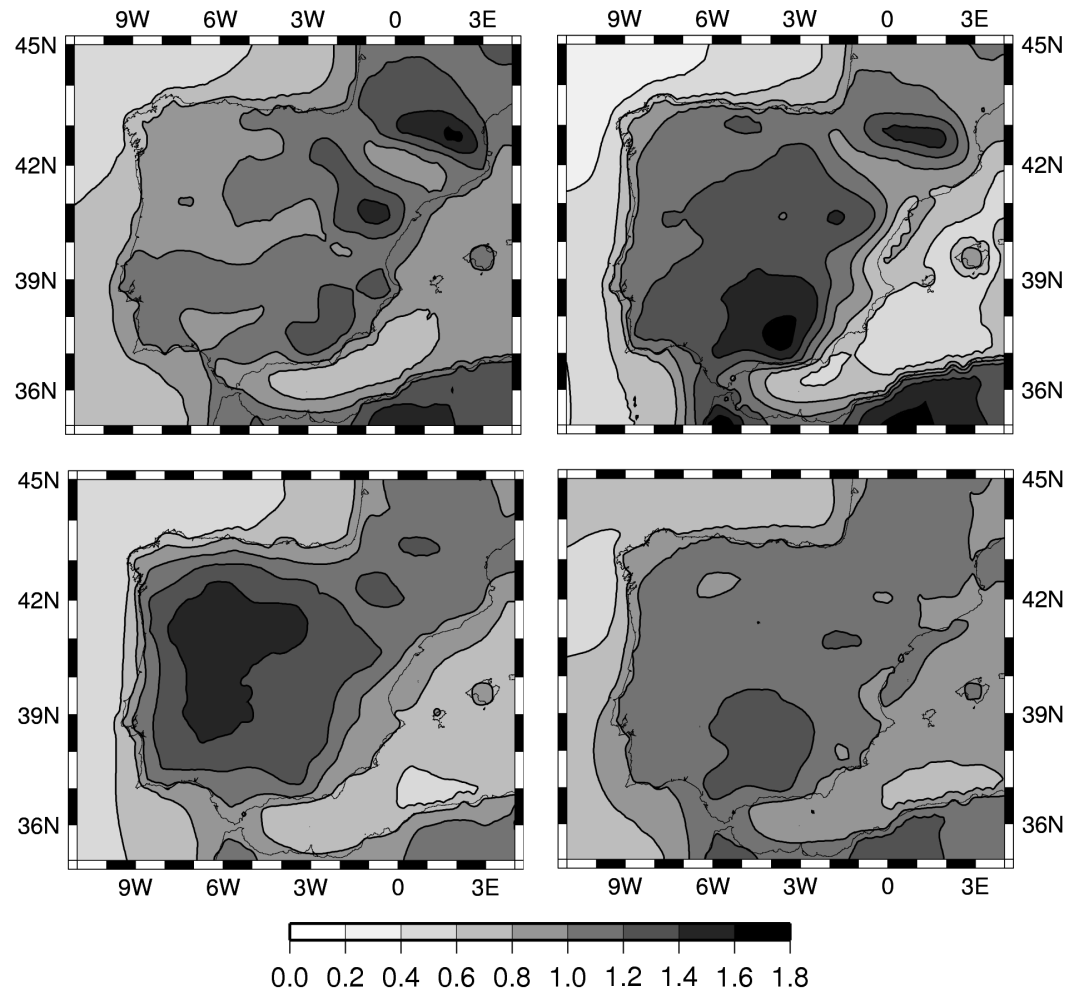
### 4.3.1 Warming patterns

Figure 4.4 (Figure 4.5) depicts the first EOF obtained for the E5A2 experiment for maximum (minimum) temperatures for January, April, July and October (one representative month per season). The rest of the months (not shown) present an intermediate behaviour. In general, warming patterns associated to maximum and minimum temperatures present some similarities, although there are important differences (discussed below).

In order to check whether the warming patterns depend on the SRES scenario, the spatial correlations between warming patterns in the E5A2 and E5B1 experiments for maximum and minimum temperatures in each month have been calculated (Table 4.3 first and second columns). In all cases the correlation is above 0.9. Similarly, the correlations between EGA2 and EGB2 experiments are shown in the third and fourth columns for maximum and minimum warming patterns, respectively. Again, the spatial correlation is very high, albeit there are some months showing some differences (correlation in October for minimum temperatures is 0.61). Hence, the spatial warming patterns hardly change under different SRES scenarios, and thus, given the same GCM, the effect of changing GHG concentrations has to be sought in the intensity of the warming, rather than in the spatial structure of the warming patterns. Similar re-



**Figure 4.3:** Trends of the monthly mean series for July for the whole simulation period in the EGA2 experiment (grey shaded) and trends for the corresponding residual series (white contours). Both data sets are expressed in Kelvin per decade.



**Figure 4.4:** First EOF obtained from maximum 2-m temperature monthly series for the E5A2 experiment. Only one representative month per season is presented: January (top left), April (top right), July (bottom left) and October (bottom right). Other months present an intermediate behaviour.

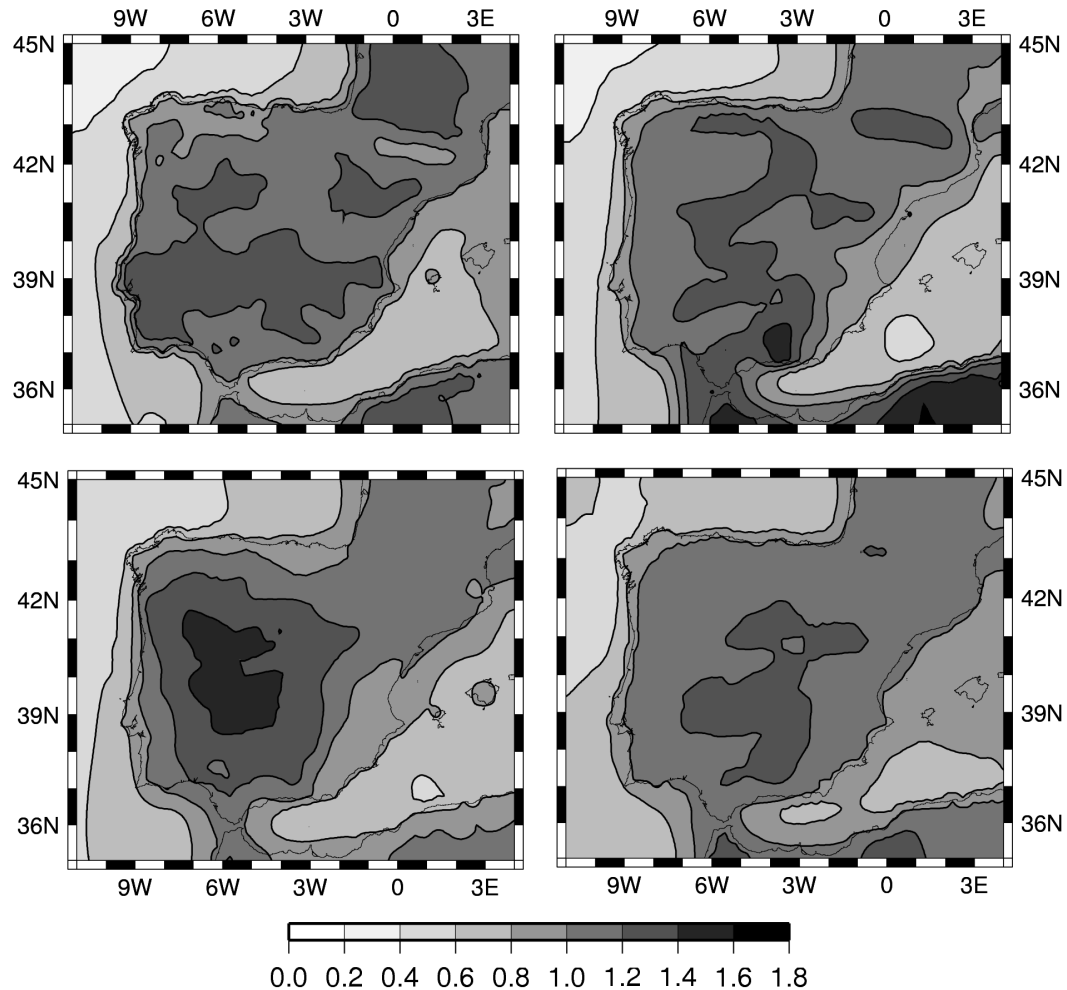


**Figure 4.5:** First EOF obtained from minimum 2-m temperature monthly series for the E5A2 experiment. Only one representative month per season is presented: January (top left), April (top right), July (bottom left) and October (bottom right). Other months present an intermediate behaviour.

Month	E5A2		E5B1		EGA2		EGB2	
	Tmax	Tmin	Tmax	Tmin	Tmax	Tmin	Tmax	Tmin
Jan	84.96	84.88	83.43	83.26	87.10	85.85	80.13	76.13
Feb	84.31	83.85	81.76	80.60	85.69	87.90	83.07	82.51
Mar	84.41	85.71	76.18	77.95	84.36	86.05	82.40	81.67
Apr	82.01	81.97	75.40	73.29	86.69	86.60	82.60	82.33
May	81.58	79.03	71.45	71.03	87.09	85.08	81.28	79.17
Jun	81.12	79.84	70.60	73.26	89.69	88.88	78.17	76.64
Jul	81.88	81.89	73.51	75.79	89.63	90.04	80.67	82.10
Aug	83.41	84.88	74.21	79.08	88.32	89.77	78.22	81.67
Sep	84.98	86.16	78.10	82.99	85.82	89.13	79.66	82.92
Oct	84.18	84.00	72.86	77.55	88.68	89.69	81.40	84.01
Nov	89.16	88.05	79.17	80.74	87.21	85.72	84.79	84.95
Dec	86.03	84.95	84.46	84.79	86.98	84.89	83.40	82.67

**Table 4.2:** Percentage of the total variance explained by the first EOF of the associated series. Information is split into variables, model runs and months (by rows).

sults have been found by [Nunez et al. \(2009\)](#) for southern South America using the future-minus-present method.

The question of whether the warming patterns depend on the GCM version driving the simulation may be explored through comparing the E5A2 and EGA2 simulations, corresponding to the same SRES scenario, A2. The correlations between warming patterns associated to these experiments are shown in Table 4.3 in columns 5 and 6. In this case, correlations are in general slightly lower than in former cases, reaching 0.61 in November for minimum temperatures. Nevertheless, the average correlation is still around 0.8, and more than 0.85 for several months. The fact that correlation between different GCM versions is lower than between different SRES scenarios means than there is more resemblance between warming patterns associated to same GCM under different scenarios than to the same scenario with different GCM. It should be emphasised that the two tested GCM were implemented with two versions of the same atmospheric model, ECHAM. This aspect will be discussed further in the conclusions.

The shapes of the warming patterns seem to be related with several geographical parameters, such as altitude and distance to the sea. Figures 4.4 and 4.5 indicate a pattern linked to the distance to the sea in the first EOF for July, meanwhile for April they seem to be related to orography. The annual cycle of these relationships is fur-

Month	E5A2 vs. E5B1		EGA2 vs. EGB2		E5A2 vs. EGA2	
	Tmax	Tmin	Tmax	Tmin	Tmax	Tmin
Jan	0.98	0.99	0.94	0.97	0.79	0.88
Feb	0.98	0.98	0.94	0.91	0.82	0.83
Mar	0.95	0.93	0.96	0.97	0.85	0.81
Apr	0.99	0.97	0.96	0.94	0.89	0.80
May	0.98	0.98	0.98	0.96	0.89	0.78
Jun	0.84	0.90	0.98	0.97	0.88	0.83
Jul	0.93	0.93	0.98	0.96	0.90	0.88
Aug	0.92	0.90	0.92	0.86	0.81	0.79
Sep	0.97	0.95	0.92	0.77	0.79	0.73
Oct	0.95	0.95	0.89	0.61	0.75	0.66
Nov	0.85	0.93	0.94	0.84	0.66	0.61
Dec	0.95	0.97	0.84	0.96	0.74	0.89

**Table 4.3:** Spatial correlation coefficient for each month between the warming patterns corresponding to different experiments. Only land points have been considered.

ther explored in Figure 4.6. Figure 4.6a depicts the correlation between the warming pattern for each month for maximum and minimum temperature in the E5A2 experiment and distance to the sea, defined as the minimum distance from the grid point to the sea. In summertime the warming patterns are mostly related with the distance to the sea, with a correlation above 0.6 for maximum and minimum temperatures. This signal disappears and even becomes negative in wintertime for maximum temperatures, but remains significant for minimum temperatures in the first months of winter, clearly showing the discrepancies between the maximum and minimum temperatures mentioned above. On the other hand, Figure 4.6b shows the correlation between patterns and altitude with respect to sea level. The relationship between them seems to be stronger in the principal mountain systems. For this reason, only grid points above 800 metres were taken into account in the calculations. This explicitly removes the IP Central Plateau, where the orographic signal is weaker. This figure shows a complementary behaviour with the former: warming patterns in the colder months are related to altitude, with correlations up to 0.5 for maximum (0.3 for minimum) temperatures in February, while in summer correlations are low or negative, giving way to the influence of the distance-to-sea pattern. Again the differences in the behaviour of the maximum and minimum patterns may be easily identified in this figure in January and

December, where the correlations between maximum and minimum warming patterns and the orography are 0.3 and -0.2, respectively.

Although there is no completely satisfactory explanation for the physical processes governing the shape of the warming patterns, the distance-to-sea pattern in the warmest months may be linked with the larger thermal capacity of oceans, which smoothes trends near coast lines. As regards the orography, it has been argued (Giorgi et al., 1997) that a positive feedback between melting snow cover on summits and albedo may be responsible for the increase of warming with altitude. This possibility has been ruled out over the IP by using two different land soil models to perform the same simulation, one of which is capable to dynamically model the snow cover while the other uses prefixed values depending on the season. The resulting warming patterns in both experiments exhibit a similar correlation with altitude (Gómez-Navarro et al., 2009). Further research should be devoted to identifying the reasons for increased warming with altitude, which may be related with changes in the global circulation.

The asymmetry in the spatial structure of the warming patterns for maximum and minimum temperatures may have important implications for the projected evolution of the daily temperature range (DTR). In particular, zones where maximum temperatures rise more than minimum temperatures tend to develop a higher DTR.

### 4.3.2 Temporal evolution

As stated in the previous section, the scenarios and GCM versions driving the regional simulations tested in this work do not strongly modify the spatial structure of the warming, which seems to be an inherent feature of the regional model configuration and the chosen domains. The effect of these factors is to modify the amplitude of the warming trend. Figure 4.7 shows the first PCs of the monthly mean of daily maximum and minimum 2-m temperatures series for the E5A2 and E5B1 experiments, while Figure 4.8 depicts the same results for EGA2 and EGB2. Generally, the stronger the GHG forcing, the larger the trend associated to maximum and minimum temperatures, as is to be expected. A difference up to 2 K in the maximum 2-m temperature series exists at the end of the XXI century for July when comparing E5A2 and E5B1 experiments, as shown in Figure 4.7. Similar results can be found for EGA2 and EGB2 experiments in Figure 4.8.

Nevertheless, this difference between scenarios depends strongly on the month, reaching just 1 K of difference in January for the ECHO-G-driven experiments, and showing negligible difference for those driven by ECHAM5. The internal variability plays an important role here. Although a 31 year running mean has been performed to

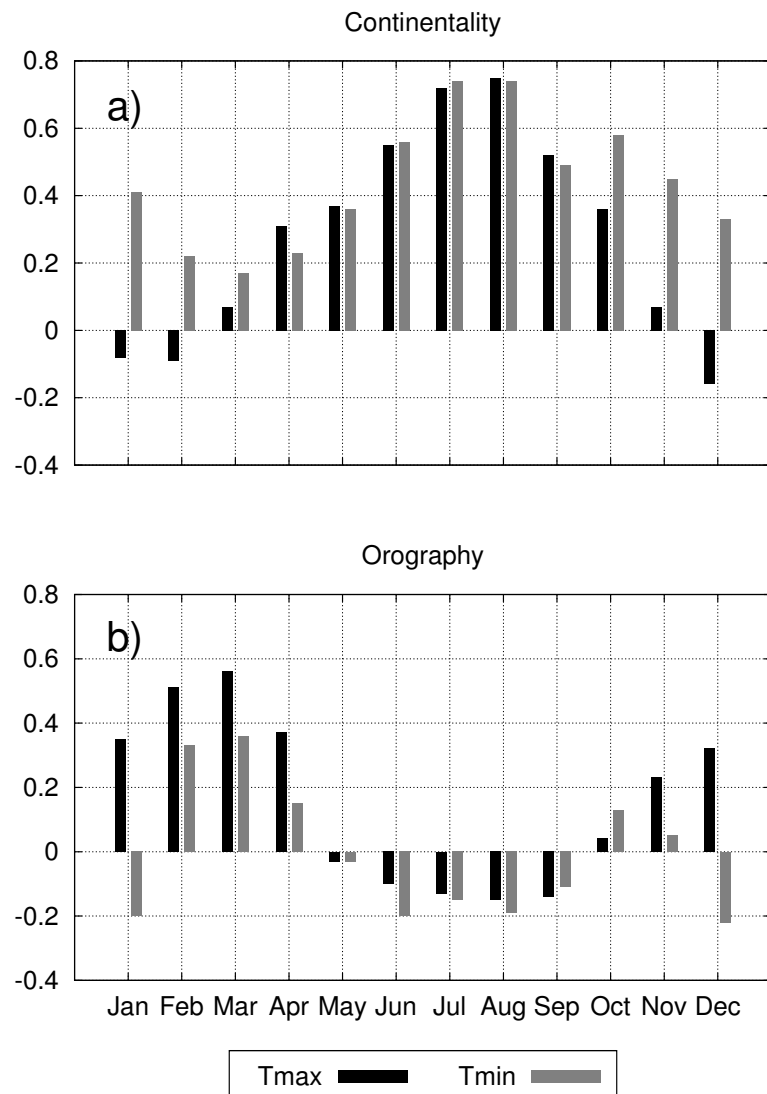


**Figure 4.6:** Annual cycle of correlation coefficients between maximum (black boxes) and minimum (grey boxes) warming patterns with: a) continentality, b) altitude referred to the sea level for the E5A2 experiment.

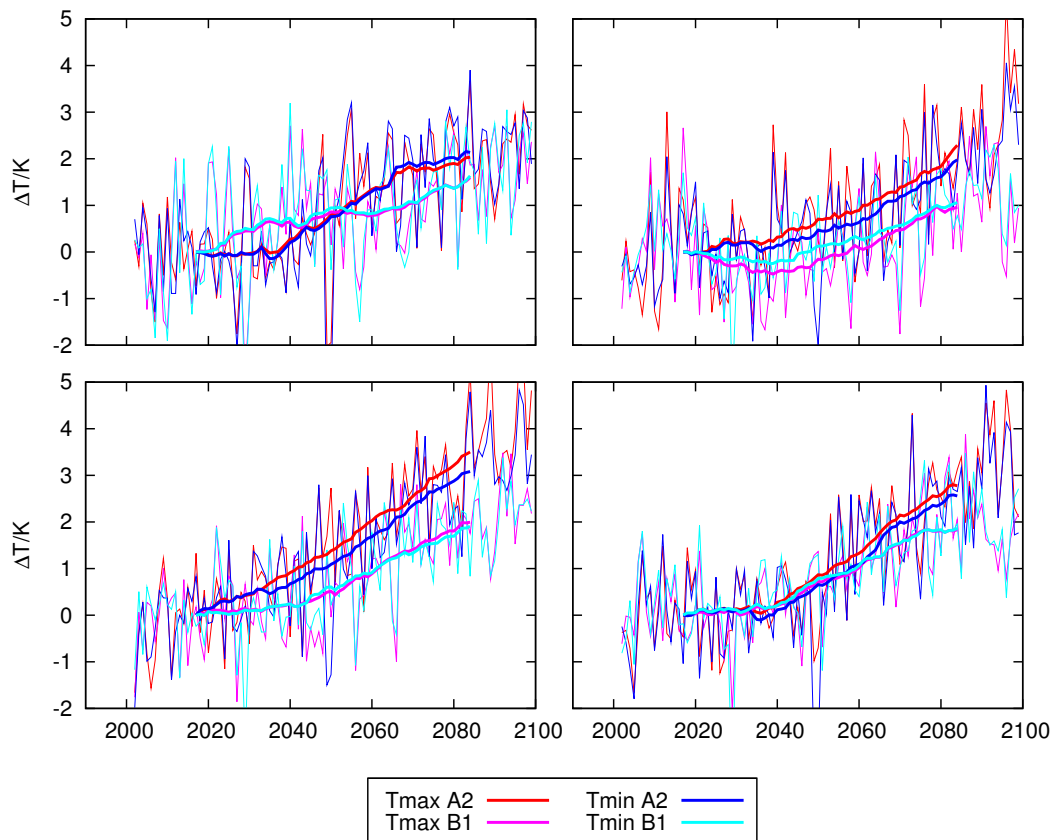


**Figure 4.7:** First PC anomalies, referred th its mean in the first 31 years, of maximum and minimum (red and blue lines, respectively) 2-m temperatures for E5A2 (dark colours) and E5B1 (light colours) experiments. Thick lines represent a 31-year running mean. Only one representative month per season is represented: January (top left), April (top right), July (bottom left) and October (bottom right).

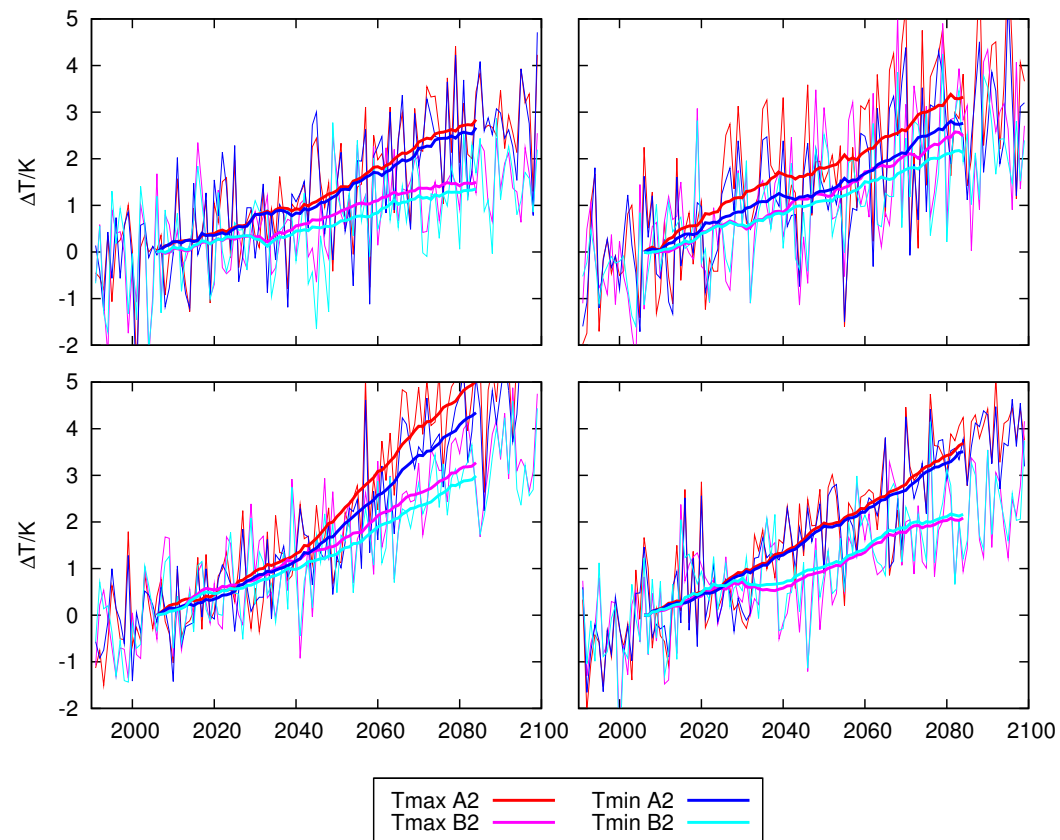


**Figure 4.8:** First PC anomalies, referred to its mean in the first 31 years, of maximum and minimum (red and blue lines, respectively) 2-m temperatures for EGA2 (dark colours) and EGB2 (light colours) experiments. Thick lines represent a 31-year running mean. Only one representative month per season is represented: January (top left), April (top right), July (bottom left) and October (bottom right).

the RCM data, the GCM has its own variability, which is passed to the RCM through the boundary conditions. This GCM natural variability explains why the model response in the E5B1 simulation for January is even greater than in the E5A2 until 2050 (top left panel in Figure 4.7). In general, given a GCM, the differences between scenarios follow an annual cycle (not shown), in which warmer months tend to be more sensitive to stronger GHG forcings. This suggests than the model projects not only warming, but also an increased difference between summer and winter.

Although the trends are positive in every case, except for April in the E5B1 experiment until 2040 (top right panel of Figure 4.7), which may be attributable to internal variability of the GCM, maximum temperatures, in general, show a more pronounced trend than the minima. This behaviour is more noticeable in warm months, as well as in the scenarios where GHG forcing is more intense, as can be appreciated in both figures. In the EGA2 experiment the difference between maximum and minimum PC anomalies at the end of the XXI century is around 1 K for July, while it is nearly 0 K for January. Similar results, although less intense, are found in the other experiments. These different trends imply a coherent increase in the DTR in this ensemble of regional projections for the XXI century, being more intense in the more pessimistic scenarios. This behaviour has been further explored by Jerez et al. (2009), who pointed to a relationship between the intensification of the DTR and the projected decrease of available moisture over the IP.

The increased DTR, as well as the differences between summer and winter, would suggest a continentalization of the climate over the IP. It should be highlighted that the only effect of imposing different SRES scenarios and GCMs is to modify the intensity and the moment when these changes occur. That is, the continentalization of the IP is a common feature of all the climate change projections discussed in this paper.

#### 4.4 Discussion

The usual approach in this kind of study is to calculate the differences between averages of each variable for two periods of time, as reference (usually several years in the past) and for the future. Instead, this work focuses on an EOF analysis, which is able to account for the warming signal, the first EOF capturing the temperature trends along the simulated period. This methodology, not used so far in RCM studies, tries to overcome the problem linked to the internal variability of RCMs, as it employ the whole transient simulation to calculate the warming patterns.

The spatial structure of the warming patterns has a marked annual cycle. In addition, there is an important asymmetry between maximum and minimum 2-m tem-

peratures. Nevertheless, these patterns depend neither on the SRES scenario nor on the GCM version used to drive the regional simulations. They are, rather, an inherent feature of the considered domains. It is nevertheless important to note that these conclusions could be modified if different RCM configurations or a larger set of GCMs are employed. In particular, the two GCM employed were implemented with two versions of the atmospheric model ECHAM. Thus, although two different ocean models were used in the GCM setup, they are not completely independent. It would be interesting to check whether these patterns remain similar under other completely independent GCMs. Such an analysis will be performed in future studies.

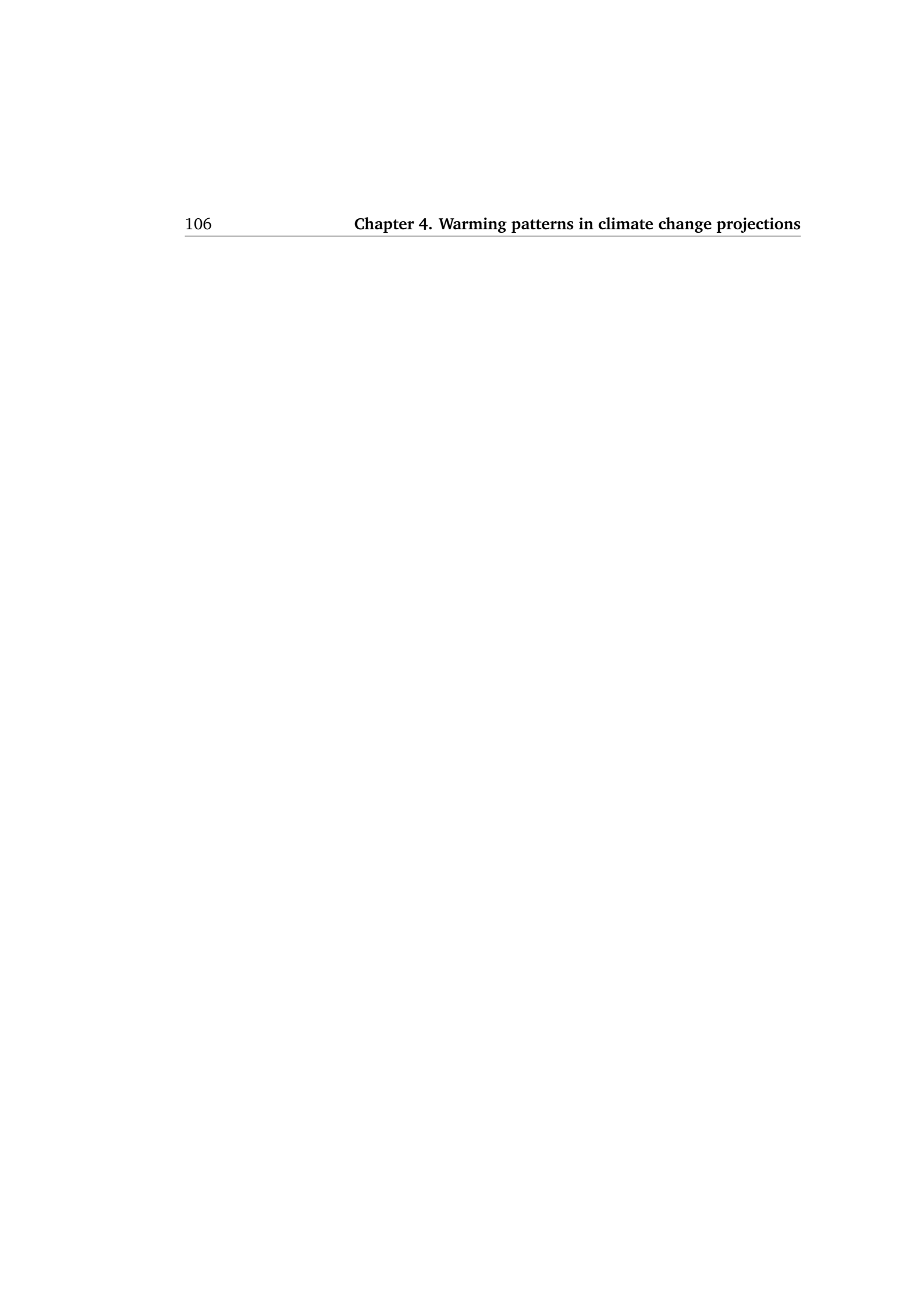
The warming patterns seem to be associated to several geographical parameters such as distance to the sea or altitude. The positive feedback between the melting of snow cover on summits and albedo as being responsible for the relationship between orography and warming has been ruled out in previous communications (Gómez-Navarro et al., 2009). In addition, the distance-to-sea pattern may be related with the larger thermal capacity of oceans. Nevertheless, there is no completely satisfactory explanation of the physical mechanisms underlying this behaviour, and further research should be devoted to an attempt to fully understand.

Maximum temperature trends are more pronounced than minimum ones. These differences also depend on the month, being stronger in summer. This asymmetry yields a continentalization of the climate over the IP for the projected period. One important result is that these projections are consistent in all the scenarios studied. The effect of changing the forcing conditions (i.e. the GHG concentrations) is to modulate the global trends over the IP, not to modify the spatial structure of the projected warming or the continentalization of the climate.

Internal variability plays an important role in the simulations, adding an important uncertainty factor to the results. Trying to overcome this problem, long full-transient simulations have been performed, and temporal series have been filtered out by means of a 31 year running mean. Nevertheless, the internal variability of the GCM is passed through the boundaries to the RCM, leading to some unexpected results, like the cooling trends seen in several months in the the E5B1 simulation. The internal variability problem can be faced by downscaling a larger set of GCM runs. For this reason, and due to the similarities between the two GCMs employed in this study, in future works a more complete set of simulations will be performed, using completely independent GCMs and different SRES scenarios in order to reinforce the present results.

It should be highlighted that the aforementioned results depend on the fact that the physics and the configuration of the domain are equal in all simulations. Further simulations should be performed modifying these factors. Such sensitivity studies would be

helpful for assessing the uncertainties linked to the dynamic downscaling process itself. Analogously, different RCMs could be employed for checking differences and similarities between models. On the other hand, it would also be interesting to check whether the patterns found are present in the pre-industrial climate, as obtained by other authors in GCM experiments ([Zorita et al., 2005](#)).



# Chapter 5

## A simulation of the European regional climate over the past 500 years

This chapter presents a high resolution (45 km) regional palaeoclimate simulation for Europe. It expands the period 1501-1990, and was driven through the boundaries by the global model ECHO-G. Both models were identically driven by three sources of external forcings: a reconstruction in the Total Solar Irradiance, the concentration of Greenhouse gases and the parametrized effect of big volcano events in the radiative balance. The skill of the simulation in reproducing a realistic climate has been assessed during the instrumental period comparing with the CRU data base. Despite a general accuracy of the model in reproducing temperature and precipitation at regional scales, some important biases are found. They can be attributed, despite some deficiencies in the regional model, to an overestimation of zonal circulation in the driving global model. We have also performed comparisons with a number of climate reconstructions of several variables for Europe in the simulated period. We find that the warming trend simulated matches the one reconstructed, which suggests that the amplitude of the external forcings used to drive the simulations is realistic. At shorter time scales, there are some periods where the agreement between the modelled and reconstructed climate is poor, which would require further exploration of the underlying causes. The model allows to test the accuracy of reconstructions. In particular, we have been able to identify an oversimplification of main variability modes in gridded reconstructions, especially for precipitation.

## 5.1 Introduction

Although the physical mechanisms conductive to global higher temperatures accompanying an increase of atmospheric concentrations of anthropogenic greenhouse gases are well understood, the magnitude of future projections of climate change are still burdened with large uncertainties (IPCC, 2007b). This is even more so at regional scales, where additional processes and feedbacks may modulate the climate response to external forcings. The comparative analysis of proxy-based climate reconstructions and climate simulations has been proposed as a means to reduce the spread in the uncertainties of climate sensitivity (González-Rouco et al., 2009; Zorita et al., 2010; Gómez-Navarro et al., 2011a), but this type of comparative analysis can furthermore provide useful information about the feedback mechanisms, about the amplitude and processes involved in unforced regional climate variations and about the skill of climate models in simulating regional climate changes. This latter point seems particularly important since the estimation of climate change impacts and possible adaptation measures depend on the level of certainty that can be placed on the simulated regional climate projections.

In this study we focus on the comparison of several climate reconstructions over Europe with climate model simulations over the past centuries conducted with the comprehensive Atmospheric Ocean Global Circulation Model (AOGCM) ECHO-G and the Regional Climate Model (RCM) MM5. The climate of the European region in the past centuries has been subject to an intense analysis based on a variety of sources (a very rich web of recorded historical evidence, very long instrumental and early instrumental climate series, tree-rings, lake sediments, etc.) and thus offers a suitable target for climate models. These sources have been combined into gridded reconstructions of monthly (and seasonal in early periods) near-surface air temperature (SAT) and precipitation, which are particularly useful for comparisons with coarse-resolution simulations with global climate model simulations. Additionally, a few very long, almost 400 hundred years instrumental temperature series, such as the Central England temperature record, are available. Although uncertainties in this record cannot be ignored, particularly in its early part, it is probably more closely ground-truthed than other indirect indicators of temperature, and this may be useful in situations when disagreements between model simulations and proxy-based reconstructions can not be completely resolved.

In this type of analysis one important drawback concerning global climate models is their limited spatial resolution, presently about 200-300 km at mid-latitudes, which hampers a direct comparison between the simulated output and individual proxy

records. Regional details like topography, coastlines, etc., may cause deviations between simulations and proxy series, which would not be *per se* indicative of a serious intrinsic deficiency of the global climate model. Regional models are a useful tool in this respect (Dudhia, 1993; Jacob et al., 2007; Gómez-Navarro et al., 2011a). Driven at the boundaries of a limited domain by the output of global models, they can represent much more realistically, thanks to their high spatial horizontal resolution of about 20 to 50 km, all those regional characteristics that can be important to interpret a particular proxy record. In some cases they can also correct the frequency or intensity of regional synoptic circulation patterns that may be deficiently represented in the global climate model, in such way that the regional imprint of a large-scale climate change signal is also better represented.

An important aspect in the comparison between simulations and reconstructions is of course the long-term, centennial scale, evolution of temperature, since it is probably driven by external climate forcings and thus is linked to the climate sensitivity, an important characteristic to evaluate future climate change. However, persistent, long-lived deviations from the externally forced trend may be also important from the regional perspective. It is actually not very well-known if the regional climate can display large multidecadal deviations from the global climate evolution, either driven by regional climate drivers, such clusters of volcanic eruptions, or due to internal climate variations. In the European region some multidecadal episodes of such deviations have been identified, which are not fully explained yet. One characteristic episode is a set of especially warm decades in the winter temperatures around 1730 (Jones and Briffa, 2006), that are more clearly seen in North-Western Europe. Another episode is shown by the summer temperatures around 1760. Between both, a very cold period of extremely cold winter temperatures around 1740 (Jones and Briffa, 2006) has been also documented. If these long-lived deviations are due to natural variations, they could in principle re-occur also in the future, thus overwhelming the expected global climate change signal, at least in the early portion of the 21st century.

After presenting the technical details of the climate simulations, together with a short summary of the proxy-based climate reconstructions employed in this study, we present in the section 3 a validation of the climate simulations in the present climate. Section 4 comprises the comparison of model simulations with the different proxy-based reconstruction, and an analysis of the model skill. Finally, the chapter is closed with the main conclusions of this study.

## 5.2 Methodology and data employed

### 5.2.1 Climate models

For this study we have performed a 490-years long regional simulation of the European climate over the period 1501-1990. The RCM employed is a climate version of the meteorological model MM5 driven by the AOGCM ECHO-G (the model configuration will be hereafter referred as MM5-ECHO-G). Both models were driven identically by reconstructions of several external forcings, further explained below.

The ECHO-G global model driving the RCM consists of the spectral atmospheric model ECHAM4 coupled to the ocean model HOPE-G (Legutke and Voss, 1999). The model ECHAM4 was used with a horizontal resolution T30 ( $\sim 3.75^\circ \times 3.75^\circ$ ) and 19 vertical levels. The horizontal resolution of the ocean model is approximately  $2.8^\circ \times 2.8^\circ$ , with a grid refinement in the tropical regions and 20 vertical levels. A flux adjustment between the atmosphere and ocean submodels, constant in time and with vanishing spatial average, was applied to avoid climate drift. A full description of this simulation can be found in (Zorita et al., 2004, 2005, and references herein). The global model simulation was driven by estimations of three independent sources of external forcings: greenhouse gas (GHGs) concentrations in the atmosphere, total solar irradiance (TSI) and an estimation of the global radiative forcing of stratospheric volcanic aerosols. The last two effects are included through the introduction of variations in an effective solar constant. The evolution of these forcings is depicted in the Figure 5.1, adopted from (Crowley, 2000).

The regional climate model used for the present study is a climate version of the Fifth-generation Pennsylvania-State University-National Center for Atmospheric Research Mesoscale Model (Dudhia, 1993; Grell et al., 1994a; Gómez-Navarro et al., 2010; Jerez et al., 2010). Two two-way nested domains were employed in the simulation with a spatial resolution of 135 km and 45 km, respectively. Figure 5.2 depicts the inner domain, with the actual topography implemented in the model. The present study focuses in this domain. The atmosphere is represented by 24 sigma levels in the vertical, with the top level at 100 hPa. The boundary conditions of the model ECHO-G are introduced into the RCM through a blending area of five grid points at the fringes of the outer domain. These areas (included in Figure 5.2) are not reliable in general and can not be taken them into account to draw the main conclusions of this study, so they and are excluded from the maps hereafter. The regional simulation was driven using the same external forcings than the global one to avoid physical inconsistencies.

The physics configuration in the RCM has been chosen in order to minimise the com-

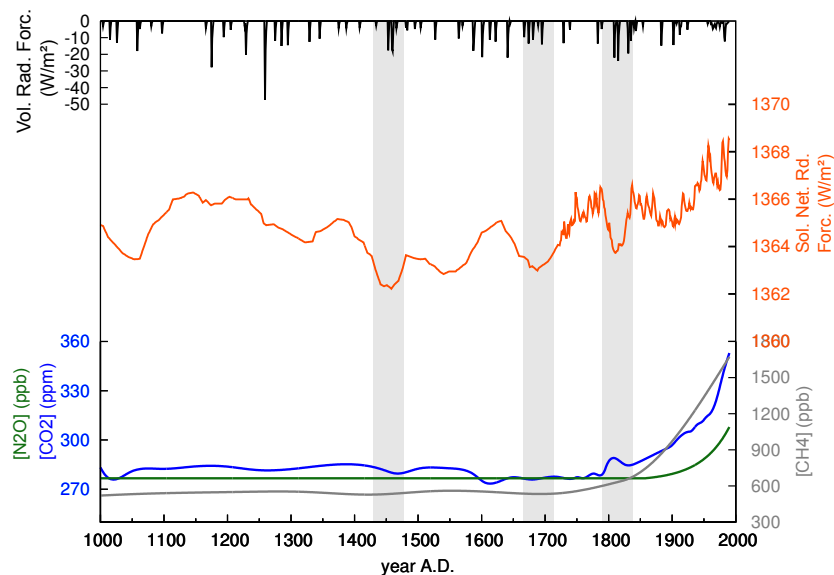


**Figure 5.1:** Reconstruction of the forcings for the last millennium employed in the simulations (Crowley, 2000). Orange line is the reconstruction of the total solar irradiance. Black line shows the estimated reduction in the effective short wave radiative balance in the top of the atmosphere due to big volcano events. The sum of both lines is the effective solar constant, which is implemented in the model to take into account both sources of external forcing. Blue, green and grey lines show the evolution in the concentration of CO<sub>2</sub>, NO<sub>2</sub> and CH<sub>4</sub>, respectively.

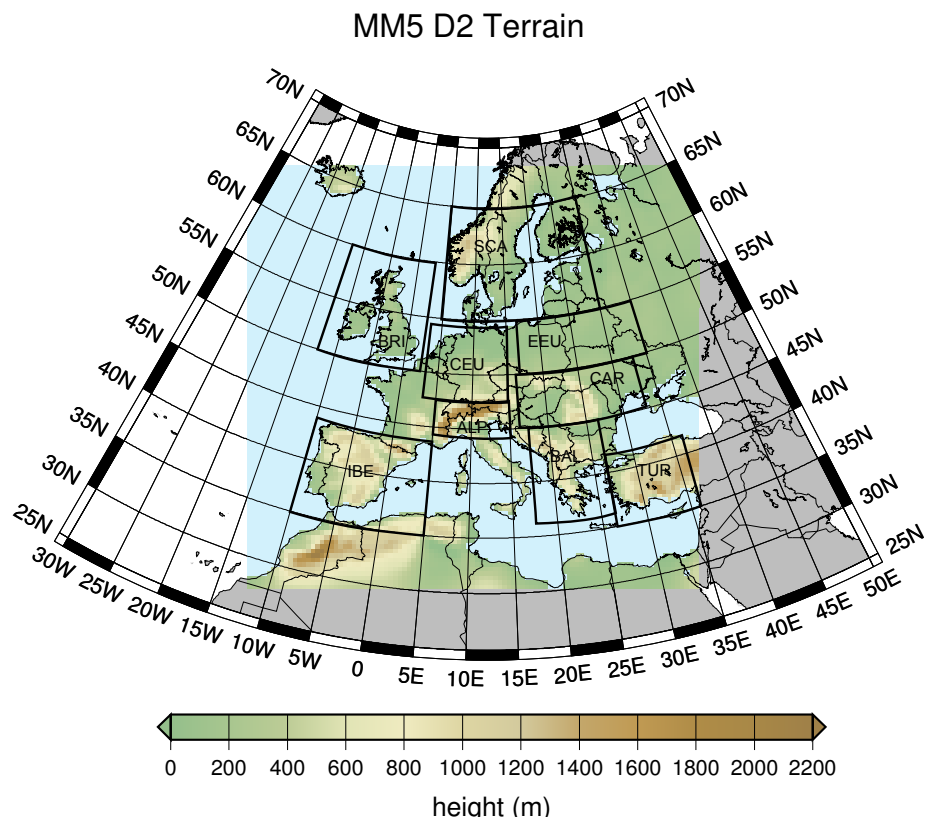


**Figure 5.2:** Topography implemented in the inner domain of the MM5 simulation, with a spatial resolution of 45 km. The mother domain covers a larger area with 135 km of resolution (not shown). Also shown 9 subregions used for more detailed analysis, based on geographical criteria. The names stand for: IBE, Iberian Peninsula; BRI, British Isles; CEU, Central Europe; EEU, Eastern Europe; SCA, Scandinavian Peninsula and Baltex Sea; CAR, Carpathian Region; BAL, Balkan Peninsula; ALP, Alps; TUR, Turkey.

putational cost, since none of the tested configurations provides the best performance for all kinds of synoptic events and regions (Fernández et al., 2007). The physical options implemented here are: Grell cumulus parametrisation (Grell, 1993), Simple Ice for microphysics (Dudhia, 1989), RRTM radiation scheme (Mlawer et al., 1997) and MRF for boundary layer (Hong and Pan, 1996). The Noah Land-Surface model (Chen and Dudhia, 2001a,b) has been used, as it simulates more accurately the climate in dry areas, specially in summer over most of the IP (Jerez et al., 2010). Boundary conditions are updated at the boundaries of the regional model every 12 hours.

### 5.2.2 Observations and reconstructions

To assess the skill of the model MM5-ECHO-G in reproducing the climate in a recent past period, we compare the seasonal mean values of SAT and precipitation in the last century with the data set provided by the Climate Research Unit (CRU) of the University of East Anglia (Mitchell and Jones, 2005). It consists on a gridded reconstruction of the evolution of SAT and precipitation (among other variables) which covers the last century entirely. It is the result of an interpolation of observational data to a high resolution regular grid ( $0.5^\circ \times 0.5^\circ$ ) that homogeneously covers the Earth over land grid-cell points. This data set is commonly used for model validation purposes in large projects such as PRUDENCE (Déqué et al., 2007). The NCEP reanalysis is used to provide a realistic data base for the evolution of SLP for during the 20th century (Kalnay et al., 1996).

We have also performed comparisons of the model results against some available proxy-based climatic reconstructions. For this we have employed several data sets, some of them are gridded reconstructions over Europe, and other are local or regional temperature reconstructions.

The gridded data sets consist of the SAT reconstruction by Luterbacher et al. (2004) and the precipitation reconstruction by Pauling et al. (2006). Both data sets consists of monthly and seasonal series in a  $0.5^\circ \times 0.5^\circ$  regular grid over Europe. They are based on a large variety of long instrumental series, indices based on historical documentary evidence and natural proxies. These reconstructions have been performed with a Climate Field Reconstruction method. The reconstruction method is based on principal components (PC) regression, by which a multivariate statistical regression model is set up between the leading Principal Components of a gridded observational data set and the available proxy records. This statistical model is then used to reconstruct the temperature or precipitation Principal Components backwards in time and, by combining the reconstructed PCs with the spatial eigenvectors, the whole spatial field.

The SLP reconstructions we use along this chapter is described by Küttel et al. (2009). It consist on a new statistically-derived  $5^\circ \times 5^\circ$  resolved gridded seasonal SLP data set covering the eastern North Atlantic, Europe and the Mediterranean area ( $40^\circ\text{W}$ ,  $50^\circ\text{E}$ ;  $20^\circ\text{N}$ ,  $70^\circ\text{N}$ ) back to 1750 using terrestrial instrumental pressure series and marine wind information from ship logbooks.

The Central European air temperature reconstruction (Dobrovolný et al., 2010) is based on documentary evidence in the period 1500-1854 from Germany, Switzerland and the Czech Republic. A dimensionless index of temperature is constructed for each country, and then averaged to get one series. Since none of the three series are complete, the number of series contributing to the mean varies with time, and correction of inhomogeneities have to be performed previous to the calibration. The instrumental period begins at 1760, and is recorded in 11 locations in the former countries plus Austria. All these series were homogenized and adjusted for the early instrumental warm-bias problem (Frank et al., 2007a,b). The calibration of the proxy dimensionless series is performed against the instrumental series in the period 1770-1816, and verified in 1760-1770 and 1817-1854. There are two version of the series, differing only in how the calibration of the proxy data to the instrumental period is performed. Nevertheless both versions depict few differences, and in this study we will focus in the version based in linear regression. Finally, although this reconstruction is available for all the 12 months, we will focus on annual and seasonal averages.

The Stockholm temperature reconstruction is also a combination of documentary evidence and instrumental records (Leijonhufvud et al., 2010). The former consists of several sub-series of estimations of the start of the sailing season after each winter in the period 1502-1892. It is known that this event is highly correlated with the average temperature in January to April, at least before the 19th century. Thereafter the ships became more capable of navigating in adverse conditions and the relationship between sailing season and average winter-spring temperature may be not that close. After homogenization, a dimensionless index can be obtained that preserves low-frequency variations. This index have to be calibrated against a instrumental period, which is available for this area from 1756 onwards. As in the case of the Central Europe series, the series corresponding to two methodologies of calibrating the proxy index to the instrumental period are available. Both results are very similar, and in this study we will focus on the series calibrated via ordinary least squares in the period of overlap 1756-1782. After 1782, the calibrated series is spliced to the instrumental record.

The model results for SAT is also compared with the Central England monthly temperature record (Parker et al., 1992). This record consists a well known instrumental series starting at 1659. Nevertheless, as pointed out by Manley (1974), data before

1720 should be considered less reliable, and in fact it is given with precision of 0.5 K.

### 5.3 Model skill in reproducing observed climate

#### 5.3.1 Climatologies

We have assessed the skill of the coupled model MM5-ECHO-G to reproduce the observed climate in the period 1960-1990 (hereafter referred as the reference period). We specifically focus on seasonal mean values and variability of SAT and precipitation. For this purpose we have used the CRU observational data base ([Mitchell and Jones, 2005](#)), thus only considering land grid-cells for the comparison.

Figure 5.3 depicts the time-averaged SAT in winter and summer for the reference period in the model (top), in the observation (middle) and their difference (bottom). In winter, the model describes relatively well the general spatial pattern, with the coldest areas in the northeastern part of the domain and the warmest in North Africa. Some deviations are nevertheless apparent when looking at the difference pattern. Although the model simulates accurately the areas close to the Mediterranean sea (with an average warm bias of 0.3 K in the areas below 45°N), it is clearly too warm in northern Europe (the averaged warm bias is 2.8 K for the areas above 45°N, and it is larger than 5 K in some areas). This picture is inverted in summer, when the model is too cold. Again, the model seems to simulate relatively well the general pattern (in particular is able to take into account the main mountain systems), but a marked difference in northern and southern Europe is clear. In this season the model is too cold, more remarkably in areas near the Mediterranean sea (the averaged cold bias over the Iberian Peninsula is -3.9 K). These warm/cold bias are within the ranges simulated, in the present climate, by other in the state-of-the art RCMs employed for climate change projections in Europe ([IPCC, 2007b](#)). Standard deviation maps (not shown) depict a large North-South gradient in winter, with values up to 3 K/year over the Baltic sea and only 1 K/year over the Iberian or Italian peninsula. Summer variability is however smaller, with rather homogeneous values around 1 K over Europe. This spatial and temporal structure of the SAT variability in the control period is correctly captured by the model.

Figure 5.4 depicts the similar information than Figure 5.3 for precipitation. Wettest areas in winter are near the western coasts and in the main mountain regions, as corresponds to a circulation dominated by the westerly moist flow. The model is able to capture this behaviour to a large extent. However, some differences appear in the model-minus-observations map (bottom row). In winter there is a clear bipolar behaviour: the model overestimates the precipitation in northern Europe, but underesti-

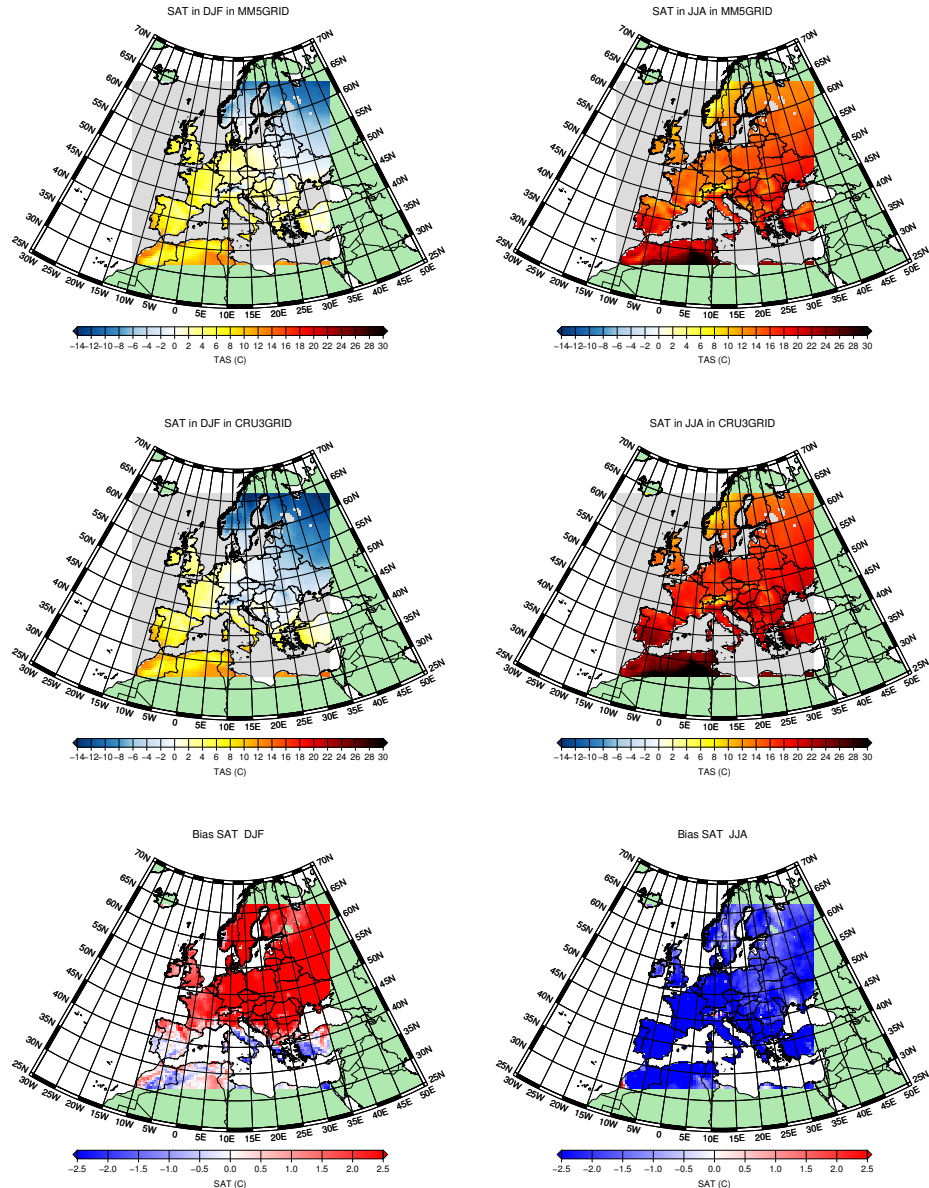


**Figure 5.3:** SAT averaged for the 1960-1990 period in winter (left) and summer (right) in the coupled model MM5-ECHO-G (top), CRU (middle) and difference between both (bottom). To perform the calculations, the CRU data has been interpolated to the model grid and only non ocean grid-cells have been considered.

mates it in the Mediterranean area, specially in the coast of Africa. The same bipolar behaviour, but inverted, is found in summer. Although the main precipitation events in summer are related to the orography (see Figure 5.2), and the resolution employed in the simulation is able to reproduce this behaviour, the model tends to strongly overestimate the precipitation near the Mediterranean, whereas it performs better in Northern Europe. Standard deviation maps for this variable (not shown) are similar to those of mean value, since mean and standard deviation are strongly correlated in precipitation records. However, difference maps in standard deviation are patchy during both seasons, and no clear structure of over neither infra estimation is easily identified.

We have further characterised the skill of the model comparing the Probability Distribution Function (PDF) in several regions as reproduced by the model and registered the CRU data base during the 20th century. This allows not only to identify biases but also the characterization of extreme seasons in different climatic areas over Europe. Figure 5.5 shows the PDF for the seasonal series of spatial-averaged SAT over the Alps, Scandinavia, Turkey and Iberia during the period 1900-1990. As discussed above, the cold bias in the model stands out in summer, whereas the model tends to be warmer in winter, specially in the Northern areas. However, despite the bias in the PDFs, its shape is remarkably similar in the simulation and observations in all areas and seasons. In particular, the model is able to reproduce correctly the characteristic bimodal PDF over Iberia or the asymmetric tails of the distribution in Scandinavia in the summer SAT series. This good match between model and observations at regional scale, although affected by a large bias, seems to indicate that the characterization of the influence of the orographic details in regional climates, together with the improved land use categories and vegetation cover, are being correctly captured by the regional model, whereas the biases could be driven by deficiencies in the characterization of the large-scale systems in the global model, as further investigated below.

Similarly, Figure 5.6 shows the PDF for precipitation in the same areas as Figure 5.5. The bipolar behaviour of the bias, discussed above, can be again identified here. In winter, the model tends to overestimate precipitation in Scandinavia, whereas underestimates it in Iberia. In summer, the situation is the opposite. In general there are larger differences between the model and observations for this variable than for temperature, but again the shape of PDFs, as well as the large differences between both seasons, is remarkably well captured by the model. The greater differences appear over the Alps, which could be due to a combination of a worse skill of the model over the mountains due to its relatively coarse resolution of 45 km, but also to the deficiencies in the observational data base due to the lack of reliable observations in complex topography areas.

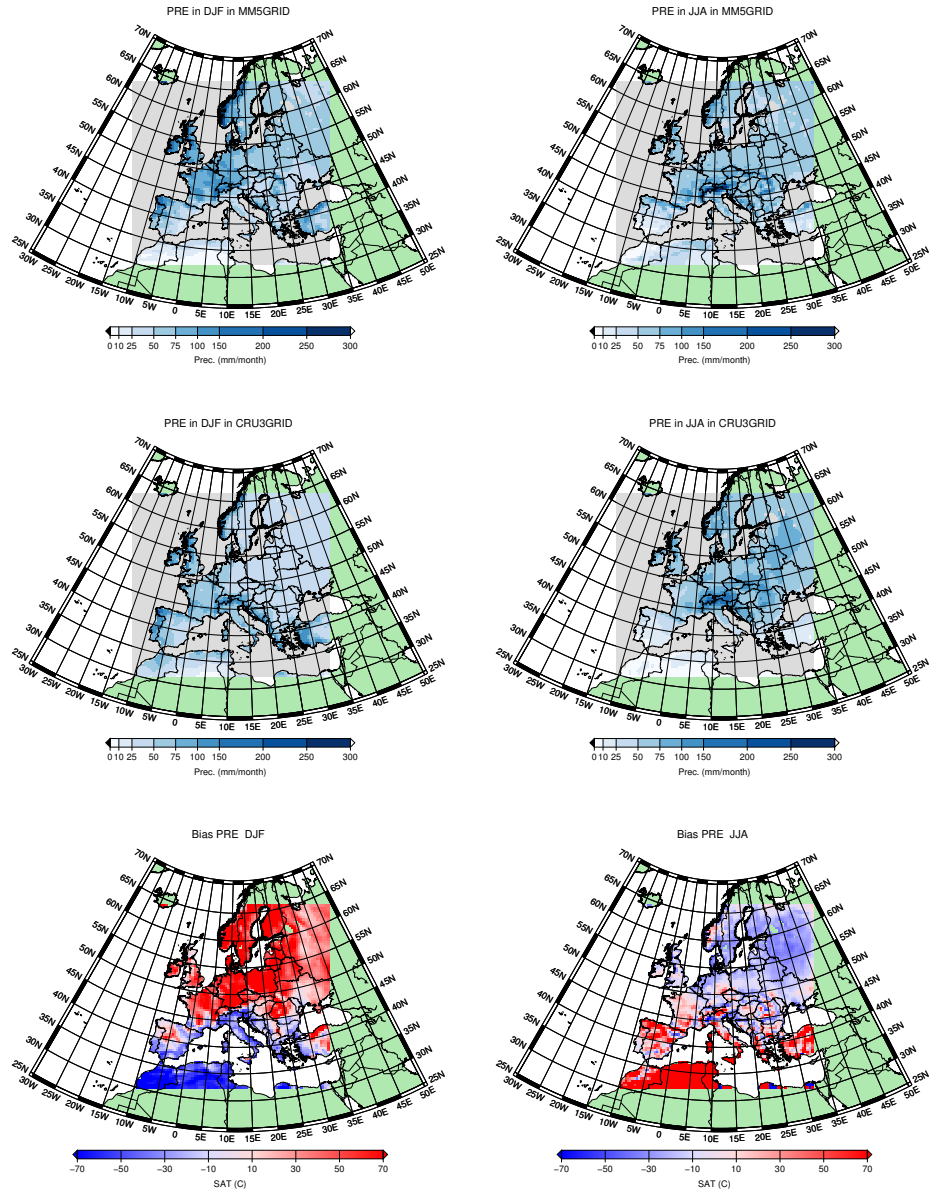


**Figure 5.4:** Precipitation averaged for the 1960-1990 period in winter (left) and summer (right) in the coupled model MM5-ECHO-G (top), CRU (middle) and difference between both (bottom). To perform the calculations, the CRU data has been interpolated to the model grid and only non ocean grid-cells have been considered.

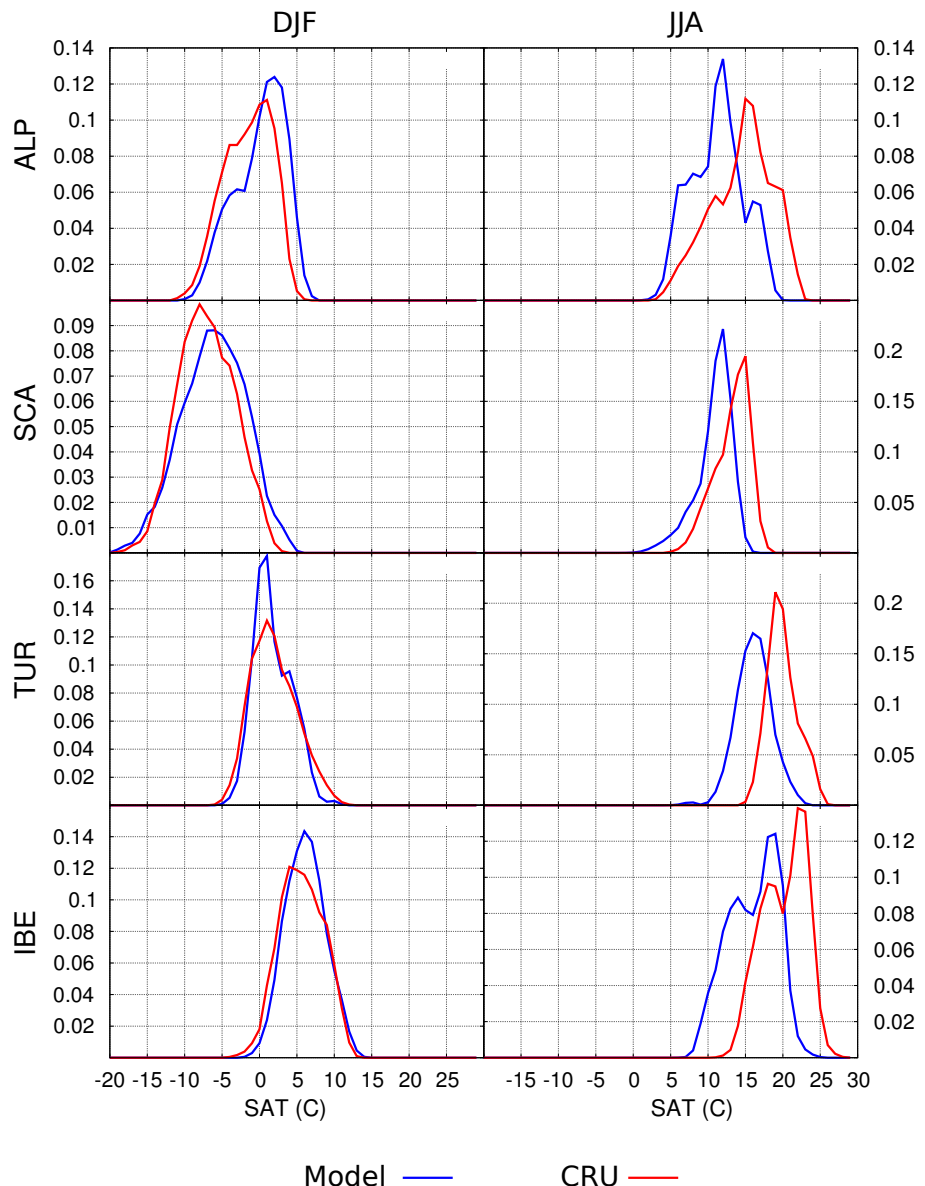


**Figure 5.5:** PDFs for SAT in winter (left column) and summer (right column) for several areas illustrating different climates over Europe. Blue line represents the simulation whereas red line represents CRU. PDFs have been calculated from the seasonal series during the period 1900-1990. From top to bottom: Alps, Scandinavia, Turkey and Iberia. These areas are shown in Figure 5.2.

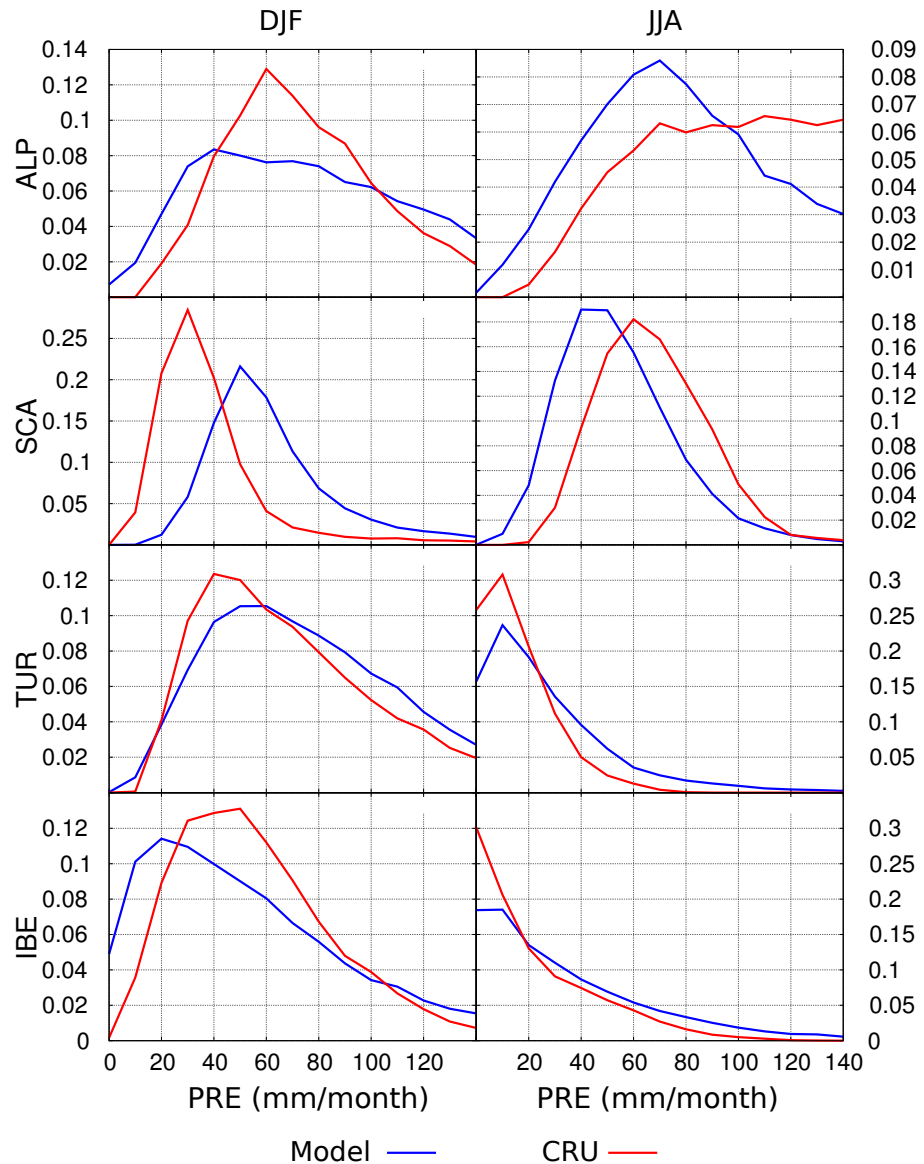


**Figure 5.6:** PDFs for precipitation in winter (left column) and summer (right column) for several areas illustrating different climates over Europe. Blue line represents the simulation whereas red line represents CRU. PDFs have been calculated from the seasonal series during the period 1900-1990. From top to bottom: Alps, Scandinavia, Turkey and Iberia. These areas are shown in Figure 5.2.

We have investigated the reasons for the biases in SAT and precipitation exposed above. The warm bias in winter is also (but greater) present in the stand-alone ECHO-G simulation, with the notably difference of a strong cold bias in the most northeastern part of the domain (not shown). In ECHO-G the warm bias is even larger near the Mediterranean, pointing to a improvement in this area due to the higher resolution of the RCM, and perhaps for changes in physical parametrizations. This warm bias in northern Europe seems to be caused by an overestimation of the strength of the zonal circulation, which carries too much warm and moist air from the Atlantic sea. This overestimation is due to a too intense pressure gradient simulated by ECHO-G over the North Atlantic, as can be appreciated in Figure 5.7, where the Sea Level Pressure (SLP) in the reference period for the NCEP reanalysis (Kalnay et al., 1996) and ECHO-G is presented. This flow is introduced into the RCM through the boundaries of the domain, warming the area in winter. The anomalous flow of warm moist air from the ocean also explains the larger precipitation amounts in this season in northern Europe.

Similarly, the cold bias in summer is also present in the ECHO-G simulation, with the exception of the main mountain systems. Here, the bias is smaller since the GCM is not able to represent the mountain ranges due to its coarse resolution (not shown). The RCM is still able to reduce the bias over these mountains, but it can not be completely corrected. Analyzing the summer mean SLP in the simulation and in NCEP in Figure 5.7, it can be identified how part of the bias is due to the same mechanism than in winter. During this season, the overestimation of the zonal circulation precludes a realistic simulation of the large-scale systems, developing a weather too similar to winter in comparison with the NCEP observations. However, another mechanism emerges during this season. Comparing Figures 5.3 and 5.4, the cold bias in summer near the Mediterranean can be linked to a too wet conditions. A possible explanation for this may involve a too extensive cloud cover and precipitation in summer, thus reducing the incoming solar radiation and cooling this area compared to observations.

### 5.3.2 Summary of the validation

Summarizing this section, the coupled model MM5-ECHO-G is able to reproduce many aspects of the present climate in Europe. Some biases in the reference period compared to the CRU data base can be found, but they are within the range of other biases reproduced by current state-of-the art RCMs employed in climate change projections<sup>1</sup>. In

<sup>1</sup>Most RCMs are validated in an observational period driven by reanalysis data, since this kind of hindcast simulation try to assess the skill of the model itself, not the driving boundary conditions. However, the simulation analyzed here are driven by a GCM not forced to follow observations. Thus, the fact that

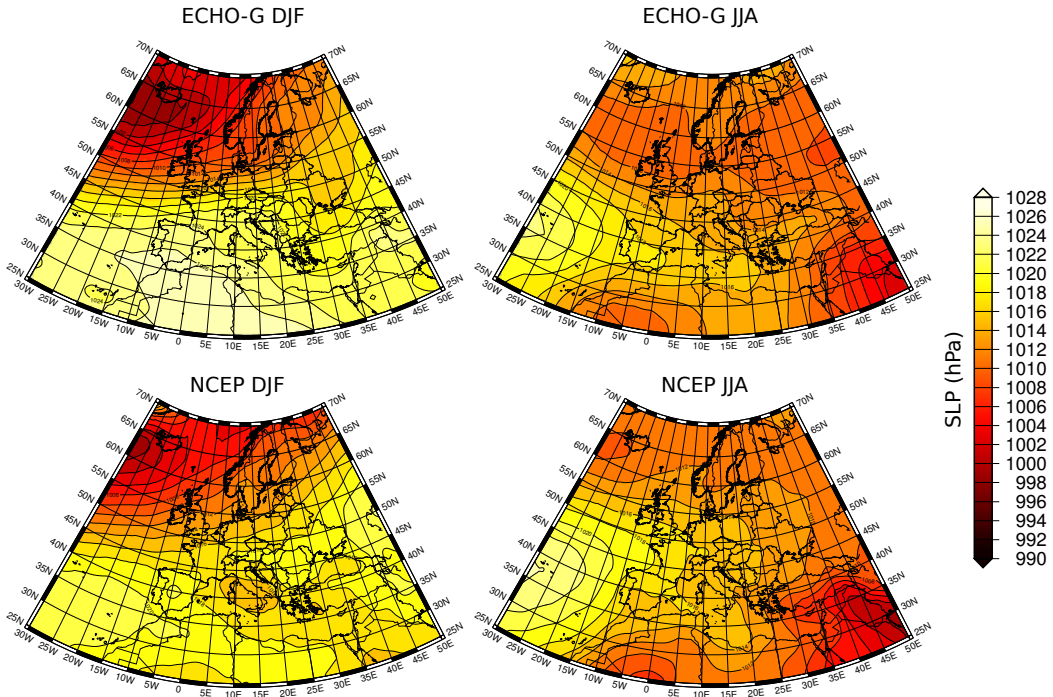


**Figure 5.7:** Mean SLP in winter (left) and summer (right) in the reference period 1960–1990 as simulated by ECHO-G (top) and in the NCEP reanalysis (bottom).

particular, winters tend to be too warm and wet, and summers too cold. This underestimation of the amplitude of annual cycle seems to be related to an overestimation of the zonal flow in the GCM, as well as to an overestimation of the precipitation amount, mostly near the Mediterranean sea in summer. Despite these bias, which must be preset when trying to use the model as a benchmark for the reconstructions, the analysis of PDFs show that the model is able to capture realistically its complex shape in different areas over Europe. This also implies that the model develops a feasible distribution of extreme seasons.

---

biases are not too large with respect to other simulations with RCMs is a even stronger prove of the skill of the model setup employed here.

## 5.4 Modeled and reconstructed climate

We have compared the climate evolution simulated by the models with a number of reconstructions of the climate in different areas of Europe during the last centuries. It is important to note that due to the high natural variability in climate models (which is also an important component of the variability in the actual climate system), one should not expect complete agreement between the temporal evolution of simulations and reconstructions at interannual timescales, even if both are perfect (Yoshimori et al., 2005). This makes the comparison difficult, specially concerning the time evolution, but does not hamper the evaluation of many other aspects of climate variability such as the amplitude of variations at centennial time scales, long-term trends, or even more sophisticated aspects like main variability modes<sup>2</sup>. An especially interesting aspect of simulations is that they allow the evaluation of the physical consistence of reconstructions. This is because although climate models only represent a limited fraction of the reality due to the many simplifications they contain, they are compounded by well-known physical laws, so their internal physical consistence is warranted. This use of the simulation to evaluate the skill of reconstructions is also illustrated through this section.

### 5.4.1 Gridded reconstructions

We have firstly computed the PDFs of SAT and precipitation in the same areas than in the former section in the reconstructions and the simulation (which was demonstrated above to be realistic in a reference period, although with clear biases). The period chosen to analyze the PDFs is 1500-1900. We do not consider the 20th century because these reconstructions are calibrated against CRU in this period, so their skill could be easily overestimated. Figure 5.8 depicts the histograms for SAT in four regions over Europe, and it is the equivalent to Figure 5.5 but in the palaeoclimatic context. The shape of PDFs is very different in different areas and seasons, but it is remarkably similar in the simulation and reconstructions, and it is also very similar to the results exposed above regarding the reference period. Since the model poses on the same physical laws in the reference and the past period, this represents independent evidence of the good skill of the reconstructions and their capability to represent a feasible realization of the past climate. Additionally, bias between both approaches are very similar to the bias found within the reference period, which indicates that the main differences can

<sup>2</sup>Obviously this kind of complex studies can only be afforded with gridded reconstructions, as it is done in the first section. In punctual reconstructions the analysis is more limited.

be attributed to problems in the simulation, rather than in the reconstructions. Figure 5.9 depicts the PDFs for precipitation. There is again a remarkable agreement in the shape of the histograms, but in this variable the disagreements are greater, as in the reference period. It is interesting however that despite the large trends simulated by the model during the 20th century (see next section), the PDFs in the model present similar aspect in the 1500-1900 period and in the last century. This suggest that in the case of precipitation differences with the model are more easily attributable to drawbacks in the reconstructions.

The next step is to compare the temporal evolution of the simulations by the model configuration ECHO-G-MM5 against the SAT and precipitation gridded reconstructions by Luterbacher et al. (2004) and Pauling et al. (2006), respectively. This is done by means of the comparison of the temporal series associated to space-averaged areas. In order to take advantage of the high resolution of the model simulation in the comparison of the series, we have avoided the use of averages over large areas. Instead, in the following analysis we have used the 9 subregions depicted in Figure 5.2. The series have been filtered to reduce the high frequency noise. However, although at longer timescales the random variability may be filtered out more effectively, and the external forcings can be more easily identified in the evolution of the variables, the degree of filtering required is not known. In this study we apply a 31-years running mean, which is a commonly employed filter in the bibliography (Zorita et al., 2010; Gómez-Navarro et al., 2011a).

Figure 5.10 shows the comparison between the evolution of SAT in the ECHO-G-MM5 model (solid lines) and the Luterbacher et al. (2004) reconstructions (dashed lines) in winter and summer. The corresponding area is labeled in each panel. In general, variability in northern areas of Europe is larger than in the south. Similarly, the winter variability in these areas is larger than in summer. It is important to note that this behaviour is coherent in the reconstruction and the simulation. The temporal agreement between both is in general better in winter for in central Europe. A clear upward trend appear in all seasons and areas of the 20th century, which is remarkably larger in the northern Europe in winter (contrastingly, the Iberian Peninsula is the only region where the trend is larger in summer, as reported by Gómez-Navarro et al. (2011a)). Nevertheless the time in point when this upward trend starts is different in the reconstructions and the simulation. In the latter it begins in all areas just after the Dalton minimum (1790-1810), a period characterised by a lower number of sun spots and hence solar activity. This cold period is not clearly present in the reconstructions. Instead, they show a cold period later, more noticeable in summer across southern Europe, around 1900, which is not present in the simulation. Around 1740 there is a clear

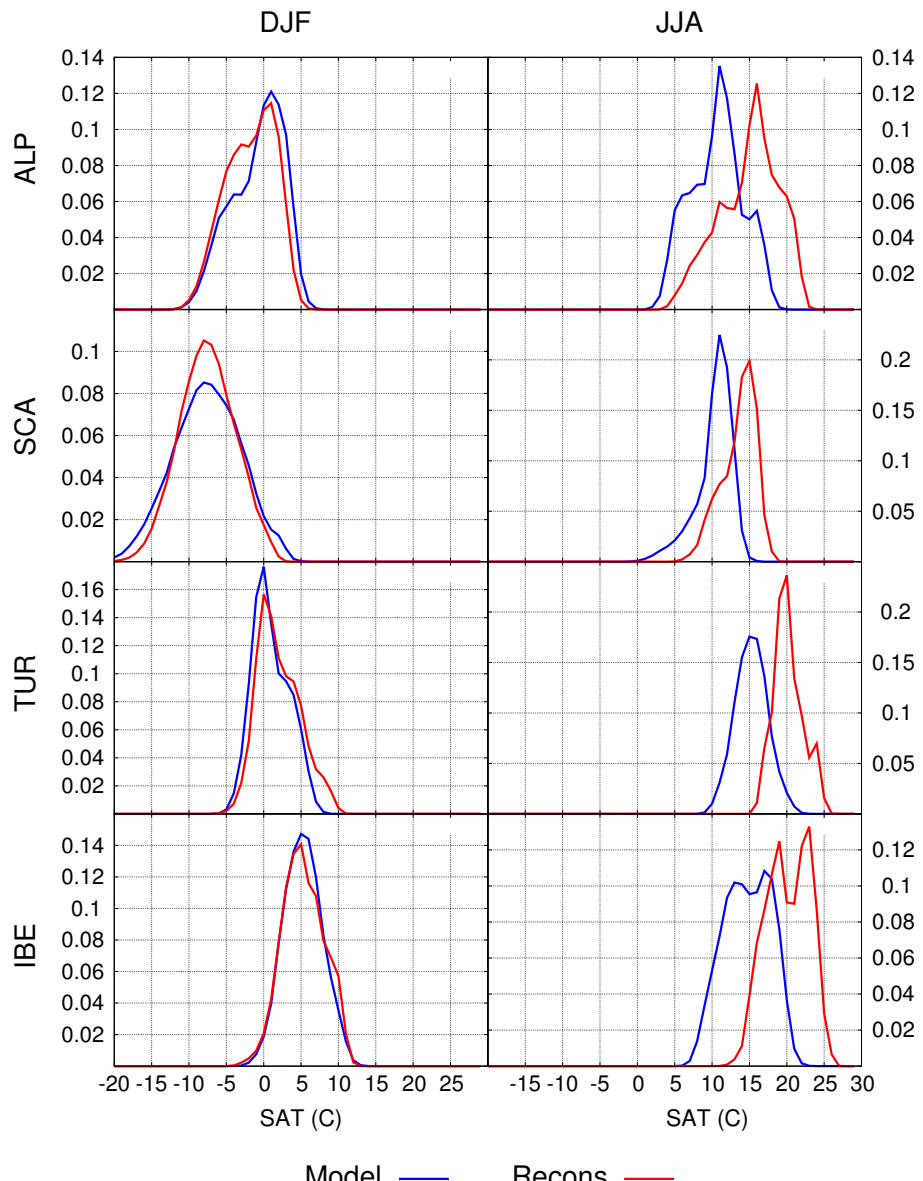


**Figure 5.8:** PDFs for SAT in winter (left column) and summer (right column) for several areas illustrating different climates over Europe. Blue line represents the simulation whereas red line represents the (Luterbacher et al., 2004) reconstructions. PDFs have been calculated from the seasonal series during the period 1500-1900. From top to bottom: Alps, Scandinavia, Turkey and Iberia. These areas are shown in Figure 5.2.

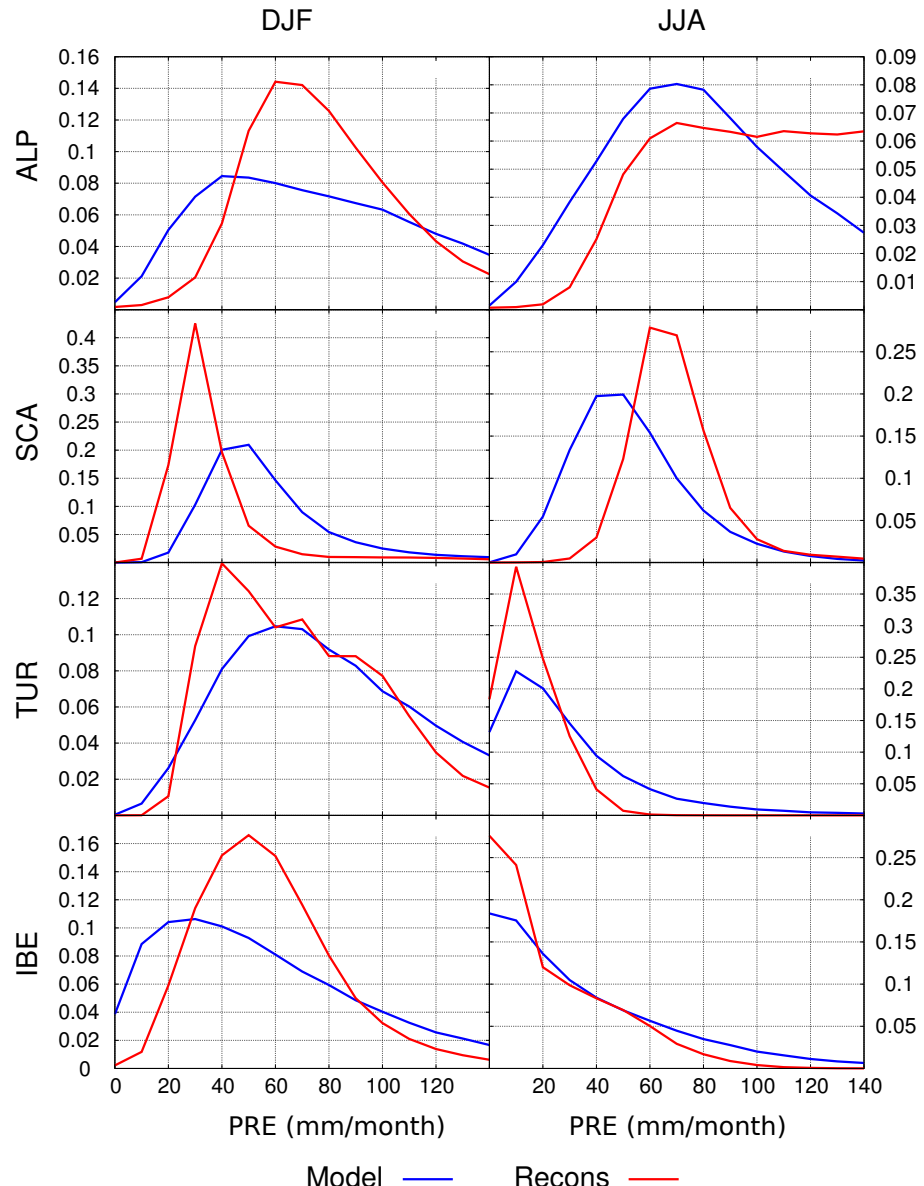


**Figure 5.9:** PDFs for precipitation in winter (left column) and summer (right column) for several areas illustrating different climates over Europe. Blue line represents the simulation whereas red line represents the (Pauling et al., 2006) reconstruction. PDFs have been calculated from the seasonal series during the period 1500-1900. From top to bottom: Alps, Scandinavia, Turkey and Iberia. These areas are shown in Figure 5.2.

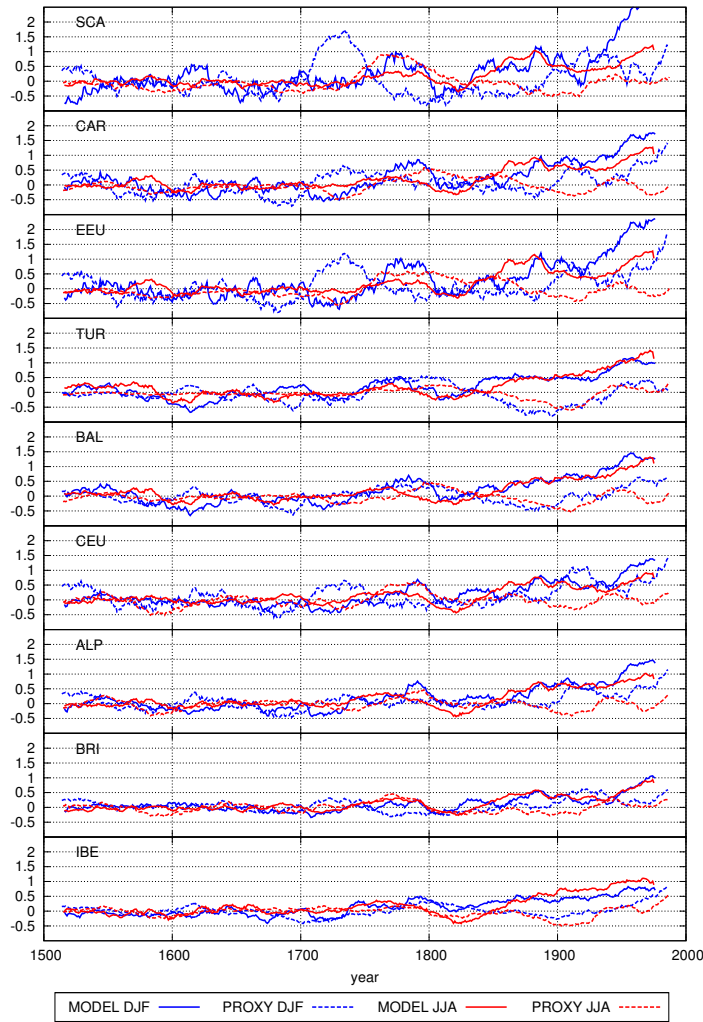


**Figure 5.10:** 31-year running mean of SAT anomaly series averaged for the 9 subregions depicted in Figure 5.2. Blue and red lines represent winter and summer, whereas solid and dashed lines represent the model and the Luterbacher et al. (2004) reconstructions, respectively. All series depict anomalies (in K) respect to the preindustrial period (1500–1850). Panels share the same scale in both axis to ease the comparison of the relative variability among different areas.

warm period a few decades long in northern Europe in the winter SAT reconstructions, which goes up to Eastern Europe, but is not present in the south. This warm period, which was analysed by Jones and Briffa (2006) based on documentary and early instrumental evidence, is not present in the simulation. It can also be identified in other independent reconstructions and instrumental records, as further commented below. In general, the 20th century temperature trends tend to be larger in the model than the reconstructions, being this tendency larger across northern areas. In fact, this larger sensitivity to climatic variations in the northern areas seems to be coherent with state-of-the-art climate change projections (IPCC, 2007b). There are two possible reasons for this mismatch. One is that, neither the GCM nor the RCM incorporate the forcing by tropospheric aerosols in the 20th century. The higher concentration of aerosols is known to have a net cooling effect, and thus its absence in the simulation can explain part of this bias. Secondly, the cold bias seem to be reduced from roughly 1800 onwards. This could be linked to a known warm bias in the summer temperature recorded by some early instruments, due to the lack of the modern screens (Frank et al., 2007a,b).

Figure 5.11 depicts the same information that Figure 5.10 for precipitation. In this case, the differences between the RCM and the GCM are larger (not shown), since precipitation processes are strongly influenced by the differences in the orography and the physical parametrisations implemented in both models (Fernández et al., 2007). As in the case of temperature, there is no significant correlation between the reconstruction and the simulation. In contrast with the evolution of SAT, precipitation presents less variability the northern areas. In particular, it seems to be specially large in mountain areas such as the Alps, Turkey or the Iberian Peninsula. This behaviour is shared between the model and the reconstructions, giving in this sense confidence to both approaches. In this case there is not a shared trend in all areas and seasons. We may however identify a positive trend in winter precipitation in some areas in the northern part of Europe, specially in the British Islands and Scandinavia, together with a negative tendency in the south, such as in the Iberian or the Balkan Peninsulas. This behaviour, which resembles the bipolar structure found for the present period in the previous section, seems to be driven by an intensification of the zonal circulation due to a strong positive phase of the NAO in the last century within the simulation (see Figure 6.6c and explanations in Chapter 6). Nevertheless this pattern can not easily be identified in the reconstructions. In summer the trends are weaker, since this season is not so influenced by this large circulation pattern. In fact, apart from the clear negative trend in the British Islands, there is no obvious trend in summer precipitation series in the model neither in the reconstructions.

Finally, we have analyzed the main variability modes in the period 1500-1900 in the

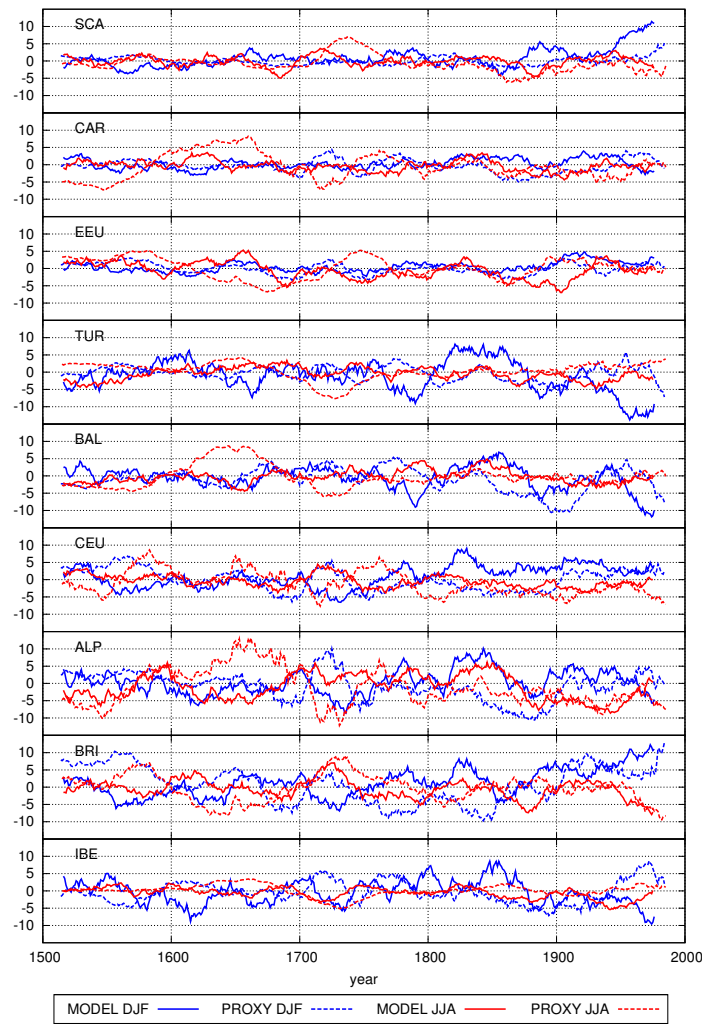


**Figure 5.11:** 31-year running mean of precipitation anomaly series averaged for the 9 sub-regions depicted in Figure 5.2. Blue and red lines represent winter and summer, whereas solid and dashed lines represent the model and the [Pauling et al. \(2006\)](#) reconstructions, respectively. All series depict anomalies (in mm/month) respect to the preindustrial period (1500-1850). Panels share the same scale in both axis to ease the comparison of the relative variability among different areas.

simulation and in the reconstructions through an EOF analysis (von Storch and Zwiers, 1999). This procedure allows to increase the signal-to-noise ratio, reducing the amount of noise in climatic fields and summarizing a large part of their variability in a reduced number of prominent modes. Figure 5.12 depicts the first three EOFs for winter SAT in the model and in the reconstructions. First EOF shows a very similar pattern, with the same sign over most of the domain, following a Northeast-Southwest gradient. Greatest differences are located near the Mediterranean, in particular over the Iberian and Turkish peninsulas. Second EOF shows a bipolar behaviour (notice the change of sign, which has no physical meaning), with its axis around the parallel at 55°N in both cases. The largest difference in this mode is that simulation includes the British Islands in the lower side of the dipole in the model. Finally, third EOF shows a clear East-West gradient, only differing in the Northern areas near the Baltic sea. Besides the good agreement in the shape of the main modes, it is noticeable the good agreement in the amount of variance explained by each EOF, shown in Table 5.1, which indicates that SAT variability is captured realistically (or at least physically consistent) by the reconstructions. Figure 5.13 analyzes the same than Figure 5.12 for precipitation. The agreement between model and reconstructions in this variable is in general worse than for temperature. First EOF shows in the model a North-South gradient which is analogous to the modes found in the CCA analysis performed above, which can be related to NAO variations, whereas reconstructions show a monopole structure, with changes of sign over West of Norway and some areas in the North of Africa. Second EOF is more similar. It depicts a North-South pattern, clearly separating the behaviour near the Mediterranean with the rest of Europe. Again, the largest differences appear in the Iberian and Turkish peninsulas. Third EOF is a patchy pattern in both data bases, and presents not good agreement in general. Analyzing the amount of variance explained in each EOF, we found further differences. The amount of variability explained by the first EOFs in reconstructions is larger than in the model. This overestimation could be associated to the reconstruction method, also based on EOF analysis, which overestimates the amplitude of variability of the main variability modes, underestimating the amount of noise in the actual climate fields.

The situation for summer is similar, as shown in Figures 5.14 and 5.15. First three EOFs for summer SAT depict similar spatial structure than for winter. However, the order of second and third EOF are swapped in the model and the reconstructions. Additionally the spatial structure of second EOF in the model (third in the reconstructions), although similar with a North-South bipolar structure, differs at great extent in the Southwest of Europe, more noticeably over the Iberian Peninsula and France. Situation becomes even worse for summer precipitation. In this case EOFs are different, and

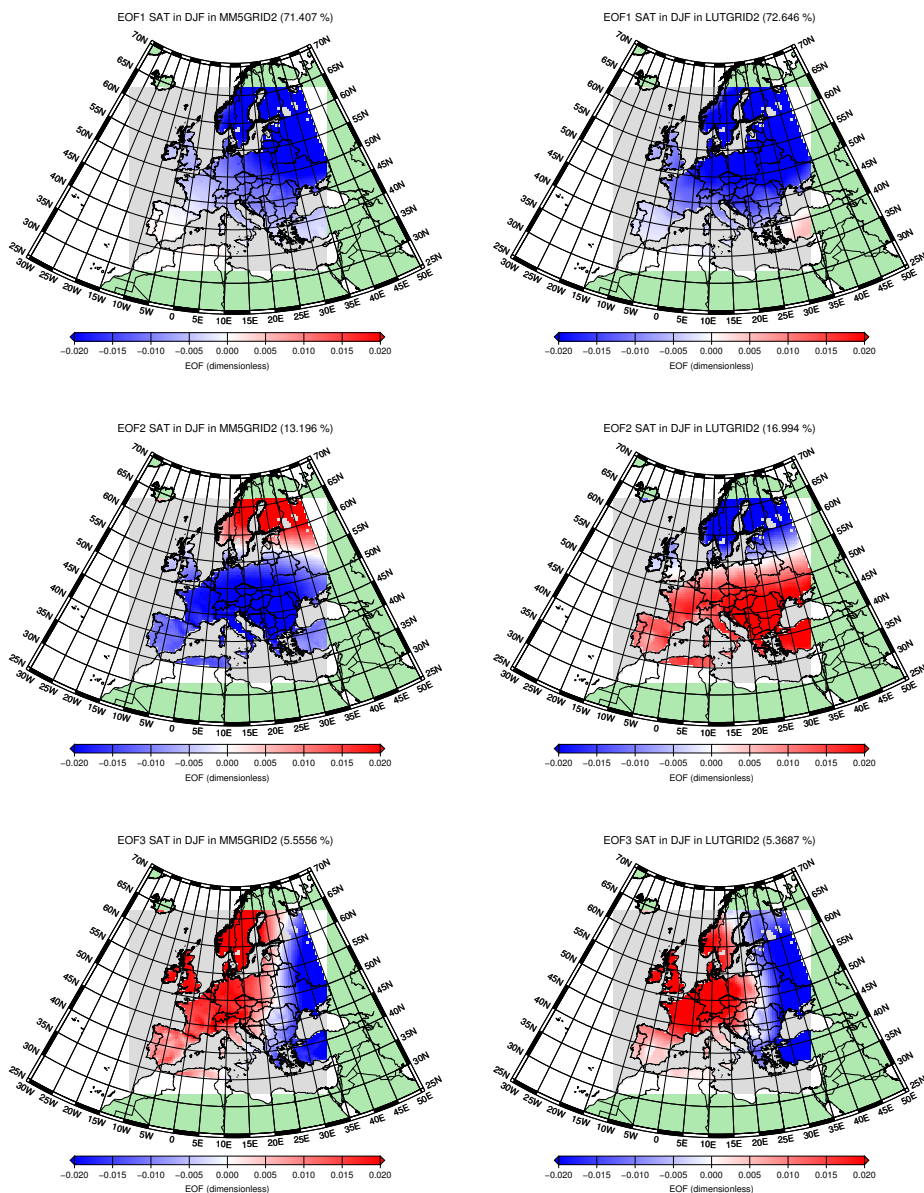


**Figure 5.12:** First EOFs for SAT in winter in the model simulation (left) and in the gridded reconstruction (right) in the period 1500-1900.

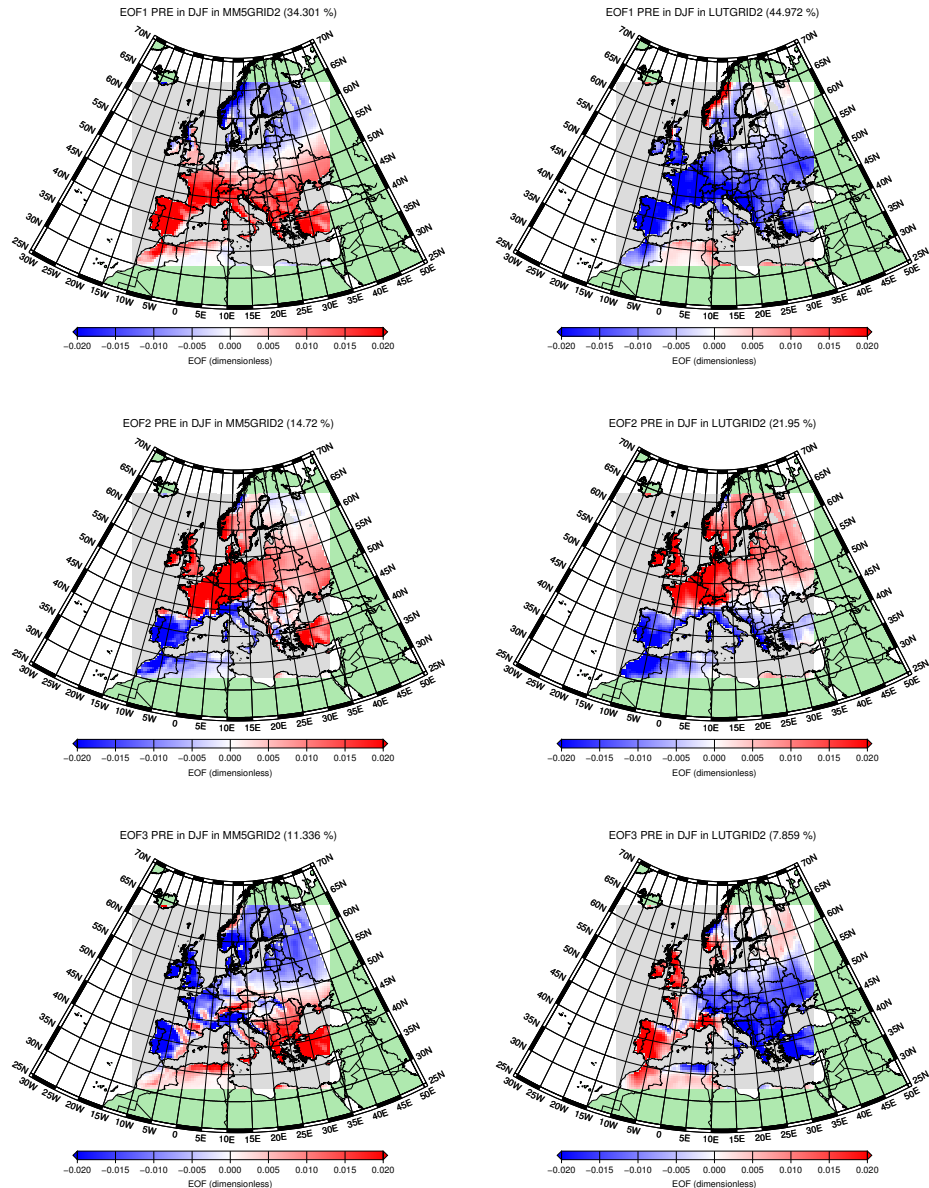


**Figure 5.13:** First EOFs for precipitation in winter in the model simulation (left) and in the gridded reconstruction (right) in the period 1500-1900.

	DJF				JJA			
	SAT		PRE		SAT		PRE	
	Model	Rec.	Model	Rec.	Model	Rec.	Model	Rec.
EOF1	71.41	72.65	34.30	44.97	57.07	48.21	11.83	38.66
EOF2	13.20	16.99	14.72	21.95	11.85	24.88	8.18	18.79
EOF3	5.56	5.37	11.34	7.86	10.57	13.13	5.25	9.01

**Table 5.1:** Percentage of variance explained by the first three EOFs in SAT and precipitation in winter and summer in the model simulation and the reconstructions in the period 1500-1900. The corresponding fields are shown in Figures 5.12 to 5.15.

again the amount of variance explained by them (see Table 5.1) is strongly overestimated in the reconstructions. This may indicate that the reconstruction method tends to infra estimate the number of independent variability models contributing to the actual variability field of precipitation.

#### 5.4.2 Reconstruction of Central European Temperature series

In this subsection we compare the results of the simulation obtained with the model MM5-ECHO-G with a Central European air temperature reconstruction (Dobrovolný et al., 2010). Figure 5.16 depicts the SAT series obtained for Central Europe by the models (ECHO-G alone and the coupled model MM5-ECHO-G) and by the reconstructions. All series represent anomalies with respect to its mean during the period 1900-1990. The correlation between the two models is remarkable in all seasons, and it is due to the forcing of the ECHO-G model, which strongly drives the MM5 SAT evolution through the boundaries of the domain (note that the large differences in the mean values shown in Figure 5.3 are not appreciated here since only anomalies are depicted). As commented above, precipitation anomalies show much larger differences between models, since this variable is more dependent on the horizontal resolution, as well as physical parametrisation of the model (not shown). Less temporal agreement can be found between the reconstruction and the models, as it could be expected. The general tendency towards warmer conditions in all seasons in the 20th century is nevertheless present in the simulation and the reconstruction, being this the major agreement between the data sets. By seasons, the agreement is in generally lower in the warmer seasons, where the model tends to be too cold. It is not easy to explain this cold bias of the model, since the proxy series were previously corrected to avoid the warm-bias problem due to insufficient protection of the thermometers against radiation. Simu-

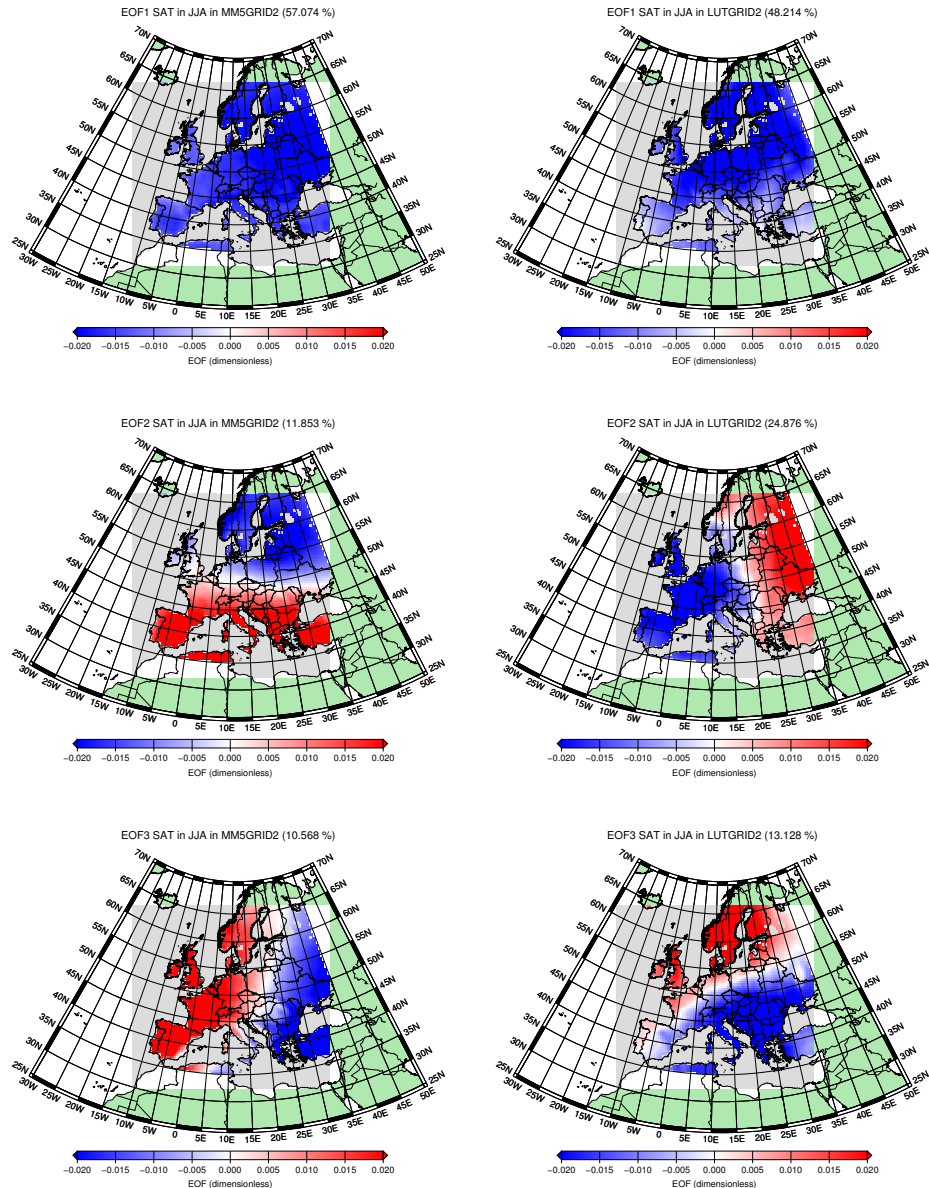


**Figure 5.14:** First EOFs for SAT in summer in the model simulation (left) and in the gridded reconstruction (right) in the period 1500-1900.

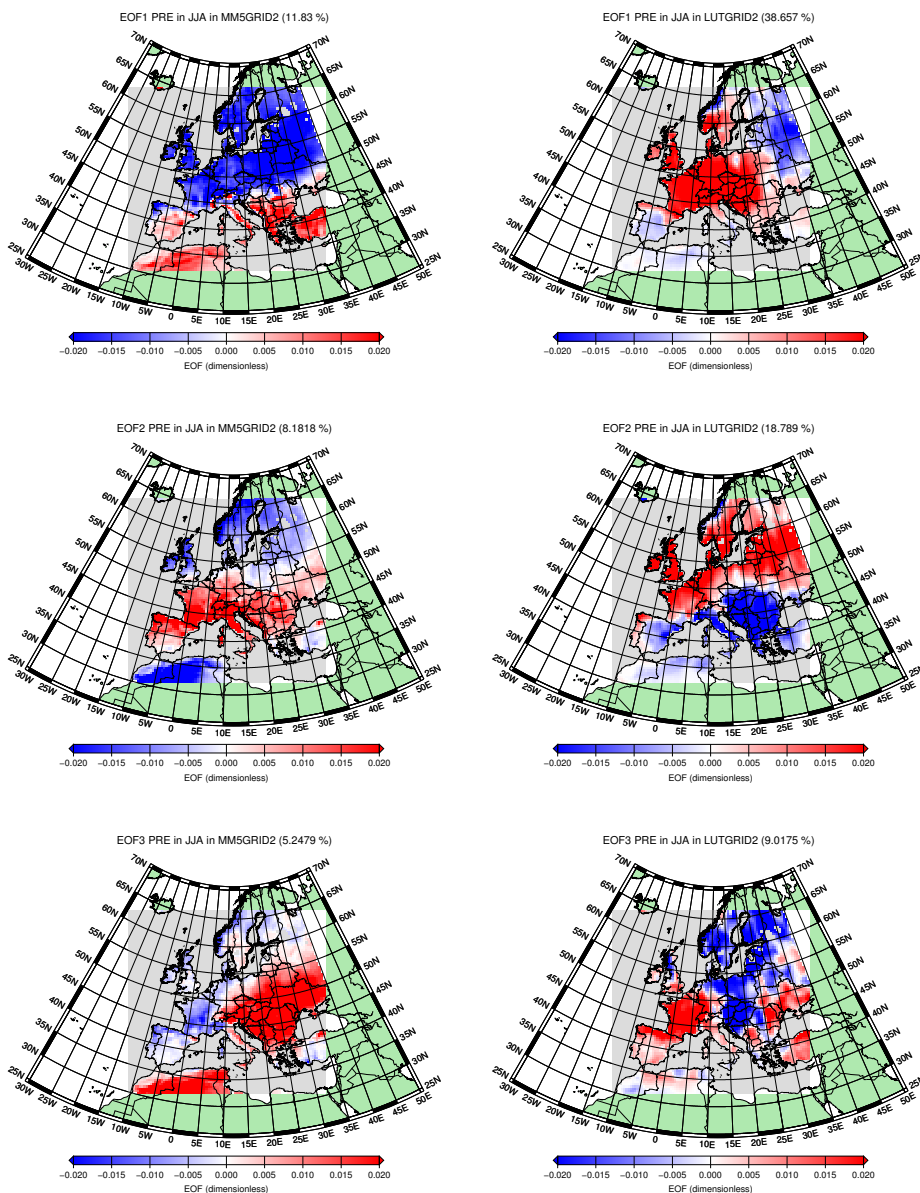


**Figure 5.15:** First EOFs for precipitation in summer in the model simulation (left) and in the gridded reconstruction (right) in the period 1500-1900.

lated and reconstructed variability is similar in winter, but the models underestimate it in summer. The models simulate a cold period around 1810 which is coincident with the Dalton minimum. Reconstructions nevertheless do not show a clear minimum in this period.

#### 5.4.3 Reconstruction of Stockholm January-to-April mean temperatures

The comparison between the model output and the Stockholm temperature reconstruction ([Leijonhufvud et al., 2010](#)) is shown in Figure 5.17. It depicts the evolution of SAT in Stockholm in the global, the regional model, and the reconstruction, all records with respect to the period mean in 1900-1990. The reconstruction is characterised by a cooling trend between 1500 and 1550s, reaching a minimum between 1550-1650, and followed by a long-term warming trend to the present. A clear peak in the 1730s, which can also be clearly identified also in the [Luterbacher et al. \(2004\)](#) reconstructions, as commented above. As before, the simulated series evolve close to each other with a rather continuous trend along the five centuries simulated, with some decadal variability superimposed. The global long-term trend in the simulations (0.47 K/century) agrees relatively well with that of the reconstruction (0.37 K/century), suggesting that the magnitude of the changes of the solar forcing in the last centuries, combined with the model sensitivity, is reasonable [Zorita et al. \(2010\)](#).

Regarding the warm anomaly in the reconstruction around 1730, it clearly can not be identified in the model simulations. Furthermore it can not be explained invoking uncertainties in the model or the reconstruction, and since this warm period is absent in different simulations with ECHO-G sharing the external forcings, this warm period seems not to be caused by the effect of variations in the external forcings prescribed in the model ([Zorita et al., 2010](#)). Another possibility is that internal variability in the ECHO-G simulation is too small. This aspect will be further investigated below.

#### 5.4.4 Modeled and observed temperatures records in Central England

Seasonal and annual series for the models and the instrumental record of Central England ([Parker et al., 1992](#)) is depicted in Figure 5.18. Although the series of both models are very similar, MM5 is up to 0.5 K colder in some periods, specially in winter. This difference is due to the better characterisation of the orography in MM5, since great part of the British Islands are covered by ocean in the GCM. The long-term trend is similar in the observation and in the simulation, and supports the idea that the choice of external forcing in the simulations was reasonable. There is nevertheless a larger trend

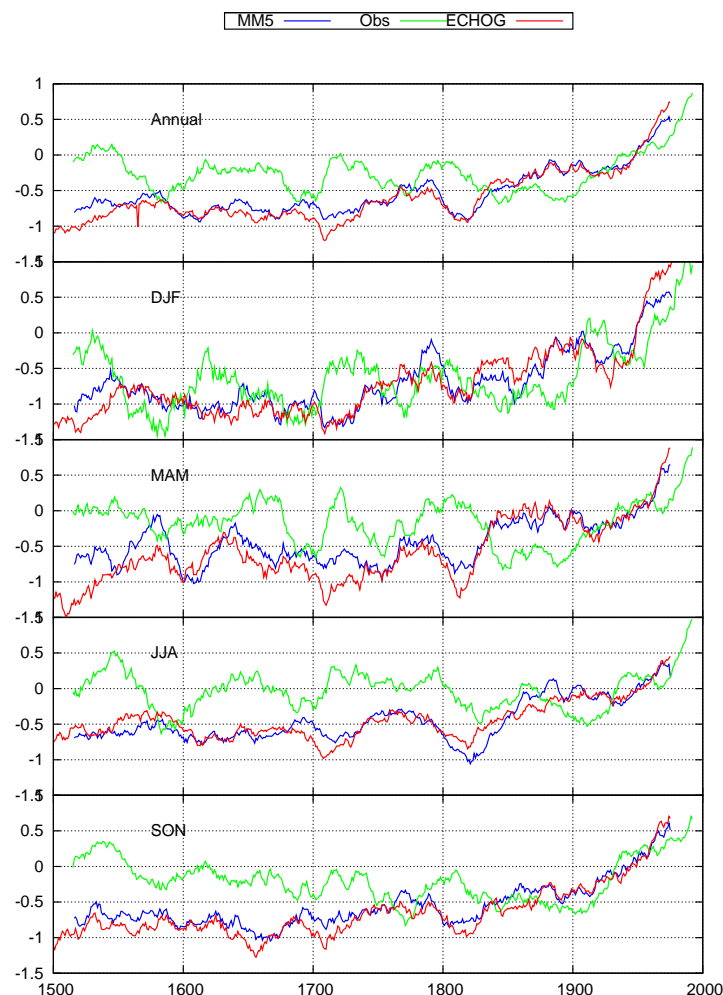


**Figure 5.16:** 31-year running mean series of SAT in Central Europe respect the period 1900-1990. Figure depicts the annual and seasonal mean series by the GCM (red), the RCM (blue) and the reconstruction by Dobrovolný et al. (2010) (green).

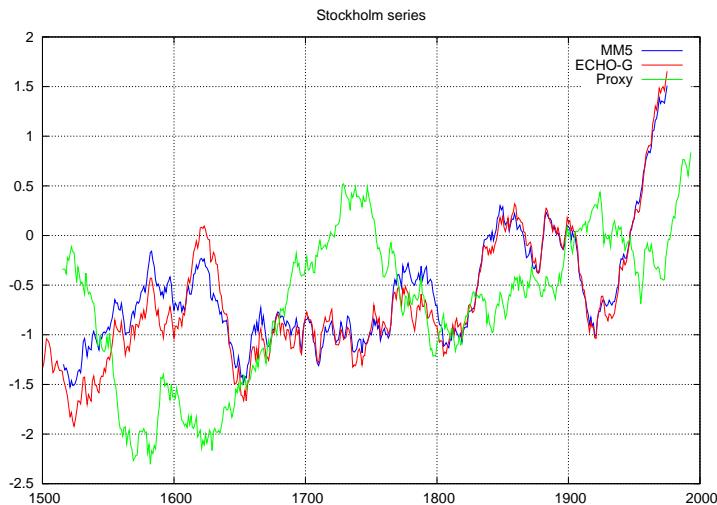


**Figure 5.17:** 31-year running mean series of SAT in Stockholm respect the period 1900–1990. Figure depicts the annual and seasonal mean series by the GCM (red), the RCM (blue) and the reconstruction by Dobrovolný et al. (2010) (green).

in the simulations, more noticeably in summer. This could be related to problems with the homogenisation of the instrumental series, in particular with the warm-bias commented earlier. Another possible cause of the larger trends in the model is the absence of aerosols in the simulations. Regarding multi-decadal variability, simulations show a cold period around 1810 which can be associated with the Dalton minimum. Although this period is present in all seasons, and more clearly identified in winter in the MM5 simulation, it can hardly be identified in the observational record.

There is again a clear disagreement between the model and instrumental series around 1730, similar to that found for the Stockholm record for mean SAT in January to April (although this warm anomaly also appears in the Luterbacher et al. (2004) reconstruction, the Central England series was employed to create the gridded reconstructions, so they can not be considered as further independent evidence of the warm period). Since this period matches well in the Central England and Stockholm records, and they have been derived independently, it is likely that it is a real phenomenon. Furthermore, the records are obtained from different places in Europe and located relatively far away, which suggests that this warm period was originated by a continental scale phenomenon, or at least affecting whole Northern Europe. This phenomenon is revisited in Chapter 6.

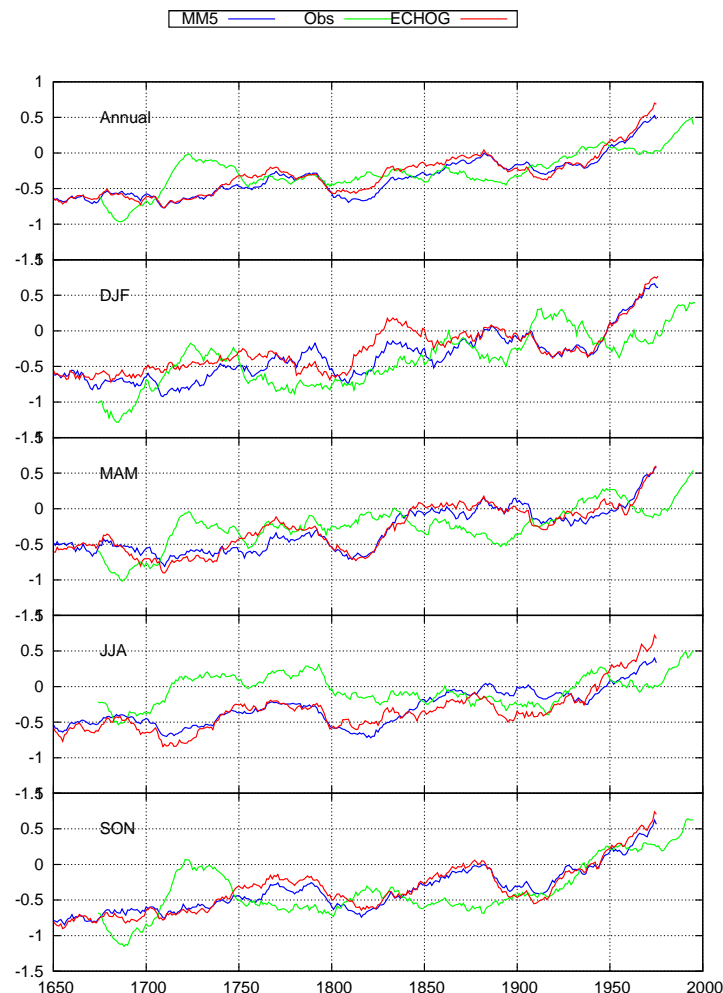


**Figure 5.18:** 31-year running mean series of SAT in Central England respect the period 1900-1990. Figure depicts the annual and seasonal mean series by the GCM (red), the RCM (blue) and the instrumental series (green).

## 5.5 Summary and conclusions

In this study we analyze a dynamic downscaling palaeosimulation for the period 1500-1990 performed with a climate version of the mesoscale model MM5, implemented with a spatial resolution of 45 Km over the European area. The regional model is driven through the boundaries by a former simulation performed with the GCM ECHO-G. Both models are identically driven by three independent sources of external forcings: GHG concentrations, solar forcing and estimations of the net effect of big volcano events.

The skills of the MM5-ECHO-G setup has been first analyzed comparing its outputs with a number of observational records, focusing the analysis in summer and winter seasons. The mean values of temperature and precipitation in a reference period (1960-1990) have been compared with observations recorded in the CRU database ([Mitchell and Jones, 2005](#)), which has been interpolated to the MM5 grid in order to perform the comparison. The mean values are well captured due to the higher resolution of the regional model. There are however some important biases, like a clear tendency to overestimate temperature and precipitation in Northern Europe in winter and underestimate temperature in summer. These biases seems to be related to the overestimation of the zonal circulation in the GCM, due to a too intense pressure gradient over the Atlantic. This drawback is a known feature of many GCMs, in particular in the ECHAM family.

The analysis of PDFs during the 20th century obtained by the simulation and recorded in observations shows more clearly in which areas and seasons the biases are more prominent. However, despite the bias, the shape of the PDS is remarkably similar in the simulation and the reconstructions. This gives confidence on the capability of the model to reproduce extreme periods, not only mean values.

Once the skill of the model has been evaluated, and its drawbacks identified, the model outputs have been compared with a number of reconstructions of climate available for this period and area. The gridded reconstructions of SAT and precipitation by ([Luterbacher et al., 2004](#)) and ([Pauling et al., 2006](#)), respectively, offer a unique opportunity to test not only the temporal evolution of the reconstruction, but their spatial distribution properties and relations with large-scale fields. We found that the PDFs for the model and the reconstructions match remarkably well during the period 1500-1900, and the differences can be attributed to biases in the model. The temporal evolution in the spacial-averaged series in several areas of Europe present similar variability and trend in both datasets, giving confidence to the skill of the reconstructions. However, the EOF analysis indicates that reconstructions tend to oversimplify the main variability modes, overestimating the percentage of variance associated to the leading modes. This

is especially noticeable for precipitation.

SAT simulated series have also been compared with a number of local reconstructions. The general tendency in the reconstructions is very similar to the one reproduced by the model. It suggests that the amplitude of the reconstructions of these forcings employed to drive the simulations is reasonable. At shorter time scales there are however some disagreements which require further analysis. A possible explanation is due to the internal variability in climate simulations, as explored in Chapter 3. A clear example of this disagreement is a warm period reconstructed around 1730, which is missing in the simulation. The model can however be used to gain insight in the underlying physical mechanism responsible for this anomaly, as further discussed in Chapter 6.

This work presents the first high-resolution palaeoclimatic simulation for entire Europe. First results point to the capacity of the model to simulate a realistic realization of the climate evolution during the last five centuries. A preliminary comparison with proxy reconstructions has allowed to identify robustness in the available gridded reconstructions, as well as some drawbacks. The temporal agreement between the model and the reconstructions can not be expected in general due to the role of internal variability (Gómez-Navarro et al., 2011b). However, some mismatches are too large to be explained by this factor, and this indicates (assuming the response of the model to the forcings is correct) that the forcings employed to drive the simulations are incompatible with the available reconstructions. Unfortunately, this study allows to identify this kind of inconsistencies, but gives no clue on which element is more reliable.

Since the data base generated is physically consistent, it allows facing many interesting questions on the evolution of past climate, such as modifications of circulation and weather types during key periods such as Maunder Minimum compared with current climate, or the relative role of external forcings compared with internal variability, which is a key aspect of the theory of anthropogenic climate warming. Additionally, further comparison with newer reconstructions, which are being currently generated by the proxy community, will be performed as they as a mean of validation of their physical consistence. All these aspects are further developed in Chapter 6.



# Some applications of regional climate palaeosimulations

## 6.1 Introduction

Models are far from perfect. They have drawbacks reproducing the observations and oversimplify the complexity of the reality in order to make its simulation possible. In addition, climate palaeosimulations can not be considered as a reconstruction of the climate. This is, they are not intended to represent the evolution of the actual climate, as climate reconstruction do. Similarly, climate change projections can not predict all the details of the climate modifications that can potentially arise from anthropogenic modifications in several elements in climate system such as GHG concentration or land uses. Thus, the point is not whether they are right or not (they are not!), but whether they are useful and complex enough for dealing with the problem you are facing. In this sense, and having in mind their limitations, climate models are very useful to study the climate evolution in the past, as well as under future emission scenarios.

Performing climate change projections is one of the most prominent applications of climate models, as explored in Chapter 4. In this respect, there exist many different models, which are compounded by many independent parts, from the dynamical core to the so-called physical parametrizations (Jerez, 2011). Each one of these elements rely on different hypothesis, which try to simulate a simplified part of the nature. None of these model configurations is perfect, and depending on the application different setups lead to different results (Fernández et al., 2007). In addition, an important component of the climate evolution is dominated by unpredictable internal variability, as

demonstrated in Chapter 3. Thus, none of the available climate change projections is completely reliable, resulting in some amount of uncertainty. For this reason, climate change projection has to be considered in an statistical approach. Due to the many different models employed nowadays, it is expected that a large ensemble of independent climate change projections is capable to sample most of the uncertainty sources, thus providing a comprehensive view on the possible evolution of climate under several hypothesis of socioeconomic evolution. This statistical approach allows to identify the most likely effects of anthropogenic climatic change but also to characterize the amount of uncertainty.

Palaeoclimatic simulations are however more scarce due to their huge computational cost and the more limited number of applications. This limits the number of conclusions that can be drawn from them. A statistical approach to characterize the amount of uncertainty in the actual evolution of climate system coming from different sources, as those performed in the climate change projections context, is currently impossible. Indeed this Thesis presents results obtained using some of the first high resolutions simulations performed nowadays covering the last millennium in Europe. However, due to the many uncertainties exposed above, which are a combination of oversimplification in the models, but also to the important role of internal variability, the simulated climate in just one or two simulations should not be considered as a climate reconstruction. This does not imply that simulation is useless. A palaeoclimate simulation relies on the adequate choice of the external forcings plus an initial condition. Later, using a number of well known physical laws, the model develops a self-consistent climate compatible with those forcings. This leads to the concept of pseudo reality (Zorita et al., 2003). The simulation can be considered as a simplified climate system where many of the properties of the actual climate system can be tested, given that in the model world all the variables are known. This allows to study the relations between different phenomena, how different parts of climate system respond to forcings, the relative role of internal variability compared to external forcing, etc. Hence, climate simulations, with acknowledged limitations, is the closest we can be of the concept of *climate experiment*.

In the former chapters some of the applications of these *climate experiments*, focusing in the model as a goal, have been exposed. However, along the last months we have contacted with a number of members of the climate reconstructions community. As a product of this experience, we have developed several applications for our simulations. This kind of interactions between model and reconstruction communities is of great interest to test the skill of the model in longer time scales (which is a key aspect of climate change projections) but also to validate some aspects of climate reconstructions. In this chapter we describe part of the results obtained from this exchange, in which the model

is the mean to test climate reconstructions. Some parts of this chapter is ongoing work which will be completed during the next months after this Thesis is defended.

## 6.2 Reconstructing climate in Andalusia from documentary evidence

This section summarizes our contribution to a paper sent to Climate of the Past (Rodrigo et al., 2011), in which running mean and standard deviation of seasonal series of temperature and precipitation over Andalusia during the period 1701-1850 is reconstructed from documentary evidence by using a novel methodology developed by Rodrigo (2008). In the paper a new reconstruction based in new evidences is presented, and the pseudoreality of the model is used to test the skill of the reconstruction methodology.

### 6.2.1 Reconstruction methodology

The reconstruction methodology is based on the fact that a modification in mean and standard deviation in a given variable is accompanied by variations of the associated Probability Distribution Functions (PDFs), which also modifies the occurrence of extreme events. The aim here is to study the inverse problem, that is, infer changes in mean and standard deviation from the frequency of extreme events, having in mind that documentary data basically reflect the occurrence of extreme events through their impacts. This methodology has the advantage of avoiding subjectivity introduced by the researcher, and does not need an overlapping period with instrumental data to obtain quantitative estimates of climate variables during the past.

The method simply consist in counting the number of extreme events registered in a given temporal window of  $n$  years, only considering two kinds of extreme events for each variable, extremely low or extremely high, resulting in two numbers,  $n_l$  and  $n_h$ , respectively (note that this method does not consider different degrees of severity in the definition of extreme events, but only their frequency in a given period). Then, if  $F_X$  is the PDF associated to a given variable  $X$ , the frequency of occurrence of both kind of extreme events are related with the PDF through

$$\begin{aligned} \frac{n_l}{n} &= \Pr(X \leq q_l) = F_X(q_l) \rightarrow q_l = F_X^{-1}\left(\frac{n_l}{n}\right) \\ \frac{n_h}{n} &= \Pr(X > q_h) = 1 - \Pr(X \leq q_h) = 1 - F_X(q_h) \rightarrow q_h = F_X^{-1}\left(1 - \frac{n_h}{n}\right) \end{aligned}$$

where  $q_l$  and  $q_h$  are percentiles of the unknown PDF  $F_X$ . If we now assume, as a hypothesis in which the method rely, that  $F_X$  is a normal distribution whose mean  $u$

and standard deviation  $s$  are unknown, the former percentiles can be related with these two parameters through

$$s = \frac{c_h - c_l}{q_h - q_l}$$

$$u = c_h - sq_h = c_l - sq_l$$

where  $c_l$  and  $c_h$  and the corresponding percentiles of the  $N(0, 1)$  distribution. Hence, if we consider that a climate event is present in the documentary records when it has exceeded a given threshold of probability, let us say 10% (90%) for low (high) events, and consider a temporal window of 31 years, we can count the number of events in the documentary evidence, and the former equations allow to estimate  $u$  and  $s$  during such temporal window.

Despite the discussed advantages of this method, it has several limitations. First one is that it needs the analyzed variable to follow a normal distribution, which is not always the case. Second, it is only able to reconstruct the long-term evolution of a given variable, this is running statistics. Finally, the model yields no results if the number of extreme events recorded in a given period is 0.

### 6.2.2 Building pseudoproxies

This methodology can be tested within the context of the pseudoreality of the climate simulation. The underlying idea is that even if the evolution of the simulation does not match perfectly the actual evolution of the climate in the past millennium, it represents a feasible evolution of the climate, since it is physically self-consistent. Thus, the statistical properties of the simulated variables, and their physical relationships, are a reliable version of the actual ones. An obvious advantage of using a climate model is that within the simulation the information is available at all temporal and spatial scales. Thus, one can construct a pseudoproxy inside the model for a given variable, apply the reconstruction methodology to be tested and generate a pseudoreconstruction. It can be later compared with the simulated evolution of the variable, which is perfectly known. It is important to note that this exercise does not validate the model, but the methodology used to reconstruct the actual climate.

The procedure to create the pseudoproxy is as follows. A reference period has to be chosen, as well as a probability threshold to define what an extreme event is. Once this is fixed,  $c_h$  and  $c_l$  can be found. The next step is to compare the simulated seasonal means with these percentiles, to get a series of 0's and 1's representing the occurrence

or not of an extreme season. Using a running window of 31 yr, the number of extreme seasons in a given period,  $n_l$  and  $n_h$ , can be counted, which are the pseudoproxy.

### 6.2.3 Results

An important drawback applying the above methodology is that a reference period, as well as a probability threshold to define an event extreme, has to be arbitrary defined. Thus, the reconstruction methodology is in principle sensible to this choice, introducing an uncertainty factor which is important to assess. In order to quantify this uncertainty, four different combinations have been tested in the present study: two reference periods (the 31-year periods 1885–1915 and 1960–1990) with two pairs of probability thresholds (percentiles 10–90 and 25–75), receptively. This exercise has been applied to the simulated winter mean series of temperature and precipitation (the results for other seasons are similar, and are not shown) to reconstruct the simulated evolution of these variables during the last millennium.

The results are shown in Figures 6.1 and 6.2 which show the results for the reconstruction of  $u$  and  $s$ , respectively. The two top panels of each figure show the reconstruction for temperature, whereas the two bottom ones show it for precipitation. Black line is the “reality”, this is, the series simulated by the model spatially averaged for Andalusia, and smoothed through a 31-years running mean, to make reconstructed and “observed” series comparable between them. The period chosen to define what an extreme event is according to a given threshold is 31 years around 1900 and 1975, and the result for each choice are shown in the panels labeled accordingly. Finally, red and blue represent the reconstructions using different percentiles.

The reconstruction of mean temperature is better achieved when the reference period is chosen around 1900 instead of 1975. This is due to the too warm period simulated in the last years of the run, producing too large percentiles, which are used later on to determine what an extreme event is. This yields to many periods in the reconstruction where no extreme events are found compared to the reference period (specially in cold periods), a situation which produces a missing value in the reconstruction. There are however no large differences in the reconstruction when the percentiles used to define the extreme event, 10–90 or 25–75, are used (obviously when the more restrictive ones are chosen, the reconstruction presents more gaps). Reconstruction of precipitation behaves differently. It shows no so large differences when the two periods are employed as reference. This is because both periods are not extreme compared with the 1000 years series. The reconstruction in this case behaves slightly better when the percentiles 25–75 are chosen. When the more restrictive percentiles are chosen, the

Period Percentile	1900		1975	
	10-90	25-75	10-90	25-75
$u$ (SAT)	0.12 (739)	0.08 (925)	0.18 (355)	0.24 (636)
$s$ (SAT)	0.11 (738)	0.16 (923)	0.19 (355)	0.27 (636)
$u$ (PRE)	15.18 (878)	12.21 (952)	13.99 (844)	9.02 (952)
$s$ (PRE)	13.71 (878)	21.02 (952)	16.35 (844)	17.72 (952)

**Table 6.1:** RMSE of mean and standard deviation in the pseudoreconstructios for winter temperature (in °C) and precipitation (in mm) compared with the actual path of the simulation. The calculations cover the two reference periods and the two choices of percentiles for both variables. In parenthesis is shown the number of elements in the series used to compute RMSE (it differs depending on the number of missing values).

resulting series is too sharp, with large steps.

Reconstructions for standard deviation are less skillful. As before, when the warm period is used as reference a large amount of missing values are produced, whereas using the period around 1900 as reference, standard deviation for temperatures is reconstructed more accurately. Precipitation is not so correctly captured, and there is a general tendency to overestimate the variability. This is due to the non-normality of the distribution of seasonal precipitation, which is a hypothesis of the methodology. The hypothesis of normality has been tested in the observations of the instrumental period of temperature and precipitation in Andalusia, and only the variables and seasons following this distribution have been considered in the reconstruction (only summer precipitation fails to be fitted to a normal distribution). However, slight departures from normality yields to worse result, as is the case of winter precipitation.

In general, the method is capable to reconstruct with great accuracy the “observed” running mean of temperature and precipitation. A measure of the agreement between the original series and the reconstructions is the Root Mean Square Error (RMSE). It varies among the four tested reconstructions (see Table 6.1), ranking from 0.08 to 2.4 °C in mean temperature, and from 9.02 to 15.18 mm in mean precipitation. Similarly, the standard deviation reconstructions vary from 0.12 to 0.24 °C and from 13.71 to 21.00 mm in temperature and precipitation, respectively. However, there is no a clear relationship between a lower RMSE and the chosen period or percentile. The mean value of the RMSE in the four pseudoreconstructions can be considered as a measure of the uncertainty in the methodology due to the arbitrary choice of the references, and it is used as the error bar when reconstructing the actual climate.

Further results on the accuracy of the methodology and the conclusion that can

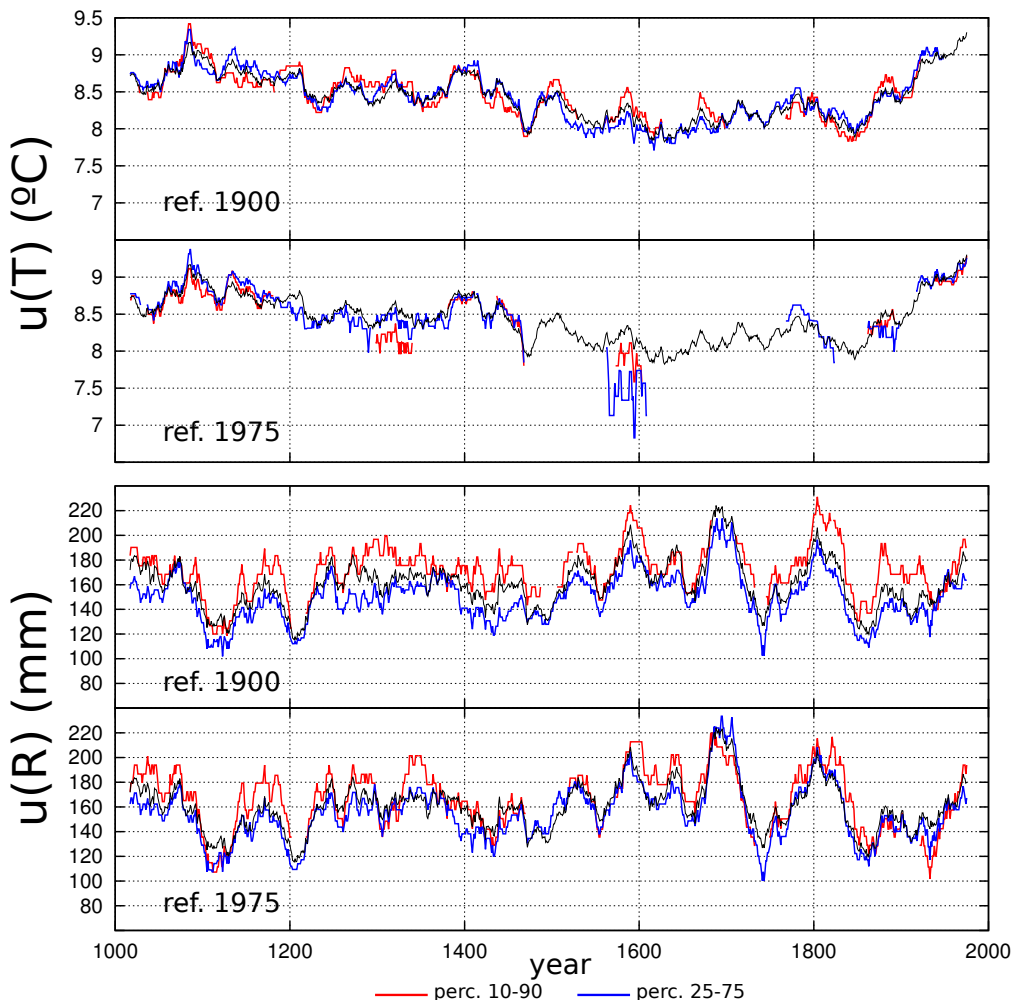


**Figure 6.1:** Evolution (in black) of the 31-year running mean of temperature (two upper panels) and precipitation (two lower panels) in the climate simulation for the last millennium. Four pseudoreconstructions are shown, using the periods 1885–1925 (first panel and third panels) and 1960–1990 (second and fourth panels) using the 10–90 percentiles (red lines) and 25–75 (blue lines).

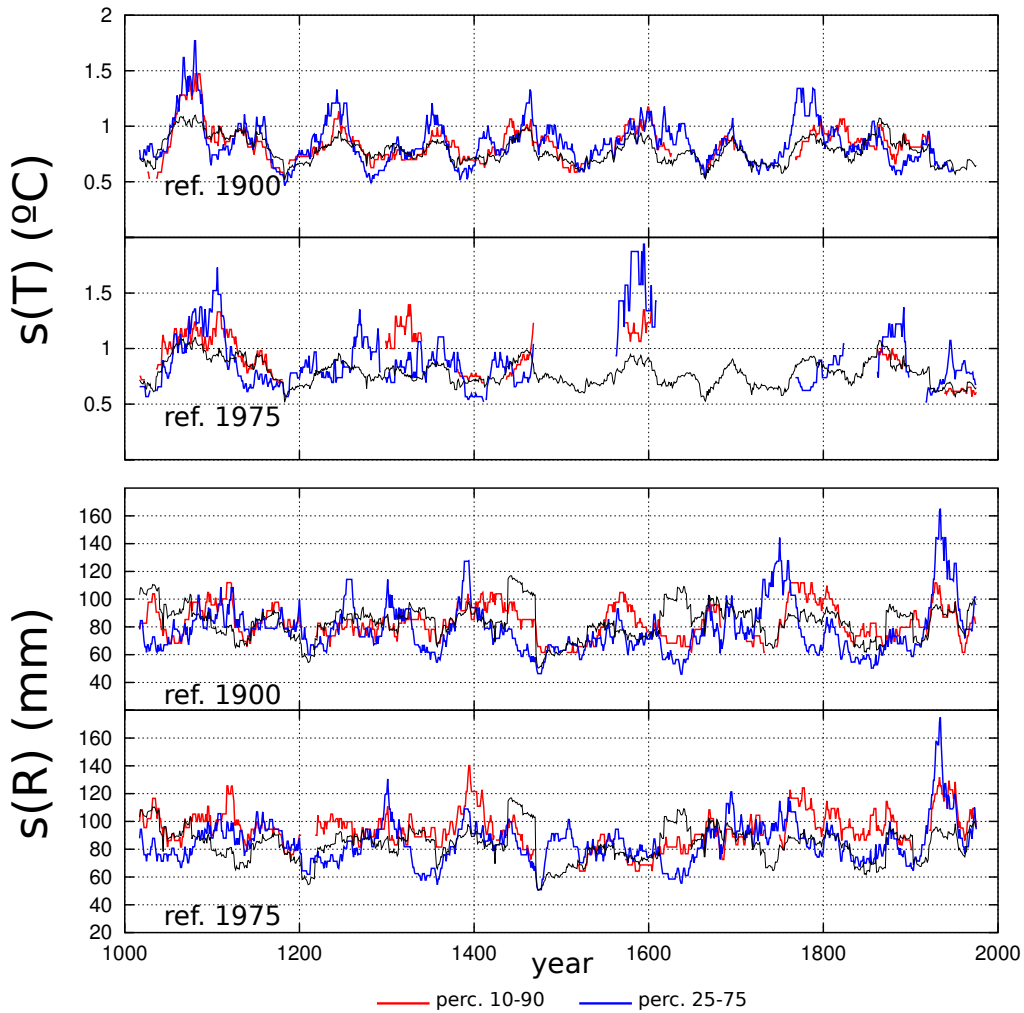


**Figure 6.2:** Evolution (in black) of the 31-year running standard deviation of temperature (two upper panels) and precipitation (two lower panels) in the climate simulation for the last millennium. Four pseudoreconstructions are shown, using the periods 1885–1925 (first panel and third panels) and 1960–1990 (second and fourth panels) using the 10–90 percentiles (red lines) and 25–75 (blue lines).

be drawn when applied to actual documentary evidence is presented in [Rodrigo et al. \(2011\)](#).

### 6.3 Testing physical consistence of the Westerly Instrumental Index (WII)

This section describes some calculations performed with the model outputs in order to asses the physical consistence of a new climate index defined in terms of wind directionality in the area of the English Channel. This index can be extended back in time until 1685, thus providing a new invaluable source of paleoclimate variability evidence. The information employed to build this index consists on wind direction, recorded for centuries in ship's logbooks of the Royal Navy. Thus, it is a quasi-instrumental index, rather than based on proxy indicators, which contains a large amount of information on the large-scale circulation variability during last centuries. A brief description of this reconstruction can be found in ([Alvarez-Castro et al., 2011](#)), although most of the details exposed here were provided by personal communication. Unfortunately the main results of this study have not been published yet, so this section only describes some very preliminary results that still have to be extended and published during the next months. The details of the simulation employed in the following analysis can be found in Chapter [5](#).

#### 6.3.1 Definition of the Index

The Westerly Instrumental Index (WII) is a monthly index defined as the percentage of days that wind blows from the West in a given month (this is, wind velocity is a vector pointing toward the 90°arc defined from Northeast to Southeast) in the English Channel. The WII is a dimensionless monthly index defined between 0 and 1, which accounts for the zonallity of the wind over this area. Note that the index do not consider wind speed, but only direction. The WII has two important features: it can be built back in time using documentary evidence from ship's logbooks until 1685 (it has the important advantage of being quasi-instrumental, instead of proxy based indicators), and it can be related with large-scale fields such as temperature and precipitation, since this index can be closely related to the North Atlantic Oscillation (NAO), although there are periods where the coupling between both indices becomes lower. Assessing this last point, i.e. the consistence between the WII and several climatic variables, is the aspect that has been explored within the simplified world of the simulation and is described in this Thesis.

Defining a pseudo WII in the pseudoreality of the simulation is straightforward. First, a rectangular area between 5°W, 4°W and 48°N, 49°N has been selected, which contains 6 grid points in the English Channel. The simulation was recorded every 3 hours, so the daily mean of the 8 values of zonal and meridional components of the wind can be calculated separately, and then averaged for the 6 grid points. This yields an average wind vector per day in this area. The next step is to obtain the monthly percentage of days this vector falls within the 90°sector described above.

This pseudo WII can be compared with the corresponding fields of temperature, precipitation, or even with other indices such as the NAO, also defined in the simulation world. This allows to analyze the physical relations between different climate variables (and more importantly their temporal evolution) found in observations in the real world, in the simplified but physically self-consistent climate of the model.

### 6.3.2 NAO vs. WII

The WII index accounts for wind zonality in the area of the English Channel. Hence it reminds the physical meaning of the NAO pattern. We have explored this relation in Figure 6.3, where the evolution of NAO index and WII are shown simultaneously for winter (we focus on this season because NAO pattern is normally only defined for it). As expected, there is an overall positive correlation between the two series. In particular, they share a positive long-term trend, more clear in the last century. However some mismatches in a number of periods are evident, like in 1520-1560 or 1710-1740. Although there is no a completely satisfactory explanation for these decouplings, a possible explanation are changes in the large-scale spatial structure of NAO pattern, which modify the physical links between SLP and wind in a very local area such as the English Channel. This aspect is further explored in next section.

Figure 6.3 also depicts the evolution of the actual WII index reconstructed from documentary evidence. In general the agreement is not good, and indeed both series are not statistically correlated, neither share a common trend. However this should not be considered as evidence of a mismatch between the reconstruction and the climate model. The evolution of large-scale dynamics is, to a large extent, dominated by internal variability in the simulations (Gómez-Navarro et al., 2011b), and thus a direct comparison between the two series is not meaningful. In other words, even if both series would match perfectly, it could be due to chance, and should only be interpreted in these terms. Nonetheless, the model should reproduce realistically the physical link between the WII index and other climate fields within the simulation. This aspect is further developed in the next section.

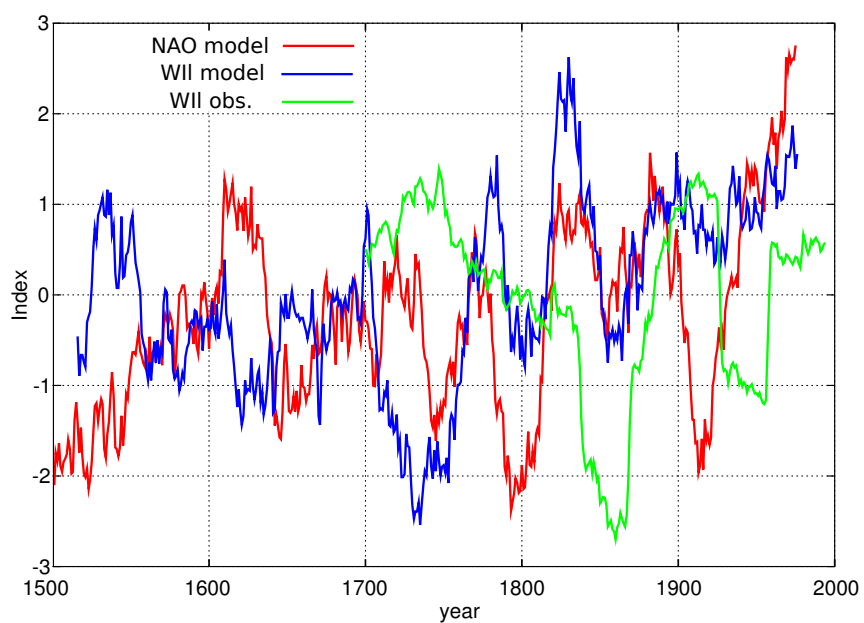


**Figure 6.3:** WII index and its relation with NAO in winter. Red line represents NAO index in the simulations, defined as the standardised series of the principal component associated to the leading EOF of the mean SLP in winter in the geographical box  $70^{\circ}\text{W}$  to  $50^{\circ}\text{E}$  and from  $20^{\circ}\text{N}$  to  $75^{\circ}\text{N}$ . Blue line is the WII index in the model, whereas green line is the WII index obtained from observations. All series have been normalised.

### 6.3.3 Large-scale relations found in the simulation

The physical connection between the WII and large-scale patterns of temperature and precipitation in winter and summer is illustrated in Figure 6.4, where the temporal correlation between the index and these fields is shown. In general, the connection between wind zonality and both climate fields is greater in winter. There is a clear bipolar behaviour of precipitation. Northern Europe is positively correlated with WII, whereas in the South this behaviour is inverted. The physical explanation for this mechanism is straightforward: larger zonality implies large transport of moist water from the ocean, which produces larger precipitation rates over most of Europe. However, this larger zonality is accompanied by a strengthening of the high pressures belt around mild latitudes, which tends to reduce precipitations over these areas, in this case over the Mediterranean. Indeed, this negative relation between larger zonal flow and decreased precipitation over the IP was explored in Chapter 2 in this Thesis. Figure 6.4 also shows the relation between WII and temperature. During winter, an increase of zonal flow is accompanied by a larger transport of warm air from the Atlantic Ocean, whereas this mechanism has the opposite effect during the summer, although less intense.

Thus, the model setup is able to develop some well established characteristics of the links between large-scale circulation and temperature and precipitation. The WII index simulated in the pseudoreality behaves similarly as NAO. However it still shows a strong signal in summer, a feature that makes this index stronger. The WII reconstructed has been tested by [Alvarez-Castro et al. \(2011\)](#) by using observations in an instrumental period and they have found similar physical links. Future research will concentrate in assessing at what extent these large scale connection in the observation have their counterpart in the simulation, bearing in mind the advantage of the simulation of having a longer periods to assess the time evolution of these links.

### 6.3.4 Temporal consistence of the relations

Despite the simplistic realization of the climate that simulations produce, they have several advantages. Long palaeoclimate simulations allow to assess the long-term temporal evolution of the climate beyond the short period of the instrumental records, but also provide a complete physical picture of the climate, where all variables at all temporal and spatial scales are known. In this sense, WII researchers have explored the relation between the WII index and the longer instrumental record available for Europe, this is, the Central England temperature series ([Manley, 1974](#)). They have calculated the correlation between these two series in different seasons, using running windows of

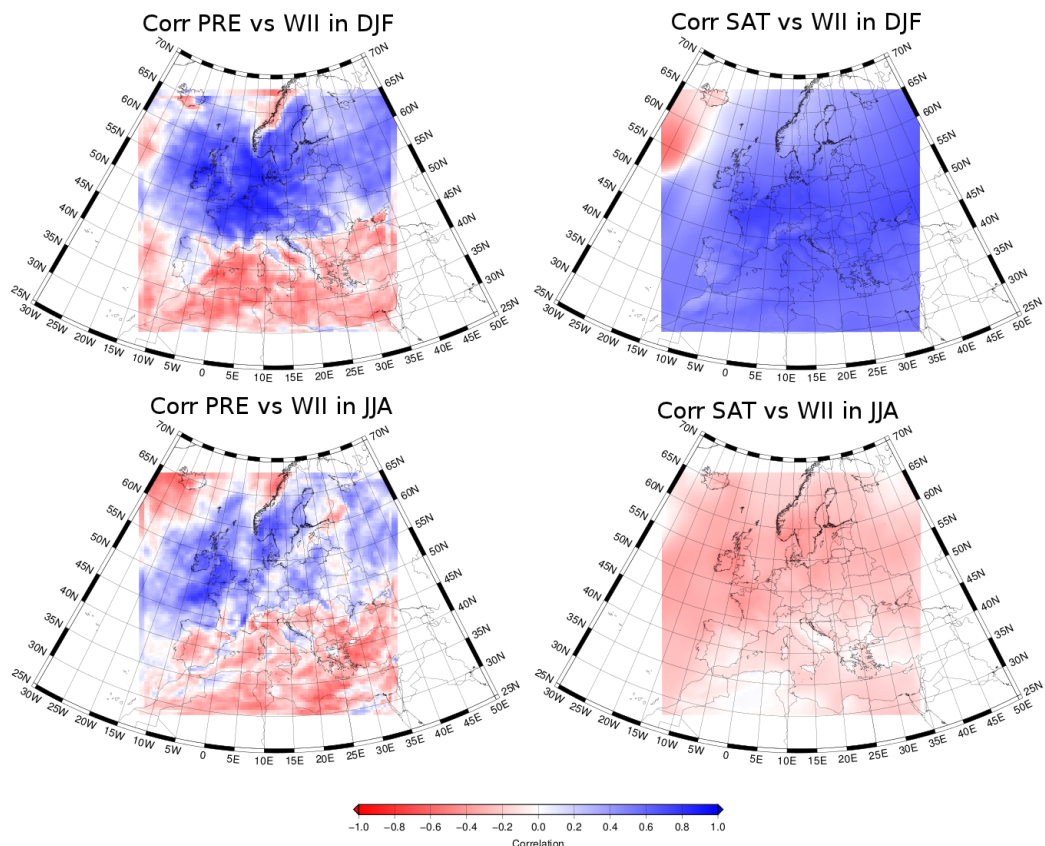


**Figure 6.4:** Correlations between the WII index defined in the model and the corresponding fields of precipitation (left column) and temperature (right column) for winter (top row) and summer (bottom row). Before computing correlations, the series have been filtered out with a 31-year running mean to reduce the high-frequency noise.

several lengths. This allows them to assess whether there are periods where the coupling between the two series becomes weaker. However, given that these series do not contain information on the large-scale systems, it is not easy to address whether these decoupling periods have a physical meaning or it is just a statistical artifact. Climate simulations may play an important role in testing whether these decouplings have a counterpart in the simplified but physically self-consistent world of the simulation, and even more importantly in providing a feasible physical explanation for these phenomenon.

Trying to address this point, Figure 6.5 shows the correlations calculated within the model between the pseudo WII and the temperature series averaged over an area in Central England. The figure shows the correlation value with colours. Vertical axis indicates the width of the moving window, whereas horizontal axis is the year in which the window is centered to perform the calculation. The relation between the two variables is overall greater in winter, as discussed above, whereas transition seasons show an intermediate behaviour. In winter the correlation is positive regardless the length of the window and the period. However, when shorter windows are chosen, the correlation exhibits more variability, with large values in some periods, although in hardly any period it becomes negative. Nevertheless, in summer there are periods where correlation becomes even negative in a large variety of moving windows. At longer time scales, the average correlation becomes very weak or even null.

These findings contrast with the results found in the reconstruction (not shown for being unpublished work). In the reconstruction, the correlations for winter show the same behaviour. However, correlation in summer presents a surprising behaviour. Before 1850, the correlation is negligible, whereas after this year it becomes negative and very strong. Correlation in spring also exhibits a completely different behaviour before and after that year. Correlation is positive before this year, but becomes null after it. The reasons for these sudden changes are unknown, but given that this behavior can not be found in any period in the last 500 years simulated, our first guess is that it is incompatible with the model. This difference might be due to several reasons, such as statistical inhomogeneities in the records (if this behaviour turns out to be not real) or failures in the model to capture the behaviour of the climate system.

#### **6.4 Warm anomaly in Northern Europe in 1730s**

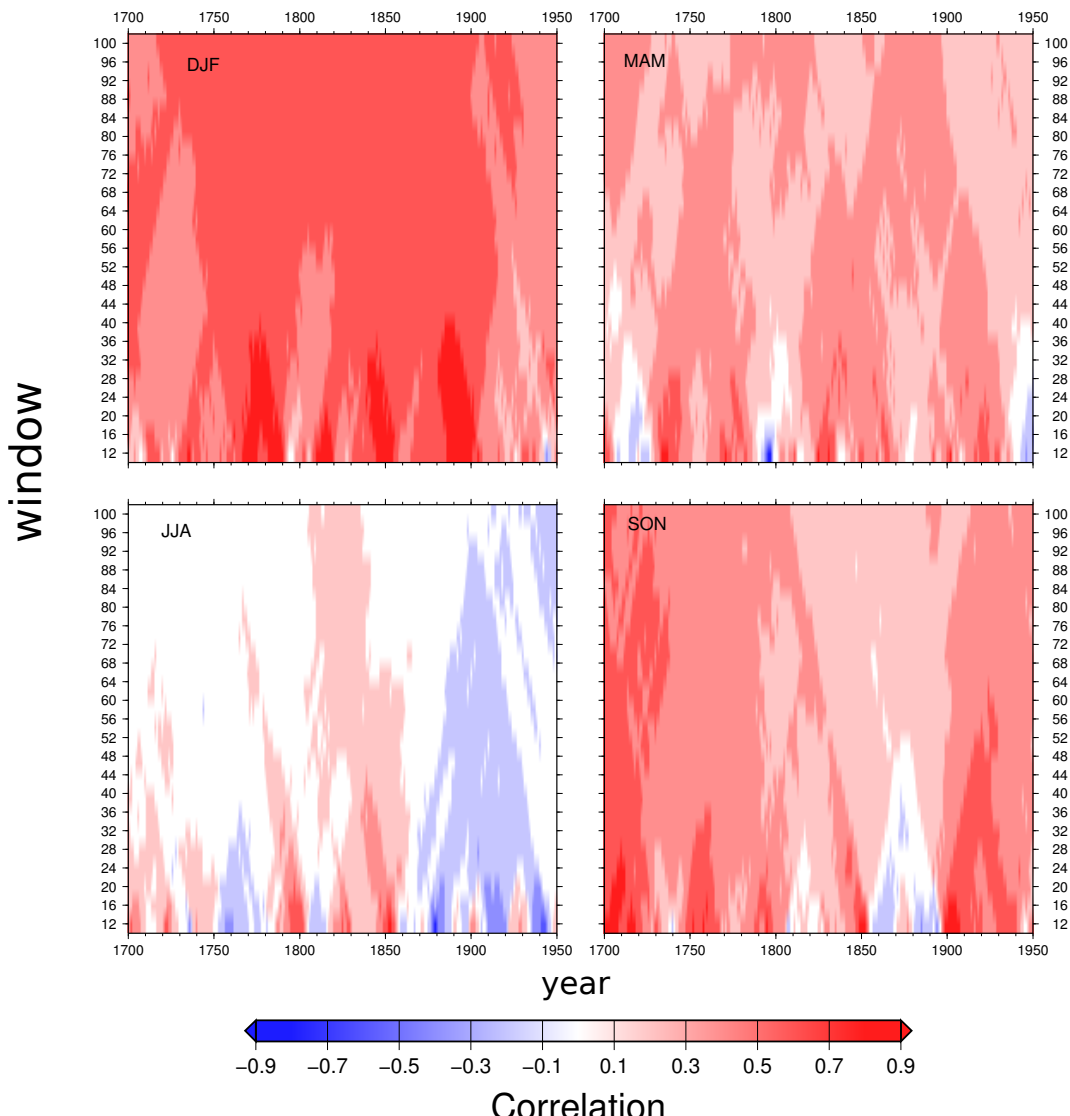


**Figure 6.5:** Running correlations between the WII index and temperature in Central England through several seasons within the model simulation. Colours show the correlation value. Vertical axis indicates the width of the window used to calculate correlation, whereas horizontal axis indicates the central year of this interval.

### 6.4.1 Evidence in climate reconstructions

Chapter 5 discusses a comparison between a climate simulation for Europe and the Luterbacher et al. (2004) reconstructions. This reconstruction depicts a clear warm period around 1735, which is present mostly in Northern Europe areas in winter. It can also be identified in the Central England series (Parker et al., 1992), which is not surprising since the latter is implicit in the former. Further independent evidence of this warm period is nevertheless found in the Central Europe (Dobrovolný et al., 2010) and Stockholm (Leijonhufvud et al., 2010) reconstructions.

To gain more insight into the spatial structure of the warm anomaly, Figure 6.6a depicts the winter SAT anomalies in the period 1700-1750 with respect to the mean in 1600-1700 in the Luterbacher et al. (2004) gridded reconstruction. The warm anomalies are strongest in Scandinavia, with values above 2 K in some areas. They are however less intense (around 1 K) in Central Europe, and even become cold anomalies in the Iberian Peninsula and Turkey.

The appearance of this warm period in several independent reconstructions suggests that this phenomenon was real, rather than a statistical artefact.

### 6.4.2 Lack of evidence in the simulation and pseudoreality

Although it seems that this anomalous period was real, there exists no evidence of changes in external forcings around that period which could explain it. Additionally, since the simulation does not include any input information capable to take into account explicitly this period, the model does not simulate this period, neither any other equivalent warm period in the whole record, which already suggests that the possible contribution of forced variability, if at all, may not be very strong.

Jones and Briffa (2006) studied this period using early instrumental evidence of SAT and MSLP, and found that it was characterised by an unusual atmospheric circulation, yielding sudden swings from warm conditions to an extreme cold winter in 1740. Thus, a plausible explanation for this phenomenon could be an anomalous circulation driven by natural variability, rather than by changes in climate forcings.

The physical consistency of the model can be used to gain insight in this hypothesis. For this exercise, we employ the Europe simulation described in Chapter 5. The hypothesis to test is that these wide-spread anomalies are due to a prolonged, and anomalously large, positive phase of the NAO. Note that this NAO anomaly might be linked to the increased solar irradiance at the end of the 17th century and the first half of the 18th century, but it could also have been the result of internal dynamics. Al-

though the relationship between the NAO and the anomalous warm decades can be in principle contrasted with the available NAO reconstructions, these reconstructions do not quite agree in this period. In particular the reconstruction by (Luterbacher et al., 1999) present a positive anomaly in this period, meanwhile it can not be identified in more modern reconstructions (Cook et al., 2002; Trouet et al., 2009).

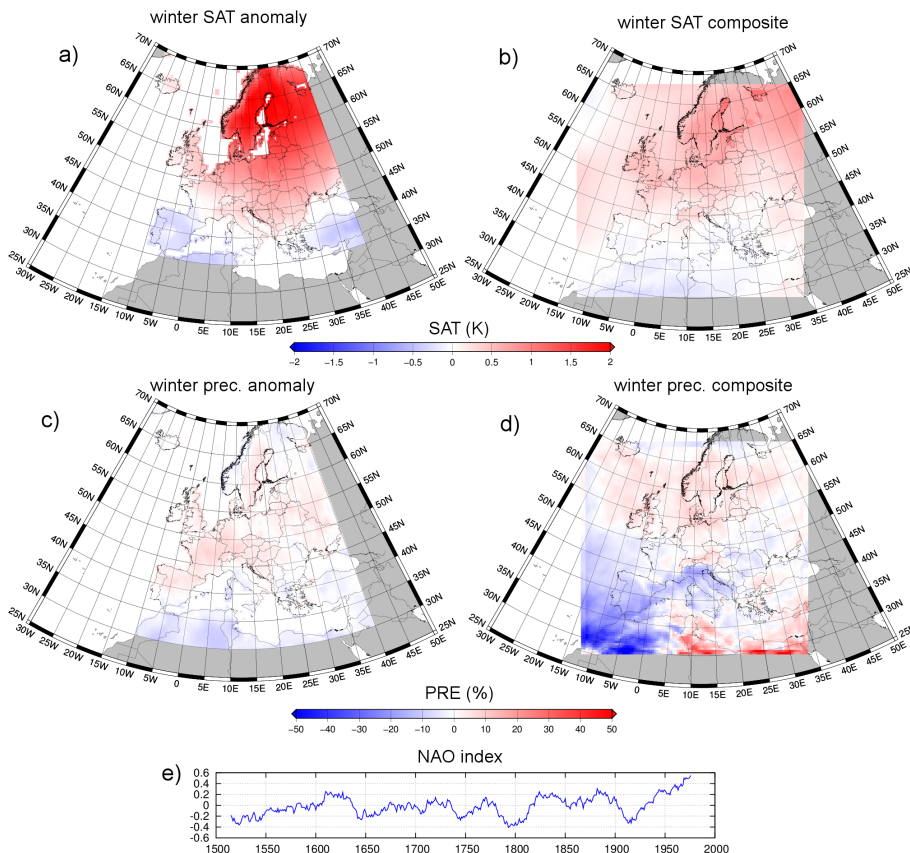
### 6.4.3 Results

Figure 6.6e shows the NAO index simulated by ECHO-G, defined as the Principal Component associated to the leading EOF of the winter Sea Level Pressure in the North Atlantic sector ( $20^{\circ}\text{W}$  to  $40^{\circ}\text{E}$  and  $30^{\circ}\text{N}$  to  $65^{\circ}\text{N}$ ). There are a series of maxima and minima, with a clear final trend towards a more intense NAO phase in the 20th century. By selecting periods of strong positive NAO with respect weak phases, we can perform a composite of SAT to assess, within the pseudo-reality of the model, the impact in this variable of a modification of this important circulation mode. In particular, we have calculated the mean SAT in the periods 1820-1850 and 1870-1900 minus in the periods 1770-1820 and 1850-1870. The result of this composite is shown in Figure 6.6b. There is a warm anomaly which is specially intense in Northern Europe. The anomaly is weaker toward the south, and it turns out to be positive in the Iberian Peninsula and north Africa. In general the temperature anomaly pattern is very similar to those shown by the reconstructions, although it is less intense in the model. These results indicate that a more intense phase in this important circulation mode, persistent over a few decades, is a plausible explanation for the anomalies found in reconstructions.

There are two conclusions we can draw from the previous that should be highlighted. The fact that the composite pattern of the model simulation is weaker than in the reconstruction seems to indicate an underestimation in the amplitude of the variations of the NAO in the model, or equivalently, a extremely anomalous atmospheric circulation in this period which the model is unable to reproduce. In any case, the model seems to develop too stereotypical climatic situations which can not account for the variability shown by the reconstructions in this extreme period. On the other hand, if the strong-NAO hypothesis were true, a increase in precipitation should have been registered in this period in Northern Europe. The precipitation anomalies in this period are depicted in Figure 6.6c, and the same composite than previously performed for SAT within the model is also shown for precipitation in Figure 6.6d. The model exhibits a strong decrease of precipitation over the Iberian Peninsula and the Mediterranean sea, together with an increase of rainfall in the British Islands, Central Europe and the Scandinavian Peninsula. This pattern is coherent with the strong positive phase which

defines the composite, and has to be compared with the results for the precipitation anomalies reconstructed for this period to test the consistence among reconstructions. In the precipitation reconstructions (Pauling et al., 2006) there is a relative maximum in the smoothed series of averaged winter precipitation in some areas such as the British Islands or Central Europe. Nevertheless we can neither identify the expected maximum in precipitation in the Scandinavian area nor the negative anomaly in the Iberian Peninsula. Indeed, the spatial structure of the anomalies depicted in Figure 6.6c shows a too flat structure, which only slightly reproduces the expected clear bipolar structure in the presence of a strong NAO phase. Thus, either the SAT and precipitation gridded reconstructions are inconsistent in this aspect, or a positive NAO phase can not explain the observed warm anomaly in this period in the reconstructions.

There is another warm period easily noticeable in the Luterbacher et al. (2004) reconstructions in summer around 1770. Summer SAT anomalies in the period 1750-1800 with respect to 1650-1750 show a similar spatial structure as those for the winter season analysed above (spatial correlation 0.92), although are less intense (not shown). Nevertheless no equivalent study to that performed for winter (Jones and Briffa, 2006) has been reported so far. As in the warm winter anomaly case, this period with intense summer temperature anomalies is not reproduced in the simulation, but physical relationships responsible for these climatic events can be examined within the model. In particular we have calculated the summer NAO index (Folland et al., 2009), and performed a composite of SAT in the strong versus the weak phases of this circulation mode for summer, a similar calculation as for winter performed above. In this case the resemblance between the anomaly pattern in the reconstruction and in the model composite is lower (not shown). In fact we studied the general link between the SAT anomalies and the MSLP in summer in the model by means of canonical correlation analysis, and we found no significant correlation between both patterns in this season. Canonical correlation analysis (von Storch and Zwiers, 1999) is a multivariate linear method to identify the patterns in two variables with the highest correlation possible. Significance tests for the canonical correlation can be conducted using Monte Carlo methods. It was found that, in the model, summer means of European temperature and summer means of SLP are not statistically significantly correlated. Thus, the warm anomaly in summer in the European mean temperatures detected in the reconstructions, if real, have to be explained by other mechanism than by anomalous MSLP.



**Figure 6.6:** Up: winter warm anomaly in the Luterbacher et al. (2004) reconstruction. Period 1700-1750 minus 1600-1700. Medium: winter warm anomaly in MM5-ECHO-G performing high NAO composites. Periods 1820-1850 and 1870-1900 minus 1770-1820 and 1850-1870. Bottom: winter NAO defined as PC of the leading EOF of MSLP over the Atlantic.

## 6.5 Comparison between tree-ring reconstructions and simulations in the Pyrenees

This section describes a comparison between several climate simulations and a set of tree-ring proxy based temperature reconstructions for the Pyrenees. It briefly summarizes the study presented by [Dorado-Liñán et al. \(2011\)](#).

### 6.5.1 Reconstructions methodology

[Dorado-Liñán et al. \(2011\)](#) developed a set of regional reconstructions of May-to-September mean temperature for the Pyrenees in the period 1260-2005 based on maximum density (MXD) tree-ring chronologies. They created 22 local chronologies, built from a total of 804 individual tree-ring series, and aggregated them to generate regional chronologies for the Pyrenees area. However, tree-ring reconstructions are hampered by a number of uncertainties in the statistical methods employed to post-process the tree-ring density data. Trying to sample most of this uncertainty, several complementary methodologies were used, and an ensemble of reconstructions was generated, instead of just one.

In order to generate the chronologies, four methods for the standardization of the series were employed: Regional Curve standardization (RCS), Regional Curve standardization preceded by a power transform to stabilize the variance of the individual series (RCSPT), 300 years cubic smoothing with a 50% frequency-response cut-off (300sp) and 300 years cubic smoothing with a 50% frequency-response cut-off preceded by a power transform (300spPT). Additionally, three methods for aggregating the local chronologies into a regional one were employed: computing a simple arithmetic average of the 22 individual MXD chronologies (RCS\_mean, RCSPT\_mean, 300sp\_mean, 300spPT\_mean), computing a single chronology including all 804 individual series in a run (RCS\_chrono, RCSPT\_chrono, 300sp\_chrono, 300spPT\_chrono) and by Principal Component Analysis, computed separately for each time segment with a constant number of MXD chronologies to produce nested PCA regional chronologies (PCs\_RCS; PCs\_RCSPT; PCs\_300sp; PCs\_300spPT). Thus, a total of 12 regional chronologies were developed for the Pyrenees region. Each one was later on used to generate a reconstruction using two different methodologies: simple linear regression and variance-matching (scaling). Hence, a total of 24 different regional reconstructions of May-to-September mean temperature were generated. They were calibrated in the first half of the instrumental temperature record (1900-1952) and validated in the second half (1953-2005), and vice versa to check the consistency of the reconstruction.

### 6.5.2 Comparison with simulations

The 24 regional May-to-September temperature reconstructions were compared with the analogous series in four climate simulations: the two high-resolution regional climate simulations employed to assess internal variability in Chapter 3, and the corresponding simulations performed with the driving global model of the former ones.

Comparison is shown in Figure 6.7. In the figure, grey shadow represents the range of variability of the 24 reconstructions, while the instrumental record, available only in the last century is shown in red. Simulated May-to-September temperatures show a good agreement with the instrumental record for the first part of the 20th century (Fig. 7a) However, from 1940 onwards the discrepancies arise at the inter-annual time scale. At inter-decadal scale, the two global (ERIK1 and ERIK2) and the regional MM5-ERIK2 simulations display a marked positive trend for the entire calibration period, in disagreement with the instrumental series. This negative temperature trend in the latest part of the 20th century is only reproduced by the regional simulation MM5-ERIK1. Amplitude of the temperature variations is larger for the regional simulations compared to the global simulations (Fig. 6.7c), which is due to the larger spatial average performed implicitly by the coarser resolution of the GCM.

Global and regional simulations show large inter-decadal changes that are in agreement with those displayed by the collection of Pyrenees MXD based May-to-September temperature reconstructions (Fig 6.7b). A high synchrony is found among the simulations and the tree-ring based reconstructions in periods with large negative temperature anomalies observed at the end of the 18th century, during the Dalton and Spörer solar minima, and during periods of positive anomalies as well e.g.: middle 15th century, middle-end 16th century and middle of 18th century. The positive trend displayed by the simulations from 1800AD onwards is also in accordance with the increase in temperature described by the proxy based reconstructions, though more pronounced in the case of the model outputs. Some simulations lack large negative periods which are present in the reconstructions, as the Late Maunder solar minimum. The simulations ERIK1 and MM5-ERIK1 display an identical period of negative anomalies corresponding to the Maunder solar minima, in agreement with the one displayed by the set of reconstructions. In the simulations ERIK2 and MM5-ERIK2 this negative period is delayed. In general terms, ERIK1 and MM5-ERIK1 seems to simulate better the negative anomalies.

The comparison between the output of the model simulations and the range established by the different reconstructions show that, overall the agreement between reconstructed and simulated May-to-September temperatures at the Pyrenees is good, especially at intermediate to low frequencies. At multi-decadal timescales, the different

series show their up and downs swings synchronized and all series show a similar behavior, with a warmer century from 1300 AD to 1400AD, a colder between 1600-1800 AD (little ice age, LIA), the solar minima and the modern warming. Thus, the external forcing applied to the model matches the timing of the main past periods of anomalous temperatures in the Pyrenees region.

At higher frequencies, i.e. decadal time scales, the agreement between model simulations and reconstructions is lower because the climate variability at this time scales is mostly internal, not driven by the external forcing ([Gómez-Navarro et al., 2011b](#)). For instance, the warm episode with the maximum around AD 1730 discussed in last section displayed by the Pyrenees reconstructions is not reproduced by any of the four simulations and does not match any maximum of the external forcing. Therefore it should not necessarily appear in the simulations with the same timing as in the reconstructions.

Finally, the instrumental data used for the Pyrenees describe a pronounced cooling from 1950 until approximately 1980, which is visible in the reconstructions but not in the simulation, and that does not agree with the increasing warming trend replicated by simulations for the second part of the 20th century. It is important to note that these four simulations do not include tropospheric aerosol forcing and vegetation changes, which may have a cooling effect. Hence, the increasing trend in temperatures described by the simulations is only due to the increase in solar irradiance and greenhouse gases forcing. However, the Pyrenees has experienced an increase in the vegetation cover and active vegetation successions processes from 1950 onwards, which is not included in these simulations. Whether this increase in vegetation coverage can produce negative temperature trend which explains this mismatch is an open question. Anyway, it seems that there is some cooling factor influencing the temperature variation at the Pyrenees on the second half of the 20th century which is missing in the external forcing of model simulations. However, since one of the simulations (MM5-ERIK1) displays a minima on the 20th century, the described regional cooling could also be due to internal variability without the need to involve vegetation changes or aerosol forcing.

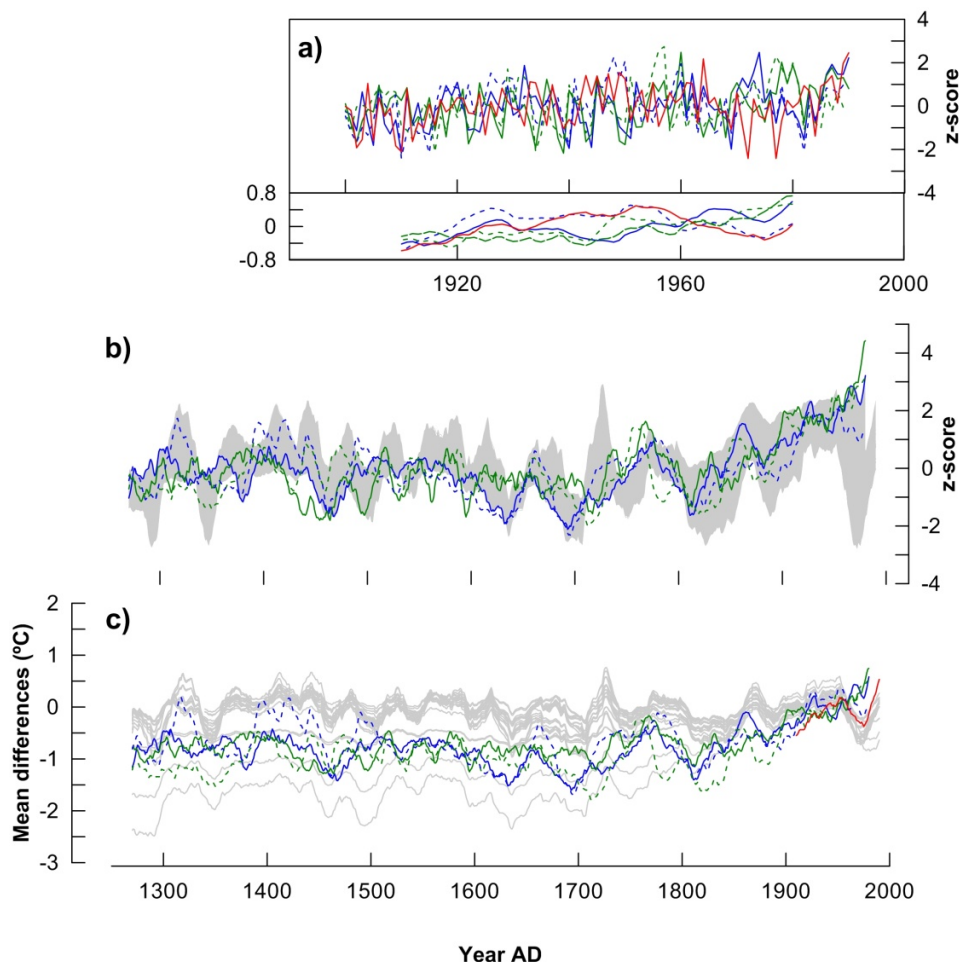


**Figure 6.7:** Comparison of reconstructed and simulated May to September temperature for the last 750 years. Grey lines/shade corresponds to the range of the 24 MXD based temperature reconstructions developed at the Pyrenees. Colored lines correspond to the different model outputs: Erik1 (blue), Erik2 (green), MM5-Erik1 (dashed blue) and MM5-Erik2 (dashed green). All series smoothen with a 20-years centered moving average. a) Comparison of the simulated May to September temperatures and the instrumental record (black line). b) Series scaled to mean 0 and standard deviation 1. c) Series in anomalies (differences from reference period 1900-2005). Source: Dorado-Liñán et al. (2011).



Chapter **7**

## General conclusions

Most of the main conclusions obtained in this Thesis are exposed along the respective chapters. However, here we summarize them to provide a general overview of the content of this Thesis.

One of the most prominent objectives of this Thesis was to develop a large database of high-resolution regional climate simulations over the Iberian Peninsula (IP) and Europe which allows to study the long-term evolution of the climate over these areas. This study requires a large number of climate simulations to be designed, run and analyzed. Nearly 3000 years of regional climate simulations (which are currently being used by several research groups) have been performed, including:

- Two transient 990-year long simulations for the IP covering the period 1000-1990 with a spatial resolution of 30 km. These simulations were forced identically by three external forcings: variations in solar constant, concentration of greenhouse gases and the parametrized effect of big volcano events in the radiative balance. The GCM driving these simulations is ECHO-G. The only difference between these two simulations was the initial condition used for running the GCM. These two simulations are further described in Chapters [2](#) and [3](#).
- A simulation for the period 1500-1990 for all Europe with a resolution of 45 km. This simulation was driven by ECHO-G, using the same external forcings as the simulations for the IP. This simulation is described in Chapter [5](#).
- Four regional climate change projections for the 21st century with 30 km of spatial resolution over the IP. These four simulations are transient runs which cover

continuously the period. Two GCMs were used to drive these simulations, each one under two different scenarios (A2 and B2 for ECHO-G and A2 and B1 for ECHAM5). Details of these simulations are presented in Chapter 4.

- A hindcast simulation driven by the ERA40 reanalysis with the same domain configuration than the one employed for the IP paleosimulations.

The skill of this model setup has been assessed through comparisons with observational databases in the instrumental period. This comparison was performed in Chapters 2 and 5. The main conclusions obtained were:

- The high spatial resolution of regional climate simulations represents an added value to previous palaeosimulations performed with ECHO-G. By means of a comparison with a dynamical downscaling performed with reanalysis data, MM5 was able to improve significantly the skill of ECHO-G in reproducing the observed climate over the IP for the 1961-1990 period. In particular, differences between the climate simulated by ERA40 and ECHO-G are larger than those for the corresponding downscaled datasets.
- MM5 is able also to narrow differences between the climate developed by ECHO-G and the E-OBS database over the IP. This supports the idea that the downscaling of GCM paleosimulations may improve their quality at regional scales. These improvements pertain to the modification of the seasonal variability, which is modified by MM5 bringing it closer to the observations in the reference period.
- The assessment of the skill of the model has also included the comparison of the main variability modes of the simulation and the observations. It has been analyzed through an EOF analysis of the seasonal series of temperature and precipitation. The model develops very similar patterns to those observed, and the amount of variability explained by each EOF is of similar magnitude in both datasets.
- The simulation for Europe has also been tested. The skill of the MM5-ECHO-G setup has been first analyzed comparing its outputs with a number of observational records, focusing the analysis on summer and winter seasons. The mean values of temperature and precipitation in a reference period (1960-1990) have been compared with observations recorded in the CRU database. Mean values are well captured due to the higher resolution of the regional model. There are however some important biases, like a clear tendency to overestimate temperature and precipitation in Northern Europe in winter and underestimate temperature

in summer. These biases seem to be related to the overestimation of the zonal circulation by the GCM, due to a too intense pressure gradient over the Atlantic.

- The PDF analysis during the 20th century obtained for the European simulation and in observations shows more clearly the areas and seasons with more prominent biases. However, despite the bias, the shape of the PDFs is remarkably similar in the simulation and the observations, and more importantly it evolves similarly through different seasons. This gives confidence on the capability of the model to reproduce extreme events.

Another objective of this Thesis was the use of climate experiments to describe the past climate of the IP and Europe, which allows to put the recent warming in a longer climate context. The main conclusions drawn in Chapters 2 and 5 were:

- External forcings have an important role in the simulation. There is a series of minima and maxima in the effective TSI that can be linked with corresponding cold/warm periods, and that matches several known historical periods. In particular, the models are able to simulate the Little Ice Age and the Medieval Climate Anomaly as a direct response to radiation forcing. On the other hand, in the last 150 years of the 20th century there is an increase of the temperature, which seems to be linked to the continuous rise of GHGs concentrations characteristic of the industrial period.
- Although domain-averaged values of temperature and precipitation in the RCM simulation are very similar to those of the AOGCM in the same area, some important differences appear at regional scales. These can be more clearly found in the high-frequency evolution of the regional climate, or in the shape and intensity of temperature and precipitation anomaly patterns in a given period.
- Through comparison with observations, the ECHO-G-MM5 configuration has shown to be able to develop a realistic link between NAO variability and precipitation over Europe and the IP in particular.
- Simulations draw a Little Ice Age influenced by a weak NAO phase, which produces wetter-than-usual conditions over the IP during this cold period. However, this result should be taken carefully due to the role of internal variability in large-scale dynamics.

The analysis of the role of internal variability in regional climate simulations over the IP was another important objective of this Thesis, which is explored in Chapter 3. The main conclusions obtained were:

- The long-term evolution of temperature is strongly affected by the external forcings driving the simulation. This variable responds to the external factors very homogeneously over the IP at most temporal scales.
- Evolution of precipitation is however more strongly governed by chaotic variability at regional scale. In particular, there are few areas over the IP where the precipitation is significantly driven by external forcings.
- The influence of the external forcing on precipitation is specially weak in winter. This is due to the nature of the winter precipitation over the IP which is dominated by variations in the NAO. The NAO seems to be quite insensitive to the external forcing in the simulations at the investigated timescales. Once the NAO signal is removed from the precipitation series, the leading variability pattern corresponds quite well with the areas which more clearly are able to respond to forcings. We have identified that the physical mechanism capable to link the evolution of precipitation and forcing during this season is through modification in the condensation level, driven by air temperature changes.
- Precipitation in summer is more strongly affected by variations in the forcing. We have demonstrated that this precipitation mode is dominated by modulation of the large-scale SLP by the external forcing in summer.
- The significance of the correlation used to detect the role of external forcing emerges at regional scales, and is blurred when a spatial average is performed. This stresses the importance of high resolution simulations in exercises comparing the model results with proxy reconstructions of precipitation

Several comparison exercises between climate simulations and reconstructions have been performed through Chapters 2, 5 and 6. They deal with validating the skill of climate reconstructions and the methodologies employed to generate them, as well as drawback in the models. The main conclusions extracted from these chapters were:

- We have compared the results of the model simulation over the IP with the temperature and precipitation reconstruction of Luterbacher et al. (2004) and Pauling et al. (2006). The model results tend to be colder than the reconstruction,

more noticeably in the LIA. Winter temperature variability is similar, although the model overestimates it. However, in summer the reconstruction depicts clearly less variability. There is a relatively good agreement in the final trend in the 20th century. Precipitation series show similar variability in the model and in the reconstructions, although the correlation between both is low. In particular, the positive anomaly in precipitation simulated by the model does not seem to reproduce the reconstruction in the past centuries.

- A similar comparison was performed with the simulations covering the whole Europe. It offers a unique opportunity to test not only the temporal evolution of the reconstruction, but their spatial distribution properties and relations with large-scale fields. We found that the PDFs for the model and the reconstructions match remarkably well during the period 1500-1900, and most of the differences can be attributed to biases in the driving model.
- The temporal evolution in the spacial-averaged series over several areas of Europe presents similar variability and trend in simulation and reconstructions, giving confidence to the skill of the latter.
- However, the EOF analysis indicates that reconstructions tend to oversimplify the main variability modes, overestimating the percentage of variance associated to the leading modes. This leads to an oversimplification of the reconstructed variability, a drawback of reconstructions which is especially noticeable for precipitation.
- The comparison with local reconstructions in Stockholm and Central Europe, as well as the instrumental series of Central England, shows some agreements and some other important disagreements. The long-term trend is similar in the reconstructions and the simulation, suggesting a good choice of the amplitude of external forcings used to drive the simulation. However, the model tends to overestimate the warming in the 21st century, something that could imply that other factors not included in the simulations, such as anthropogenic aerosols or vegetation cover changes, could have played an important role in the last century.
- An important disagreement between model and reconstruction is a warm period around 1730, which is not present in the simulation. Since there is no evidence of a change in external forcings during that period, a plausible explanation for this anomaly could be a change in large-scale dynamics. This hypothesis is explored

within the model performing a temperature composite based on strong-minus-weak NAO phases, which yields an anomaly pattern that mimics the one found in temperature gridded reconstructions. Thus, the hypothesis of non-forced variability can not be ruled out.

- The simulations with the global circulation model ECHO-G and the regional model MM5 agree with the tree-ring based reconstructions over the Pyrenees at decadal to interdecadal time scales. However, the comparison also highlights differences that need to be understood, such as the amplitude of the temperature variations and the discrepancies in the 20th century trends.
- The physical consistence of the model has been used to test the methodology developed by [Rodrigo \(2008\)](#) to reconstruct running mean and standard deviation from documentations recording extreme events. The methodology has demonstrated its robustness, and the simulation allows to estimate a confidence level for the reconstruction.

Finally, the analysis of climate change projections was presented in Chapter 4. The main conclusions obtained were:

- Our approach focuses on an EOF analysis, which is able to account for the warming signal, the first EOF capturing the temperature trends along the simulated period. This methodology, not used so far in RCM studies, tries to overcome the problem linked to the internal variability of RCMs, as it employs the whole transient simulation to calculate the warming patterns.
- The warming patterns found depend neither on the SRES scenario nor on the GCM version used to drive the regional simulations. They are, rather, an inherent feature of the considered domains and the model setup.
- The effect of changing the forcing conditions (i.e. the GHG concentrations) is to modulate the global trends over the IP not to modify the spatial structure of the projected warming or the continentalization of the climate.
- The spatial structure of the warming patterns has a marked annual cycle. In addition, there is an important asymmetry between maximum and minimum 2-m temperatures.

- The warming patterns seem to be associated to several geographical parameters such as distance to the sea or altitude. Nevertheless, there is no completely satisfactory explanation of the physical mechanisms underlying this behaviour, and further research should be devoted to an attempt to fully understand them.
- Maximum temperature trends are more pronounced than minima. These differences also depend on the month, being stronger in summer. This asymmetry yields a continentalization of the climate over the IP for the projected period.

In general, the present Thesis assesses the possible effect of anthropogenic emissions of greenhouse gases to the atmosphere during the next century, but also contextualize this human-forced variability in the longer palaeoclimatic context of the last millennium. Nearly 3000 years of regional climate simulations have been performed, trying to take into account many of the underlying uncertainties, like those related on internal variability and climate forcings. However, uncertainties linked to the model itself are not covered by this Thesis, since this issue is carried out in the Thesis by Jerez (2011), developed in our research group. The generated database has been used, and it is being currently used, by various scientists in different research areas related to climate (Dorado-Liñán et al., 2011; Jiménez-Guerrero et al., 2011; Rodrigo et al., 2011, among others). Hence we expect that our results contribute to a better understanding of climate variability and its effects in our environment.

As future work, there are several aspects of these simulations which have not been exploited yet, but we plan to do it within the next months (some of them have been outlined in Chapter 6). There are several climate reconstructions for the IP which are currently under development in the context of the SALVA-SINOBAS project. Comparison between these reconstructions and climate simulations will allow to assess their physical consistence. In the framework of this project, further studies about the impact of droughts and the effect of big volcano events during the last centuries will be evaluated. On the other hand, Europe is an area where high-quality reconstructions are available. Thus, the European simulation described in Chapter 5 will be employed to study these reconstructions. Other works include the analysis of changes in circulation pattern over Europe during anomalous periods such as the Dalton Minimum, and to characterize whether these changes can be driven by volcanic, solar forcing, or both. Other important issue we plan to address in the future is the use of regional ocean models. In this respect, the project SPEQ-TRES, funded by the Ministry of Science and Innovation, includes a set of simulations performed with the regional model WRF coupled to a ocean regional model ROMS. The results of these simulations will be compared

with the simulations analyzed through this Thesis, to characterize the role of the ocean model and address its added value.

# Bibliography

- Alley, R.B., Marotzke, J., Nordhaus, W.D., Overpeck, J.T., Peteet, D.M., Pielke, R.A., Pierrehumbert, R.T., Rhines, P.B., Stocker, T.F., Talley, L.D., and Wallace, J.M.: Abrupt climate change, *science*, 299, 2005–2010, 2003.
- Alvarez-Castro, M.C., Barriopedro, D., Gallego, D., Garcia-Herrera, R., Hernandez, E., Peña-Ortiz, C., Ribera, P., and Wheeler, D.: Westerly Index: A new quasi-instrumental climatic index for the North Atlantic westerlies (1685–2008), in: EMS Anual Meeting Abstracts, vol. 8, p. 435, 2011.
- Ammann, C.M., Joos, F., Schimel, D.S., Otto-Bliesner, B.L., and Tomas, R.A.: Solar influence on climate during the past millennium: Results from transient simulations with the NCAR Climate System Model, *Proceedings of the National Academy of Sciences of the United States of America*, 104, 3713–3718, doi:10.1073/pnas.0605064103, 2007.
- Barnett, T.P., Pierce, D.W., and Schnur, R.: Detection of Anthropogenic Climate Change in the World's Oceans, *Science*, 292, 270–274, doi:10.1126/science.1058304, 2001.
- Barriendos, M. and Rodrigo, F.S.: Study of historical flood events on Spanish rivers using documentary data, *Hydrological sciences journal*, 51, 765–783, 2006.
- Beltrami, H.: Earth's long-term memory, *Science*, 297, 206–207, 2002.
- Bigg, G.R., Jickells, T.D., Liss, P.S., and Osborn, T.J.: The role of the oceans in climate, *International Journal of Climatology*, 23, 1127–1159, doi:10.1002/joc.926, 2003.

- Boo, K.O., Kwon, W.T., and Baek, H.J.: Change of extreme events of temperature and precipitation over Korea using regional projection of future climate change, *Geophysical Research Letters*, 33, L01 701, 2006.
- Bradley, R.S. and Jones, P.D.: 'Little Ice Age' summer temperature variations: their nature and relevance to recent global warming trends, *The Holocene*, 3, 367–376, doi:10.1177/095968369300300409, 1993.
- Bradley, R.S., Hughes, M.K., and Diaz, H.F.: Climate in Medieval Time, *Science*, 302, 404–405, doi:10.1126/science.1090372, 2003.
- Brázdil, R., Pfister, C., Wanner, H., Storch, H.V., and Luterbacher, J.: Historical climatology in Europe – the state of the art, *Climatic Change*, 70, 363–430, 2005.
- Briffa, K.R., Osborn, T.J., and Schweingruber, F.H.: Large-scale temperature inferences from tree rings: a review, *Global and planetary change*, 40, 11–26, 2004.
- Büntgen, U., Tegel, W., Nicolussi, K., McCormick, M., Frank, D., Trouet, V., Kaplan, J.O., Herzig, F., Heussner, K.U., Wanner, H., Luterbacher, J., and Esper, J.: 2500 Years of European Climate Variability and Human Susceptibility, *Science*, 331, 578–582, doi:10.1126/science.1197175, 2011.
- Cacho, I., Valero-Garcés, B., and González-Sampériz, P.: Review of paleoclimate reconstructions in the Iberian Peninsula since the last glacial period, in: *Climate in Spain: Past, present and future*, edited by Fiz, Perez F. and Roberta, Boscolo, pp. 9–24, Ministerio de Ciencia e Innovacion (MICINN), 2010.
- Chen, F. and Dudhia, J.: Coupling an Advanced Land Surface-Hydrology Model with the Penn State-NCAR MM5 Modeling System. Part I: Model Implementation and Sensitivity, *Monthly Weather Review*, 129, 569–585, 2001a.
- Chen, F. and Dudhia, J.: Coupling an Advanced Land Surface-Hydrology Model with the Penn State-NCAR MM5 Modeling System. Part II: Preliminary Model Validation, *Monthly Weather Review*, 129, 587–604, 2001b.
- Christensen, J.H., Hewitson, B., Busuioc, A., Chen, A., Gao, X., Held, I., Jones, R., Kolli, R.K., Kwon, W.-T., Laprise, R., Rueda, V. Magaña, Mearns, L., Menéndez, C.G., Räisänen, J., Rinke, A., Sarr, A., and Whetton, P.: *Climate Change 2007: The Physical Science Basis. Contribution of Working Group I to the Fourth Assessment Report of the Intergovernmental Panel on Climate Change*, chap. *Regional Climate Projections*, Cambridge University Press, Cambridge, United Kingdom and New York, 2007.

- Cook, E., D'Arrigo, R.D., and Mann, M.E.: A well verified multiproxy reconstruction of the winter North Atlantic Oscillation index since A.D. 1400, *Journal of Climate*, 15, 1754–1764, 2002.
- Courant, R., Friedrichs, K., and Lewy, H.: On the partial difference equations of mathematical physics, *IBM Journal of Research and Development*, 11, 215–234, 1967.
- Crowley, T.J.: Causes of climate change over the past 1000 years, *Science*, 289, 270–277, doi:10.1126/science.289.5477.270, 2000.
- Curry, J.A., Schramm, J.L., and Ebert, E.E.: Sea ice-albedo climate feedback mechanism, *Journal of Climate*, 1151, 240–247, 1995.
- Davidson, E.A. and Janssens, I.A.: Temperature sensitivity of soil carbon decomposition and feedbacks to climate change, *Nature*, 440, 165–173, 2006.
- deMenocal, P.B.: Cultural responses to climate change during the Late Holocene, *Science*, 292, 667–673, doi:10.1126/science.1059827, 2001.
- Déqué, M., Jones, R.G., Wild, M., Giorgi, F., Christensen, J.H., Hassell, D.C., Vidale, P.L., Rockel, B., Jacob, D., Kjellström, E., de Castro, M., Kucharski, F., and van den Hurk, B.: Global high resolution versus Limited Area Model climate change projections over Europe: quantifying confidence level from PRUDENCE results, *Climate Dynamics*, 25, 653–670, doi:10.1007/s00382-005-0052-1, 2005.
- Déqué, M., Rowell, D.P., Lüthi, D., Giorgi, F., Christensen, J.H., Rockel, B., Jacob, D., Kjellström, E., de Castro, M., and van den Hurk, B.: An intercomparison of regional climate simulations for Europe: assessing uncertainties in model projections, *Climatic Change*, 81, 53–70, doi:10.1007/s10584-006-9228-x, 2007.
- Diffenbaugh, N.S. and Sloan, L.C.: Mid-Holocene orbital forcing of regional-scale climate: a case study of western North America using a high-resolution RCM, *Journal of Climate*, 17, 2927–2937, doi:10.1175/1520-0442(2004)017<2927:MOFORC>2.0.CO;2, 2004.
- Diffenbaugh, N.S., Pal, J.S., Giorgi, F., and Gao, X.: Heat stress intensification in the Mediterranean climate change hotspot, *Geophysical Research Letters*, 34, L11 706, doi:10.1029/2007GL030000, 2007.
- Dobrovolný, P., Moberg, A., Brazdil, R., Pfister, C., Glaser, R., Wilson, R., van Engelen, A., Limanówka, D., Kiss, A., Halíčková, M., Mackova, J., Riemann, D., Luterbacher, J.,

- and Böhm, R.: Monthly, seasonal and annual temperature reconstructions for Central Europe derived from documentary evidence and instrumental records since AD 1500, *Climate Change*, 101, 69–107, 2010.
- Dorado-Liñán, I., Büntgen, U., González-Rouco, J.F., Zorita, E., Montávez, J.P., Gómez-Navarro, J.J., Brunet, M., Heinrich, I., Helle, G., and Gutiérrez, E.: Tree-ring proxy based temperature reconstructions and climate model simulations: Cross-comparison at the Pyrenees, *Climate the Past*, 2011.
- Dudhia, J.: Numerical study of convection observed during the winter monsoon experiment using a mesoscale two-dimensional model, *Journal of the Atmospheric Science*, 46, 3077–3107, 1989.
- Dudhia, J.: A Nonhydrostatic Version of the Penn StateNCAR Mesoscale Model: Validation Tests and Simulation of an Atlantic Cyclone and Cold Front, *Monthly Weather Review*, 121, 1493–1513, 1993.
- Ebisuzaki, W.: A method to estimate the statistical significance of a correlation when the data are serially correlated, *Journal of Climate*, 10, 2147–2153, 1997.
- Eddy, J.A.: The maunder minimum, *Science*, 192, 1189–1202, doi:10.1126/science.192.4245.1189, 1976.
- Fernández, J., Montávez, J.P., Saenz, J., González-Rouco, J.F., and Zorita, E.: Sensitivity of the MM5 mesoscale model to physical parameterizations for regional climate studies: Annual cycle, *Journal of Geophysical Research-Atmospheres*, 112, D04 101, doi:10.1029/2005JD006649, 2007.
- Fischer, E.M., Luterbacher, J., Zorita, E., Tett, S.F.B., Casty, C., and Wanner, H.: European climate response to tropical volcanic eruptions over the last half millennium, *Geophysical Research Letters*, 34, L05 707, doi:10.1029/2006GL027992, 2007.
- Folland, C.K., Knight, J., Linderholm, H.W., Fereday, D., Ineson, S., and Hurrell, J.W.: The Summer North Atlantic Oscillation: Past, Present, and Future, *Journal of Climate*, 22, 1082–1103, 2009.
- Font-Tullot, I.: *Climatología de España y Portugal*, Ediciones Universidad de Salamanca, Salamanca, 2<sup>a</sup> edn., 2000.

- Frank, D., Büntgen, U., Böhm, R., Maugeri, M., and Esper, J.: Warmer early instrumental measurements versus colder reconstructed temperatures: shooting at the moving target, *Quaternary Science Review*, 26, 3298–3310, 2007a.
- Frank, D., Esper, J., and Cook, E.R.: Adjustment for proxy number and coherence in large-scale temperature reconstruction, *Geophysical Research Letters*, 34, L16 709, doi:10.1129/2007GL030571, 2007b.
- Frei, C., Christensen, J.H., Déqué, M., Jacob, D., Jones, R.G., and Vidale, P.L.: Daily precipitation statistics in regional climate models: Evaluation and intercomparison for the European Alps, *Journal Geophysical Research*, 108, 1–19, 2003.
- Fritts, H.C.: Tree rings and climate, London, New York, San Francisco.: Academic Press, 1976.
- Giorgi, F.: Climate change prediction, *Climatic Change*, 73, 239–265, 2005.
- Giorgi, F.: Climate change hot-spots, *Geophysical Research Letters*, 33, 11 217–11 222, 2006.
- Giorgi, F. and Bi, X.: Updated regional precipitation and temperature changes for the 21st century from ensembles of recent AOGCM simulations, *Geophysical Research Letters*, 32, L21 715, doi:10.1029/2005GL024288, 2005.
- Giorgi, F., Brodeur, C.S., and Bates, G.T.: Regional climate change scenarios over the United States produced with a nested regional climate model, *Journal of Climate*, 7, 375–399, 1994.
- Giorgi, F., Hurrel, J.W., and Marinucci, Maria Rosaria: Elevation Dependency of the Surface Climate Change Signal: A Model Study, *Journal of Climate*, 10, 288–296, 1997.
- Giorgi, F., Bi, X., and Pal, J.S.: Mean, interannual variability and trends in a regional climate change experiment over Europe.I. Present-day climate (1961–1990), *Climate Dynamics*, 22, 733–756, doi:10.1007/s00382-004-0409-x, 2004a.
- Giorgi, F., Bi, X., and Pal, J.S.: Mean, interannual variability and trends in a regional climate change experiment over Europe. II: climate change scenarios (2071–2100), *Climate Dynamics*, 23, 839–858, doi:10.1007/s00382-004-0467-0, 2004b.

- Gleckler, P.J., Taylor, K.E., and Doutriaux, C.: Performance metrics for climate models, *Journal of Geophysical Research*, 113, D06 104, 2008.
- Gómez-Navarro, J.J., Montávez, J.P., Jerez, S., and García-Valero, J.A.: On the relationship between warming and orography in regional climate change projections (in Spanish), in: *Clima en España: Pasado. Presente y futuro. Contribución a un informe de Evaluación del Cambio Climático Regional: Resúmenes del congreso*, p. 132, Madrid, 2009.
- Gómez-Navarro, J.J., Montávez, J.P., Jerez, S., Jiménez-Guerrero, P., Lorente-Plazas, R., González-Rouco, J.F., and Zorita, E.: A regional climate simulation over the Iberian Peninsula for the last millennium, *Climate of the Past*, 7, 451–472, doi:10.5194/cp-7-451-2011, 2011a.
- Gómez-Navarro, J.J., Montávez, J.P., Jiménez-Guerrero, P., Jerez, S., Lorente-Plazas, R., González-Rouco, J.F., and Zorita, E.: Internal and external variability in regional simulations of the Iberian Peninsula climate over the last millennium, *Climatic of the Past Discussions*, 7, 2579–2607, doi:10.5194/cpd-7-2579-2011, 2011b.
- Gómez-Navarro, J.J., Montávez, J.P., Jiménez-Guerrero, P., Jerez, S., García-Valero, J.A., and González-Rouco, J.F.: Warming patterns in regional climate change projections over the Iberian Peninsula, *Meteorologische Zeitschrift*, 19, 275–285, 2010.
- González-Rouco, J.F., Heyen, H., Zorita, E., and Valero, F.: Agreement between Observed Rainfall Trends and Climate Change Simulations in the Southwest of Europe, *Journal of Climate*, 13, 3057–3065, doi:10.1175/1520-0442(2000)013<3057:ABORTA>2.0.CO;2, 2000a.
- González-Rouco, J.F., Heyen, H., Zorita, E., and Valero, F.: Agreement between observed rainfall trends and climate change simulations in the southwest of Europe, *Journal of Climate*, 13, 3057–3065, 2000b.
- González-Rouco, J.F., von Storch, H., and Zorita, E.: Deep soil temperature as proxy for surface air-temperature in a coupled model simulation of the last thousand years, *Geophysical Research Letters*, 30, 1–4, doi:10.1029/2003GL018264, 2003.
- González-Rouco, J.F., Beltrami, H., Zorita, E., and Stevens, M.B.: Borehole climatology: a discussion based on contributions from climate modeling, *Climate of the Past*, 5, 97–127, 2009.

- Goosse, H., Renssen, H., Timmermann, A., and Bradley, R.S.: Internal and forced climate variability during the last millennium: a model-data comparison using ensemble simulations, *Quaternary Science Reviews*, 24, 1345–1360, 2005.
- Graham, L. P., Olsson, J., Kjellström, E., Rosberg, J., Hellström, S., and Berndtsson, R.: Simulating river flow to the Baltic Sea from climate simulations over the past millennium, *Boreal Environment Research*, 14, 173–182, 5th Study Conference on BALTEX, Kuressaare, Estonia, Jun 04–08, 2007, 2009.
- Grell, G.A.: Prognostic evaluation of assumptions used by cumulus parameterizations, *Monthly Weather Review*, 121, 764–787, 1993.
- Grell, G.A., Dudhia, J., and Stauffer, D.R.: A description of the fifth-generation Penn State/NCAR Mesoscale Model (MM5), Tech. Rep. December, NCAR, Boulder, Colorado, 1994a.
- Grell, G.A., Dudhia, J., and Stauffer", D.R.: A description of the fifth-generation Penn State/NCAR Mesoscale Model (MM5), Tech. Rep. NCAR/TN-398+STR, National Center for Atmospheric Research, 1994b.
- Hannachi, A., Jolliffe, I.T., and Stephenson, D.B.: Empirical orthogonal functions and related techniques in atmospheric science: A review, *International Journal of Climatology*, 27, 1119–1152, doi:10.1002/joc.1499, 2007.
- Hansen, J., Lacis, A., Rind, D., Russell, G., Stone, P., Fung, I., Ruedy, R., and Lerner, J.: Climate sensitivity: Analysis of feedback mechanisms., *The Warming Papers*, pp. 154–190, 2011.
- Hawkins, E. and Sutton, R.: The potential to narrow uncertainty in regional climate predictions, *Bulletin of the American Meteorological Society*, 90, 1095–1107, doi: 10.1175/2009BAMS2607.1, 2009.
- Haylock, M.R., Hofstra, N., Tank-Klein, A.M.G., Klok, E.J., Jones, P.D., and New, M.: A European daily high-resolution gridded data set of surface temperature and precipitation for 1950–2006, *Journal of Geophysical Research-atmospheres*, 113, D20 119, doi:10.1029/2008JD010201, 2008.
- Hegerl, G., Luterbacher, J., González-Rouco, J.F., Tett, S.F.B., Crowley, T., and Xoplaki, E.: Influence of human and natural forcing on European seasonal temperatures, *Nature Geoscience*, 4, 99–103, doi:10.1038/ngeo1057, 2011.

- Held, I.M.: Water Vapor Feedback and Global Warming, *Annual Review of Energy and the Environment*, 25, 441–475, 2000.
- Hewitson, B.C. and Crane, R.G.: Climate downscaling: techniques and application, *Climate Research*, 7, 85–95, 1996.
- Hofstra, N., Haylock, M., New, M., and Jones, P.D.: Testing E-OBS European high-resolution gridded data set of daily precipitation and surface temperature, *Journal of Geophysical Research*, 114, D21 101, doi:10.1029/2009JD011799, 2009.
- Hong, S.Y. and Pan, H.L.: Nonlocal boundary layer vertical diffusion in a medium-range forecast model, *Monthly Weather Review*, 124, 2322–2339, 1996.
- Hostetler, S.W., Bartlein, P.J., Clark, P.U., Small, E.E., and Solomon, A.M.: Simulated influences of Lake Agassiz on the climate of central North America 11,000 years ago, *Nature*, 405, 334–337, 2000.
- Houghton, J.T., Ding, Y., Griggs, D.J., Noguer, M., van der Linden, P.J., Dai, X., Maskell, K., and Johnson, C.A., eds.: *Climate Change 2001: The Scientific Basis. Contribution of Working Group I to the Third Assessment Report of the Intergovernmental Panel on Climate Change*, Cambridge University Press, New York, 2001.
- Hurrell, J. W. and van Loon, H.: Decadal variations in climate associated with the North Atlantic Oscillation, *Climatic Change*, 36, 301–326, 1997.
- Huybers, P and Curry, W.: Links between annual, Milankovitch and continuum temperature variability, *Nature*, 441, 329–332, doi:10.1038/nature04745, 2006.
- IPCC: *Climate Change 2007: Contribution of Working Group I to the Fourth Assessment Report of the Intergovernmental Panel on Climate Change*, S. Solomon, D. Qin, M. Manning, Z. Chen, M. Marquis, K.B. Averyt, M. Tignor and H.L. Miller (eds.). Cambridge University Press, Cambridge, UK and New York, USA, 2007a.
- IPCC: *Climate Change 2007: The Physical Science Basis: Contribution of Working Group I to the Fourth Assessment Report of the Intergovernmental Panel on Climate Change*, Cambridge University Press, New York, 2007b.
- Jacob, D., Barring, L., Christensen, O. B., Christensen, J. H., de Castro, M., Déqué, M., Giorgi, F., Hagemann, S., Lenderink, G., Rockel, B., Sanchez, E., Schaer, C., Seneviratne, S. I., Somot, S., van Ulden, A., and van den Hurk, B.: An inter-comparison

- of regional climate models for Europe: model performance in present-day climate, *Climatic Change*, 81, 31–52, doi:10.1007/s10584-006-9213-4, 2007.
- Jerez, S.: Climate simulations over the Iberian Peninsula: study of the role of the parameterisation schemes and characterisation of climate change patterns, Ph.D. thesis, University of Murcia, Spain, 2011.
- Jerez, S., Montávez, J.P., Jiménez-Guerrero, P., Gómez-Navarro, J.J., and González-Rouco, J.F.: Influence of soil moisture-near surface temperature feedback on present and future climate simulations over the Iberian Peninsula, in: 21st Century Challenges in Regional-scale Climate Modelling, 41, pp. 261–262, Lund University, 2009.
- Jerez, S., Montávez, J.P., Gómez-Navarro, J.J., Jiménez-Guerrero, P., Jiménez, J.M., and González-Rouco, J.F.: Temperature sensitivity to the land-surface model in MM5 climate simulations over the Iberian Peninsula, *Meteorologische Zeitschrift*, 19, 1–12, 2010.
- Jiménez-Guerrero, P., Gómez-Navarro, J.J., Jerez, S., Lorente-Plazas, R., García-Valero, J.A., and Montávez, J.P.: Variation of Secondary Inorganic Aerosols (SIA) in Europe for the 21st century (1991–2100), *Atmospheric Environment*, 45, 1059–1063, 2011.
- Jones, P.D. and Briffa, K.R.: Unusual climate in northwestern Europe during the period 1730 to 1745 based on instrumental and documentary data, *Climate Change*, 79, 361–379, 2006.
- Jones, P.D., Osborn, T.J., and Briffa, K.R.: The evolution of climate over the last millennium, *Science*, 292, 662–667, 2001.
- Jones, P.D., Briffa, K.R., Osborn, T.J., Lough, J.M., van Ommen, T.D., Vinther, B.M., Lutherbacher, J., Wahl, E. R., Zwiers, F.W., Mann, M.E., Schmidt, G.A., Ammann, C. M., Buckley, B.M., Cobb, K.M., Esper, J., Goosse, H., Graham, N., Jansen, E., Kiefer, T., Kull, C., Kuettel, M., Mosley-Thompson, E., Overpeck, J.T., Riedwyl, N., Schulz, M., Tudhope, A.W., Villalba, R., Wanner, H., Wolff, E., and Xoplaki, E.: High-resolution palaeoclimatology of the last millennium: a review of current status and future prospects, *The Holocene*, 19, 3–49, doi:10.1177/0959683608098952, 2009.
- Jungclaus, J.H., Lorenz, S.J., Timmreck, C., Reick, C.H., Brovkin, V., Six, K., Segschneider, J., Giorgetta, M.A., Crowley, T.J., Pongratz, J., Krivova, N.A., Vieira, L.E., Solanki, S.K., Klocke, D., Botzet, M., Esch, M., Gayler, V., Haak, H., Raddatz, T.J., Roeckner, E., Schnur, R., Widmann, H., Claussen, M., Stevens, B., and Marotzke, J.: Climate and

- carbon-cycle variability over the last millennium, *Climate of the Past*, 6, 1009–1044, 2010.
- Jungclaus, J.H., Keenlyside, N., Botzet, M., Haak, H., Luo, J. J., Latif, M., Marotzke, J., Mikolajewicz, U., and Roeckner, E.: Ocean circulation and tropical variability in the coupled model ECHAM5/MPI-OM, *Journal of Climate*, 19, 3952–3972, 2006.
- Kalnay, E., Kanamitsu, M., Kistler, R., Collins, W., Deaven, D., Gandin, L., Iredell, M., Saha, S., White, G., Woollen, J., Zhu, Y., Leetmaa, A., and Reynolds, R.: The NCEP/NCAR 40-Year Reanalysis Project, *Bulletin of the American Meteorological Society*, 77, 437–470, 1996.
- Kittel, T.G.F., Giorgi, F., and Meehl, G.A.: Intercomparison of regional biases and doubled CO<sub>2</sub>-sensitivity of coupled atmosphere-ocean general circulation model experiments, *Climate Dynamics*, 14, 1–15, 1998.
- Kjellström, E., Brandefelt, J., Näslund, J., Smith, B., Strandberg, G., Voelker, A.H.L., and Wohlfarth, B.: Simulated climate conditions in Europe during the Marine Isotope Stage 3 stadial, *Boreas*, 39, 436–456, doi:10.1111/j.1502-3885.2010.00143.x, 2010.
- Kleidon, A., Fraedrich, K., and Heimann, M.: A green planet versus a desert world: estimating the maximum effect of vegetation on the land surface climate, *Climatic Change*, 44, 471–493, 2000.
- Knutti, R., Stocker, T.F., Joos, F., and Plattner, G.K.: Constraints on radiative forcing and future climate change from observations and climate model ensembles, *Nature*, 416, 719–723, 2002.
- Krivova, N. and Solanki, S.: Models of solar irradiance variations: Current status, *Journal of Astrophysics and Astronomy*, 29, 151–158, 10.1007/s12036-008-0018-x, 2008.
- Küttel, M., Xoplaki, E., Gallego, D., Luterbacher, J., García-Herrera, R., Allan, R., Barriendos, M., Jones, P.D., Wheeler, D., and Wanner, H.: The importance of ship log data: reconstructing North Atlantic, European and Mediterranean sea level pressure fields back to 1750, *Climate Dynamics*, 34, 1115–1128, 2009.
- Lawrence, M.G.: The Relationship between Relative Humidity and the Dewpoint Temperature in Moist Air: A Simple Conversion and Applications., *Bulletin of the American Meteorological Society*, 86, 225–233, 2005.

Legrand, M. and Mayewski, P.: Glaciochemistry of polar ice cores: a review, *Reviews of Geophysics*, 35, 219–243, 1997.

Legutke, S. and Voss, R.: The Hamburg atmosphere-ocean coupled circulation model ECHO-G, Tech. rep., DKRZ, Hamburg, Germany, 1999.

Leijonhufvud, L., Wilson, R., Moberg, A., Söderberg, J., Retsö, D., and Söderlind, U.: Five centuries of winter/spring temperatures in Stockholm reconstructed from documentary evidence and instrumental observations, *Climate Change*, 101, 109–141, doi:10.1007/s10584-009-9650-y, 2010.

Liang, X., Kunkel, K.E., Meehl, G.A., Jones, R.G., and Wang, J.X.L.: Regional climate models downscaling analysis of general circulation models present climate biases propagation into future change projections, *Geophysical Research Letters*, 35, L08 709, doi:10.1029/2007GL032849, 2008.

Lorenz, E.: Empirical Orthogonal Functions and Statistical Weather Prediction, Tech. rep., Massachusetts Institute of Technology, 1956.

Lorenz, E.: Deterministic nonperiodic flow, *Journal of the Atmospheric Sciences*, 20, 131–141, 1963.

Luterbacher, J., Xoplaki, E., Dietrich, D., Jones, P.D., Davies, T.D., Portis, D., González-Rouco, J.F., von Storch, H., Gyalistras, D., Casty, C., et al.: Extending North Atlantic oscillation reconstructions back to 1500, *Atmospheric Science Letters*, 2, 114–124, 2002.

Luterbacher, J., Gómez-Navarro, J.J., Montávez, J.P., González-Rouco, J.F., Werner, J.G., and Zorita, E.: Comparison of century-long regional climate experiments with proxy based climate reconstructions over the Iberian Peninsula (Invited), in: AGU Fall Meeting Abstracts, vol. 1, pp. PP53A–04, 2010.

Luterbacher, J., Schmutz, C., Gyalistras, D., Xoplaky, E., and Wanner, H.: Reconstruction of monthly NAO and EU indices back to A.D.1675, *Geophysical Research Letters*, 26, 2745–2748, 1999.

Luterbacher, J., Dietrich, D., Xoplaki, E., Grosjean, M., and Wanner, H.: European seasonal and annual temperature variability, trends, and extremes since 1500, *Science*, 303, 1499–1503, 2004.

- Manley, G.: Central England Temperatures: monthly means 1659 to 1973, *Q.J.R. Meteorol. Soc.*, 79, 389–405, 1974.
- Mann, M.E., Zhang, Z., Hughes, M.K., Bradley, R.S., Miller, S.K., Rutherford, S., and Ni, F.: Proxy-based reconstructions of hemispheric and global surface temperature variations over the past two millennia, *Proceedings of the National Academy of Sciences of the United States of America*, 105, 13 252–13 257, doi:10.1073/pnas.0805721105, 2008.
- Mann, M.E., Woodruff, J.D., Donnelly, J.P., and Zhang, Z.: Atlantic hurricanes and climate over the past 1,500 years, *Nature*, 460, 880–883, doi:10.1038/nature08219, 2009.
- Mitchell, T.D. and Jones, P.D.: An improved method of constructing a database of monthly climate observations and associated high-resolution grids, *International Journal of Climatology*, 25, 693–712, doi:10.1002/joc.1181, 2005.
- Mlawer, E.J., Taubman, S.J., Brown, P.D., Iacono, M.J., and Clough, S.A.: Radiative transfer for inhomogeneous atmospheres: RRTM, a validated correlated- model for the longwave, *Journal of Geophysical Research*, 102, 16 663–16 682, 1997.
- Montávez, J.P., Fernández, J., González-Rouco, J.F., Saenz, J., Zorita, E., and Valero, F.: Climate change projections over the Iberian Peninsula (in Spanish), in: V Asamblea Hispano Portuguesa de geodesia y geofísica, Ministerio de Medio Ambiente, Sevilla, 2006.
- Montávez, J.P., Jerez, S., Gómez-Navarro, J.J., and González-Rouco, J.F.: Evaluation of soil models coupled to a RCM in simulating the Iberian Peninsula Climate, in: *Eos Trans. AGU. Fall Meet. Suppl.*, vol. 89, pp. GC53A–0706, 2008.
- Neelin, J.D., Battisti, D.S., Hirst, A.C., Jin, F.F., Wakata, Y., Yamagata, T., and Zebiak, S.E.: ENSO theory, *Journal of Geophysical Research*, 103, 14 261–14 290, 1998.
- North, G.R., Cahalan, R.F., and Coakley, J.A.: Energy balance climate models, *Reviews of Geophysics and Space Physics*, 19, 91–121, 1981.
- Nunez, M.N., Solman, S.A., and Cabre, M.F.: Regional climate change experiments over southern South America. II: Climate change scenarios in the late twenty-first century, *Climate Dynamics*, 32, 1081–1095, doi:10.1007/s00382-008-0449-8, 2009.
- Oreskes, N.: The scientific consensus on climate change, *Science*, 306, 1686, 2004.

- Parker, D.E., Legg, T.P., and Folland, C.K.: Five centuries of winter/spring temperatures in Stockholm reconstructed from documentary evidence and instrumental observations, *Jounal of Climate*, 12, 317–342, 1992.
- Patterson, W.P., Dietrich, K.A., Holmden, C., and Andrews, J.T.: Two millennia of North Atlantic seasonality and implications for Norse colonies, *Proceedings of the National Academy of Sciences of the United States of America*, 107, 5306–5310, doi:10.1073/pnas.0902522107, 2010.
- Pauling, A., Luterbacher, J., Casty, C., and Wanner, H.: Five hundred years of gridded high-resolution precipitation reconstructions over Europe and the connection to large-scale circulation, *Climate Dynamics*, 26, 387–405, doi:10.1007/s00382-005-0090-8, 2006.
- Pongratz, J., Reick, C.H., Raddatz, T., and Claussen, M.: Effects of anthropogenic land cover change on the carbon cycle of the last millennium, *Global Biogeochemical Cycles*, 23, GB4001, 2009.
- Raisanen, J.: CO<sub>2</sub>-induced climate change in CMIP2 experiments: Quantification of agreement and role of internal variability, *Journal of Climate*, 14, 2088–2104, 2001.
- Raisanen, J., Hansson, U., Ullerstig, A., Doscher, R., Graham, L.P., Jones, C., Meier, H.E.M., Samuelsson, P., and Willen, U.: European climate in the late twenty-first century: regional simulations with two driving global models and two forcing scenarios, *Climate Dynamics*, 22, 13–31, doi:10.1007/s00382-003-0365-x, 2004.
- Renssen, H., Isarin, R.F.B., Jacob, D., Podzun, R., and Vandenberghe, J.: Simulation of the Younger Dryas climate in Europe using a regional climate model nested in an AGCM: preliminary results, *Global And Planetary Change*, 30, 41–57, Workshop on Rapid Climatic Warming at the End of the Last Glacial - Palaeodata Analysis and Climate Modeling, Haarlem, Netherlands, Feb 22–24, 2000, 2001.
- Rind, D., Goldberg, R., Hansen, J., Rosenzweig, C., and Ruedy, R.: Potential evapotranspiration and the likelihood of future drought, *Journal of Geophysical research-atmospheres*, 95, 9983–10 004, 1990.
- Robock, A.: State of the planet, chap. Climate impacts of volcanic emissions, pp. 125–134, American Geophysical Union, Washington D.C., first edn., 2004.

- Rodrigo, F.S.: A new method to reconstruct low-frequency climatic variability from documentary sources: application to winter rainfall series in Andalusia (Southern Spain) from 1501 to 2000, *Climatic Change*, 87, 471–487, 2008.
- Rodrigo, F.S., Gómez-Navarro, J.J., and J.P. Montávez: Climate variability in Andalusia (southern Spain) during the period 1701–1850 AD from documentary sources: evaluation and comparison with climate model simulations, *Climate of the Past Discussions*, 7, 2297–2339, 2011.
- Schneider von Deimling, T., Meinshausen, M., Levermann, A., Huber, V., Frieler, K., Lawrence, D. M., and Brovkin, V.: Estimating the permafrost-carbon feedback on global warming, *Biogeosciences Discussions*, 8, 4727–4761, doi:10.5194/bgd-8-4727-2011, 2011.
- Serrano, A., García, J.A., Mateos, V.L., Cancillo, M.L., and Garrido, J.: Monthly Modes of Variation of Precipitation over the Iberian Peninsula, *Journal of Climate*, 12, 2894–2919, doi:10.1175/1520-0442(1999)012<2894:MMOVOP>2.0.CO;2, 1999.
- Servonnat, J., Yiou, P., Khodri, M., Swingedouw, D., and Denvil, S.: Influence of solar variability, CO<sub>2</sub> and orbital forcing between 1000 and 1850 AD in the PSLCM4 model, *Climate of the Past*, 6, 445–460, doi:10.5194/cp-6-445-2010, 2010.
- Shanahan, T.M., Overpeck, J.T., Anchukaitis, K.J., Beck, J.W., Cole, J.E., Dettman, D.L., Peck, J.A., Scholz, C.A., and King, J.W.: Atlantic Forcing of Persistent Drought in West Africa, *Science*, 324, 377–380, doi:10.1126/science.1166352, 2009.
- Shapiro, A.I., Schmutz, W., Rozanov, E., Schoell, M., Haberreiter, M., Shapiro, A.V., and Nyeki, S.: A new approach to the long-term reconstruction of the solar irradiance leads to large historical solar forcing, *Astronomy and Astrophysics*, 529, D07107, doi:10.1051/0004-6361/2, 2011.
- Soden, B.J., Wetherald, R.T., Stenchikov, G.L., and Robock, A.: Global cooling after the eruption of Mount Pinatubo: A test of climate feedback by water vapor, *Science*, 296, 727–730, 2002.
- Solman, S.A., Nunez, M.N., and Cabre, M.F.: Regional climate change experiments over southern South America. I: present climate, *Climate Dynamics*, 30, 533–552, doi: 10.1007/s00382-007-0304-3, 2008.

- Stenchikov, G., Hamilton, K., Stouffer, R.J., Robock, A., Ramaswamy, V., Santer, B., and Graf, H.: Arctic Oscillation response to volcanic eruptions in the IPCC AR4 climate models, *Journal of Geophysical Research*, 11, D07 107, doi:10.1029/2005JD006286, 2006.
- Stensrud, D.J.: Parameterization schemes: keys to understanding numerical weather prediction models, Cambridge University Press, 2007.
- Stevens, M.B., González-Rouco, J.F., and Beltrami, H.: North american climate of the last millennium: underground temperatures and model comparison, *Journal of Geophysical Research - Part F - Earth Surfaces*, 113, F01 008, doi:10.1029/2006JF000705, 2008.
- Stott, P.: Attribution of regional-scale temperature changes to antrropogenic and natual causes, *Geophysical Research Letters*, 30, 1728–1731, 2003.
- Strandberg, G., Brandefelt, J., Kjellström, E., and Smith, B.: High-resolution regional simulation of last glacial maximum climate in Europe, *Tellus, Series A: Dynamic Meteorology and Oceanography*, 63, 107–125, 2011.
- Swingedouw, D., Terray, L., Cassou, C., Volodioire, A., Salas-Mélia, D., and Servonnat, J.: Natural forcing of climate during the last millennium: fingerprint of solar variability, *Climate Dynamics*, 36, 1349–1364, doi:10.1007/s00382-010-0803-5, 2010.
- Taylor, K.E.: Summarizing multiple aspects of model performance in a single diagram, *Journal of Geophysical Research-Atmospheres*, 106, 7183–7192, 2001.
- Tett, S.F.B., Betts, R., Crowley, T.J., Gregory, J., Johns, T.C., Jones, A., Osborn, T.J., Oestroem, E., Roberts, D.L., and Woodage, M.J.: The impact of natural and anthropogenic forcings on climate and hydrology since 1550, *Climate Dynamics*, 28, 3–34, 2007.
- Thompson, L.G., Yao, T., Mosley-Thompson, E., Davis, M.E., Henderson, K.A., and Lin, P.N.: A high-resolution millennial record of the South Asian monsoon from Himalayan ice cores, *Science*, 289, 1916–1919, 2000.
- Trenberth, K.E.: Climate system modeling, Cambridge University Press, 2010.
- Trenberth, K.E. and Paolino, D.A.: The Northern Hemisphere sea-level pressure data set-Trends, errors and discontinuities, *Monthly Weather Review*, 108, 855–872, 1980.

- Trigo, R.M. and Palutikof, J.P.: Precipitation scenarios over Iberia: A comparison between direct GCM output and different downscaling techniques, *Journal of Climate*, 14, 4422–4446, 2001.
- Trigo, R.M., Pozo-Vazquez, D., Osborn, T.J., Castro-Diez, Y., Gamiz-Fortis, S., and Esteban-Parra, M.J.: North Atlantic oscillation influence on precipitation, river flow and water resources in the Iberian peninsula, *International Journal Of Climatology*, 24, 925–944, doi:10.1002/joc.1048, 2004.
- Trouet, V., Esper, J., Graham, N.E., Baker, A., Scourse, J.D., and Frank, D.C.: Persistent positive North Atlantic Oscillation model dominated the Medieval Climate Anomaly, *Science*, 324, 78–80, doi:10.1126/science.1166349, 2009.
- Ulbrich, U., Leckebusch, G.C., and Pinto, J.G.: Extra-tropical cyclones in the present and future climate: a review, *Theoretical and Applied Climatology*, 96, 117–131, 2009.
- Uppala, S.M., Kallberg, P.W., Simmons, A.J., Andrae, U., Bechtold, V.D., Fiorino, M., Gibson, J.K., Hinesler, J., Hernandez, A., Kelly, G.A., Li, X., Onogi, K., Saarinen, S., Sokka, N., Allan, R.P., Andersson, E., Arpe, K., Balmaseda, M.A., Beljaars, A.C.M., van De Berg, L., Bidlot, J., Bormann, N., Caires, S., Chevallier, F., Dethof, A., Dragosavac, M., Fisher, M., Fuentes, M., Hagemann, S., Holm, E., Hoskins, B.J., Isaksen, L., Janssen, P.A.E.M., Jenne, R., McNally, A.P., Mahfouf, J.F., Morcrette, J.J., Rayner, N.A., Saunders, R.W., Simon, P., Sterl, A., Trenberth, K.E., Untch, A., Vasiljevic, D., Viterbo, P., and Woollen, J.: The ERA-40 re-analysis, *Quarterly Journal of the Royal Meteorological Society*, 131, 2961–3012, doi:10.1256/qj.04.176, 2005.
- van der Linden P. and J.F.B. Mitchell (eds.): ENSEMBLES: Climate Change and its Impacts: Summary of research and results from the ENSEMBLES project, Met Office Hadley Centre, FitzRoy Road, Exeter EX1 3PB, UK, 2009.
- von Storch, H.: Inconsistencies at the interface of climate impact studies and global climate research, *Meteorol. Zeitschrift*, 4, 72–80, 1995.
- von Storch, H. and Zwiers, F.W.: Statistical Analysis in Climate Research, Cambridge University Press, 1999.
- Wagner, S. and Zorita, E.: The influence of volcanic, solar and CO<sub>2</sub> forcing on the temperatures in the Dalton Minimum (1790–1830): a model study, *Climate Dynamics*, 25, 205–218, doi:10.1007/s00382-005-0029-0, 2005.

- Walker, M., Johnsen, S., Rasmussen, S.O., Popp, T., Steffensen, J., Gibbard, P., Hoek, W., Lowe, J., Andrews, J., Björck, S., Cwynar, L.C., Hughen, K., Kershaw, P., Kromer, B., Litt, T., Lowe, D.J., Nakagawa, T., Newnham, R., and Schwander, J.: Formal definition and dating of the GSSP (Global Stratotype Section and Point) for the base of the Holocene using the Greenland NGRIP ice core, and selected auxiliary records, *Journal of Quaternary Science*, 24, 3–17, doi:10.1002/jqs.1227, 2009.
- Weiss, H. and Bradley, R.S.: Archaeology - What drives societal collapse?, *Science*, 291, 609–610, doi:10.1126/science.1058775, 2001.
- Wilby, R.L., Wigley, T.M.L., Conway, D., Jones, P.D., Hewitson, B.C., Main, J., and Wilks, D.S.: Statistical downscaling of general circulation model output: A comparison of methods, *Water Resources Research*, 34, 2995–3008, 1998.
- Xie, S.P., Miyama, T., Wang, Y., Xu, H., de Szoeke, S.P., Small, R.J.O., Richards, K.J., Mochizuki, T., and Awaji, T.: A Regional Ocean-Atmosphere Model for Eastern Pacific Climate: Toward Reducing Tropical Biases, *Journal of climate*, 20, 1504–1522, 2007.
- Xoplaki, E., González-Rouco, J.F., Luterbacher, J., and Wanner, H.: Wet season Mediterranean precipitation variability: influence of large-scale dynamics and trends, *Climate Dynamics*, 23, 63–78, doi:10.1007/s00382-004-0422-0, 2004.
- Yoshimori, E.M., Stocker, T.F., Raible, C.C., and Renold, M.: Externally forced and internal variability in ensemble climate simulations of the Maunder Minimum, *Journal of Climate*, 18, 4253–4270, 2005.
- Zorita, E. and von Storch, H.: The Analog Method as a Simple Statistical Downscaling Technique: Comparison with More Complicated Methods, *Journal of Climate*, 12, 2474–2489, doi:10.1175/1520-0442(1999)012<2474:TAMAAS>2.0.CO;2, 1999.
- Zorita, E., González-Rouco, J.F., and Legutke, S.: Testing the Mannetal.(1998) Approach to Paleoclimate Reconstructions in the Context of a 1000-Yr Control Simulation with the ECHO-G Coupled Climate Model, *Journal of Climate*, 16, 1378–1390, 2003.
- Zorita, E., González-Rouco, J.F., von Storch, H., Montávez, J.P., and Valero, F.: Natural and anthropogenic modes of surface temperature variations in the last thousand years, *Geophysical Research Letters*, 32, 755–762, 2005.

- Zorita, E., von Storch, H., González-Rouco, J.F., Cubasch, U., Luterbacher, J., Legutke, S., Fischer-Bruns, I., and Schlese, U.: Climate evolution in the last five centuries simulated by an atmosphere-ocean model: global temperatures, the North Atlantic Oscillation and the Late Maunder Minimum, *Meteorologische Zeitschrift*, 13, 271–289, doi:10.1127/0941-2984/2004/0013-0271, 2004.
- Zorita, E., Moberg, A., Leijonhufvud, L., Wilson, R., Brázdil, R., Dobrovolny, P., Luterbacher, J., Böhm, R., Pfister, Ch., Glaser, R., Söderberg, J., and González-Rouco, J.F.: European temperature records of the past five centuries based on documentary information compared to climate simulations, *Climatic Change*, 101, 143–168, doi: 10.1007/s10584-010-9824-7, 2010.